CFD Analysis of Subcutaneous Deposition and Dispersion of Insulin in Adipose Tissue

Ryan Christopher Lubbers

A Thesis Submitted to the Graduate Faculty of

GRAND VALLEY STATE UNIVERSITY

In

Partial Fulfillment of the Requirements

For the Degree of

Master's in Biomedical Engineering

Padnos School of Engineering and Computing

August 2021

Acknowledgements

I would first like to extend my deepest gratitude to my committee who helped to shape the success of this study. A special thanks to my committee chair Dr. Mokhtar, who was willing to endeavor into this project with me. His expertise in CFD was essential for the accurate development of the computational model of the adipose tissue and understanding the results. Secondly, I would like to express my appreciation for all the professors that have influenced my work throughout my years at Grand Valley State University, better shaping my skills as an engineer. I also would like to thank my family for their continued support throughout my schooling and as I pursued my graduate degree. I also would like to mention my puppy Kimber, who always reminded me when it was take a break and move around or go to bed. Finally, I would like to give all the glory to God, who has given me not only the strength to face my own health difficulties each day, but also the gifts to excel at a higher level of education.

Abstract

Drug delivery is the most important factor of many therapies, but a lack of technology and research have led to a very generalized understanding of drug kinetics. Insulin pump therapy for the treatment of Type 1 Diabetes depends on precise delivery of the hormone into the adipose region between the dermis and underlying muscle. The kinetics of insulin within the adipose tissue environment is not well understood and varies greatly case to case. The use of computation fluid dynamics (CFD) models to study insulin kinetics in relation to influential factors will lead to a better understanding of the characteristics of insulin infusion.

Previously published studies revealed a single study using CFD to analyze insulin delivery, which indicated CFD research of insulin delivery was viable, but also needed more development for a complete biological computational model to simulate insulin delivery. Other studies have presented research in many of the key areas needed to create such a CFD model incorporating interstitial adipose tissue fluid flow and insulin delivery. Important characteristics were able to be identified from published research aiding in the development of an adipose tissue CFD model.

A porous media CFD model simulating the interstitial flow within adipose tissue was developed and modified to include insulin infusion in the model. The insulin deposition modeling was verified through the agreement with published study results. A study to analyze the effect of infusion set design and adipose tissue thickness on insulin deposition and dispersion was developed. This study considered the five most common cannula geometries currently on the market as well as adipose tissue thicknesses found across the body mass index range of patients, resulting in the parametric analysis of twenty-five cases.

Through the use of both graphic and statistical analysis, the results of the study indicated that both the cannula design and adipose tissue thickness have a significant effect on deposition and dispersion of insulin. Further, there was a clear difference between the thin adipose tissue and thick adipose tissue insulin deposition and dispersion observed. It was also found that as the lower angle cannulas decreased the dispersion of insulin within the tissue, but the cannula length at these infusion angles did not significantly impact the deposition and dispersion of insulin. In conjunction with previous understanding of insulin kinetics, the results indicated using a similar cannula geometry in lean and thick adipose tissue would result in largely different drug absorption characteristics. Further there would likely be a large variation in the insulin kinetics even within a singular patient due to adipose tissue thickness deviation.

Therefore, further research in the area of insulin kinetics with relation to the cannula design and tissue thickness is highly warranted, especially with autonomous insulin pumps already on the market. The best way to further improve insulin treatment would be to achieve a more precise delivery and absorption across each adipose environment within a singular patient's anatomy. This study proved the use of computational models such as CFD is a very useful technology for such research in insulin delivery, but additional studies are required to further utilize computational models to enhance the understanding of insulin delivery kinetics within adipose tissue and the different factors effecting it.

Table of Contents

List of Figures

List of Tables

Symbols and Abbreviations

A – area of the control surface the fluid is flowing thru

b – factor dependent upon particular flow and medium

CFD – computational fluid dynamics

D – characteristic length

d_p – average pore diameter

E – energy

IU – insulin unit

K – permeability of medium (Darcy number)

k_c – capillary permeability

L – capillary length

$\dot{m}$ – mass flow rate

p – pressure

P_i – inertial term

P_v – viscous term

p_c – blood hydrostatic pressure

p_i – interstitial fluid hydrostatic pressure

∇p – pressure differential

q – heat flux

Re – Reynolds number

Re_D – Darcy Reynolds number

Re_P – Pore Reynolds number

S_E – heat source

S_M – body forces on fluid

U – flow velocity

$\overline{U}$ – intrinsic average velocity

u – fluid velocity in x-direction

$\bar{u}$ – Darcy velocity

u_L – velocity at positional length

u_0 – characteristic maximum velocity

u_y – capillary permeation velocity

V – fluid velocity

v – fluid velocity in y-direction

w – fluid velocity in z-direction

x – position length

α – volumetric porosity

θ – diffusion permeability

λ – tortuosity

μ – dynamic viscosity

π_c – blood osmotic pressure

π_i – interstitial fluid osmotic pressure

ρ – fluid density

τ – shear stress

1. Introduction

Type I Diabetes treatment advancements have been one of the greatest developments of managing autoimmune conditions in the past several decades. This has come through the successful synthesis of a human insulin analog, the introduction of continuous pump infusion, and even the use of constant glucose monitor technology to give continuous glucose updates leading to almost completely autonomous pump control. The more treatment methods develop, the greater the trend toward individualized management on a patient-by-patient basis. For this step to completely take place though, it requires the ability to understand and predict the influence of factors on a patient's insulin uptake and dispersion. There has been no readily available way to easily measure and simulate the anatomical conditions found in the subcutaneous adipose region where the insulin is infused but utilizing tools such as computational fluid dynamics (CFD) and individualize tissue models could lead to a better understanding of the flow and kinetics of the drug within the biological tissue. The use of patient models could better help determine management decisions for each individual such as which infusion set, insulin, and delivery rate would be best suited for their condition treatment.

1.1 Background

The human body has a complex network of systems which are responsible to control various functions or maintain life sustaining levels of molecules throughout the body. One of these important molecule levels to be maintained is the amount of glucose in the blood. The homeostatic balance of blood glucose is maintained through the release of either glucagon or insulin by the pancreas to prevent hyper or hypoglycemia based on the current blood glucose concentration as shown in Figure 1. Diabetes is a disease which disrupts this cycle of blood glucose control, resulting in the inability to maintain a healthy homeostatic blood glucose. The homeostatic system can be interrupted in two major ways, which create the classifications of Type I and Type II Diabetes.

Type II Diabetes is associated with a resistance to insulin, typically related to several factors including the individual patient's genetic, body mass index, and daily dietary and exercise routine. The condition can often be managed by lifestyle changes as well as supplementary drugs to change metabolism, boost insulin sensitivity, or give a small amount of supplemental insulin. In very severe cases, full time insulin therapy may be required.

Type I Diabetes on the other hand is a completely autoimmune condition where the beta cells of the pancreas that produce insulin are completely destroyed by the patient's own immune response. Little is known about why this happens or what triggers it, and the onset can be soon after birth or even into one's mid to late 20s. Therefore, the only treatment for a Type 1 Diabetic to maintain a healthy blood glucose level is by frequent insulin bolusing, whether through shots or continuous infusion. This insulin therapy requires constant blood glucose monitoring and insulin adjustment for conditions such as eating, activity, sickness, and many other daily factors that in healthy individuals would be regulated by pancreatic insulin production. These insulin boluses are delivered into the subcutaneous fatty tissue, called adipose tissue.

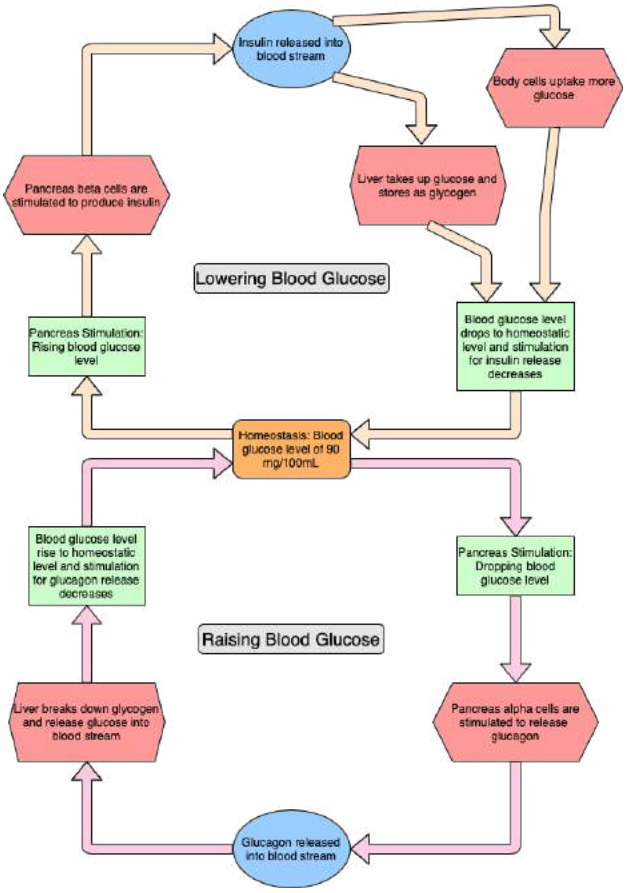

Figure 1. Homeostatic cycle of blood glucose control.

1.2 Adipose Tissue

The adipose tissue into which insulin is injected is a special connective tissue composed of white adipocytes suspended in a fibrous collagen network [1, 2, 3]. The adipocyte function to store

excess energy from carbohydrate consumption in the form of triglycerides [1]. This fatty tissue is found between the dermis and muscles layers, as shown in Figure 2.

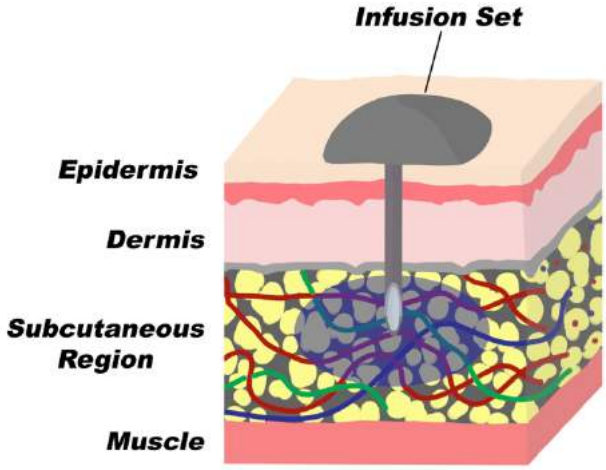

Figure 2. Adipose tissue and subcutaneous bolus into the region.

A more in depth look at the adipose tissue anatomy depicts the tissue not only contains the fatty adipocytes, but also there are blood capillaries and lymphatic capillaries flowing through the tissue as well. Each of the adipocytes is in contact with at least one capillary for the transfer of nutrients for energy storage [1, 4, 5]. These capillaries are also responsible driving the flow of interstitial fluid found in the space between adipose cells as the fluid is transferred through the capillary walls into the extracellular space and then back into either the blood capillaries or lymphatic capillaries driven by osmotic pressure gradients.

1.3 Subcutaneous Drug Delivery

A drug being injected into this subcutaneous tissue area fills the interstitial space around the adipocytes, mixing with the interstitial fluid. Figure 2 illustrates an example of a bolus of insulin in this adipose area of tissue looks like between the dermis and muscle. Once the drug is in in the space it is either absorbed into the blood capillaries, putting the drug directly into the blood stream, or it is absorbed through the lymphatic capillaries becoming part of the lymphatic fluid filtered in the lymph nodes before being added back into the blood stream. The path the drug takes depends on the drug type and molecule size, but also may depend on the delivery location and interstitial flow once the drug is in the tissue [2].

Interstitial drug delivery has posed many potential benefits, the first of which is the various areas available on the body appropriate for administration. As shown in Figure 3, there are large deposits of adipose tissue around the body including the upper arms in the area between the biceps, triceps, and shoulder, the abdominal region, the upper back, the thighs, and the upper buttocks/hip region, as well as the calf region being proposed for viable drug delivery [6, 7]. Also, since injection sites are not directly into the blood stream or quickly absorbing muscular tissue, the risk for systematic infection is much lower in a subcutaneous drug delivery system than in an intravenous or intramuscular system [8]. The diffusion and absorption dynamics of drugs injected into the adipose region could also be conducive for a more biologic method of supplementing or replacing secreted hormones such as insulin. These benefits of subcutaneous drug delivery make it a very viable solution for self-administered treatments and condition management.

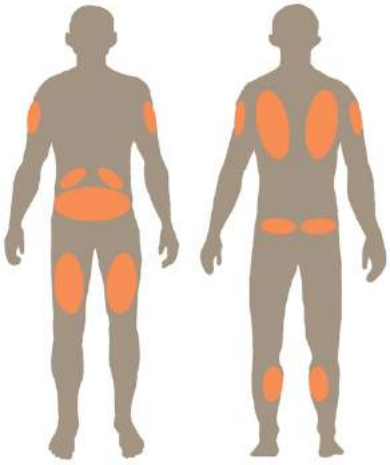

Figure 3. Suitable subcutaneous drug injection areas of body.

Subcutaneous drug delivery does have its limitations though, including a limited volume of infusion, degradation of therapeutic and injection site over time, localized reactions, and variability in inter-individual doses across adipose tissue deposits [8, 9, 10]. Many of these limitations are associated with single point injection administration though, which has been shown to limit the volume of drug able to be administered and mechanical dispersion characteristics of the drug in the adipose tissue, especially when considering large molecules [2, 8]. Also, the conditions affecting the dynamics of drug absorption are not clearly understood in human patients

by current research due to complexity of the tissue region, leading to more variability in drug therapy than is desired in a single patient's treatment [12, 13, 14]. Even given the current weaknesses of subcutaneous drug delivery systems though, there are many applications for subcutaneous injections throughout therapeutics, including immunoglobulins immunodeficiency treatment, hydration, and nutrition supplementations, Treprostinil hypertension treatment, pain killers, and the cancer drug trastuzumab, which are proven as viable for subcutaneous delivery [3, 15, 16, 17]. The most large-scale use of subcutaneous delivery in the medical field currently though would be the 1.15 million Type 1 Diabetics in the United States alone that depend daily on self-administered subcutaneous injections or infusions of insulin to sustain glycemic homeostasis [18].

1.4 Continuous Insulin Infusion

Continuous insulin infusion, which is more commonly known as pump therapy, has been gaining momentum as the best method for insulin delivery in the majority of patients over the past several decades. Pump therapy replaced injections of insulin using manual syringes with an automated pump to deliver the insulin, and a cannula placed in the subcutaneous tissue as the means of delivery rather than a small gauge hypodermic needle. A pump system compared to the typically used pen syringe and needle system used to deliver insulin are shown in Figure 4 below.

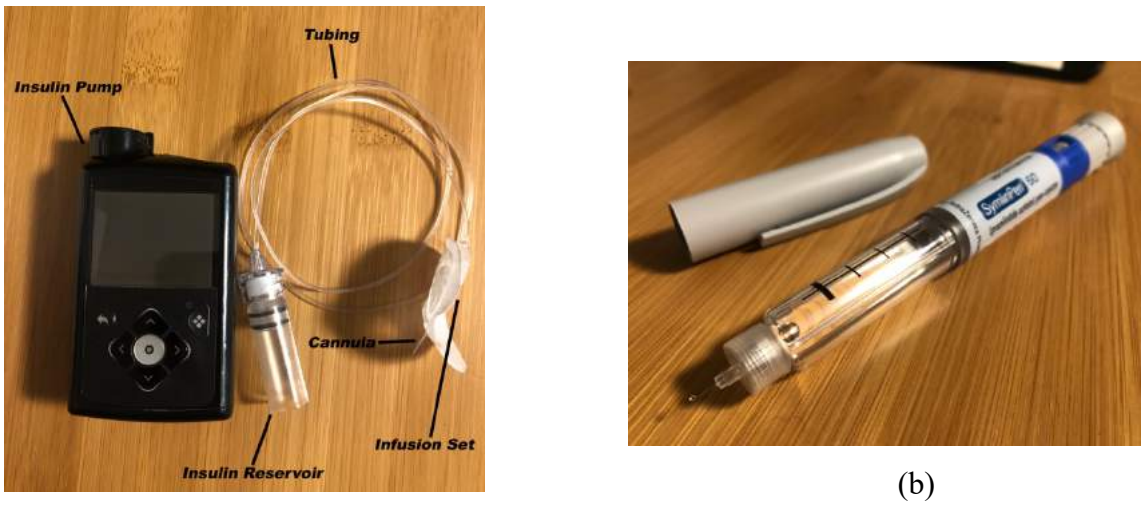

(a) (b)

Figure 4. (a) Insulin pump system versus (b) injection pen and hypodermic needle.

Using pump therapy allows for small amounts of insulin to be continuously administered throughout the day, where manual injections required more injections and even different types of insulin to maintain a consistent basal level of insulin in the patient for the best glycemic control. A pump system often fits better into patient's lifestyle, as it requires less intensive injection site management (the cannula only needs to be changed every 2 to 3 days). Further, newer systems have incorporated constant glucose monitoring (CGM) technology to better help insulin decisions or allow for fully autonomous basal insulin control based on the interstitial glucose concentration and trends returned by the sensor. Studies have indicated that the use of pump therapy has been rapidly increasing in Type 1 Diabetic patients, with a 52% increase in use from 1995 to 2017, from 1% up to 53% respectively [19]. This drastic increase would be expected to continue to grow as CGM, and therefore autonomous insulin delivery, continue to improve over the next several years.

One of the key components in the pump system is the infusion set that contains the cannula, which is directly responsible for accurate and consistent insulin delivery into the adipose tissue. The interface between the cannula and adipose tissue is responsible for the successful delivery of the insulin to the body, which depends on the dispersion within the tissue over time as well. Currently there are 4 major design types of the infusion sets with a multitude of minor variations such as cannula length or material between each pump manufacturer. These major designs include a 90-degree cannula angle, 45-degree cannula angle, a 30-degree cannula angle, and a "flexible" cannula angle (designed to be inserted at very low angles in subcutaneous tissue). Even though these variations are present, the majority of the infusion set for international distribution are actually manufactured in one factory in Denmark [8]. The major designs also have not significantly changed since the introduction of early insulin pumps onto the market in the late 1980s.

1.5 Current Evaluation Systems of Infusion Sets

Evaluation of infusion sets for use in insulin pump therapy is completed in two ways, one by the manufacturers, and one by the patients and their doctors. The evaluation completed by the manufacturers of the infusion sets is required by the drug administration agencies around the world to prove the system as a whole is fit for use in insulin delivery. These evaluations are required to prove the system in fact does deliver insulin accurately and does not provide an added danger the patient's health, but the exact regulations about this vary from agency to agency around the world.

The second evaluation is very patient dependent, as it is the determining of which infusion set on the market is in fact the best for their own use. This process is currently very subjective, and often comes down to trial and error, comfort, and in the end preference. This has resulted in varying trends of which infusion set designs are used in the different international areas [8, 20]. Often, there is input from an Endocrinologist in the infusion set decision, but it still relies heavily on experience, availability, and preference, with little to no ability to predict how the given infusion set would in fact work to deliver the insulin to each given patient based on their body condition. Through the use of CFD modeling to create a simulated adipose tissue environment and prediction of the insulin deposition and dispersion, a greater understanding of insulin kinetics could be achieved. This understanding could lead to applications to current infusion of insulin as well as a step in the direction of individualized patient care based off their own body parameters.

2. Literature Review

CFD has just begun to break into the medical field in the past decade, and therefore only one significant study into the simulation of insulin delivery by pump therapy using CFD was able to be located. The literature review was able to indicate the various components that would be required to make an accurate CFD model of adipose tissue fluid flow for the basis of studying insulin kinetics though by analysis of similar CFD studies considering flow in other tissues, known mechanics of drug and insulin dispersion in tissue, as well as characteristics unique to adipose tissue.

2.1 Subcutaneous Therapeutics Delivery

The subcutaneous region is a complex and variable region of tissue, which has diverse characteristics depending on the area of the body and the patient. The development of models and simulations of drug dynamics in the tissue is difficult due to these individualized and unique characteristics of the tissue. Animal simulation have even been shown to produce very different results from human tissue, as the vascular uptake and biodistribution often happens at very different rates between species [21]. There are many factors contributing to these varied results in drug distribution and absorption after administration, including but not limited to peptides and enzymes present, species, temperature, aggregation at injection site, etc., as shown by a summarization of the factors within a subcutaneous drug delivery system in Figure 5. The impact of many of these factors on drug absorption has not been clearly quantified in humans though, resulting in the varied results observed in drug administration. These varied results are attributed to factors such as molecule size, injection rate, age and sex, and foreign body reaction in the human physiology associated with subcutaneous drug delivery as currently understood through research [3, 16, 21, 22].

The first factor in a subcutaneous drug delivery system to influence the biotherapeutics of drug diffusion and absorption in the tissue is the size of the injected molecule. As shown in Figure 5, the size of the molecule delivered determines the route in which the drug is transported systemically to the body. Smaller water-soluble molecules from <1 kDa and even reportedly up to <20 kDa can be directly absorbed into the capillaries running through the tissue by the oncotic pressure gradients [2, 16, 21]. The drug can be completely absorbed in several hours, or even minutes, based on its size, the capillary flow in the tissue, and the oncotic pressure gradients.

In the case of larger molecules though, in the range of >20 kDa, the method of absorption would be through the bulk fluid flow in the lymphatic capillary system [2, 16, 21, 23]. This is a much slower route of delivery, as lymphatic flow is about 0.2-2% the rate of blood, indicating drug absorption and systemic delivery can take days or weeks to reach peak levels [16, 21]. Therefore, by the characteristic differences in the routes of absorption based on molecule size, it can be noted the absorption rate of the drug is often directly proportional to size. This can play an important role in the desired rate of absorption, as using the same adipose tissue can be used to optimize both slow and fast absorbed drugs based primarily only on designing the molecule to fit the size specification matching the absorption rate desired.

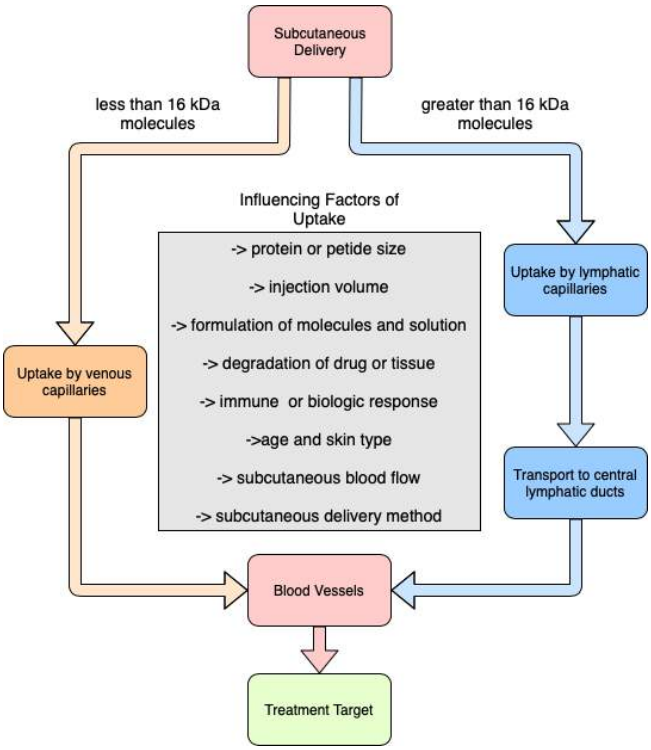

Figure 5. Factors influencing drug delivery through a subcutaneous delivery system.

Insulin specifically can be delivered as a monomer, dimer, and hexamer with respective molecular weights of 6 kDa, 12 kDa, and 36 kDa [24]. The insulin monomers and dimers are absorbed into the blood capillaries due to their size, but the hexamers are reliant on the lymphatic system for absorption due to being larger than 20 kDa [24]. These two paths of absorption are

what separate “rapid-acting” from “slow-acting” insulin, as lymphatic absorption results in a longer delay before the drug reaches the blood stream [2, 16, 21, 23, 24].

The injection rate of the drug can have significant impact on the drug dispersion into the adipose tissue and the absorption into the capillary or lymphatic system, and therefore play a critical role in the mechanics of the drug delivery. Drug solution transportation through a tissue has been modeled as a fluid flowing through a porous medium, and therefore have been assumed to follow the Navier-Stokes equation in correlation to subcutaneous drug injection/infusion [16].

Injection rate research has also shown that the depth of permeation of the drug into the tissue can be inversely related to the rate of drug injection. A faster rate of delivery results in a more planar spread of diffusion parallel to the surface of the tissue, while a slow drug injection rate results in a deeper permeation into the subcutaneous tissue with the drug [16]. This understanding could pose great importance for subcutaneous drug delivery systems, as depending on the composition of the tissue across the anatomical areas used for delivery, the injection rate can help to target areas with a high concentration of vascular capillaries or lymphatic capillaries, especially in connection to the size molecule being delivered.

Different infusion rates could be utilized for the different injection/infusion viable regions based on the physical tissue properties in order to yield consistent drug metabolism across each site on the patient. For example, in a patient’s abdominal subcutaneous tissue, differences in capillary and lymphatic capillary concentrations have been noted from proximal regions on the body to distal regions on the body [21]. Using CFD to simulate different combinations of local tissue characteristics, infusion set designs, and injection rates could lead to a better patient dependent insulin delivery, and even consistent delivery across the different anatomical regions used to deliver the drug.

2.2 Insulin Specific Drug Delivery

In addition to an understanding about drug absorption from the anatomical function of the adipose tissue region, there has been studies completed to quantify the ex vivo mechanics of insulin delivery into adipose tissue. One of these such studies was considering insulin injection pens, and the relationship of the interstitial pressure related to delivering insulin. This was of importance to understand how delivery devices such as insulin pens and pumps need to overcome the force create by the delivery of insulin into the tissue that already is saturated with interstitial fluid [25]. In the

case of the injection delivery, which has a typical delivery rate of 100 µl/s, the delivery flow rate into the tissue was found to significantly decrease when the insulin was delivery into the tissue and a counter pressure was developed while it the drug took time to disperse into the porous medium and interstitial fluid [25]. Through this, a model of the permeability of the adipose tissue region was able to be developed based upon the insulin injection delivery which was found to be in the range of $(8.9 \pm 4.7) \times 10^{-11}$ m^2 [25].

Another study was completed to study the development of the insulin depot immediately after an insulin bolus using by insulin pump and 90° x 8 mm long infusion set cannula. This research was completed in order the better understand the dynamics of the insulin with the subcutaneous adipose region during delivery. The insulin was dyed with food colorant then delivery into porcine tissue that was 15 min postmortem at an infusion rate of 120µL/min for a 150 µL bolus. The samples were then flash frozen to preserve the insulin depot formation. The depot of each sample was then digitally reconstructed by imaging the stain tissue area every 100 µm into the tissue [26]. Analysis of the samples showed the insulin was distributed in channels between the adipocytes of the tissue, with no adverse effects on the cells. The deposition pattern observed was a very branched structure and was quite variable from sample to sample [26]. Massaging the sample during infusion was shown to have increased the insulin distribution distance, but the overall observed reconstructions of the deposits showed very little patterns in their appearance [26].

The study infusing insulin through a pump did show one general observation about insulin delivery to adipose tissue, which was that the insulin did not deposit in a round pattern around the end of the cannula. It instead created an elliptical depot, that had the largest outreach from the cannula at the plane in line with the end of the cannula. Therefore, it was concluded the previous assumption that insulin deposition was spherical about the cannula tip did not fit the actual kinematic deposition of the insulin delivered to the tissue [26]. The study also proposed that the formation of the channels through which the insulin flowed, which were observed between the adipocytes, depends directly on the mechanical properties of the collogen matrix supporting the adipocytes in the adipose region. The overall force driving distribution of the insulin was concluded to be the related to the hydraulic flow and resistance for lateral spreading compared to fluid resistance to pass through to another collogen layer [26].

2.3 Interstitial Fluid Flow in Tissue

Flow of fluid through tissue could be called the highway of transportation in the body. Fluid dynamics in the body governs how different molecules are able to be transported around the body to the areas and cells that require them. To this extent, there are various body fluid compartments found throughout the body, each containing various concentrations of the water found in the body. Adipose tissue contains a low water content at only 10% to 20% compared to skin and muscle which have a water content of 70% to 80% [27]. No matter the water content though, this fluid is continually flowing through the extracellular space in the tissue, driven by the osmotic interface between the capillary fluid and interstitial fluid in the tissue [27, 28]. Fluid dynamics within tissue have been shown to play an important role in physiological functions in the body, especially tissue that the vascular density has been documented to be low such as ligaments and tendons [28-32]. Although in vivo and ex vivo experiments have documented that this interstitial fluid flow can be vital for certain biologic functions and mass transport, there are few in vivo direct measurements of interstitial fluid flow characteristics, especially relating to adipose tissue fluid flow [33, 34]. It has been documented though that flow velocities on the order of 0.1-2.0 μm/s are found in tissue, with velocities reaching even up to 4.0 μm/s [35].

2.4 CFD in Interstitial Fluid Flow and Drug Delivery

It was found that CFD models have found uses in various biological and medical scenarios over the past decade in order to better understand biological processes or drug administration, especially in the areas of cerebral spinal fluid flow, tumor drug delivery, and studying interstitial fluid flow in tendons and ligaments [33, 35-40].

It has been presented that the development of computational models could be used to understand spinal flow, as well as overcome drug delivery barriers that currently hinder therapeutic agents for chronic and degenerative diseases [36]. Using a CFD model coupled with diffusion-tensor imaging, an advanced 3D fluid transport model of the spinal region was able to be presented and validated by prior in vivo experimentation [36]. It can be noted that diffusion-tensor imaging is a non-invasive technology used to track the water diffusion along white matter tracts in the brain [36]. In another study, a CFD model was developed to further understanding of the pharmacokinetics of the regenerative molecular therapy anti-Nogo-A for spinal cord injuries [37]. It was discovered that while the assumption that biological factors such as breathing and cardiac

cycles are the primary driving effect on the drug distribution were valid, the drug injection velocity, injection needle orientation, and bolus amount also did have an effect on the drug distribution pattern in the spinal canal [37]. This gave insight into the challenges of drug delivery targeting using the cerebral spinal fluid as a delivery mechanism.

Similar to looking at drug kinetics being delivered in the spinal region, CFD has also been used in analyzing drug kinetics around tumors. Drug delivery to tumor tissue is highly influences by both therapy and biological factors, which has limited therapeutic methods. Porous media CFD models have opened the door to better understand the factors affecting penetration depth of therapeutic drugs into the tumor, and therefore provide the basis to attempt the optimization of drug delivery for tumor penetration [38]. A more recent study has looked at the fluid flow between the healthy tissue around a diseased region in relation to drug uptake as well. Using a combination of a CFD model and in vivo imaging, a prediction of heterogenous uptake and spatial distribution of therapeutics was able to be made [38]. The study was even able to predict the effect of on the vascular structure of a tumor by the uptake of a vascular disrupting agent [38]. Further, a study found that the permeability of nanoparticle to diffuse into a tumor was highly dependent on the pressure gradients within a tumor using a CFD model driven by oncotic pressure [39].

While the previous studies discussed were able to indicate a viability for use of porous media CFD models to be used in studying drug delivery and dispersion, subcutaneous tissue fluid flow modeling presents its own unique challenges, as it is a tissue region whose fluid mechanics is driven by the fluid exchange between the interstitial region and the capillaries running through the tissue. There have however been several studies completed to compare different computational modeling theories as well as parameters affecting interstitial fluid flow. The three mathematical models used to describe interstitial flow in the fibrous matrix are the Stokes, Brinkman, and Darcy equations [40-45].

It can be noted that the Stokes equation was built upon the assumption of incompressible flow, where the Navier-Stokes equation can be applied based on flow velocities. Since very low Reynolds numbers are characteristic of the interstitial flow, the inertial term of the Navier-Stokes equation can be described as negligible compared to the viscous term. Therefore, all that remains would be the Stokes equation [28, 42]. The Brickman and Darcy equations are instead based upon the hydraulic permeability of the matrix of the porous media being considered. The Brickman equation reduces to the Darcy equation when the permeability is small [28, 42]. It was found in

this comparative study that major difference between the Stokes and Darcy models was the velocity distribution in the cross-sectional area. Also, the Brinkman equation was similar to the Stokes equation when the permeability was large (permeability > 1.0×10^{-8} m^2), and an ample approximation of the Darcy equation at lower permeabilities (permeability < 5.0×10^{-12} m^2) [28]. A conclusion also made was that there was little effect on the interstitial flow when considering the material as anisotropic versus isotropic [28].

Using these principles, work has been done to simulate interstitial fluid flow in both the interosseous membrane as well as ligaments [28, 33, 41, 42]. These areas have capillaries that are parallel to the length of tissue, causing the driving interstitial flow in the lengthwise direction of the tissue based off the Starling relationship for fluid transmission between the capillaries and the interstitial region based on hydrostatic and oncotic pressure [28, 33, 41, 42]. This has allowed for the study of the interstitial velocities in these tissues as well as considering the stress on the wall of an interstitial cell due to the interstitial flow [28, 33, 41, 42].

2.5 CFD in Insulin Delivery

There was a single published research study, a master's thesis by Zedelmair in 2016, using CFD to study the deposition and dispersion of insulin into subcutaneous tissue using pump therapy. This study did create a CFD representation of adipose tissue to study insulin delivery, looking especially at the drug deposition concentration patterns after delivery and several different cannula designs the author created [46]. From this, the study was able to provide conclusions of how insulin delivery looks in a 2D and 3D domain. The study also considered the use of differing porosities in the primary axis domain directions to simulate the anisotropic nature of the depot development noted in a prior ex vivo study that result in an elliptical insulin depot shape [26, 46]. The use of this anisotropic porosity in the CFD model presented was found to accurately model the insulin depot in accordance with the previous ex vivo research. Zedelmair was also able to indicate there were noticeable difference in the size and shape drug deposit in the tissue after delivery between cannula designs and insulin flow rates.

While this study was a CFD model of insulin delivery, there were a few things noted though that were assumed or not included in the model, the largest of which was the assumption the interstitial fluid was stagnant in the adipose tissue. As previously discussed, the interstitial fluid in the adipose region is constantly moving, as it is essential for biologic function within the body.

This fluid flow within the extracellular area of the adipose region would have an impact on the insulin deposition and dispersion, especially over time.

In connection with this also, the 3D model domain described was a quarter cylinder, with an outlet in one direction and a symmetry axis assumption about the axis of the cannula [46]. This assumption would be valid considering stagnant interstitial fluid as the discussed study presented, but not if the interstitial fluid would be considered as a flowing fluid in the 3-dimensional space of the domain. Therefore, if interstitial adipose tissue fluid flow is being modeled with the insulin delivery, the CFD model domain would not be able to consider the deposition area as symmetric around the axis of the cannula as presented by Zedelmair.

Finally, the study did not consider the factors of currently available infusion set geometries or adipose tissue thickness and their effect on insulin delivery. While the research did look at several different cannula designs, these designs were created by the author, with no indication of being models of currently marketed designs available to patients. Further, the study did not consider the adipose region in various tissue thicknesses but assumed one thickness of 13.9 mm for the duration of the research [46]. Therefore, while this previously published research did present and use a CFD model to study insulin delivery, there were various factors of the research that did not allow for application to be made to current patient therapy decisions.

2.6 Adipose Tissue Characteristics

Though several studies on interstitial fluid flow using CFD were able to be found, adipose tissue has a number of special characteristics that make it unique compared to the dermis or muscle tissue around it. Two of the main factors to consider are the adipose tissue thickness and vascularization.

Adipose tissue has variable thickness throughout the body, as well as between individual patients. It has been presented that the subcutaneous adipose tissue thickness has a direct effect on insulin therapy and the chance for intramuscular delivery if the adipose region was penetrated completely, thus making the adipose thickness one of the primary factors in needle and infusion set selection [47]. Various studies have been performed looking at the adipose tissue thickness in different control groups, even comparing different anatomical regions within the sets of individuals [48-50]. The most notable results in the studies found was using a set of adults which ranged from

lean to obese, with a body mass index (BMI) range of 18.6-40.3 kg/m^2 [48]. The results presented in this study are found in Table 1.

These results indicate a very large range of adipose tissue thicknesses can be present in one patient as well as across the entire spectrum of body sizes, considering the range in the adipose tissue thickness was found be from 5 mm all the way up to 30 mm in the regions presented as suitable for insulin delivery in patients [48]. Considering tissue thickness has been mentioned as one of the large contributing factors to insulin absorption, this range in adipose tissue thickness could be a significant factor in insulin absorption and dispersion.

Table 1. Median observed adipose tissue thickness in lean and obese patients [47].

Anatomic Location	**Lean Median Thickness (mm)**	**Obese Median Thickness (mm)**
Upper Abdomen	6	28
Lower Abdomen	10	31
Distal Triceps	5	6
Lateral Thigh	9	19
Frontal Thigh	5	8
Medial Calf	3	6

Another critical factor that sets adipose tissue apart from other anatomical regions would be the vascularization of adipose tissue. The capillaries in other tissues studied for interstitial flow have a patterned longitudinal capillary direction, but adipose tissue has a much more meandering pattern throughout the tissue [4, 51, 52]. Also, it has been found that conditions such as obesity lower the capillary density in the subcutaneous adipose tissue [53]. Therefore, the vascular and lymphatic capillary density can largely vary from patient to patient as well in their respective adipose tissue region.

Similarly, adipose tissue has a more uniform structure lending itself to produce a more bidirectional interstitial fluid flow pattern compared to muscular or ligament tissue, which has been shown to have very a longitudinal anisotropic interstitial fluid flow [5, 33, 41, 42, 54]. This structure is due to the unique generation of adipocytes in the extracellular matrix in an organized manner, grouping adipocytes into lobules, and forms a well-organized network for proper adipose

tissue function [5, 54]. Adipose tissue has still been observed to have an anisotropic flow component though, especially with respect to drug delivery. The extracellular matrix layers that support the adipocyte network have been shown to buffer the vertical drug dispersion [3, 21, 26]. The exact mechanics of how these lower permeable extracellular matrix layers affect the hydrodynamic forces and permeation within the tissue though is not well quantified, it has only been observed as an influencing factor of drug deposition and dispersion in adipose tissue [3, 26].

A property of adipose tissue that has not been well documented is the tortuosity, which has not been well quantified for any biologic tissue. Tortuosity is defined as the ratio between the shortest distance a fluid particle takes to the shortest straight-line distance from the entry point to the exit point of the domain [55, 56, 57, 58]. Therefore, this would indicate a particle taking a straight path from one end of the domain to the other end of the domain would result in a tortuosity of 1, and as the particle path deviates toward a more sinusoidal path, the tortuosity would increase. If just considering a porous medium with a homogenous packing of uniform particle sizes, the largest contributing factor to tortuosity would be the porosity [55]. There is little described about adipose tissue in relation to its tortuosity, but tortuosity of tissue and bone has become of importance in previous years. This is because tortuosity has become an important factor in scaffolding design for tissue and bone reconstruction [55, 56, 57]. Similarly, tortuosity has been studied in respect to the extracellular space around the brain, giving light to how tortuosity would be affected by the porosity of the matrix as well as the type of matrix the domain is composed of. It was found at low porosities, the tortuosity of both 2D and 3D models follow very closely with the "narrow channel approximation" as well as the Maxwellian prediction, giving tortuosity values decreasing from 1.23 to 1.12 in the porosity range of 0 to 0.5 [58]. For low porosity cases, the tortuosity can be estimated by Equation 1:

$$\lambda^2 = \frac{1}{\theta} \tag{1}$$

where λ is tortuosity and θ is a diffusion permeability. This diffusion permeability can be approximated using the "narrow channel approximation", which is shown below:

$$\theta = \frac{2}{3-\alpha} \tag{2}$$

where α is the volumetric porosity of the medium. These approximations have been shown to be viable to predict the tortuosity of tissue with low permeability, whether it was a cube construct with varying gap widths, loosely dispersed spheres, or random 3D geometry of convex polyhedral [58].

2.7 Summary of Research

Summarizing all the published studies found indicated there are a multitude of published works in major component areas overlapping with using CFD techniques to study insulin delivery into adipose tissue, but only one published work by Zedelmair considered using CFD to study insulin delivery. Table 2 shows an overview of all these topics covered in the previously published studies. It can be noted the critical topic columns for the current presented study are highlighted in orange. It can be clearly observed that there was a clear divide between studies considering subcutaneous drug delivery and its biologic components and those studies modeling biologic tissues using porous media models and CFD techniques.

Many of the studies considering subcutaneous drug delivery and more importantly insulin delivery in Type 1 Diabetics emphasize how important understanding the mechanics behind the drug delivery and dispersion are to better manage condition treatment, but at this point in time there has not been a clear link studied between the available infusion sets on the market and which are most viable for drug delivery in different thickness tissues. The current evaluation method to determine which infusion set works for an individual patient is vastly lacking and time consuming. It could be greatly improved through the use of an accurate model to understand how each infusion set delivers insulin in different adipose tissue conditions. This could help to improve effective drug interaction in the body as well as improve overall homeostatic balance of blood sugars in Type 1 Diabetic patients no matter what anatomical area of adipose tissue is being used to infuse the insulin.

Although the simulation of insulin delivery using CFD was studied by Zedelmair, various parameters were not considered in the model, such as interstitial flow, varied adipose tissue thickness, and the different cannula designs that are currently available on the market. Therefore, based off the published research, an even more comprehensive model of adipose tissue to study the effect of different available infusion sets and adipose tissue thicknesses on the delivery of insulin in a patient could be developed based upon the research found. This model was able to be used to further the understanding of current insulin delivery methods available to Type 1 Diabetics.

Table 2. Research summary of previous studies published.

Citation	CFD Analysis	CFD Theory	Porous Media	Mathematical Modeling	Interstitial Flow	Adipose Tissue	Tissue Structure	Tortuosity	Turbulence	Vascularization	Subcutaneous Drug Delivery	Drug Uptake	Trans-vascular Flow	Insulin Delivery	Infusion Sets	Pump Therapy	In vivo/Ex vivo
1						X	X										
2					X	X	X				X	X	X				
3						X	X				X	X	X				X
4						X				X							
5				X		X	X										X
7						X					X				X		X
8						X					X	X		X	X	X	
9							X				X	X					
10											X	X					
11				X		X					X						X
12						X					X	X		X	X	X	
13						X					X	X		X	X	X	
14						X					X	X		X	X	X	
15											X	X					X
16											X	X					
17											X	X					X
19											X			X		X	
20						X					X	X		X	X	X	
21						X	X				X	X	X				
22						X	X			X	X	X			X		
23										X	X	X					X
24					X					X	X	X	X	X			X
25						X					X			X			X
26						X					X			X	X	X	X
27				X	X								X				
28	X	X	X	X	X		X										
29					X		X										X
30			X	X	X	X	X				X	X	X				
31					X		X										
32					X												
33	X	X	X	X	X		X			X							
34					X	X	X			X			X				
35	X	X	X	X	X												X
36	X	X	X	X	X												
37	X	X	X	X	X							X					
38	X	X	X	X	X		X										X
39	X	X	X	X	X					X			X				
40	X	X	X	X	X		X					X					X
41	X	X	X	X	X		X						X				
42	X	X	X	X	X		X						X				
43		X	X	X													
44	X	X	X	X	X		X										
45	X	X	X	X	X		X										
46	X	X	X	X	X	X	X				X	X		X	X	X	
47						X	X				X	X		X	X	X	
48						X	X										
49						X	X										
50						X	X										
51						X	X			X							X
52						X	X			X							
53						X	X			X				X			X
54				X		X	X										
55				X	X		X	X									
56				X	X		X	X									
57					X		X	X									
58				X	X			X									
59							X										X
60											X			X		X	
62	X	X	X	X	X	X	X										
63	X	X	X	X			X										
64	X	X	X	X			X										
65		X	X		X		X										
67		X	X														
68	X	X	X						X								
69			X	X													
71						X	X			X			X				X
72						X	X			X			X				X
73					X		X						X				
75					X								X				
77				X		X	X				X						
78						X											X
80						X	X			X							X
81	X	X	X	X													

3. Methodology

Therefore, considering the background and discussed research, the main research components were as follows:

First, a steady state porous media CFD model was developed to simulate the delivery of insulin the subcutaneous adipose tissue space using the CFD software Star CCM+ developed by Siemens Digital Industries Software. This model incorporated both the insulin being delivered by a cannula as well as the interstitial fluid flow driven by the blood and lymphatic capillaries present in adipose tissue. This model was able to obtain results similar to those found in previously performed insulin delivery studies presented in published research [26, 46].

Secondly, a parametric study was completed using the CFD model in order to study how different important factors of insulin delivery affect the delivery and dispersion patterns of the drug in the tissue. These factors included the adipose region thickness and infusion set cannula geometric design. These results were compared using post processing tools and graphics in the Start CCM+ software as well as a design of experiments statistical analysis of the insulin depot size formed in the adipose tissue model domain.

Through these steps of the study, conclusions concerning insulin delivery for Type 1 Diabetic patients were able to be drawn and discussed using the results obtained. The analysis of the insulin delivery cases using the developed CFD model did produce results indicating the cannula geometry and tissue thickness do both affect the kinematics of insulin delivery in the tissue. Further, observations made from the results were able to indicate further investigation into factors affecting insulin delivery would be warranted, as later discussed.

3.1 Research Goals

To accomplish the research components, a set of goals was set forth as follows in order to build upon the published research as well as explore new applicable areas:

- Develop a steady state porous-media CFD model for subcutaneous adipose tissue fluid flow
- Incorporate insulin infusion into the subcutaneous adipose tissue fluid flow CFD model
- Compare the deposition and flow of insulin using current market cannula designs within the known adipose tissue thickness range using the developed CFD model

- Complete a parametric study to analyze the effects of different cannula geometries and tissue thicknesses on insulin deposition and dispersion

The first goal to develop a steady state model for adipose tissue fluid flow was a necessary step to more accurately be able to simulate insulin flow into and through the tissue region. Having an accurate model of how fluid flows through the interstitial space in the adipose tissue is essential to accurately depicting the movement of insulin in the tissue. This was of great importance especially in a time dependent study as it would drastically affect the dispersion over time of the insulin. The previous studies that have looked at insulin delivery did not include this important factor into the models that were developed though. Considering the results of previous research in interstitial fluid flow in other tissue regions anatomically, the capillary driven flow would have a direct impact on the flow patterns and dispersion of drugs being injected into the adipose region.

The vascularization patterns of adipose tissue also provided reason for the need to include capillary exchange induced interstitial flow in an adipose tissue model, as the vascularization of adipose tissue can be described as more meandering than patterned compared to muscular tissue. Prior studies showed that the vascularization patterns in muscle and ligaments directly influenced the flow velocities, directions, and even impact on cells in the tissue region, which would indicate a direct impact on the flow of injected drugs into the tissue region as well [27-35]. Therefore, given that the capillaries are more randomized in adipose tissue, this could be assumed to have a direct impact on how drugs flow in the tissue. This indicates that the first step to building a CFD model to study insulin treatments in Type 1 Diabetic patients would be to develop a CFD model that properly models the fluid flow found in the adipose tissue without an insulin injection.

After a foundation model for the adipose tissue fluid flow was developed, the actual insulin infusion could be added to the model. The results of prior studies concerning insulin infusion were able to be used here to indicate whether the model developed did in fact give results that are similar to what have been previously observed in insulin delivery. It should be noted these studies have been completed using a pump at a much larger flow rate than was used in the cases of the current study. Therefore, the higher insulin flow rate was used to verify the model with previous published results but were not a significant component for the results of this study. The verification was able to be done by reproducing the conditions of the study presented by Leuenberger Jockel et al. [26]

as well as comparing the results obtained for the CFD model with the ex vivo results observed in the previous ex vivo study.

Once the developed porous media CFD model was able to provide viable results compared to previous published data, the *current infusion sets were introduced into the model with the goal of using this new model to accurately simulate insulin delivery with each cannula design used on the market today*. One of the biggest unknowns in current pump therapy is which infusion set to use for each patient, let alone whether different anatomic locations on a patient should be used with different infusion set designs to gain consistent treatment results. This has led to the current trial and error approach, where an infusion set is used, and if it does not have an observable positive effect on blood glucose control, another infusion set may be tried in an attempt to get better control. Little study has been done actually to determine if simulations can viably indicate which infusion set should be used for individual patients based on their individual body characteristics. A model that looks at the different possible infusion sets paired with the different adipose tissue thicknesses could be used to better understand where each infusion set design distributes the insulin paired with different tissue thicknesses. This could give better insight into which infusion set should be used for different body types, rather than having to go through the time-consuming process that is currently used to decide which infusion set a patient should use.

Finally, a parametric design of experiments (DOE) study was instrumental in differentiating whether the infusion set, tissue thickness, or both are significant in the insulin delivery pattern. A combination of comparing generated graphical images of the insulin flow development through the deposition area as well measurements of these areas were able to be used to draw conclusions concerning how the factors of interest, namely cannula geometry and tissue thickness, affected the insulin delivery. Using the DOE helped to understand the different trends found in the results and helped to determine if the cannula geometry and/or tissue thickness was significant factor in insulin deposition and dispersion. This led to the conclusion about potential direct impact on current pump therapy, as well as indicating which areas warrant more research.

3.2 Case Studies

Considering these goals, a study set of twenty-five cases were designed, as presented in Table 3, where there are 5 adipose tissue thicknesses that will be considered as well as 5 infusion set cannula geometric designs. These case-studies were built around two major factors that have

been suggested by previous research greatly impact subcutaneous drug delivery treatment success, which are the cannula geometry (length and insertion angle) and the adipose tissue thickness. These cases studies were built using a CFD model, as shown in Figure 6, that considers a domain of adipose tissue modeled as a porous medium with capillary fluid exchange driving the fluid flow in the tissue. It can be noted various elements of the model are shown here, including the capillaries inducing the interstitial fluid flow in the model and velocity vectors indicating the interstitial fluid flow direction and magnitude.

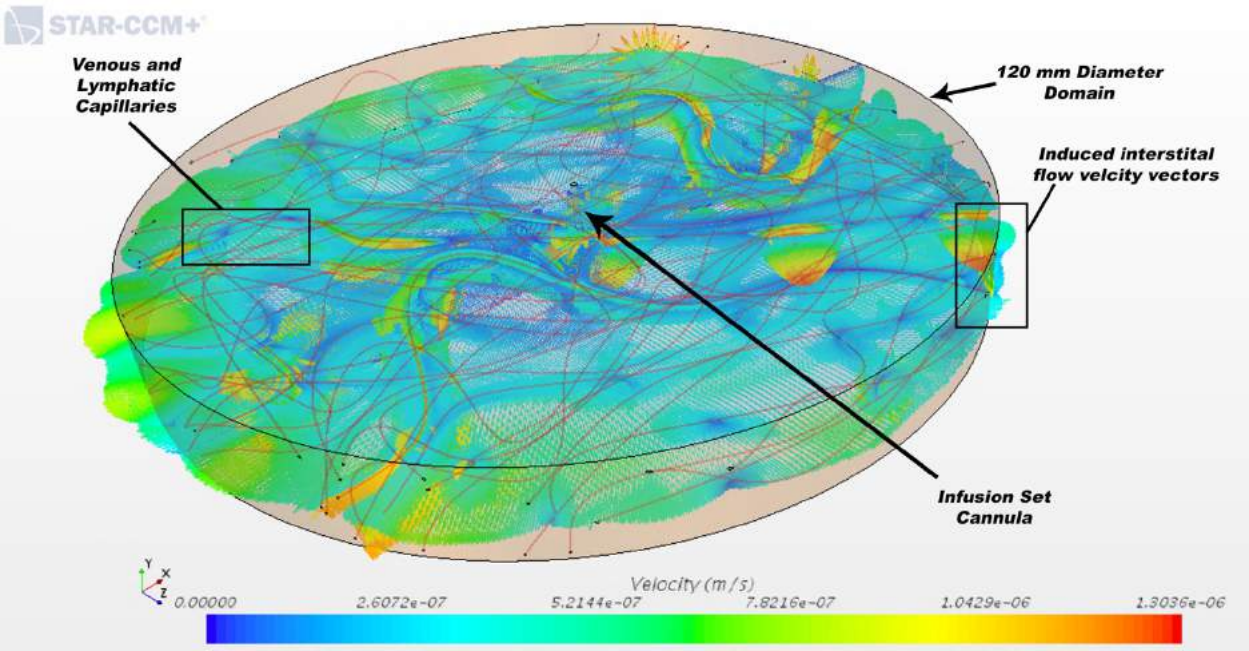

Figure 6. Adipose tissue fluid flow and insulin infusion CFD model domain and elements.

Based off the previously completed studies considering adipose tissue thickness in adults, a range from 6.0 mm to 30.0 mm was found reasonable to encompass the average range of adipose tissue thickness [48-50]. This includes the different anatomical areas used for insulin injections as well as the range of body types from lean to obese. Considering this range of tissue thickness was able to show whether insulin delivery can be affected by the thickness of the tissue it has been delivered into, as well as indicate how the insulin disperses in the tissue. This is especially important when considering different infusion set designs may result in better insulin delivery in

different adipose tissue thickness ranges. A 6 mm tissue thickness step size was used between the cases in each set to fully encompass the range of tissue thickness.

Table 3. Matrix of case sets and parameters.

	Number of Cases	**Cannula Design (insertion angle x length)**	**Tissue Thickness (mm)**
Set 1	5	90° x 8mm	6, 12, 18, 24, & 30
Set 2	5	45° x 13mm	6, 12, 18, 24, & 30
Set 3	5	30° x 13mm	6, 12, 18, 24, & 30
Set 4	5	20° x 13mm	6, 12, 18, 24, & 30
Set 5	5	20° x 17mm	6, 12, 18, 24, & 30

Another property that was involved in the modeling of the tissue that directly related to the position of the cannula in the adipose tissue region was the thickness of the dermis layer above the adipose tissue. Although the dermis thickness is variable anatomically just as the adipose tissue is, it was assumed the dermis had a thickness of 2.5 mm for each case. This tissue thickness for the layer found above the adipose tissue fits within the published study results looking at this anatomical region of the tissue of 1185 μm to 3616 μm in human tissue [59]. It can be noted that one case in Set 2, with the 6 mm adipose tissue, required the assumption that the dermis had a thickness of 3.5 mm to keep the cannula within the adipose tissue without delivering into the muscular region below. This assumption still fits within the published range as discussed above.

In considering the infusion set design, there are four typical insertion angles that are used for subcutaneous cannula geometries used in insulin pump therapy internationally, which are 90-degrees, 45-degrees, 30-degrees, and 20-degrees. It can be noted that there are some infusion sets that are inserted without a guide, so the angle can be between one of these identified angles, such as the Medtronic MiniMed™ Silhouette™, but the insertion angle range for this infusion set is still 20 to 45 degrees. Each pump manufacturer has these options in their infusion sets product lines, varying only in either the locking mechanism on the infusion set or the cannula material and diameter, but the insertion angle remains the same. Therefore, the presented insertion angles for the cannulas should accurately represent the infusion sets that are available to Type 1 Diabetic patients currently. Figure 7 indicates how the geometry of the different cannula lengths and

insertion angles are defined for the infusion sets. The figure also shows this in reference to the cannula being inserted in a tissue sample.

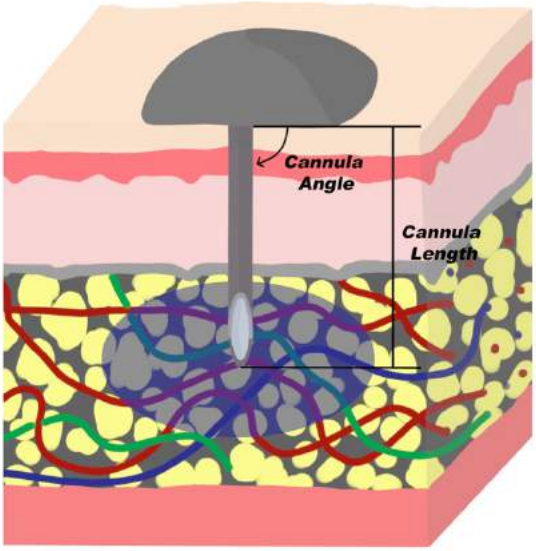

Figure 7. Cannula geometry definition with respect to adipose tissue.

Similarly, the cannula lengths are established across the market that correspond with the different angles of insertion for specific infusion sets. Infusion sets designed for 90-degree insertion typically have a cannula length of 6mm or 8mm. An 8mm to 10mm cannula length was identified as the recommended general use cannula by health officials in a previous study, and therefore an 8 mm cannula for the 90° insertion angle cannula geometry was used in the respective cases [8]. Cannulas of infusion sets designed to have a more acute insertion angle come in the lengths of either 13mm or 17mm across each pump manufacturers product lines in order to get the depth required to get past the dermis and into the adipose tissue below. Most often endocrinologist recommend the shortest cannula, as to alleviate the chance of intramuscular infusion from the cannula passing through the target adipose tissue into the muscle below. It was therefore decided to consider each of the more acute insertion angles as the shorter 13mm cannula length. In order to still consider the longer 17mm cannula though in this study, it has been included as a second 20-degree insertion angle case, which would be the most likely candidate for the longer cannula length because it has such an acute angle of insertion that the penetration depth into the adipose tissue would still be only about 4.5mm.

Each of these twenty-five cases would be considered using the injection rate of two of the most common insulin pumps on the market today, the entire line of Medtronic pumps, and Tandem t:slim X2 pump. This rate of delivery is 1.5 units of insulin (IU) per minute [60]. Although there are slightly different insulin delivery rates in other pumps that are not as common on the market as well as insulin pen injections, the main considerations of this study are to look at the infusion sets and adipose tissue thickness. Therefore, the most common injection rate found in the current insulin pumps available can be considered in each case. Also, the cannula for each case set was assumed to be a 25-gauge size, which is standard for the infusion sets on the market such as the Medtronic MiniMed™ Silhouette™ previously mentioned. Further, it was assumed across the study that the cannula was perfectly seated into the tissue, and therefore no fluid could be lost around the cannula and dermis interface. This was validated by the fact even in previous published ex vivo insulin delivery studies, no leakage was observed around the infusion site [26].

4. CFD Theory

CFD is a numerical method used to solve fluid flow problems in the areas of fluid flow, heat transfer, chemical reactions, and even fluid and structure interactions. This computational numerical method is based upon a set non-linear differential equations, which are derived from the physic principles of conservation of mass, Newton's Second Law, and the First Law of Thermodynamics. Further, due to the structure of adipose tissue, the additional theoretical solutions concerning porous media as well as porous media turbulence must also be taken into account to make a viable computational model of the adipose tissue domain.

The fundamental of CFD therefore is considering constructing the model based off small differential volume elements of fluid. These differential elements are used to create a discrete domain in which the flow field can be solved for at each point on the differential element, while the other areas are approximated by interpolation. Therefore, the discretized element can be represented as shown in Figure 8, with its center at (x, y, z) and length of δx, δy, and δz in the respective coordinate directions. Due to the small size of the elements in respect to the domain being considered, the properties of the fluid flow can be accurately expressed in the first two terms of a Taylor series expansion [61].

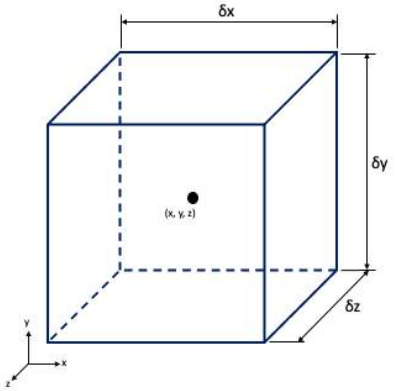

Figure 8. Control volume of differential element for discretized domain.

4.1 Conservation of Mass

The first principal equation governing CFD is the conservation of mass, as shown generally in Equation 3 below, which is a scalar equation, indicating the solution is not direction dependent.

$$Rate\ of\ mass\ tranfer = Mass\ flow\ in - Mass\ flow\ out \tag{3}$$

The mass flow rate can be written in terms of fluid flow parameters, as shown in Equation 4:

$$\dot{m} = \rho VA \tag{4}$$

Where $\dot{m}$ is mass flow rate, ρ is the fluid density, V is the fluid velocity, and A is the area of the control surface the fluid is flowing thru. Based on the directions of the fluid flowing in the differential element and a Taylor series expansion, as shown in Figure 9, it can be shown that in each coordinate axial direction there is one control surface with positive flow of mass into the element, and one surface with a negative mass flow [61]. It can be noted that u, v, and w indicate the flow velocity in the respective x, y, and z directions independently on the element.

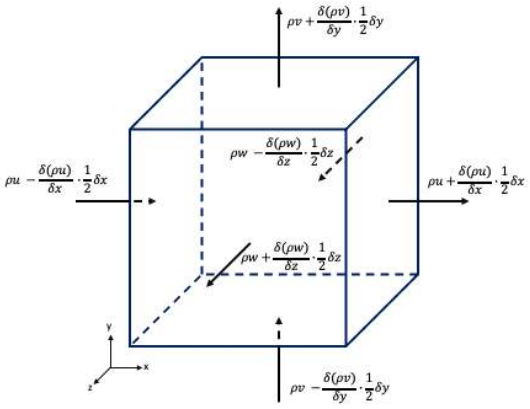

Figure 9. Differential element for the conservation of mass.

The net rate of mass transfer across the boundaries of the element can be calculated by multiplying the respective directional velocities by the differential areas of the surface, and subtracting the mass outflow from the mass inflow, resulting in the total mass transfer as shown in Equation 5.

$$\frac{\partial \rho}{\partial t} + \frac{\partial (\rho u)}{\partial x} + \frac{\partial (\rho v)}{\partial y} + \frac{\partial (\rho w)}{\partial z} = 0 \tag{5}$$

This generalize solution for the conservation of energy can be simplified based on several conditions of the fluid flow being considered. If the flow is steady, the time dependance of the solution can be removed, since $\frac{d}{dt} = 0$. Similarly, when a liquid is considered incompressible, that is the density is not variable across the domain, the density may be considered constant, so $\frac{d\rho}{dt} = 0$. Although no flow is completely incompressible, in most cases where low velocities of air (below Mach 0.3) or a liquid is being considered, it can be assumed the fluid is incompressible [61]. This results in the differential equation describing the conservation of mass to be,

$$\frac{\partial(u)}{\partial x} + \frac{\partial(v)}{\partial y} + \frac{\partial(w)}{\partial z} = 0 \tag{6}$$

as the density is constant across the domain being considered. This results in significantly less computational requirements for each iteration of the model solution.

4.2 Conservation of Momentum

The second principal governing equation of CFD is Newton's Second Law, or the conservation of momentum. The generalized equation indicated that across the differential element, momentum is conserved, as shown in Equation 7.

$$Sum\ of\ forces = Rate\ of\ momentum\ increase \tag{7}$$

Unlike the conservation of mass, momentum is a direction dependent equation, resulting in three governing equations, one in each principal direction respectively [61]. Therefore, considering the forces on each surface of the differential element, there is a stress component in each principal direction, as shown in Figure 10. Each face has one pressure component perpendicular to the face, and two viscous stresses parallel to the face.

The force on each of these surfaces is the product of the stress and the differential surface area. Therefore, each face has a force corresponding to each principal axial direction, as exemplified in Figure 11 for the x-direction stresses, where p denotes pressure. This results in the net sum of forces for the x-direction be described as in Equation 8 below:

$$\left[\left(\frac{\partial(-p+\tau_{xx})}{\partial x}\right)+\left(\frac{\partial(\tau_{yx})}{\partial y}\right)+\left(\frac{\partial(\tau_{zx})}{\partial z}\right)\right](dxdydz) = Sum\ of\ forces \quad (8)$$

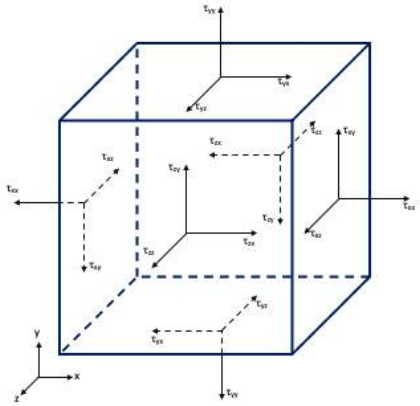

Figure 10. Stress components on differential element surfaces.

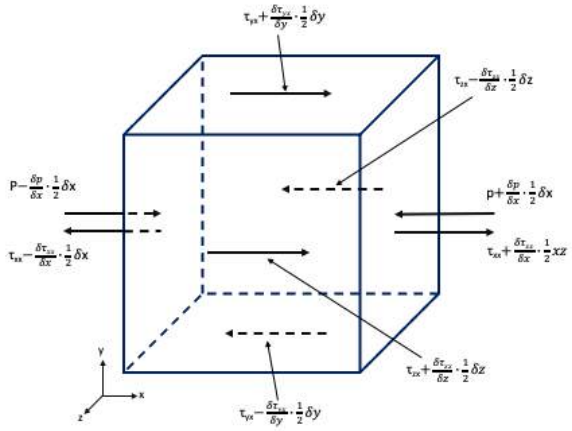

Figure 11. Stress components in the x-direction on differential element.

The y-direction and z-directions are similar, only varying where the pressure term is found in the equation with respect to the axis direction being considered. The rate of moment increase is found by considering each principal axis direction related to momentum being the product of mass and velocity,

$$\left[\frac{\partial(\rho u)}{\partial t}+\frac{\partial(\rho uu)}{\partial x}+\frac{\partial(\rho vu)}{\partial y}+\frac{\partial(\rho wu)}{\partial z}\right](dxdydz) = Rate\ of\ momentum\ increase \quad (9)$$

Therefore, the overall generalized governing equation for the x-direction would be as follows in Equation 10.

$$\left(\frac{\partial(-p+\tau_{xx})}{\partial x}\right)+\left(\frac{\partial(\tau_{yx})}{\partial y}\right)+\left(\frac{\partial(\tau_{zx})}{\partial z}\right)+S_{Mx}=\rho\frac{Du}{Dt} \quad (10)$$

Where S_M indicates body forces that act on the fluid, which would commonly include gravity and other forces such as centrifugal, electromagnetic, and Coriolis forces [61]. In a practical understanding, the right side of the equation accounts for all inertial forces, while the first component if the left side is the normal pressure, and the second and third component of the left side account for the shear forces on the differential element with respect to the x-direction. This can be transferred to y and z directions, resulting in two more equations as shown in Equation 11 and 12.

$$\left(\frac{\partial(\tau_{xy})}{\partial x}\right)+\left(\frac{\partial(-p+\tau_{yy})}{\partial y}\right)+\left(\frac{\partial(\tau_{zy})}{\partial z}\right)+S_{My}=\rho\frac{Dv}{Dt} \quad (11)$$

$$\left(\frac{\partial(\tau_{xz})}{\partial x}\right)+\left(\frac{\partial(\tau_{yz})}{\partial y}\right)+\left(\frac{\partial(-p+\tau_{zz})}{\partial z}\right)+S_{Mz}=\rho\frac{Dw}{Dt} \quad (12)$$

Several simplifications can be considered here too, based on knowing different fluid properties or making assumptions. First, if the flow is incompressible, $\frac{d\rho}{dt}=0$ again respectively. Similarly, if the flow is only two-dimensional, one principal direction will be assumed negligible. Lastly, if the flow is being considered as non-viscous, the shear components may be neglected as friction is the cause for the fluid element shear stresses [61].

4.3 Conservation of Energy

The final principal equation governing CFD is the First Law of Thermodynamics, or conservation of energy. General, this is defined as in Equation 13:

$$Rate\ of\ change\ of\ energy = Rate\ of\ heat\ added + Rate\ of\ work\ done \quad (13)$$

This general is a scalar equation, resulting in one more governing equation for the computational model. The result is composed of considering the rate of heat flux across each surface and work done on each surface. The result is a general energy equation, as follows in Equation 14.

$$\rho \frac{DE}{Dt} = \left[\left(\frac{\partial(u(-p+\tau_{xx}))}{\partial x}\right) + \left(\frac{\partial(u\tau_{yx})}{\partial y}\right) + \left(\frac{\partial(u\tau_{zx})}{\partial z}\right)\right] + \left[\left(\frac{\partial(v\tau_{xy})}{\partial x}\right) + \left(\frac{\partial\left(v(-p+\tau_{yy})\right)}{\partial y}\right) + \left(\frac{\partial(v\tau_{zy})}{\partial z}\right)\right] + \left[\left(\frac{\partial(w\tau_{xz})}{\partial x}\right) + \left(\frac{\partial(w\tau_{yz})}{\partial y}\right) + \left(\frac{\partial(w(-p+\tau_{zz}))}{\partial z}\right)\right] - \left[\left(\frac{\partial(q_x)}{\partial x}\right) + \left(\frac{\partial(q_y)}{\partial y}\right) + \left(\frac{\partial(q_z)}{\partial z}\right)\right] + S_E \quad (14)$$

Where E signifies energy, q is the heat flux in the given direction, and S_E is a heat source in the fluid element. This equation is a general form, that can be converted to be written in terms of temperature, enthalpy, internal energy, and kinetic energy [61].

This equation can be simplified by noting that if the fluid is frictionless, the shear stress terms will be zero. Also, in isothermal cases, there will be no heat flux across the element boundaries, resulting in the heat flux term being zero.

4.4 Porous Media

A porous medium is described as a medium whose volume is composed of a solid matrix of material with an interconnected void throughout the domain [62]. The main factor in the material is the porosity, or ratio of the void space to the total volume of the solid. A very important factor in porous media modeling, especially in medical CFD modeling, is the tortuosity, which is the resistance to diffusion of the flow by local parameters such as viscosity or boundaries [62]. This porous media modeling has been used as a means to understand and predict heat transfer in human tissue, as well as transport models around or within biologic tissue [33, 35-45, 62-64]. The utilization of porous media models has allowed for useful description of different biological functions and have been found to have an abundance of applicable areas in medical applications especially related to tissue regeneration and even drug transportation [62].

4.5 Navier-Stokes Equations

The previous equations do form a set of differential equations that could solve for fluid flow but fail to yield a solution for the viscous shear stress components. However, these viscous stress components can be related to the principal direction velocity components u, v, and w. Under

the assumptions that the fluid is isotropic and Newtonian, the Navier-Stokes equation can be applied down to a microscopic scale [61, 65]. The Navier-Stokes equation is defined as follows in the independent x, y, and z directions of the domain,

$$\rho\left(\frac{\partial u}{\partial t}+u\frac{\partial u}{\partial x}+v\frac{\partial u}{\partial y}+w\frac{\partial u}{\partial z}\right)=-\frac{\partial p}{\partial t}+\mu\left(\frac{\partial^2 u}{\partial x^2}+\frac{\partial^2 u}{\partial y^2}+\frac{\partial^2 u}{\partial z^2}\right)+S_{Mx} \tag{15}$$

$$\rho\left(\frac{\partial v}{\partial t}+u\frac{\partial v}{\partial x}+v\frac{\partial v}{\partial y}+w\frac{\partial v}{\partial z}\right)=-\frac{\partial p}{\partial t}+\mu\left(\frac{\partial^2 v}{\partial x^2}+\frac{\partial^2 v}{\partial y^2}+\frac{\partial^2 v}{\partial z^2}\right)+S_{My} \tag{16}$$

$$\rho\left(\frac{\partial w}{\partial t}+u\frac{\partial w}{\partial x}+v\frac{\partial w}{\partial y}+w\frac{\partial w}{\partial z}\right)=-\frac{\partial p}{\partial t}+\mu\left(\frac{\partial^2 w}{\partial x^2}+\frac{\partial^2 w}{\partial y^2}+\frac{\partial^2 w}{\partial z^2}\right)+S_{Mz} \tag{17}$$

Where μ is the dynamic viscous friction of the fluid, and in a steady state $\frac{\partial}{\partial t}=0$ and if there are no body forces such as gravity S_M is also zero. In considering porous media, the Reynolds number should be considered also, as with a small Reynolds number (Re <<1), the Navier-Stokes equation can be simplified to just the Stokes equation since the inertial forces are small compared to the viscous forces [28, 33, 42, 40, 62, 65, 66]. Therefore, the set of equations 15, 16, and 17 becomes

$$\frac{\partial p}{\partial t}=\mu\left(\frac{\partial^2 u}{\partial x^2}+\frac{\partial^2 u}{\partial y^2}+\frac{\partial^2 u}{\partial z^2}\right) \tag{18}$$

$$\frac{\partial p}{\partial t}=\mu\left(\frac{\partial^2 v}{\partial x^2}+\frac{\partial^2 v}{\partial y^2}+\frac{\partial^2 v}{\partial z^2}\right) \tag{19}$$

$$\frac{\partial p}{\partial t}=\mu\left(\frac{\partial^2 w}{\partial x^2}+\frac{\partial^2 w}{\partial y^2}+\frac{\partial^2 w}{\partial z^2}\right) \tag{20}$$

with the assumption there are also no body forces affecting the fluid flow as well.

4.6 Darcy's Law

In considering porous media, the Navier-Stokes equation can be applied to the flow inside the pores of the media but cannot be applied in a generalized form to the entire macroscopic media domain [66, 67]. Considering a steady state isothermal Newtonian fluid flow in a porous material

though, the governing equation called Darcy's law can be applied [28, 33, 42, 40, 62, 65-67]. Darcy's law indicates there is a linear proportionality between flow velocity and the applied pressure difference [62]. The model is expressed by:

$$\frac{\partial p}{\partial x} = -\frac{\mu}{K}\bar{u} \tag{21}$$

Where K is the permeability of the porous medium or Darcy number, and $\bar{u}$ is the Darcy velocity (the fluid velocity average across the cross section) [62]. It can be noted Darcy's model can be obtained by simplification of the Navier-Stokes equation for a porous medium, or by starting with the Brinkman system in a porous medium with a very small Darcy number [28, 33, 42, 40, 65]. The Darcy model is therefore a good prediction when considering media with very low permeability and low Reynolds numbers.

4.7 Turbulence Modeling in Porous Media

Although turbulent flow in porous media is often present, and even in case a design factor in CFD studies, there is a significant lack of published literature in this area [68]. In order to understand what the turbulence in a porous material may look like, or even if there would be significant turbulence to be considered, the Reynolds number of the system must be established. The most generalized form of considering the Reynolds number in relation to turbulence in a porous media is known as the pore or particle Reynolds number defined as:

$$Re_P = \frac{\rho||\boldsymbol{U}||d_P}{\mu} \tag{23}$$

where Re_P is the pore Reynolds number, **U** is the intrinsic average velocity, and d_P is the average pore diameter (or be assumed the particle diameter) [68]. There is also a definition of the Reynolds number based upon the Darcy number, which is as follows:

$$Re_D = \frac{\rho||\boldsymbol{U}||\sqrt{K}}{\mu} \tag{24}$$

Where Re_D is the Darcy Reynolds number [68]. Due to the structure of porous media, and the small scale, different microscale flow field properties can be defined based on the estimated Reynolds numbers of the system. There are 5 major ranges that have been presented, as shown in Table 4 below.

Table 4. Different regimes of porous turbulence based on Reynolds number [68].

Regime	Reynolds Number Range
Darcy Regime	$Re_P < 25$, $Re_D < 10$
Inertial Regime	$25 < Re_P < 375$, $10 < Re_D < 150$
Unsteady Laminar (transitional) Regime	$375 < Re_P < 750$, $150 < Re_D < 300$
Turbulent Regime	$750 < Re_P < 3{,}400$, $300 < Re_D < 1{,}360$
Asymptotic Regime	$Re_P > 3{,}400$, $Re_D > 1{,}360$

Each regime has a different flow field associated with it but is quite qualitative based on rough Reynolds number criteria ranges. The Darcy regime can have the flow field approximated very well by Stokes flow with no significant turbulence. In the inertial regime, inertial effects of the fluid begin to appear, with very different velocity profiles compared to the Darcy regime with even some steady vortical structures having been observed in this range. Unsteady transitional flows are observed in the Unsteady Laminar regime, with periodic vortexes and even some exhibition of intermittency. The Turbulent regime is where the flow within pore spaces begins follow the characteristics of typical turbulent flows. Finally, in the Asymptotic regime, turbulence is able to be approximated as being isotropic over the majority of the pore volume [68].

4.8 Ergun Equation

Considering the adipose tissue could be considered a packed bed of adipocytes in this modeling case, giving rise the description of the flow of the fluid past the adipocyte in the domain by the Ergun equation. While Darcy's Law applies to creeping flows, as would be observed in adipose interstitial fluid that has a Reynolds number much smaller than 1, as previous research has mentioned, the relationship between the pressure gradient and flow velocity becomes much more nonlinear as flow velocity increases [28, 35, 40-45]. This would apply to the area around the

injection site in adipose drug delivery, as the drug would have a much higher velocity while being delivered than the interstitial fluid. To account for this change, Dupuit and Forchheimer proposed the addition of a quadratic term known as the Forchheimer, as shown by Equation 25 [69].

$$-\nabla p = \frac{\mu}{K}\bar{u} + b\rho|\bar{u}|\bar{u} \tag{25}$$

Where ∇p is pressure differential and b is a factor dependent upon the particular flow and medium (normally determined through experimentation) [69]. The Ergun equation is a specific example of this Forchheimer equation, which is an empirical model to describe the pressure drop over a length of the domain through a packed bed [70]. This is described as shown in equation 26:

$$-\frac{\nabla p}{L} = P_v + P_i = \frac{150\mu(1-\alpha)^2\bar{u}}{\alpha^3 d_p^2} + \frac{1.75\rho(1-\alpha)\bar{u}^2}{\alpha^3 d_p} \tag{26}$$

where P_v is the viscous term and P_i is the inertial term. Therefore, it can be scene comparing Equations 25 and 26 that the permeability and b factor can be described as follows:

$$\frac{1}{K} = \frac{150(1-\alpha)^2}{\alpha^3 d_p^2} \tag{27}$$

$$b = \frac{1.75(1-\alpha)}{\alpha^3 d_p} \tag{28}$$

Therefore, the use of the Ergun equation can be applied to the case of injecting insulin into the adipose tissue considering the relatively large velocity of the insulin entering the tissue compared to the interstitial fluid velocity as well as the adipocytes being constructed in the tissue similar to a packed bed.

5. Domain and CFD Model Development

The Domain and CFD models were developed using a combination of physical measurements, previous study principles and results, and justified assumptions based on known or published biological factors. The model was developed using first known values for parameters such as specific adipose tissue and capillary characteristics. The unknown or assumed parameters that may have an influence on the flow and results of the model were studied individually, to determine what would create the most accurate outcome based on previous studies as well as know kinetics of interstitial flow and insulin delivery. These developments and parameters are discussed in further detail in the following sections. The evolution of the presented CFD model took several iterations to compare results and refine the design as well as input parameters to accurately model the interstitial flow and deposition of insulin into the model.

5.1 Domain Modeling

The model domain was created using the SolidWorks 2018 software package. The first consideration required in the development of the model was determining of the domain size. The thickness of the adipose tissue sample domain would vary by the tissue thickness range being studied as discussed in the cases, but the length and width of the domain would remain the same for each simulation case. Based on the cannula designs and anatomical measurements with an infusion set inserted, it was determined that a domain size of 120 mm x 100 mm would be sufficiently large to give acceptable results in the simulation. Further validation of this would be that 120 mm was about ten times greater than the insulin deposit outreach overserved in previous research [26].

One of the most important factors in the domain size was keeping the domain large enough to reduce the chance for domain induced anomalies, but small enough that the micro-scale mesh could be refined enough and remain computationally feasible. The domain size of the adipose tissue sample was further refined by considering which shape domain resulted with expected interstitial flow. The three domain shapes considered were a rectangular domain 120 mm x 100 mm, a 120 mm square domain, and a round domain with a 120 mm diameter. Each of these domain shapes tested can be seen in Figure 12.

After running a simulation on each of the trial domains, as seen in Figures 13-15, it was able to be concluded that the round domain would be the selected choice for the CFD model being developed for interstitial fluid flow.

The first indicator of this was that compared to the rectangular domain, there was a higher mesh volume element to domain volume ratio, as the circular domain had a similar number of mesh elements to the rectangular domain, even though it had a 6% decrease in volume compared to the rectangular domain. The square domain on the other hand had a 16% increase in mesh volume elements, which would be expected as the volume of the square domain was 20% larger than that of the rectangular domain. Therefore, the round domain could be said to have the most efficient use of resources based on volume elements, which was a major factor in the design of the model.

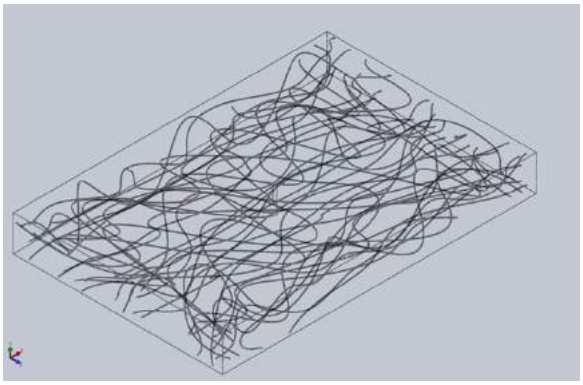

(a)

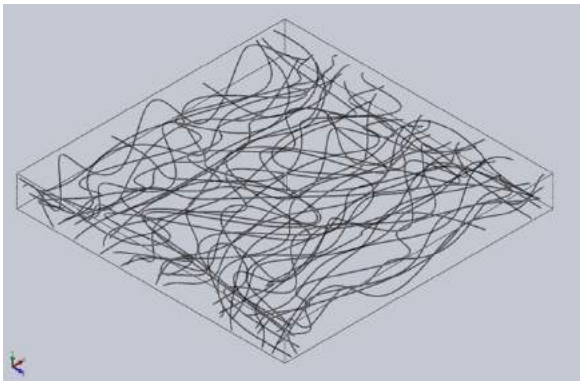

(b)

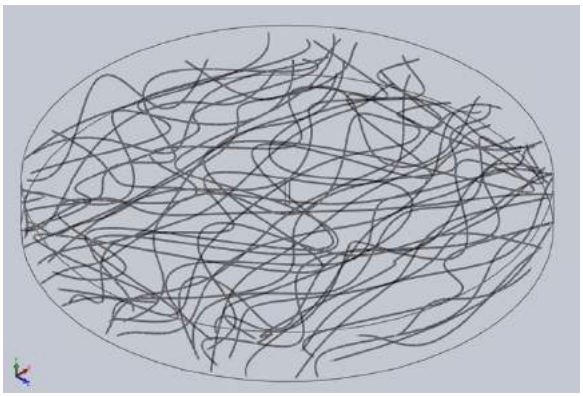

(c)

Figure 12. Three tissue domains tested for interstitial adipose fluid flow. (a) 120 mm x 80 mm rectangular domain (b) 120 mm square domain (c) 120 mm diameter round domain.

Secondly, there was no noticeable change in fluid flow between the domain shape options, as shown by the velocity profiles in Figures 13-15.

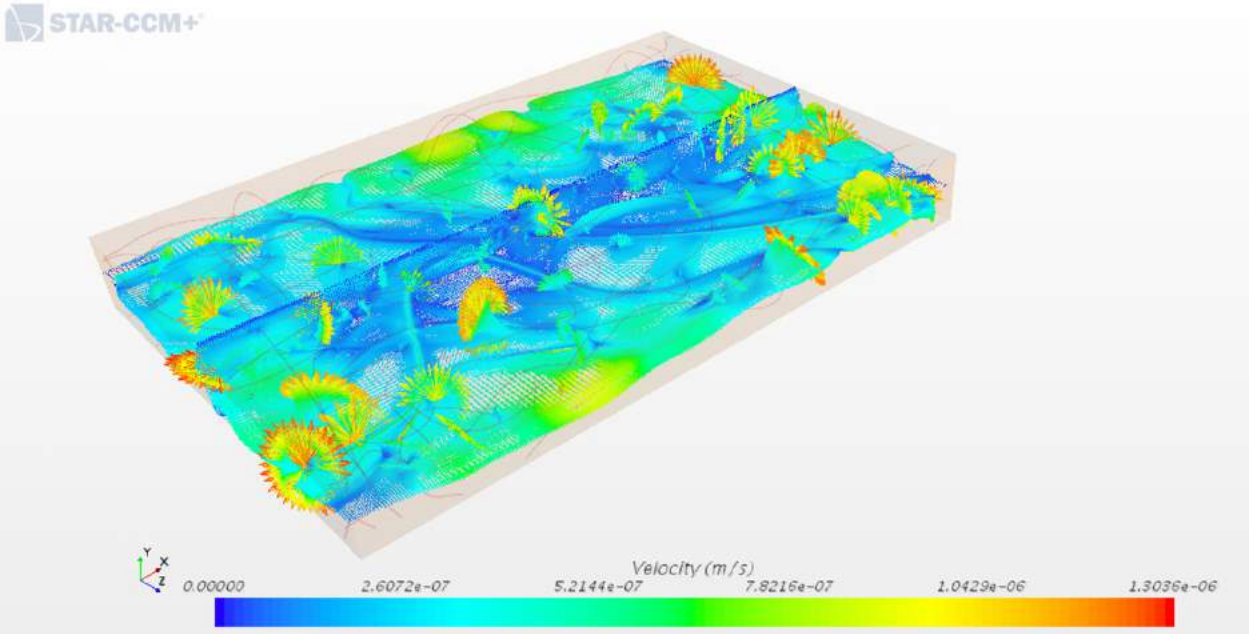

Figure 13. Adipose fluid flow trial with 120mm x 100 mm rectangular domain.

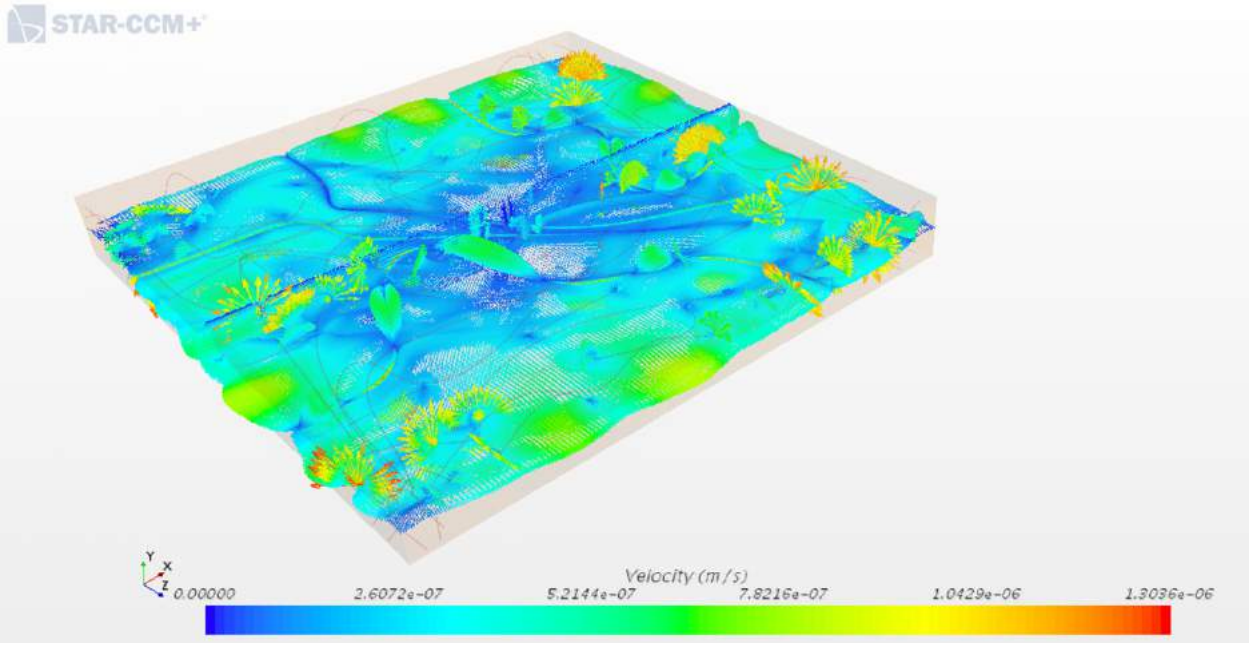

Figure 14. Adipose fluid flow trial with 120mm square domain.

It can be noted the only major difference observed was between the round domain and the two other domains, which was the stagnant area of flow in the corners of the flat side domains.

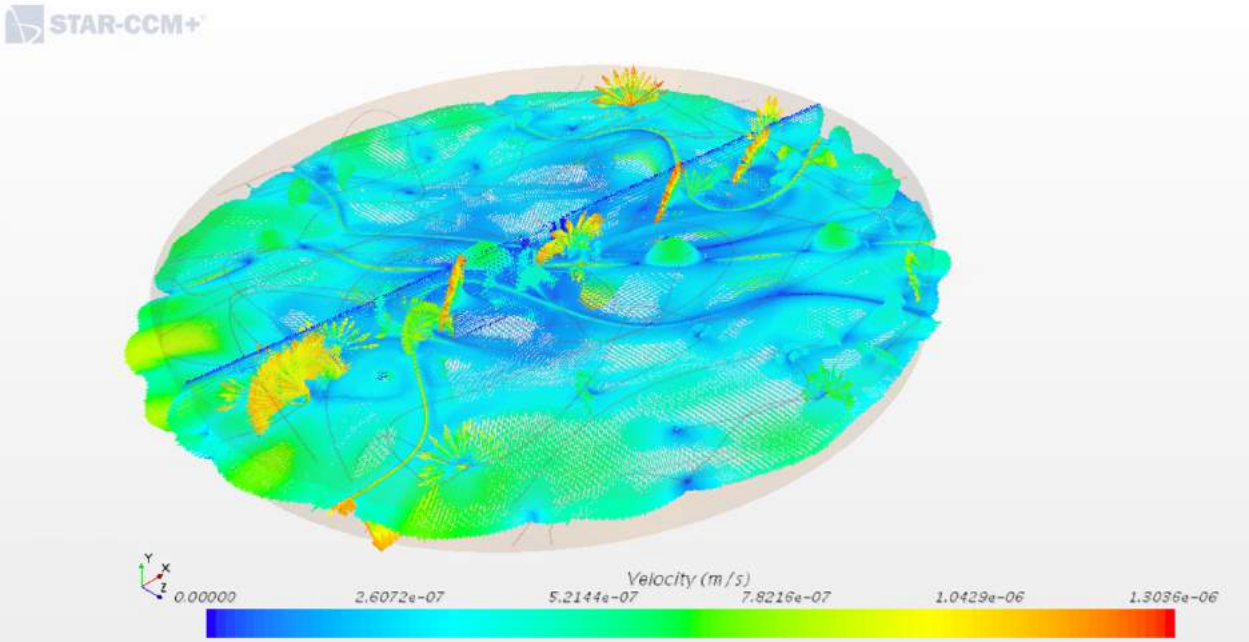

Figure 15. Adipose fluid flow trial with 120mm diameter round domain.

This would be expected due to the characteristic of fluid flowing out of a corner of a domain but would not be necessary for the consideration of this study, and therefore could be considered an inefficient use of volume in the domain. Because of this, the round domain again can be said to be the more efficient domain shape for considering the interstitial fluid flow in adipose tissue and insulin deposition.

The other major consideration with the design of the adipose tissue domain was how the capillaries should be modeled to induce the interstitial fluid flow in the CFD model. The biggest difficulty was that the capillaries in the adipose tissue have a lumen diameter of 2-10 μm, which is extremely small to model in both the CAD and CFD environments [71, 72]. Also, along with the micro scale of the capillaries was unpredictable pattern of capillaries found in adipose tissue. Therefore, there were three options looked at for the model, the first being assuming the fluid flow was induced through the faces of the domain. This meant that a combination of the upper and lower surfaces of the modeled tissue sample (representing the lower layer of the dermis on the top and muscular bed on the bottom) and the side faces would be used as velocity inputs in the CFD

model to drive the flow through the porous media domain created. An example of what the fluid velocity pattern noted in the model domain with this type of interstitial flow induction can be seen in Figure 16.

The second and third options involved modeling the capillaries throughout the domain to drive the interstitial flow, represented as either a repeated pattern across the domain or a meandering path through the domain. After creating a volume mesh for several trial CFD models, a capillary lumen diameter of 0.25 mm was found to be the smallest diameter able to be meshed feasibly with the computational resources available, as later discussed in section 5.6 respectively. This lumen diameter is much greater than anatomically correct 5-10 μm diameter, but was concluded acceptable based upon the limited computation resources available and the variability that would be found in the vascularization of adipose tissue throughout the body [4, 51-53]. The second way to model the capillaries was geometrically repetitive across the domain, such as a lattice pattern going from one end of the model domain to the other as well as across from side to side, while inducing a flow from using the capillary walls as a velocity output. An example of this flow induction can be seen in Figure 17. The final option was to model the capillaries in a much more randomized manner across the domain, utilizing 3-dimensional splines, as is shown in Figure

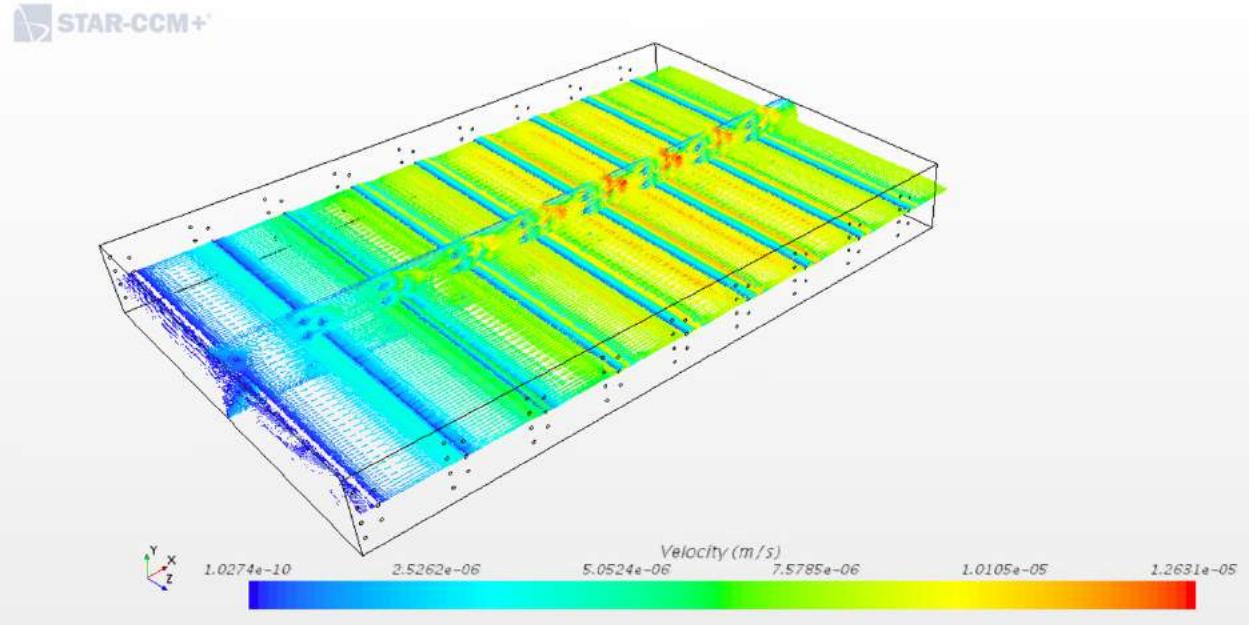

Figure 16. Capillary exchange induced interstitial flow from top and bottom faces.

18. Using 3-dimensional splines would be a much more anatomically correct representation of the capillaries found in adipose tissue, but much more time consuming and resource heavy to model.

The figures of the different capillary induced flow models show there was drastic differences noted between each type of capillary design simulated for the model. First, the flow induced from only the top and bottom face of the model developed such that as the flow moved through the domain, the flow in the central region across the domain increased in velocity as well as becoming more compact as it reached the outlet face.

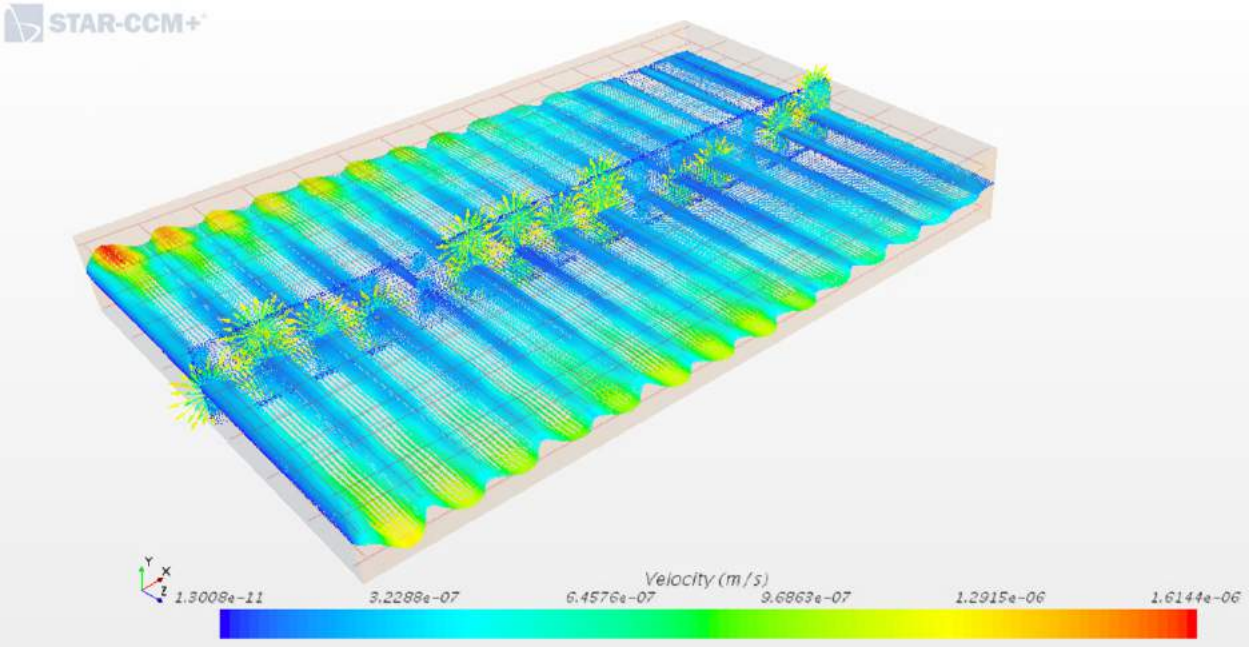

Figure 17. Lattice modeled capillary exchange induced interstitial flow.

It can be noted that the model was simulated with influx fluid velocity from the top and bottom faces only, with the side faces as symmetry planes and the rear face an outlet. This could be described as very similar to what would be seen in a pipe, with a boundary layer developing across the flow domain on the walls. However, this very developed boundary layer and pipe style flow would not be expected in a sample of adipose tissue with the interstitial fluid flow induced by capillaries running throughout the tissue. Also, there was about a ten times greater maximum velocity magnitude in the fluid flow than the other models trialed, which could likely be attributed to the large surface area acting as a fluid inlet. It was able to be concluded from this that inducing

the flow from faces on the domain, though computationally less taxing, was not the most accurate method to model the adipose tissue interstitial fluid flow.

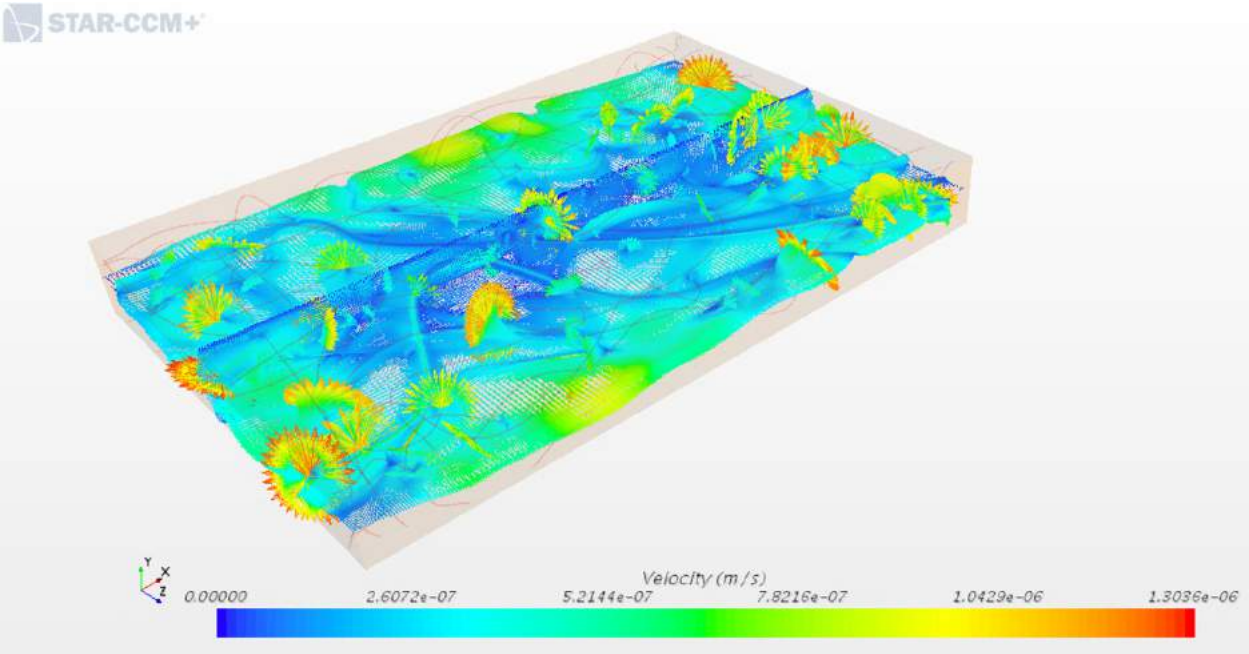

Figure 18. Spline modeled capillary exchange induced interstitial flow.

Considering the lattice hatched pattern model of the capillaries throughout the tissue domain, it can be seen there was a very geometrically symmetric flow induced by this type of design. The flow across the domain was very patterned based on the flow velocities coming out of the capillary walls across the model. This was much closer to what would be expected based on prior published studies as well as adipose tissue characteristics compared to flow being induced from the top and bottom of the tissue domain. The flow was much too patterned throughout the domain though to be the most accurate representation achievable in a model of adipose tissue fluid flow.

Therefore, the selected representation of modeling the capillaries in the adipose tissue for the presented CFD model would be using 3-dimensional splines. Although computationally splines are much more computationally costly, it can be seen in Figure 18 that the flow pattern induced by the capillaries being modeled as splines produces a much less repetitive flow development throughout in the tissue domain. Using 3-dimensional spline creates a much closer representation of what tissue studies have revealed the pattern of vascularization in the adipose region

anatomically looks like [4, 51, 52]. Further, the flow developed across the domain as was described to develop on a smaller scale by previous studies of interstitial fluid flow within subcutaneous tissues [42, 73]. For these reasons, the 3-dimensional spline representation of the capillaries was selected for the representation of the capillaries in the developed CFD model.

Using these previously discussed sizing and capillary criteria, the five tissue domains to be used in each of the case sets designed was created. These domains for each respective tissue thickness are shown in Figure 19.

The domains were generated in a manner to reduce the chance for a difference in the capillaries in each of the domains to greatly affect the results of the CFD simulations between the different tissue thickness domains. This was done by creating 35 capillaries of 0.25 mm in diameter that were non-intersecting and well distributed within the 6 mm adipose tissue domain. The 12 mm tissue domain was then created from this 6 mm domain by extruding an extra 6 mm of thickness onto the domain. The existing capillaries were then geometrically repositioned in the new 12 mm domain to be roughly equally distributed in the domain depth again. There were three more capillaries added to reach a better distribution through the tissue domain, resulting in the 12 mm, 18 mm, 24 mm, and 30 mm tissue domains a total of 38 capillaries distrusted in the adipose tissue model. This extrusion and redistribution process was repeated until the 18 mm, 24 mm, and 30 mm adipose tissue domains had been generated. Developing each adipose tissue domain in this manner greatly reduced the variability for flow differences due to drastically different capillarization patterns.

Using the above-described process to generate the tissue domains did allow for the capillarization pattern to remain very similar across the five tissue thicknesses, but it did also result in a reduction in capillary density in the tissue domain from the 6 mm tissue to the 30 mm tissue models. This phenomenon of a lower capillarization density in the thicker adipose tissue would be anatomically correct though, and therefore was assumed to be acceptable in this study [53]. Similarly, since the pattern in which adipose tissue is vascularized has not been well quantified and has been shown to be variable within and across individual patients, it could be assumed the generated capillary pattern for the domains would allow for viable results in this study [4, 51, 52].

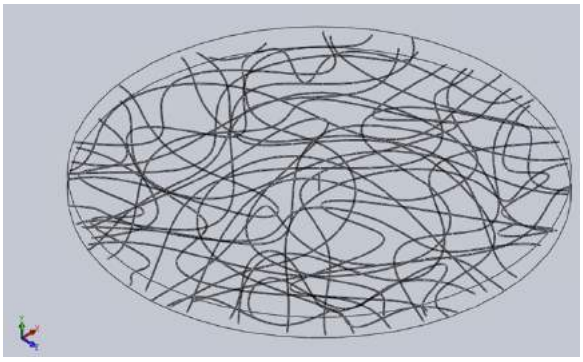

(a)

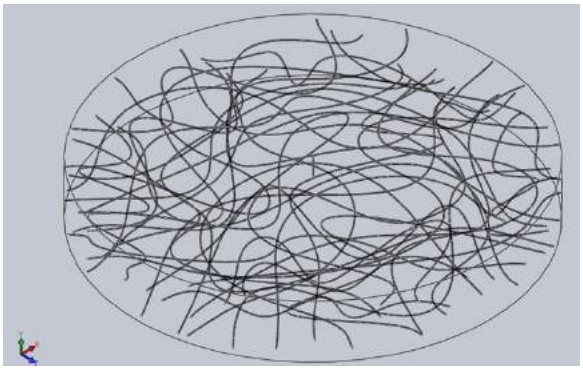

(c)

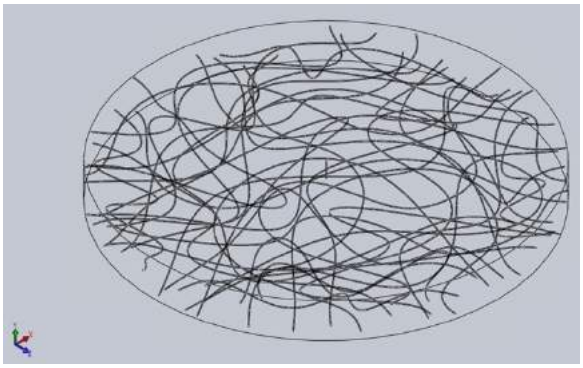

(b)

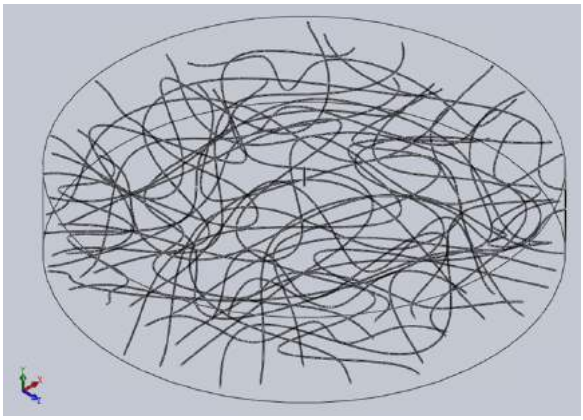

(d)

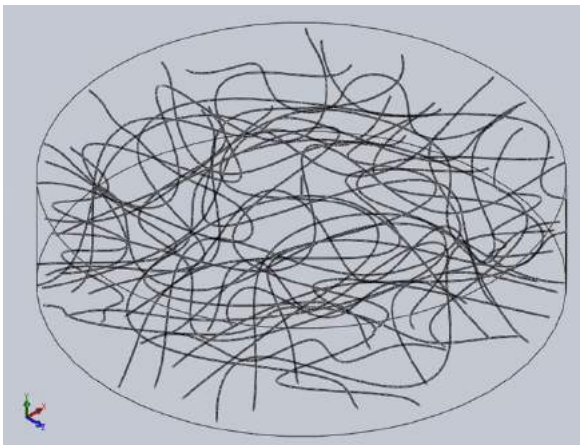

(e)

Figure 19. Adipose tissue domains with capillaries (a) 6 mm thick (b) 12 mm thick (c) 18 mm thick (d) 24 mm thick (e) 30 mm thick.

5.2 Capillary Exchange Driven Flow

One of the most critical components to the model is the interstitial flow through the tissue. This flow is driven from the exchange of fluid between the interstitial space and vascular and lymphatic capillaries, as previously discussed. Therefore, the flow direction and velocity through the tissue is directly driven by this exchange between the capillaries and interstitial space. In the model, this velocity could be simplified by considering the relationship between velocity, capillary permeability, and hydrostatic and osmotic pressures shown in Equation 29 [28, 33, 42]:

$$u_y = k_c[(p_c - p_i) - (\pi_c - \pi_i)] \tag{29}$$

Where u_y is flow velocity from capillary, k_c is capillary wall permeability, p_c is hydrostatic pressure in blood, p_i is hydrostatic pressure in interstitial fluid, π_c is osmotic pressure in blood, and π_i is osmotic pressure in interstitial fluid. The published properties to find the characteristic velocity of the flow coming out of the capillary at both the venule and arteriole side of the capillary are found in Table 5. Given these parameters, the characteristic output velocity range of fluid across the capillary wall can be calculated at the arteriole and venule ends of the capillaries in the tissue. This would be assuming the interstitial pressure is constant across the domain of the tissue, which considering the tissue sample is macro sized, the assumption of constant interstitial fluid can be stated to be valid.

Given equation 25 and the parameters of Table 5, the characteristic across capillary wall velocity range can be said to be 1.33 μm/s to -0.665 μm/s from the arteriole to venule ends of the capillary. It can be noted that although there are both venous capillaries and lymphatic capillaries in the adipose tissue, the physiological parameters of both are very similar, but a large difference in the fact that lymphatic capillaries only have an uptake of interstitial fluid [74, 75]. The lymphatic system only uptakes about ten percent of the fluid transferred between the vascular system and the interstitial space [76]. The lymphatic system would therefore have a significantly lower impact on the interstitial fluid flow. Therefore, the assumption was made for this study that the capillaries of the domain were all modeled to have venous capillary physiological and transfer properties.

The flow velocity from the capillaries into the adipose tissue can be assumed linear across the length of the capillary, as demonstrated in prior studies, being able to be described by Equations 30 and 31 [28, 33, 41, 42].

Table 5. Physiologic parameters of capillaries and fluids [33].

Parameter	Value
Permeability coefficient of capillary's wall ($k_c/(m^2 \bullet s \bullet kg^{-1})$)	5×10^{-10}
Plasma colloid osmotic pressure (π_c/kPa)	3.72
Interstitial fluid colloid osmotic pressure (π_i/kPa)	0.67
Pressure at the arteriole section of capillary (p_a/kPa)	5.32
Pressure at the venule section of capillary (p_v/kPa)	1.33
Hydrostatic pressure of interstitial fluid (p_i/kPa)	-0.40

$$u_y = u_0 - \frac{u_L}{L}x \tag{30}$$

$$u_L = u_0 + \frac{u_0 + |k_c[(p_v - p_i) - (\pi_c - \pi_i)]|}{L}x \tag{31}$$

Where u_0 is characteristic maximum velocity, u_L is velocity at x along the capillary, L is capillary length, and x is position length along capillary. This velocity profile was able to be used to drive the interstitial adipose tissue fluid flow in the model based on the position within the model domain. Since the capillaries were modeled to stretch the length of the domain, the capillary exchange velocity described was further modeled as a sinusoidal pattern for some of the capillaries in the model. This reduced velocity patterning noticed in early models where stagnation regions in the domain were created from assuming only the linearized exchange velocity profiles (as shown by Figure B-1 in Appendix B). The three resulting flow velocity magnitude curves based upon the length direction domain position used in the CFD model simulations can be seen in Figure 20 respectively. It can be seen that one linearized profile was created starting at the front of the domain and one at the back of the domain. The capillary exchange velocity profiles were also used to

described three additional capillary groups dependent upon the position across the domain rather than the length of the domain.

This flow pattern was also found to produce interstitial fluid flow velocities in the adipose tissue model domain consistent with those published be associated with interstitial flow, which would be in the range of 0.1-4.0 μm/s [35]. Therefore, it could be said that this velocity profile was adequate to induce a fluid flow in the porous media model that was within the range of what would be expected to be observed in the adipose region of tissue anatomically.

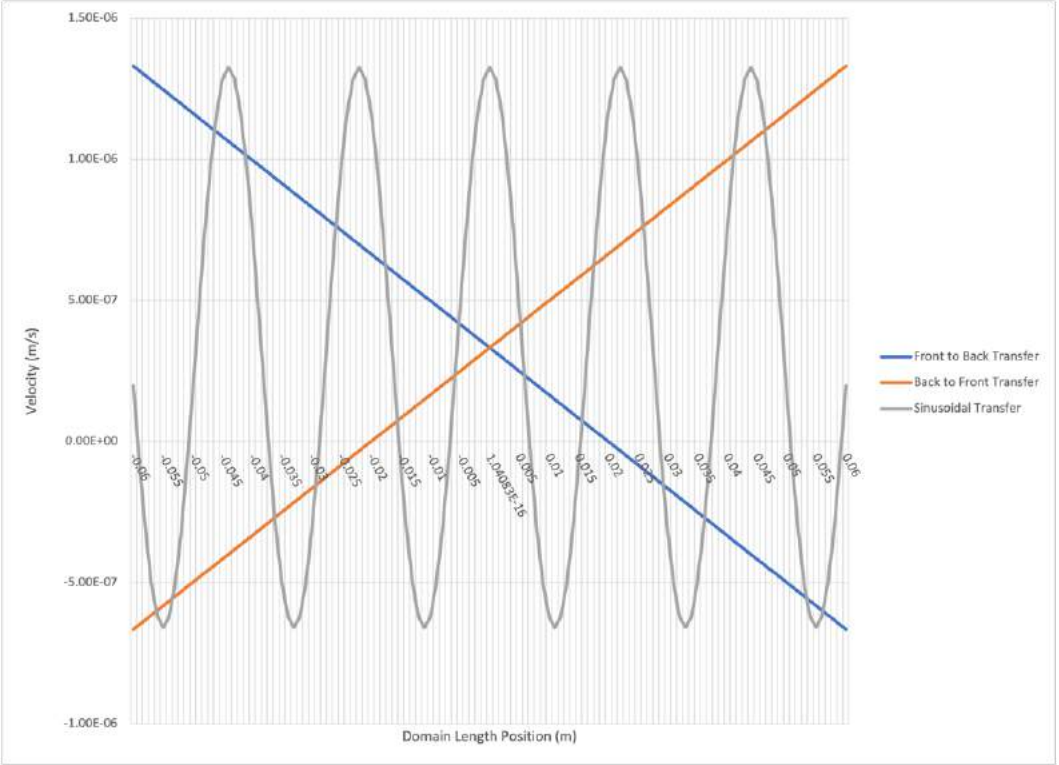

Figure 20. Capillary velocity output curves to generate interstitial flow in domain.

5.3 Model Parameters Identified

There were specific parameters that were able to be identified from previous publications or mathematical models needed for the generation of the presented CFD model. These can be found in Table 6 and Table 7 respectively. The major parameters needed pertain to the adipose tissue itself, and characteristics of interstitial fluid and insulin to fully define the domain for accurate flow simulation.

Table 6. Adipose tissue model parameters.

Parameter	Value
Porosity	0.2 [77]
Density (kg/m^3)	916.6 [78]
Specific Heat (J/kg-K)	2348 [79]
Thermal Conductivity (W/m-K)	0.21 [79]
Tortuosity	1.221
Interstitial Fluid Density (kg/m^3)	1000 [28, 30, 41, 42, 46]
Interstitial Fluid Viscosity (kg/m-s)	0.001 [46]

The porosity of the adipose tissue was one of the most important characteristics to identify, as the porosity of the tissue was the main component to creating the porous media domain, and the largest factor affecting the flow development. The tortuosity of the tissue was not able to be found as a readily available value, with ranges from 1.062 to 1.542, but using Equations 1 and 2 in conjunction with the porosity of the adipose tissue, a reasonable tortuosity was able to be determined [55, 57]. This calculation looks as follows, starting with Equation 2 to estimate the diffusion permeability:

$$\theta = \frac{2}{3-\alpha} = \frac{2}{3-0.02} = 0.67114 \tag{32}$$

And this diffusion permeability estimate can be used in Equation 1 to result in an estimation of the square tortuosity:

$$\lambda^2 = \frac{1}{\theta} = \frac{1}{0.67114} = 1.49 \tag{33}$$

Taking the square root of this results in the best estimate for the tortuosity of the tissue:

$$\lambda = \sqrt{\lambda^2} = \sqrt{1.49} = 1.221 \tag{34}$$

Therefore, the best estimation for the tortuosity of the presented porous media CFD model for adipose tissue interstitial fluid flow would be 1.221. This estimate does fall within the range of published values estimated in studies previously mentioned as well.

Table 7. Insulin model parameters.

Parameter	Value
Insulin Density (kg/m^3)	998.2 [46]
Insulin Viscosity (kg/m-s)	0.001 [46]
Insulin Mass Flow Rate (kg/s)	2.2125×10^{-7}

Both the given values for the interstitial and insulin densities shown are accurate to each of the respective fluids, but the assumption can be made that both interstitial fluid and the insulin drug being injected have the density of saline at 1000 kg/m^3. Interstitial fluid is composed almost entirely of water and sodium that permeated the capillary walls into the interstitial space with its solutes such as hormones, neurotransmitters, and glucose. Therefore, interstitial fluid was assumed to have the same density as saline, given it its composition. This assumption was also made in prior studies as well [28, 30, 41, 42, 46]. Similarly, the injected insulin drug is a composite of the insulin hormone dissolved into saline giving it near the same composition as interstitial fluid with only one hormone solute instead. Therefore, the assumption of the insulin drug solution having the density of saline was justified for the use in the model. This assumption was further able to be justified by the fact both interstitial fluid and insulin have negligible different in their fluid viscosity compared to saline.

For the use of simplifying the insulin delivery in the model, a unit conversion from the typically defined insulin delivery unit for infusion pumps of IU per minute was used to define the insulin delivery rate as a mass flow rate in the CFD domain instead. Therefore, the unit conversion from the previously define pump delivery rate of 1.5 IU/min for the case studies resulted in a mass flow rate from the cannula to the adipose tissue interstitium of 2.5125×10^{-7} kg/s of insulin. This full conversion of units can be seen in Appendix A.

A further assumption made about the adipose tissue was that it can be modeled as a bi-directional anisotropic medium. Although previously discussed, the arrangement of the adipocytes gives a very uniform geometry, adipose tissue has an extracellular matrix that is the connective

tissue giving the region its structure [5, 33, 41, 42, 54]. The region is geometrically very similar volume filled with spheres, but as shown by previous ex vivo research, the way insulin depots form during infusion follows channels that appear to form at the end of the cannula in the extracellular matrix parallel to the muscular and dermis boundaries. Therefore, although the adipose tissue region would have some isotropic properties, the assumption was made that the region had a combined porosity of 0.2, with respective porosities of 0.25 in the x-direction and z-direction and 0.15 in the y-direction of the model domain. This anisotropic assumption was previously show by Zedelmair to produce similar stagnant deposition results to that of previous ex vivo studies [25, 26, 46].

5.4 CFD Model Physics

The choices of the physics in the CFD software were very important to create an accurate simulation model for the tissue domain model created. The physics used to define the CFD model and domain are shown below in Figure 21. First in the physics parameters would be the assumption

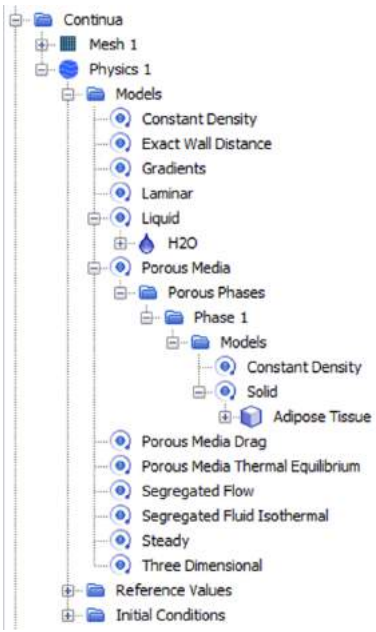

Figure 21. CFD model continua physics settings.

that the domain was all a constant density. Based on the previously discussed characteristics of adipose tissue as well as the assumption that the infusion set was placed in an ideal position anatomically, constant density in the model would be a valid assumption.

The next important physics parameter that had to be determined for the model was whether the flow needed to be modeled as turbulent or could be assumed to be a laminar flow. The previously published studies on CFD modeling of interstitial flow had all assumed laminar flow, but this assumption could also be proved by considering Equation 23 in relation to porous media models and turbulence [28, 30, 41, 42, 68]. The parameters necessary to solve the theoretical pore Reynolds number, Re_P, are already known for the fluid and tissue. This includes the interstitial fluid density (1000 kg/m^3), interstitial fluid viscosity (0.001 kg/m-s), and particle diameter, which would be 80 μm for the adipocytes in the adipose tissue [46, 80]. Therefore, the only parameter that was needed to solve the pore Reynolds number was the intrinsic average velocity, which could be found from simulating the model. This intrinsic average velocity was able to be found by looking at the average velocity of the fluid leaving the domain of the adipose tissue in the CFD model. The pore Reynolds number was found as follows:

$$Re_P = \frac{\rho||\boldsymbol{U}||d_P}{\mu} = \frac{\left(1000\,\frac{kg}{m^3}\right)(3.868059\times10^{-2}\ \text{m/s})(80\ \mu m)}{0.001\,\frac{kg}{m\cdot s}} = 3.094472 \tag{35}$$

Since this value of 3.09 is significantly lower than 25, that classifies the flow as being the Darcy regime, which indicates laminar flow. Therefore, the assumption of laminar flow was able to be justified further for the model by not only considering the assumptions of previous publications, but also considering the flow properties of the trial CFD models create [28, 33, 41, 42]. It can be noted that even if this calculation shown in Equation 30 was completed assuming the maximum velocity seen in the CFD model of 7.54×10^{-2} m/s, the resulting pore Reynolds number of 6.029 would still be within the Darcy regime as well.

Considering the liquid and porous media components of the physics in the CFD environment, the liquid was considered assumed to be water and the adipose tissue medium was created. The assumption of water for both the interstitial fluid and insulin was used based on the previously justified grounds. The adipose tissue medium was created for the porous region based on the identified characteristics of the tissue as presented in Table 5 above respectively. The domain was set to be a porous media domain, as well as be in thermal equilibrium. Thermal equilibrium could be assumed as both interstitial fluid, adipose tissue could be said to be body temperature. Similarly, since the insulin in the pump would be at room temperature, and since the

tubing between the pump and infusion set would likely be in direct contact with the body due to being routed between clothing and skin on the patient, the insulin could be assumed to be roughly the same temperature as the tissue and interstitial fluid.

The final several parts of the physics continua of the CFD domain were set based on many of the previously discussed properties of the model being designed. First, segregated flow could be assumed since the Mach number of the flow velocity was much lower than 0.2 as well as the model fluid being a liquid and therefore can be assumed incompressible. Similarly, segregated fluid isothermal could be used due to the temperature similarities between all the components of the model, the tissue, interstitial fluid and drug, as discussed previously. The model was set to steady in order to look at overall average trends in the flow structure of the interstitial tissue as well as insulin delivery. Though the model would be suitable to simulate time-dependent insulin, due to computation resources available, as well as the study being designed to compare the effect of cannula geometry and tissue thickness on the trends of insulin delivery, a steady state model was acceptable. Finally, the model should have a 3-dimensional flow, as the capillaries have been modeled as splines in a 3-dimensional domain representing the adipose tissue.

5.5 CFD Model Boundary Conditions

Considering the boundary conditions of the model, there were several different experimental simulations with various boundary conditions that were trialed during the domain shape development trials previously discussed during the development of the CAD model. It should be noted that throughout all the trials although the muscular and dermis layers bounding the top and to bottom of the adipose region were assumed to be solid boundaries even though anatomically, they as well as the adipose subspace are deformable tissues. These trials with various boundary conditions in different model domain shapes helped to develop the overall presented best domain design as well as boundary conditions, as further discussed in this section.

Initially, the boundary conditions were set up very basic in rectangular prism porous medium model, as shown in Table 8. The velocity of the inlet face on the domain was varied in the range of 7.5×10^{-7} m/s to 1.00×10^{-5} m/s in order to achieve a flow velocity through the domain on the within the published interstitial velocity range of 0.1 μm/s to 4.0 μm/s [35]. Also, it should be noted pressure outlet in STAR CCM+ works non-constraining boundary, allowing the domain to act as a sample of adipose tissue being considered within larger region of the tissue.

These conditions were set as an initial way to start working with the porous media block to be a baseline as the CFD model continued to develop. What was noted in these early simulation trials was that driving the flow from a one side to the other side of the domain with one outlet face induced a flow pattern as would be seen in a rectangular tube even considering the domain was a porous medium. A rather thick boundary layer developed on the top and bottom face representing the bottom of the dermis and muscular region respectively. A boundary layer would be expected here, as the interstitial fluid would be expected to flow within the adipose region easier due to the very low permeability of connective tissue between both the adipose tissue and the muscular bed below and dermis above the adipose tissue. The core of the flow in the rectangular prism section developed a high velocity between the boundary layers as would be expected in a rectangular pipe, and the flow direction was all parallel out the outlet side of the domain.

Table 8. Early boundary condition for a rectangular shape CFD model.

Domain Face	**Condition**
Front	Velocity Inlet
Sides	Symmetry Plane
Top and Bottom	Wall
Back	Pressure Outlet

What was observed in these early trials was that the fluid flow was very patterned as previously discussed due to the capillary design assumptions. Where this also played a part in the development of the boundary conditions was considering that the flow would not be expected to enter the dermis or muscular regions above and below the domain, but the entire region around the domain would be a continuation of the tissue. Since this continuation of the tissue would be anatomically present outside the model domain being considered, the outer face around the cylindrical tissue domain would be well suited as pressure outlet rather than constraining the interstitial fluid to exit just one side of a rectangular tissue domain.

Also, along the lines of having one pressure outlet not being ideal for the simulation, the sides being constrained as symmetry planes was not the most accurate choice for the CFD model. In considering the anatomic space being considered this also makes sense, as the flow in the body may have a net direction in the interstitial space, it would still be expected that the flow be able to

have a component in different directions, especially when nearing another capillary or cell that are exchanging fluid from the interstitium. Therefore, the boundary constraints that were selected for modeling this tissue sample of adipose tissue are as presented in Table 9.

Table 9. Adjusted boundary condition for adipose CFD model.

Domain Face	Condition
Front	Pressure Outlet
Sides	Pressure Outlet
Top and Bottom	Wall
Back	Pressure Outlet
Capillaries	Velocity Inlet

It could be noted that at this point in the CFD model development trials, it had been determined that the interstitial fluid flow in the tissue was best driven from the modeled faces of 3-dimensional spline capillaries as previously discuss in the domain modeling section. Following the conclusion these presented boundary conditions were a viable anatomical representation that could be achieved in the developed CFD model for fluid flowing in adipose tissue. The different shape domains and inlet velocity profiles were trialed as previously discussed with the boundary conditions shown in Table 10. As shown in Figure 22 below, the fluid flow in the tissue sample had exiting flow on every face, with general trends due to localized capillary flow, which would be expected in this macro scale flow due to the porous media as well as the capillary outlet and inlet of fluid [68, 80, 81].

Considering these noted justifications for the boundary conditions after trialing several different combinations for the developed CFD model, the finalized set of selected boundary conditions for the model are found in Table 9. These boundary conditions are stated in conjunction with the round geometry for the domain previously discussed as the best choice for domain shape. It can be noted there are six capillary groups in the table, each of which would have a different fluid velocity inlet profile as previously discussed.

The first would have a linearized profile described by the maximum characteristic inlet velocity induced by the osmotic pressure interface of 1.33 μm/s being at the front of the model domain, and the second being the opposite with the minimum characteristic inlet velocity induced

by the osmotic pressure interface of -0.665 μm/s being at the front of the model domain. The third capillary group would have a sinusoidal fluid velocity inlet pattern as shown in Figure 20. The fourth, fifth, and sixth capillary groups mirrored the prior three groups, only differing in their dependent being the width dimension rather than length.

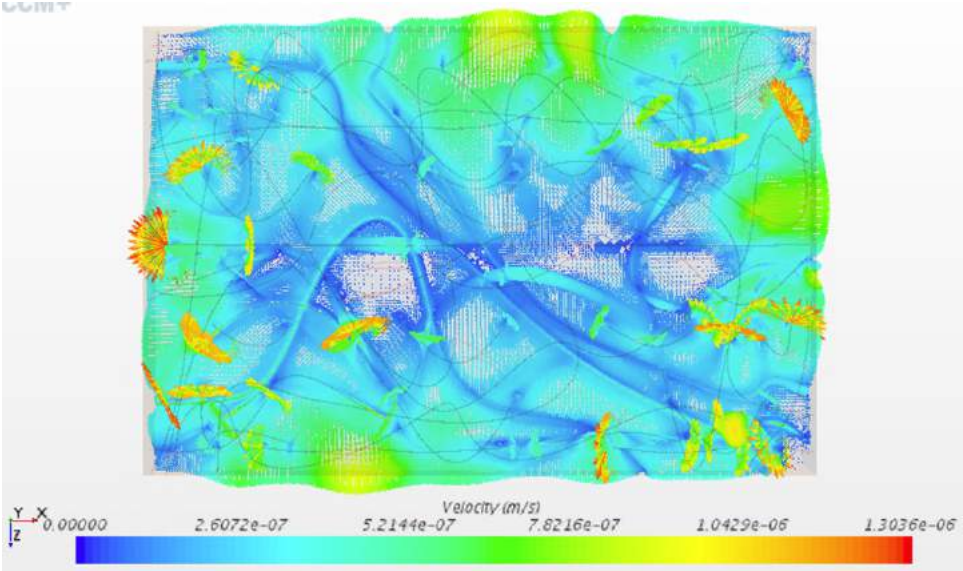

Figure 22. Adipose fluid flow trial with 120mm x 100 mm rectangular domain with all x and z axis sides as pressure outlets.

Table 10. Finalized boundary condition for adipose CFD model.

Domain Face	**Condition**
Outer Face	Pressure Outlet
Top and Bottom	Wall
Capillary Group #1	Linearized X-direction Velocity Inlet (Forward)
Capillary Group #2	Linearized X-direction Velocity Inlet (Backward)
Capillary Group #3	Sinusoidal X-direction Velocity Inlet
Capillary Group #4	Linearized Z-direction Velocity Inlet (Left)
Capillary Group #5	Linearized Z-direction Velocity Inlet (Right)
Capillary Group #6	Sinusoidal Z-direction Velocity Inlet
Cannula Outlet Face	Mass Flow Inlet (average velocity inlet)
Cannula Wall	Wall

These boundary conditions can further be identified in the CFD model domain as shown in Figure 23. It should be noted that the capillary groupings were randomly ordered while making the adipose tissue domain models and selected when creating the CFD model. This was done to keep any geometric or patterned anomalies that might affect the fluid flow to a minimum. The capillary groups were uniform between each different tissue thickness domain in the CFD simulation to reduce insulin flow anomalies due to varied interstitial fluid flow between the domains. It should be noted the cannula outlet was modeled as mass flow inlet into the adipose region, which was averaged across the surface and does not account for flow development in the tube between the pump and cannula prior to infusion into the tissue. This was assumed to be a negligible consideration in this study though since the current pumps on the market utilize an incremental delivery approach. This means that the insulin is stepped through the tubing over the course of the insulin bolus, without fully developing a characteristic tube flow pattern in the tubing or cannula that would be seen if it were a continuous flow delivery. Using these boundary conditions resulted in the fluid flow demonstrated in Figure 15 previously shown in section 5.1.

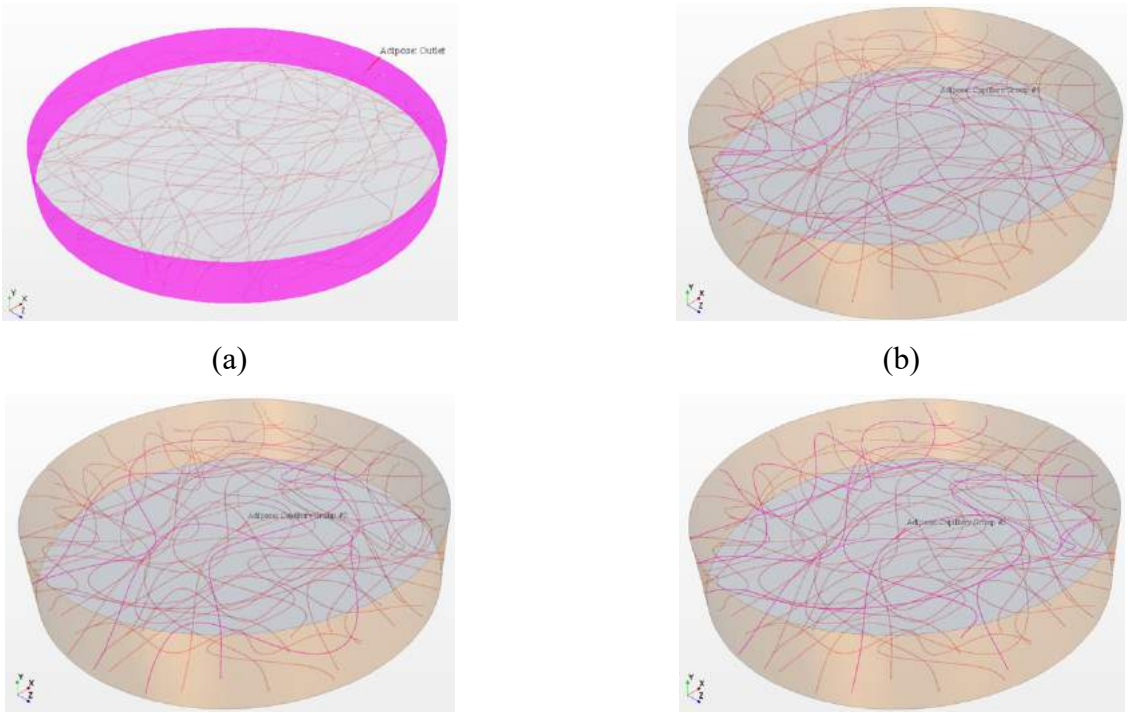

(a) (b)

(c) (d)

Figure 23. Boundary conditions in CFD domain of adipose tissue model with cannula (a) outer face (b) capillary group #1 (c) capillary group #2 (d) capillary group #3.

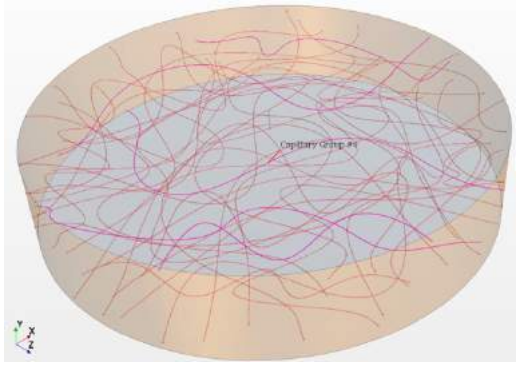

(e)

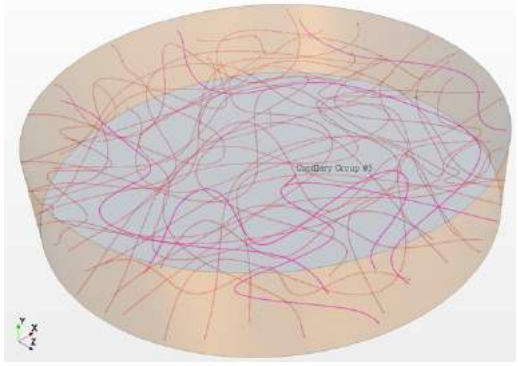

(f)

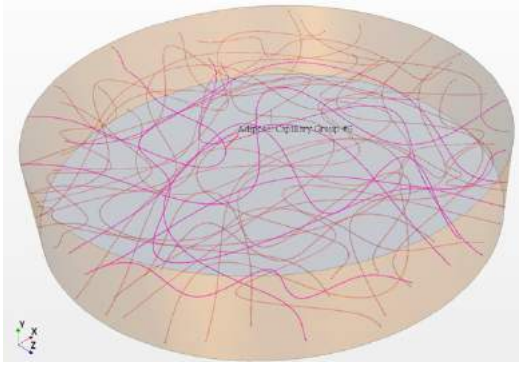

(g)

(h)

(i)

(j)

Figure 23 cont. Boundary conditions in CFD domain of adipose tissue model with cannula (e) capillary group #4 (f) capillary group #5 (g) capillary group #6 (h) cannula outlet (i) cannula wall (j) top and bottom.

A further component within the consideration of the model boundary parameters was applying the anisotropic porosity condition. The overall model porosity was set at 0.2, but the anisotropic component was incorporated using the application of the Ergun equation, using Equations 27 and 28 for the respective inertial and viscous conditions. Therefore, when the viscous

and inertial terms of the Ergun equation were utilized in the models, two field functions in the Star CCM+ software were created for both the viscous and inertial terms. One function to be applied in the x and z principal tensor directions with a porosity of 0.25, one function to be applied in the y principal tensor direction with a porosity of 0.15. This allowed for the incorporation of the anisotropic conditions that have been previously published regarding the insulin delivery environment, especially around the end of the cannula [26, 47].

5.6 CFD Model Mesh

Following the creation of the fluid domain in CAD software, it was transferred into the CFD package, and meshed using the models found in Table 11. The surface remesher model was able to be used since the CAD domain generated was designed with no intersection surfaces or other difficult geometric features that would not mesh well. Prism layers were also necessary to have as a mesh model, since the muscular and dermis face in the model would act as a wall, and therefore there would be a boundary layer developed on each in the model. Prism layers would be needed to capture this detail near to these faces. The trimmer model was not as apparent as the other mesh models given that computational limitations played a large factor in the mesh optimization of the developed CFD model. This therefore required some more meshing trials of the domain to reach the conclusion that the trimmer model was the best selection to create a mesh for the adipose tissue domain model.

Table 11. Mesh models for the CFD model.

Mesh Models
Surface remesher
Prism layer mesher
Trimmer

In starting to understand the meshing trials, it must first be mentioned that the maximum volume element count that was found to effectively run with the computational power available was twenty-million elements. Any larger mesh than this would take significantly more time to run, cause server errors, and did not significantly improve the residual error of the models being trialed. The approach therefore to determining whether the tetrahedral, polyhedral, or trimmer mesh model

was the best for the model was based around comparing the generated volume meshes by appearance as well as the number of volume elements within the mesh. This comparison was used since the micro sized features in the presented model require a fine mesh refinement, but based on the computational resources available, the volume mesh cannot surpass about twenty-million volume elements. It can be seen in Figures 24 to 26 what the results for each of these meshes was in the proposed adipose tissue CFD fluid flow model.

The meshes all shown in Figures 24 to 26 have very similar mesh densities, but there are very big differences in the meshes themselves. Using the tetrahedral mesh model, the overall mesh density of the model looked good, but when inspecting the area around the capillaries, the mesh was not acceptable as the capillary diameter was not round but rather a polygon shape due to not enough fine mesh detail in that area. Further contributing to this, the volume mesh generated had 230-million volume elements, which was ten times more than the finest mesh found to run with resources available. This volume mesh element count was after a redistribution of the mesh was attempted to reduce the mesh element number as well as gain even better mesh density around the

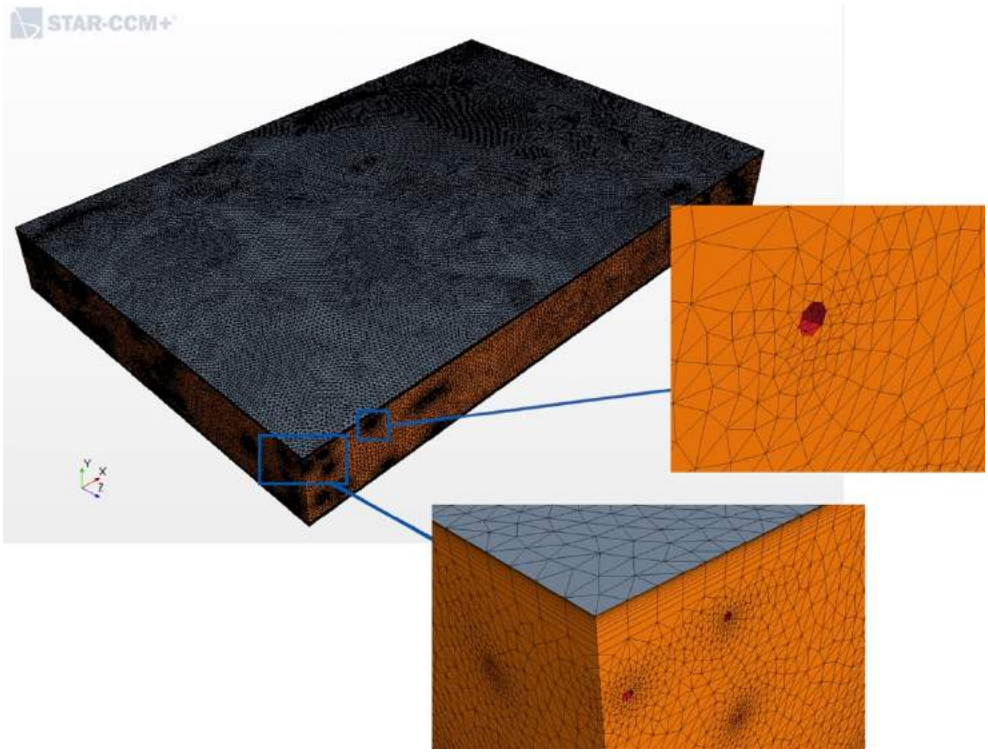

Figure 24. Volume mesh generated using the tetrahedral mesh model on the tissue domain.

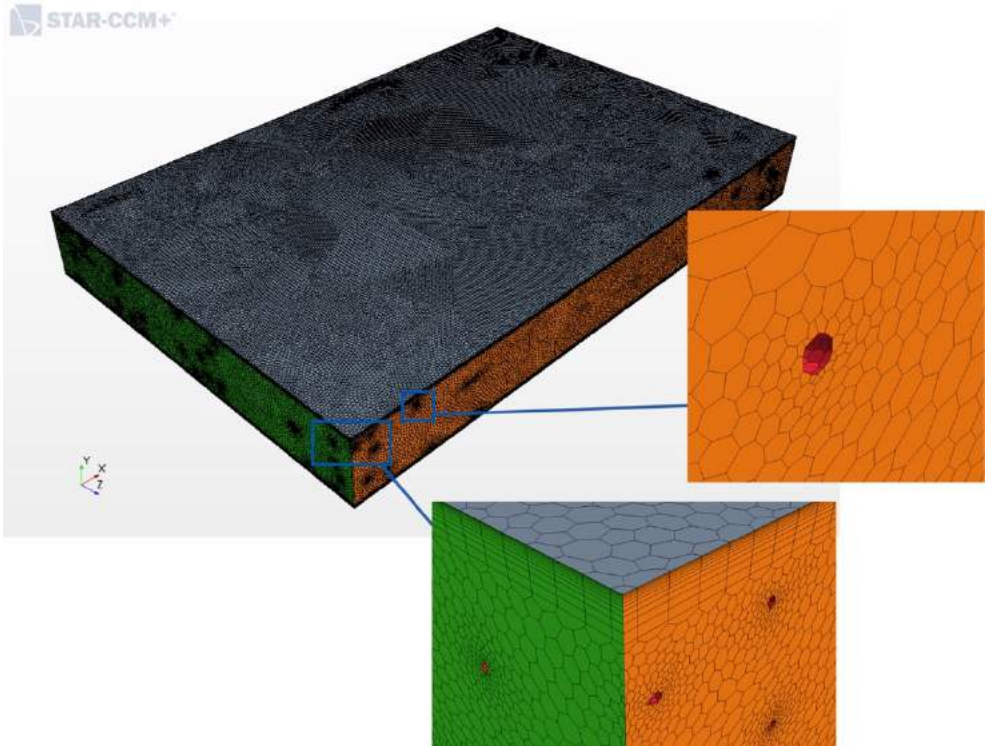

Figure 25. Volume mesh generated using the polyhedral mesh model on the tissue domain.

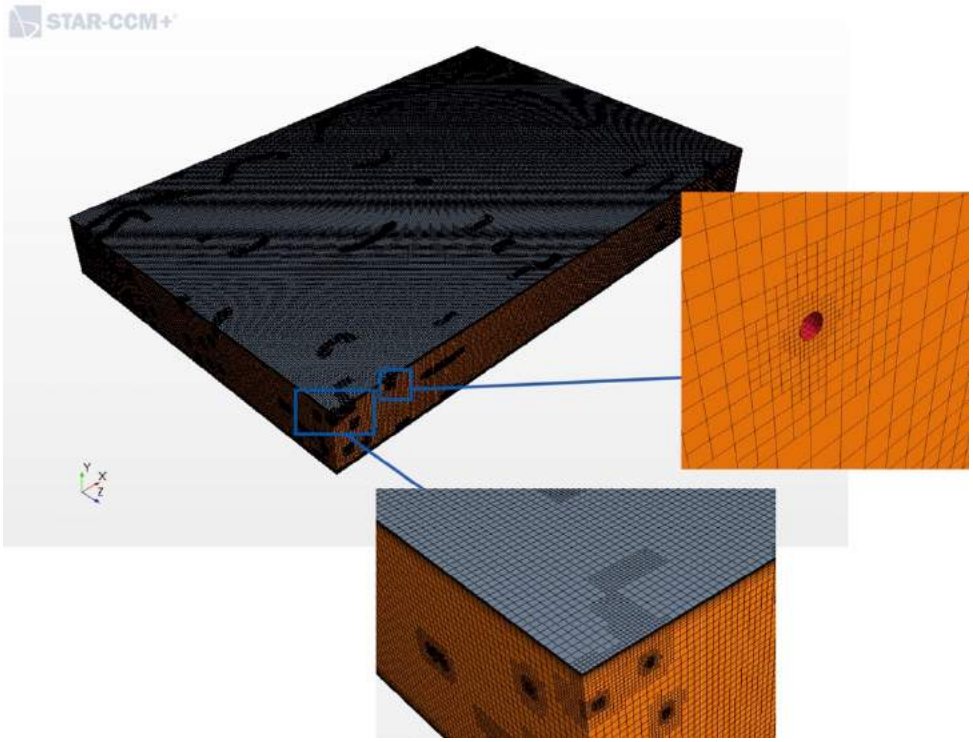

Figure 26. Volume mesh generated using the trimmer mesh model on the tissue domain.

capillaries. The polyhedral mesh model produced similar results to the tetrahedral mesh. The mesh density looked good on the overall domain, but the mesh size around the capillaries left a polygon shaped capillary rather than a round capillary shape. An attempt to redistribute this mesh was also made, but the new mesh still generated a forty-million volume element mesh, which was two times larger than was found able to run with the computational resources available. The trimmer model on the other hand generated a volume mesh that was around twenty-million volume elements when refined. Further, as shown in Figure 26, the capillary was a round shape with a very good mesh density and growth rate spreading out from the capillary. This made the trimmer meshing model the most efficient choice for the presented CFD model.

Therefore, based on the trimmer model being used on the proposed CFD model domain, the settings identified for use in the CFD model are shown in Table 12. As previously mentioned, these settings were identified based on knowing the computational power limits available and using that to distribute the mesh as best as possible to areas of most interest for the developed CFD models. This included around the capillaries and the end of the infusion set cannula. An addition feature to the mesh was created to further improve the resolution of flow around the end of the cannula which was a volume meshing constraint. A cylinder was created in each CFD simulation

Table 12. Mesh parameters for the CFD model.

Parameter	**Value**
Base Size (m)	0.1
Maximum Cell Size (% Base)	15.0
Number of Prism Layers	12
Prism Layer Stretching	1.4
Prism Layer Thickness (% Base)	0.375
Surface Curvature (#pts/circle)	100
Surface Growth Rate	1.3
Relative Minimum Size (% Base)	0.0325
Relative Target Size (% Base)	0.4
Template Growth Rate	Medium

domain with its length axis was parallel to cannula axis, with a length of 3 mm in each direction and a diameter of 6 mm, which was based on the rough size of the insulin depot in preliminary trials of the domain. This volume was then refined to have a mesh size of 0.0325% relative to the base size within its entire volume. The parameters described together generated meshes for the case simulations previously described with the characteristic ranges as shown in Table 13. Further, visual examples of the mesh details for one domain can be found in Figures 27 to 30.

Table 13. Mesh element ranges across the CFD simulation adipose tissue domains.

Parameter	Value
Minimum Vertices	22,712,356
Maximum Vertices	31,961,398
Minimum Face Elements	60,375,690
Maximum Face Elements	85,544,570
Minimum Volume Elements	19,697,903
Maximum Volume Elements	27,769,262

It can be seen in Figure 27 that the surface mesh shows very good resolution of the round capillaries as well as the cannula. This can also be seen in Figure 28 where the volume mesh generated can be seen. The volume mesh growth rate shown is acceptable given the computational power available and refinement of the mesh needed around the small feature capillaries and cannula in the domain. Figure 29 also shows the volume mesh was acceptable for the model on the inner faces as well looking at the overall mesh growth as well as the details. It can be seen the mesh was very refined around both the capillaries throughout the entire domain as well as around the cannula. The mesh settings presented could be concluded to generate a mesh acceptable for both the computational power available as well as the detail needed for the given model to study the insulin deposition and dispersion related to cannula geometry and tissue thickness.

Further, the mesh resulted in acceptable error residuals and convergence, such as shown Appendix C for each of the case simulations. The residuals for each of the cases was well below the acceptable convergence values of in the range of 10^{-3} to 10^{-4} for complicated CFD scenarios [61, 82]. The case models all converged on the order of 10^{-5} or lower. The convergence of each of the case models also was a very smooth curve, apart from a few models with some residual

bouncing observed during convergence. The residual errors and convergence observed was very good considering the micro scale of the flow model as well as the meshing limitations based on computational capacity.

Also, the mesh was developed using mesh sensitivity analysis methods. It was found from different meshing parameters with the deposition size measured in the model simulations. It was found at the mesh model size presented; the mesh had become an independent factor in the simulations. This was shown by increasing and decreasing the mesh by an overall size of 5% in a trial simulation case and observing that the insulin deposition size simulated did not significantly change. This indicated that the mesh was not a factor impacting the results of the cases, and therefore the was not of significant impact in the study. Further, this was shown by also considering factors such as the velocities vectors and gradients observed across the domain as well. There was not an observable difference in each of these results between the different mesh cases, indicating the mesh was an independent factor within the study cases.

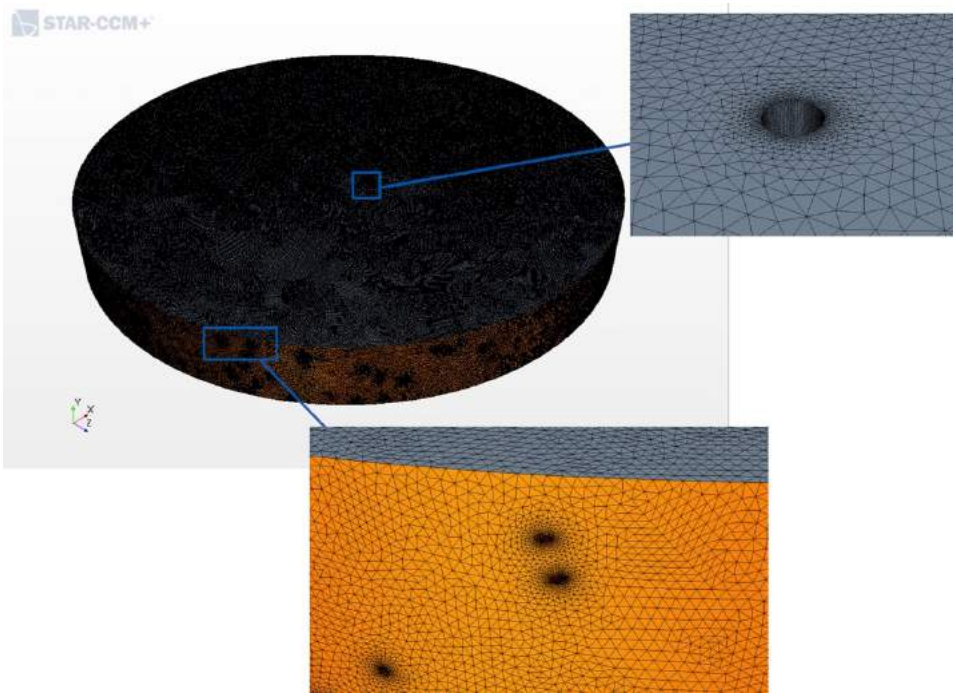

Figure 27. Surface mesh on round adipose domain using presented mesh settings.

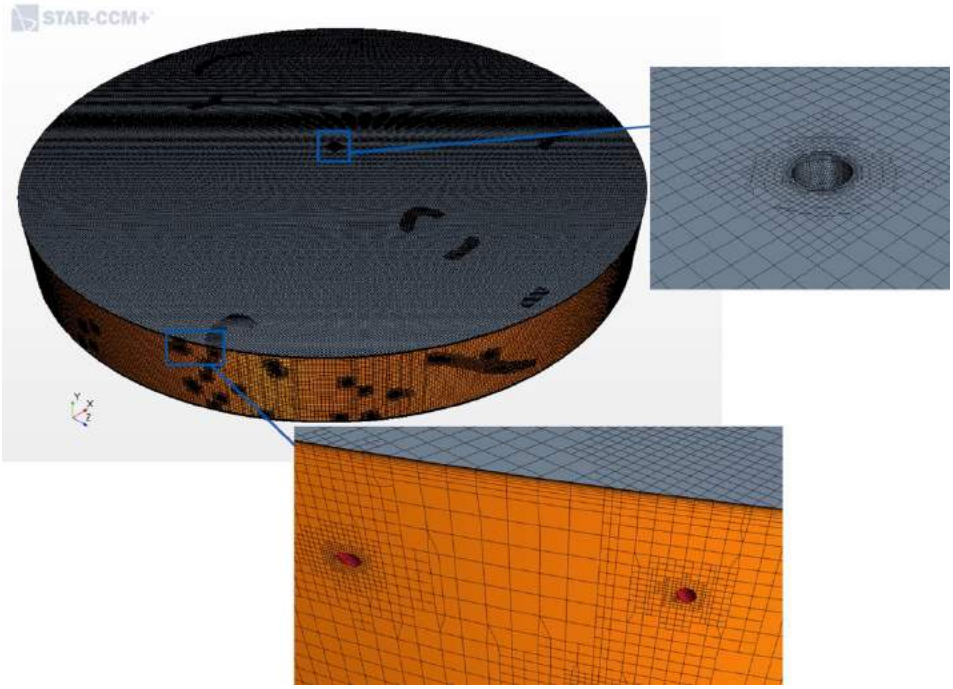

Figure 28. Volume mesh on perimeter of round adipose domain using presented mesh settings.

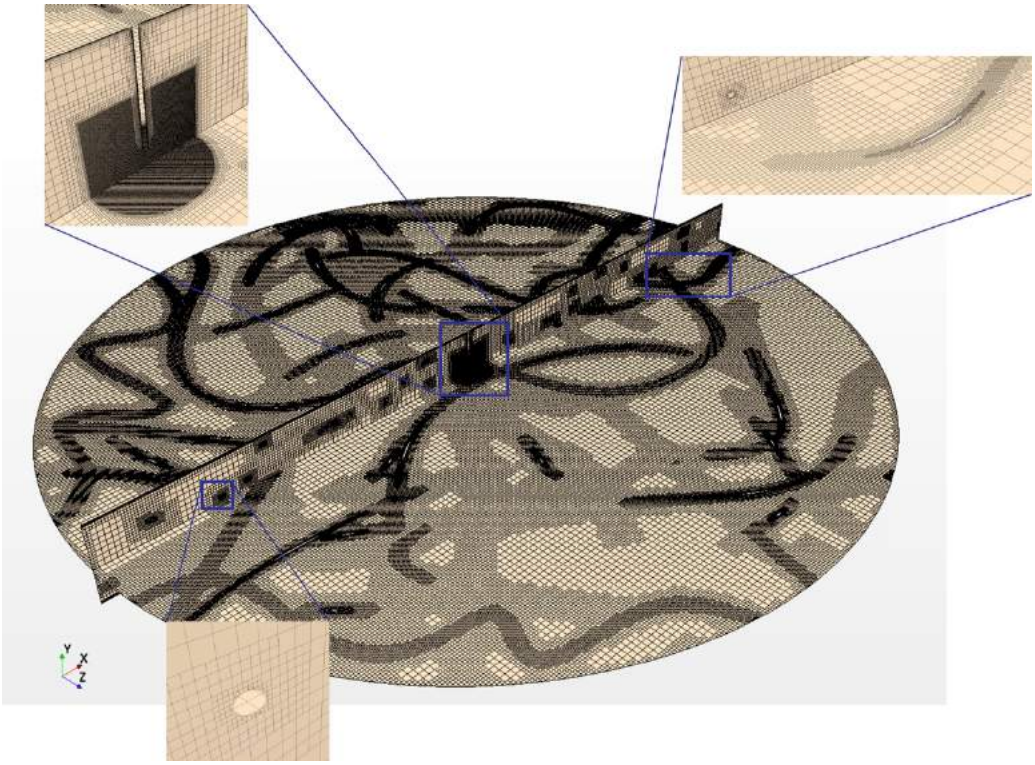

Figure 29. Volume mesh on inner surfaces of round adipose domain using presented mesh settings.

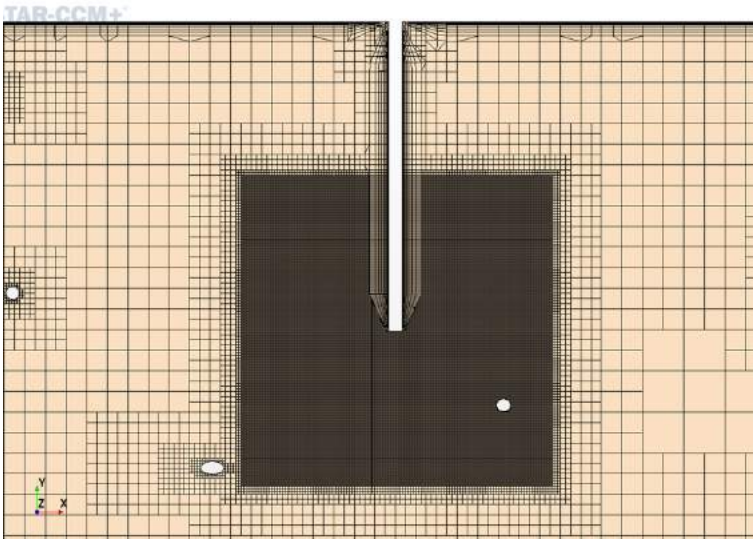

Figure 30. Cannula outlet volume element mesh constraint detail.

There were several models that were remeshed with a lower relative minimum size of 0.0324-0.0322 to obtain similar residuals to the other models. It was found that the generated mesh in these models cause error that did not allow for good convergence, which changing the relative minimum size was used to remediate this lack of convergence. The cases requiring this can be found in Appendix B Table B-1. Considering these slightly more refined meshes still attained similar residuals errors compared to the other models, the sensitivity level of the mesh was further confirmed and proved the mesh was an independent factor in the study.

6. Model Validation

Before meaningful results could be obtained in the study, the CFD model that was developed had to be validated against the previously published insulin depot characteristics and measurements, as shown by Leuenberger Jockel et al. (2013) and Zedelmair (2016), to ensure it was an accurate model. This was able to be completed using an insulin delivery rate of 12 IU/min and 90° x 8 mm long cannula to match previous ex vivo and CFD studies completed about insulin delivery [26, 46]. Further, the validation was done using a simplified time dependent unsteady CFD case as well as a complete steady state case as being considered in the current study. The results obtained through this initial step of the study indicated the model was adequate for the study of insulin delivery and the effect of cannula geometry and tissue thickness on its deposition and dispersion.

6.1 Unsteady Domain Definition

As previously mentioned, a time dependent, implicit unsteady case was developed for the validation of the presented CFD model of this study using previously published ex vivo depot formation results. A simplified domain had to be created that did not include capillaries and assumed symmetry across the z-axis intersecting the vertical center axis of the cylindrical domain. Attempts were made to utilize the complete developed model domain and CFD setup from this study in an implicit unsteady manner, with a 13.9 mm tissue thickness, as defined by the previous studies, but this was proven to be inefficient. With the time step size required to produce accurate results and the computational power available, in three weeks of continuous running at time of only 0.75 seconds was able to be simulated within the CFD model. Ten seconds was required to be simulated to reach the 2 IU threshold as done by the ex vivo study of Leuenberger Jockel et al. (2013), and therefore a simplified domain model had to be utilized to simulate this 2 IU delivery over ten seconds.

The domain for the unsteady case was created the same size as domain models used for the current study, which was a 120 mm cylinder, but did not include the capillary models. The capillaries were not a required element for this component of the current study, as they would have little effect on the insulin depot development in the adipose tissue over the course of only ten seconds [26]. Further, since no capillaries were present in the domain, a plane of symmetry could

be identified in the z-direction that intersected the central axis of the cylindrical domain and cannula. The resulting domain for this time dependent simulation is shown in Figure 31.

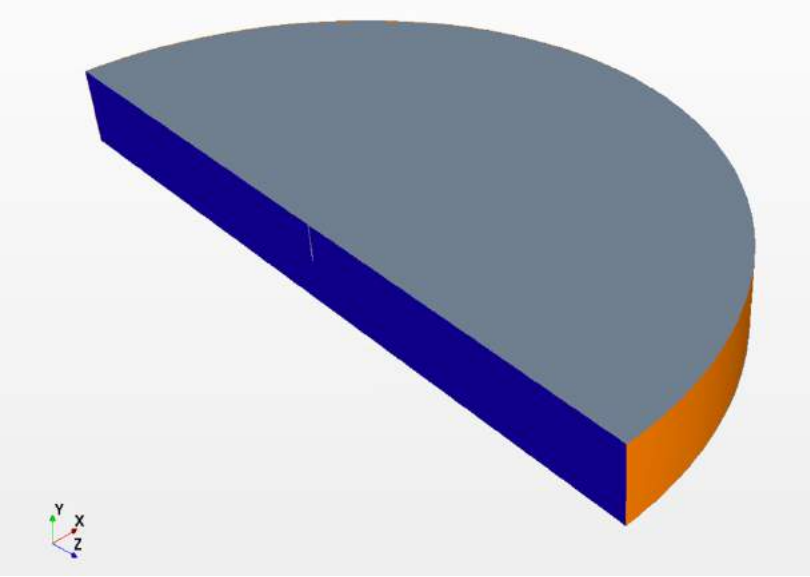

Figure 31. Time dependent validation case domain.

6.2 Unsteady CFD Model Conditions

The model conditions had to be altered in several respects to accommodate the unsteady solution compared to the physics and boundary conditions set forth in the previous chapter. First, the boundary conditions of the validation domain were a simplified set, as shown in Table 14 below.

Table 14. Boundary condition for unsteady adipose CFD model.

Domain Face	Condition
Outer Face	Pressure Outlet
Top and Bottom	Wall
Cannula Wall	Wall
Cannula Outlet Face	Mass Flow Inlet (average velocity inlet)
Vertical Mid-plane	Symmetry Plane

The boundary conditions are the same but exclude the capillary groups and instead have the addition of the symmetry plane across the middle of the cylindrical domain. This plane can be seen in blue in Figure 31 above respectively. Further, the mesh relative minimum size was made slightly larger, therefore reducing the volume elements used and the overall computational load of each iteration of the validation model. This change in the relative minimum volume element size as well as the total volume element count for this time-dependent domain developed can be seen in Table 15.

Table 15. Implicit unsteady validation case meshing parameter change and mesh result.

Parameter	Value
Relative Minimum Size (% Base)	0.05
Model Domain Volume Element Count	4,142,155

The mesh generated for this validation case domain was acceptable for the use of the domain as it still developed residual errors on the same order of the study models. The mesh can be seen in the additional figures Appendix B and the residual error plot can be found in Appendix C respectively. It should be noted that the cylindrical volume around the end of the cannula was also changed in size to be a diameter of 12 mm, to be past the the insulin deposition outreach expected in the ten second trial. Also, this volume element constraint was set to a relative volume element size of 0.05% of the base size matching the relative minimum size of the meshing parameters.

The model physics also had to be adjusted from a steady state solution to an implicit unsteady state solution. This change in physics can be noted in Figure 32. It can be compared with Figure 23 to see the only change to the physics was in in fact making the simulation an implicit unsteady case.

Given the model being unsteady, further conditions had to be set to in the model to ensure convergence and a valid simulation result. These included the implicit time step and maximum inner iterations for each time step, as shown in Table 16. These parameters were set based upon

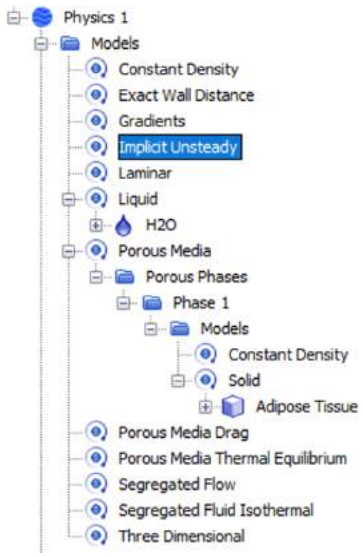

Figure 32. Unsteady validation case model physics.

trials of the model to ensure convergence of the result and maintaining a maximum Courant number of less than or equal to 1. This ensured that within one time step no fluid particles flowed across more than one volume element in the case of this fluid flow in porous media model, and therefore would cause no additional error in the model [61].

Table 16. Implicit unsteady solution parameter for time dependent adipose CFD model.

Parameter	Value
Implicit Time Step (sec)	0.001
Maximum Inner Iterations	5

6.3 Validation Results

The results from the validation compared in a 2-D planar representation of the insulin depot in the adipose tissue subcutaneous space. The reported results by the study of both Leuenberger Jockel et al. (2013) and Zedelmair (2016) were graphical measurement of the outreach of the insulin deposit from the cannula center. Note that the outreach of the depot was the measurement from the center of the cannula to the outermost edge of the insulin deposition area. Considering this, the reported outreach and height for both the 2 IU bolus as well as a 15 IU bolus from the cannula from those studies are found in Table 17.

Table 17. Previously published insulin depot measurement by pump therapy.

Measurement	Value
2 IU Depot Outreach Average (mm)	5 [26]
2 IU Depot Height Average (mm)	2 [26]
15 IU Depot Outreach Average (mm)	7 [26]
15 IU Depot Height Average (mm)	7 [26]
15 IU Depot Outreach Average (mm)	8.5 [46]
15 IU Depot Height Average (mm)	8 [46]

The results from the current validation case of the presented CFD model were found by analysis of the simulated graphical results yielded by using the case parameters of the previously published studies [26, 46]. Considering the implicit unsteady case first, the magnitude of the velocity was used to graphically show what the insulin depo shape would look like. This was a valid consideration, as the interstitial fluid in the domain was assumed to be stagnant, and therefore would have no velocity except for in the area affected by the outflow of insulin from the cannula tip. Based on this, the area in which a velocity magnitude greater than 0 m/s could be observed was used for the measurement of the outreach and height of the insulin depot. The area is shown in the entire implicit unsteady domain in the additional figures of Appendix B as well as zoomed in in Figure 33.

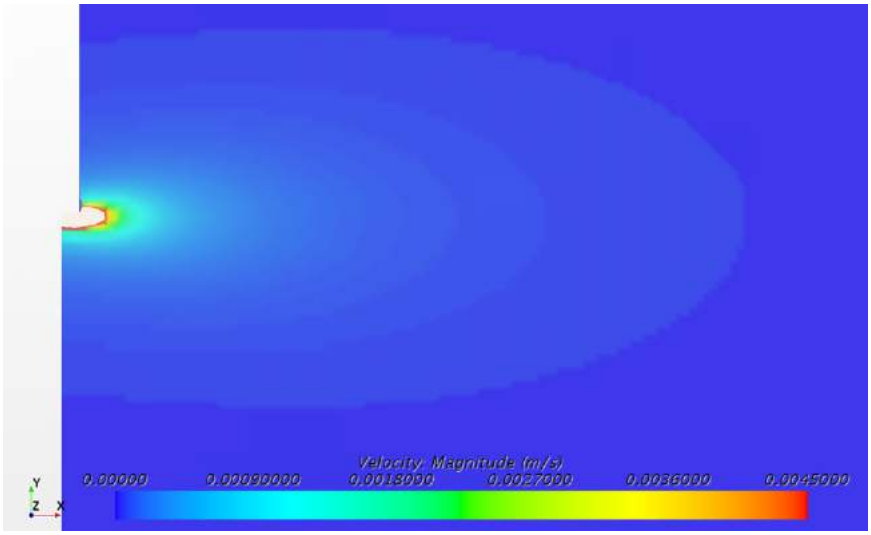

Figure 33. Implicit unsteady validation case insulin outreach.

Further, the steady state recreated scenario solution could be in a loose manner compared to the 15 IU bolus published insulin depot formation previously shown. Although both the ex vivo and previously published CFD studies were completed in the unsteady time dependent domain under the assumption the 15 IU bolus represents a large insulin bolus, that could be viewed as a semi-continuous infusion. Since a steady state solution of the presented CFD model would be representative of the average drug delivery it could be roughly correlated to the unsteady 15 IU bolus depot results published [26, 46]. Considering this, it was assumed the dense higher-pressure region around the cannula outlet in the steady state solution would be representative of the insulin depot, and the pressure gradients outside of that point indicate the insulin dispersing out into the surrounding tissue, as has been observed in previous studies considering injection pens over short periods of time [25]. This region from the steady state solution of the validation case can be found marked in Figure B-6 of Appendix B. It can further be seen in Figure 34 below where it is clearly seen as the aqua blue elliptical region around the cannula tip. Further, Figure 35 indicates how this region was measured to estimate the deposition outreach and height. It can be noted the white areas shown in the figure are areas of pressure higher than the scale shows. The scale of the figures was set to give better resolution of the boundaries of the insulin depot, which resulted in this clipping of the graphical region closest to the cannula.

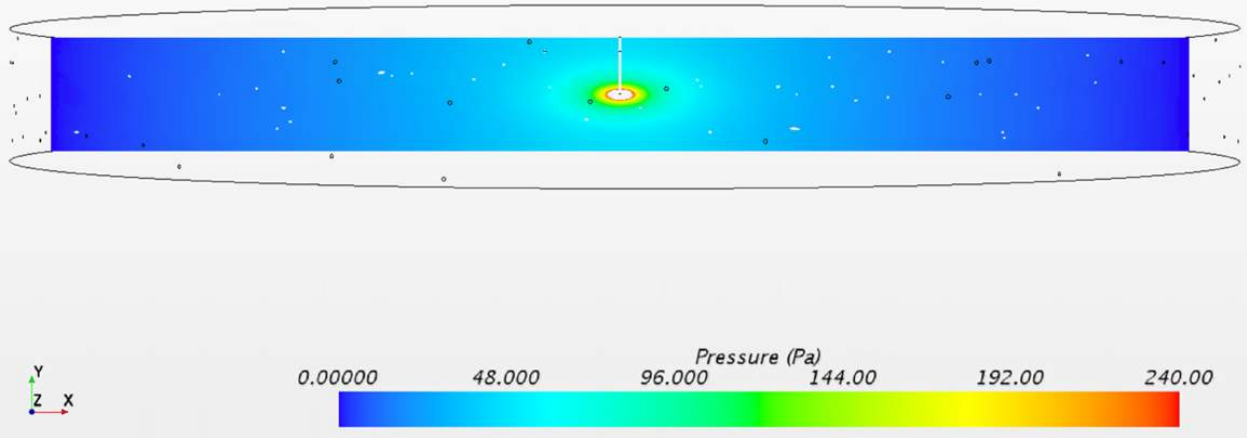

Figure 34. Steady state solution insulin injection depot by pressure distribution.

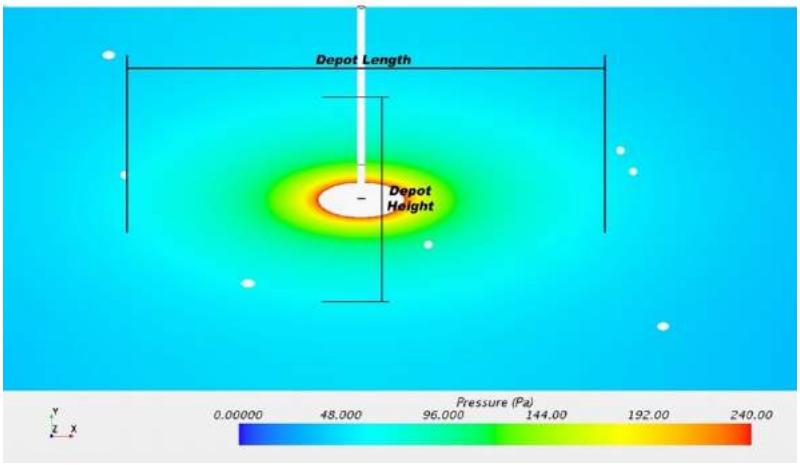

Figure 35. Insulin depot by pressure distribution size definition.

The resulting measured outreach and height of the insulin depot from the developed CFD model for the current study are shown in Table 18. In comparing these results with those of the previously published ex vivo and CFD insulin depot formation results of Leuenberger Jockel et al. (2013) and Zedelmair (2016) found in Table 17, it can clearly be seen that the CFD model developed for the current study could be concluded to produce accurate results.

Table 18. Validation case insulin depot size measurements.

Measurement	Value
2 IU Depot Outreach (mm)	5.2
2 IU Depot Height (mm)	2.8
Steady State Depot Outreach (mm)	7.3
Steady State Depot Height (mm)	6.3

Considering the 2 IU bolus, the implicit unsteady case solution for the presented model falls within 0.2 mm of the average depot outreach previously published. The height was found to have a larger deviation of 0.8 mm though. This agreement with the previously published ex vivo insulin deposition results provides significant validity that the model developed for the current study provides an accurate representation of insulin deposition within the subcutaneous adipose tissue subspace. Further emphasizing this from the previous research, the previous ex vivo study of insulin pump infusion noted that the results were quite variable within each of the samples

tested, and this was shown by the interquartile range for the outreach ranging from 3.7 mm to 7 mm [26].

In the case of the steady state solution, which followed the exact model parameters used in twenty-five cases being analyzed in the current study, a good agreement was observed between the 15 IU bolus results and this steady state insulin depot representation. The outreach interquartile range previously presented for the 15 IU bolus was 5 mm to 13.8 mm [26]. The steady state solution estimation of the insulin depot by the developed CFD model resulted in an insulin outreach of 7.3 mm, which is well within the previously published ex vivo range for a 15 IU bolus, as well as the insulin depot size previously reported by the CFD insulin depot study [26, 46]. The height of the deposition area was also within reason compared to the previously published ex vivo result of 7 mm and 8 mm.

Therefore, from these comparisons between the CFD model developed for the current study and the previously published insulin deposition studies, it could be concluded the CFD model developed for the current insulin delivery research was a valid representation for insulin infusion into adipose tissue. This was also founded within the fact the current study scope was to consider overall trends of insulin delivery and how the cannula geometry and tissue thickness might affect this delivery. The agreement of the developed model indicates that the analysis of insulin delivery trends obtained through the cases and case sets of this study are accurate and valid results.

7. Cannula Outlet Flow

The flow directly out of the cannula would have a direct impact on the development of an insulin depot within the adipose tissue subcutaneous space. Therefore, the first consideration of the study was analyzing the velocity and flow pattern coming from the cannula outlet. It can be noted that although the cannula was not modeled for the flow to develop within it, that is the cannula outlet was an averaged outlet, for the purpose of this study comparing general trends that was acceptable. The trends and velocities of each of the case sets, based on the cannula geometry, were considered independently, as well as comparing and contrasting the patterns across the different cannula geometry case sets.

7.1 90° x 8 mm Lg. Cannula

The outflow from the cannula into the adipose tissue region with a cannula geometry of 90° x 8 mm long resulted in a very symmetric velocity and flow pattern. It was found that no matter the tissue thickness, the outflow of drug at the end of the cannula yielded no discernable difference between the other tissue domains being tested. Further, it can be seen in the example Figure 36 as well as the addition figures in Appendix D that the flow pattern out of the cannula was circular in the transverse direction and semi-circular in the side profile.

It can be seen the velocity from the outlet reduces greatly in the y-direction, as would be expected due to the anisotropic property of the tissue due to the extracellular matrix, while the fluid decelerated slower in the x and z directions.

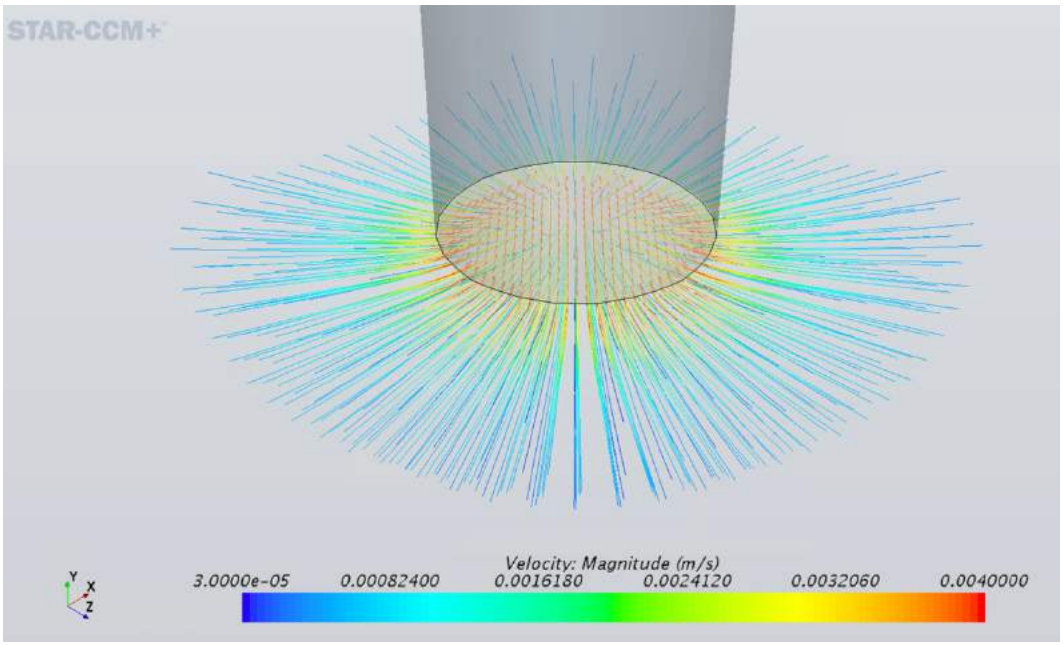

(a)

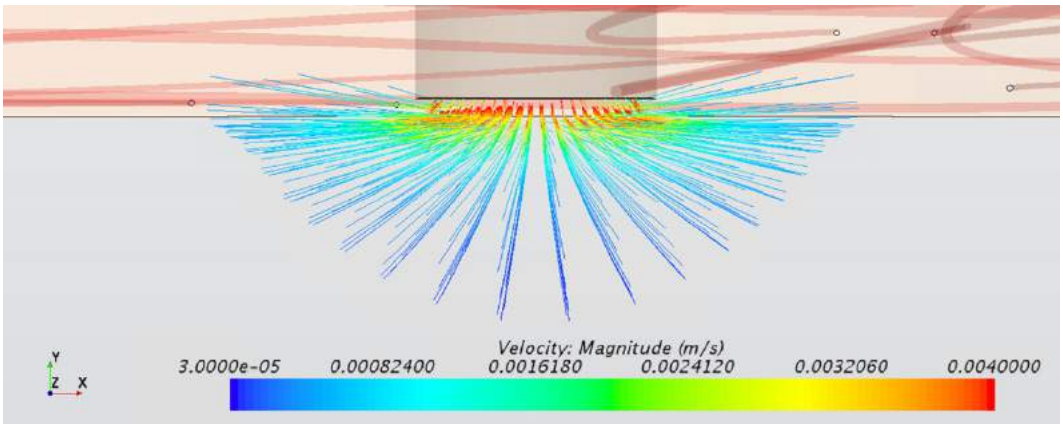

(b)

Figure 36. Outflow pattern and velocity at cannula outlet in 6 mm tissue with 90° x 8 mm Lg. cannula geometry (a) isometric view (b) side view.

7.2 45° x 13 mm Lg. Cannula

The outflow from the cannula tip with the cannula insertion angle of 45° and a length of 13 mm resulted in an elliptical velocity pattern viewed normal to the cannula end with its major axis in the z-direction of the domain, as shown in Figure 37 and the additional figures in Appendix D. Due to the anisotropic properties of the an insulin infusion domain, the path of least resistance for the flow to develop was in the x-z plane, which resulted in this elliptical velocity pattern for an

insertion angle at 45°. It can also be noted that this continues with respect to the side view of the cannula, with drastic direction changes of the fluid exiting the bottom of the cannula and turning back in the negative x-direction of the domain. Similarly, it was observed that the higher velocity density exiting the cannula was in the upper region of the cannula outlet, where the fluid could exit parallel to the x-z plane.

It was also observed that the 6 mm adipose tissue results varied from that of the thicker tissue domains. This difference was seen in the fluid flow at the lower edge of the cannula, as seen in comparing Figures 37 and 38, where the 6 mm tissue has a much greater fluid path found in the negative x-direction than the thicker counterparts with the same cannula geometry. The phenomenon could likely be attributed to the proximity of the outlet of this cannula geometry outlet to the muscular boundary in the 6 mm adipose tissue domain.

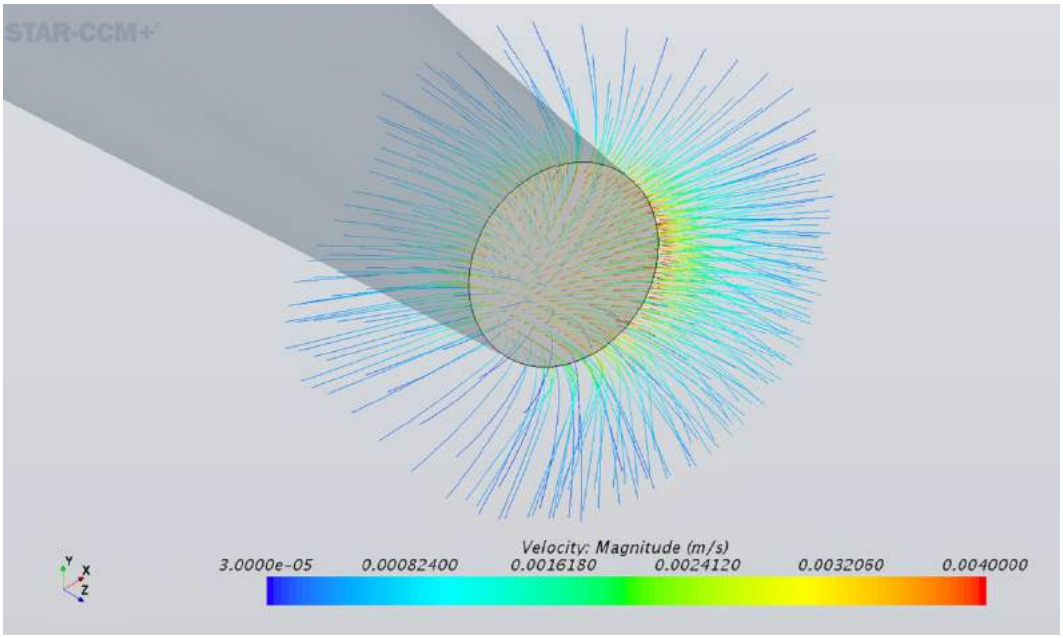

(a)

Figure 37. Outflow pattern and velocity at cannula outlet in 6 mm tissue with 45° x 13 mm Lg. cannula geometry (a) isometric view.

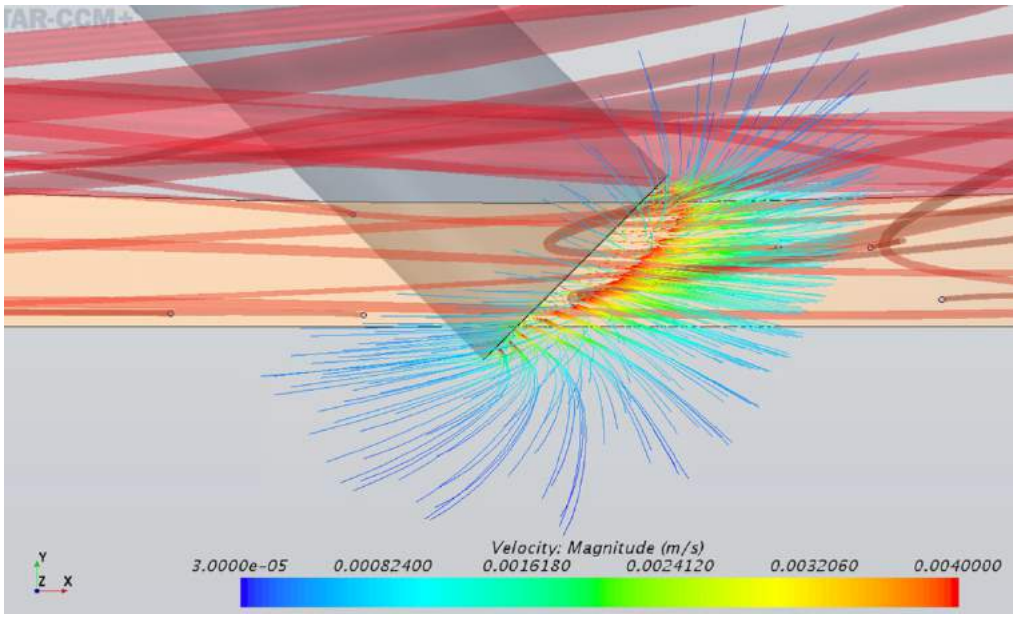

(b)

Figure 37 cont. Outflow pattern and velocity at cannula outlet in 6 mm tissue with 45° x 13 mm Lg. cannula geometry (b) side view.

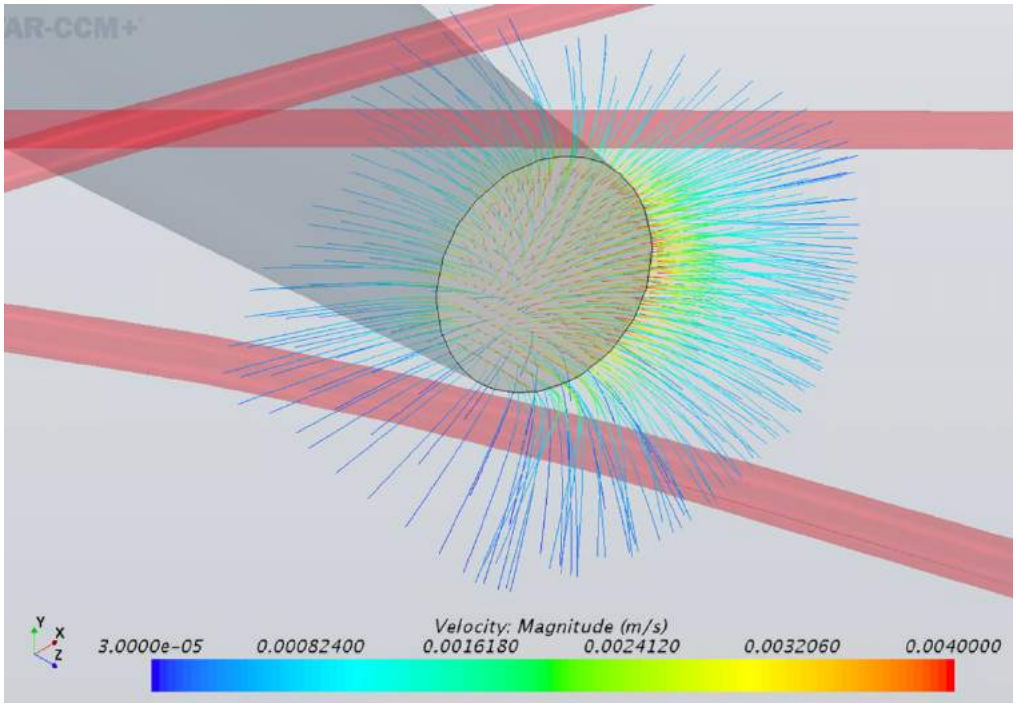

(a)

Figure 38. Outflow pattern and velocity at cannula outlet in 12 mm tissue with 45° x 13 mm Lg. cannula geometry (a) isometric view.

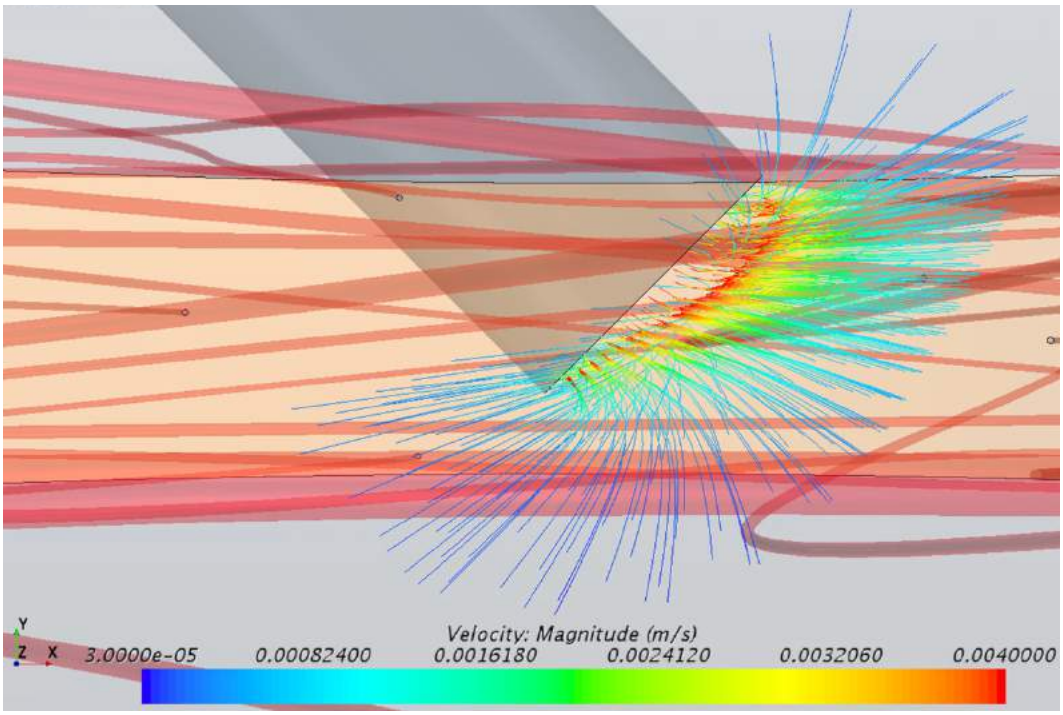

(b)

Figure 38 cont. Outflow pattern and velocity at cannula outlet in 12 mm tissue with 45° x 13 mm Lg. cannula geometry (b) side view.

7.3 30° x 13 mm Lg. Cannula

The outflow from the cannula tip with the cannula insertion angle of 30° and a length of 13 mm also resulted in an elliptical velocity pattern viewed normal to the cannula end with its major axis in the z-direction of the domain, as shown in Figure 39 and the additional figures in Appendix D. It was observed that a high density of flow was in the z-direction and x-direction, as shown by highest density of flow and highest velocities out in the z-directions from the sides and in the positive x-direction. This was especially evident looking at the high velocity region skewed toward the top of the cannula where the fluid has minimal flow bending to maintain an x-direction flow. It was also noted that the 6 mm tissue model had a slightly lower fluid velocity at the peripherals of the flow region compared to the other domains.

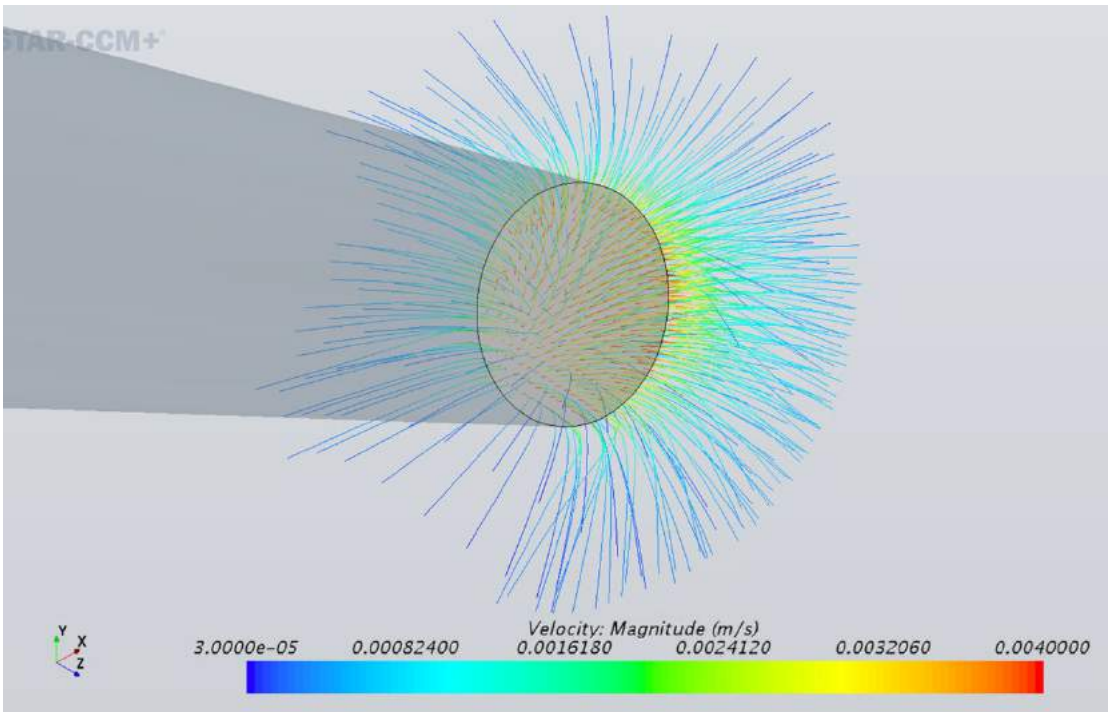

(a)

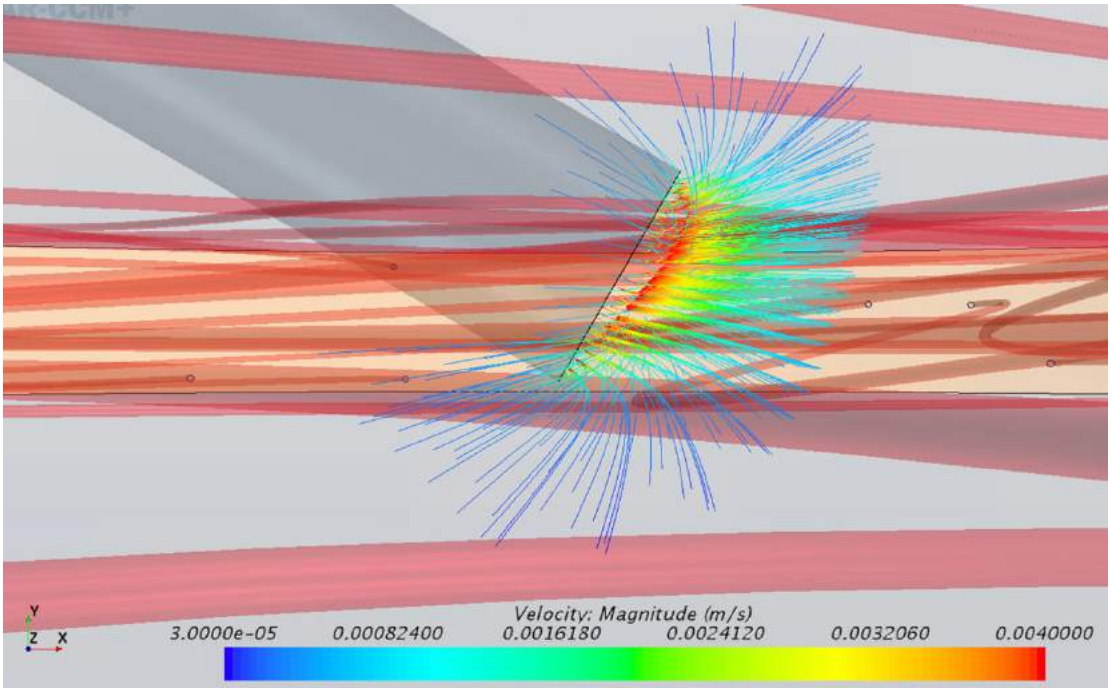

(b)

Figure 39. Outflow pattern and velocity at cannula outlet in 6 mm tissue with 30° x 13 mm Lg. cannula geometry (a) isometric view (b) side view.

7.4 20° x 13 mm Lg. Cannula

The cannula geometry with an insertion angle of 20° and a length of 13 mm again yielded an elliptical velocity pattern viewed normal to the cannula end with its major axis in the z-direction of the domain, as shown in Figure 40 and the additional figures in Appendix D. The highest flow density was overserved going out toward the side of the cannula as well as forward from the cannula end in the x-direction. There was very little flow observed to proceed around the bottom edge of the cannula. The largest portion of the flow was in the x and z directions and indicated by the velocity density and flow streams. There was no noticeable difference in the cannula outlet flow between the different adipose tissue domains for this cannula geometry.

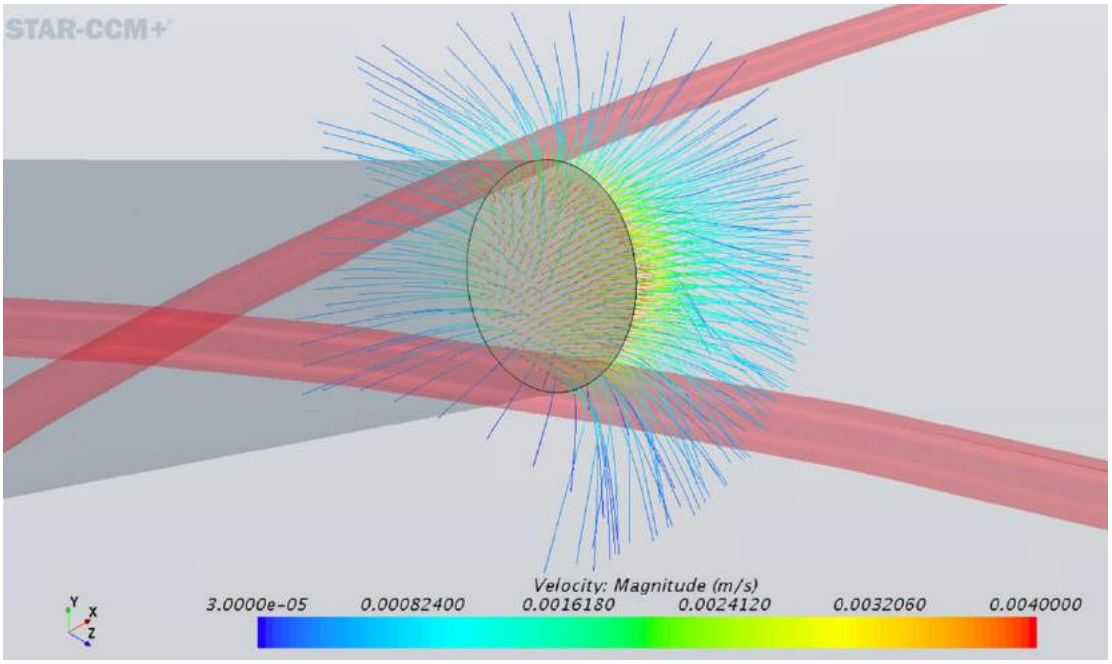

(a)

Figure 40. Outflow pattern and velocity at cannula outlet in 6 mm tissue with 20° x 13 mm Lg. cannula geometry (a) isometric view.

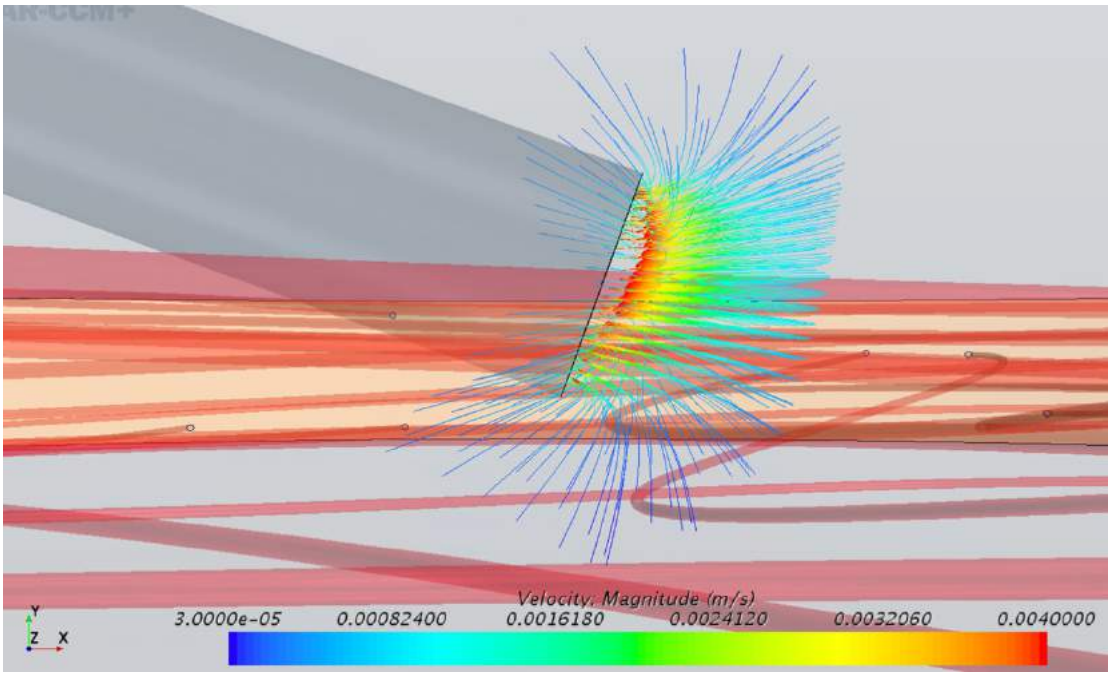

(b)

Figure 40 cont. Outflow pattern and velocity at cannula outlet in 6 mm tissue with 20° x 13 mm Lg. cannula geometry (b) side view.

7.5 20° x 17 mm Lg. Cannula

The cannula geometry with an insertion angle of 20° and a length of 17 mm, as shown by Figure 41 and the additional figures in Appendix D, again produced an elliptical velocity pattern viewed normal to the cannula end with its major axis in the z-direction of the domain. The highest flow density was overserved going out toward the side of the cannula as well as forward from the cannula end in the x-direction. There was very little flow observed to proceed around the bottom edge of the cannula and change direction. The largest portion of the flow was in the x and z directions and indicated by the velocity density and flow streams. There was no noticeable difference in the cannula outlet flow between the different adipose tissue domains for this cannula geometry.

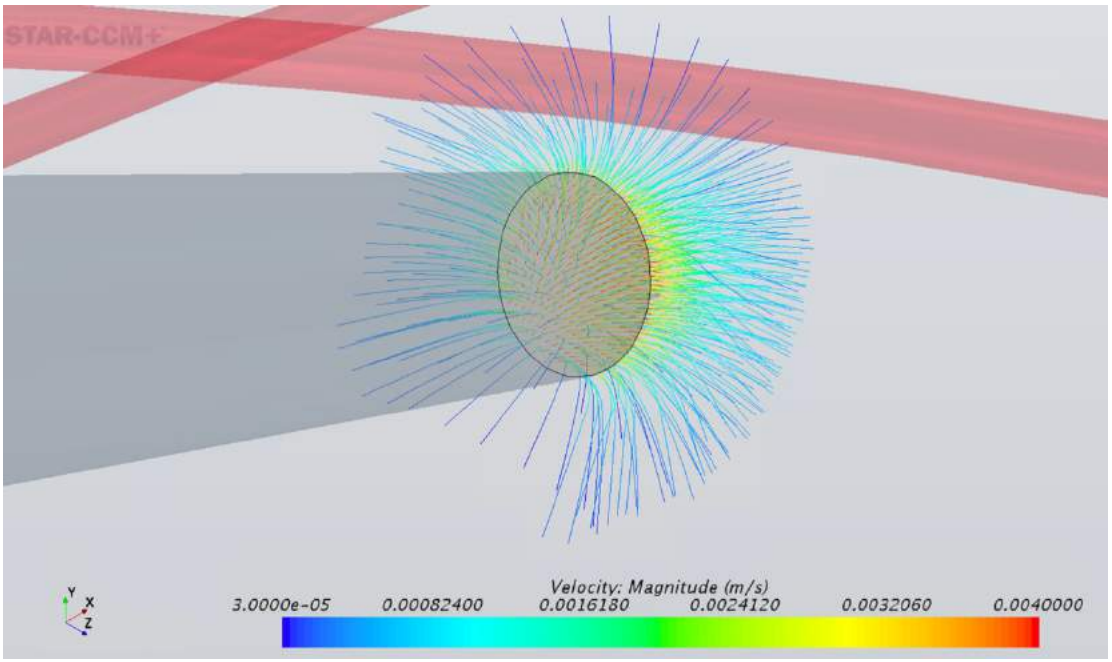

(a)

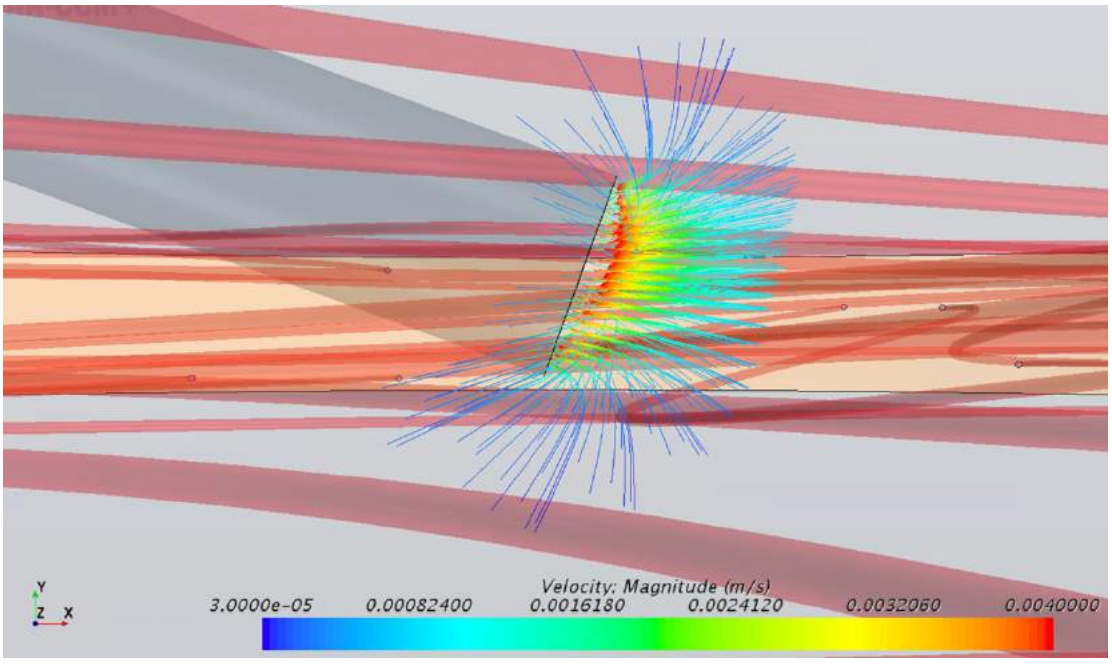

(b)

Figure 41. Outflow pattern and velocity at cannula outlet in 6 mm tissue with 20° x 17 mm Lg. cannula geometry (a) isometric view (b) side view.

7.6 Cross Case Set Analysis

Considering the insulin flow development just after leaving the cannula outlet, the flow as generally very similar across each of the cannula geometries and tissue thicknesses. The largest difference between the case sets was the 90° insertion angle cannula produced a much more rotationally symmetric flow pattern than the other cannula geometries, which were much more elliptical with a major axis in the z-direction.

Also, the velocity density pattern was much different in the lower insertion angle cannulas than the 90° cannula, which has a very even velocity distribution across the region after the insulin exited the cannula. The lower insertion angles on the other hand had a much greater density toward the region leaving near the top of the cannula. This high velocity distribution was noted to move toward the center of the cannula outlet region as the angle decreased from 45° to 20° though as shown by comparing the side view in Figure 38, 39 and 40 respectively. It was also observed there was no distinguishable difference created in the flow profile or velocity distribution by the cannula with a 20° insertion angle being of length 13 mm versus 17 mm. Further detailed analysis of these results obtained from the developed CFD model can be found in Chapter 10.

8. Drug Deposit Formation

The formation of the insulin drug deposit in the adipose tissue could be shown in the CFD model by examining the pressure gradients found withing the adipose tissue domain, as was done for the steady state validation case previously discussed in Chapter 6. A two-dimensional view of the pressure gradients was used to determine whether the cannula geometry and/or tissue thickness were significant factors in influencing the overall length and height of this drug deposit. Using both the graphic observations as well as statistical analysis the predicted drug deposition across the twenty-five cases considered were able to be analyzed and compared in regard to the insulin depot formed during delivery.

8.1 Control Cases: No Insulin Infusion

A control case for each of the tissue domains was simulated where no insulin injection through the cannula was present into the tissue. This indicated there were no anomalies present in any of the domains, especially in relation to the location of the cannula outlet, as shown by Figure 42, as well as the additional cases found in Appendix E.

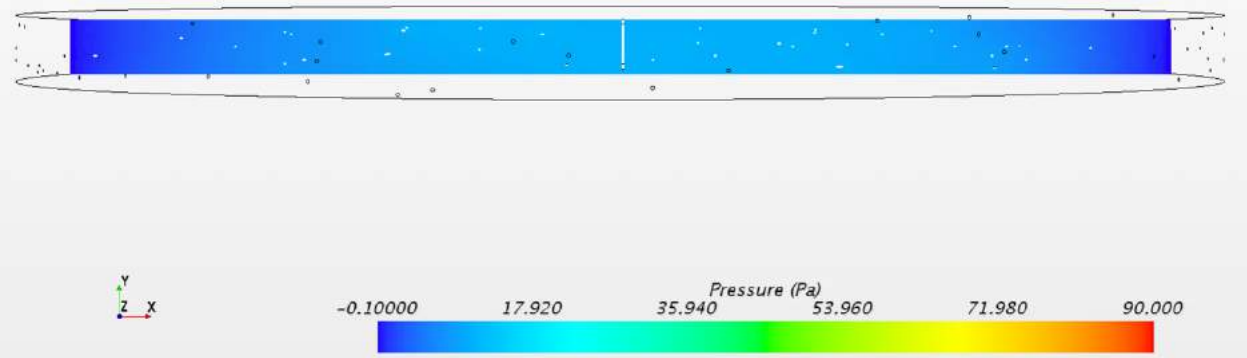

Figure 42. 6 mm tissue thickness CFD pressure gradient with no insulin delivery.

The planar graphic of the pressure is shown using the same scale found in the later deposition figures. It can be noted in Figure 42 that there were not any drastic pressure gradients around the cannula end or elsewhere in the domain plane shown. Therefore, from these control cases it was able to be concluded that the overall pressure gradients around the deposit area were due to only direct results of insulin injection being simulated in the environment and the domain factors that affect the overall deposition of the drug.

8.2 90° x 8 mm Lg. Cannula

Considering the insulin infusion deposition formation with a cannula insertion angle of 90° and cannula length of 8 mm, the deposition area was observed as represented in Figures 43 and 44. The additional tissue domain results are shown in Appendix E.

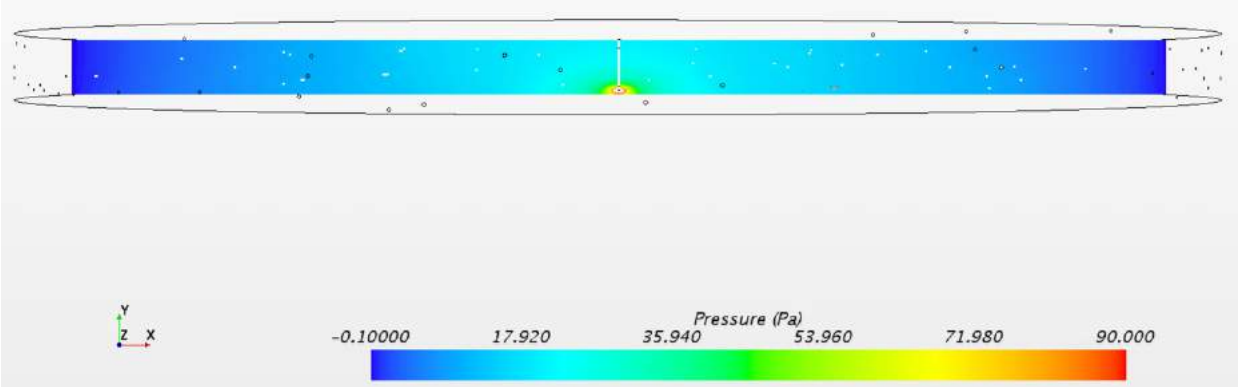

Figure 43. 6 mm tissue thickness CFD pressure gradient with 90° cannula.

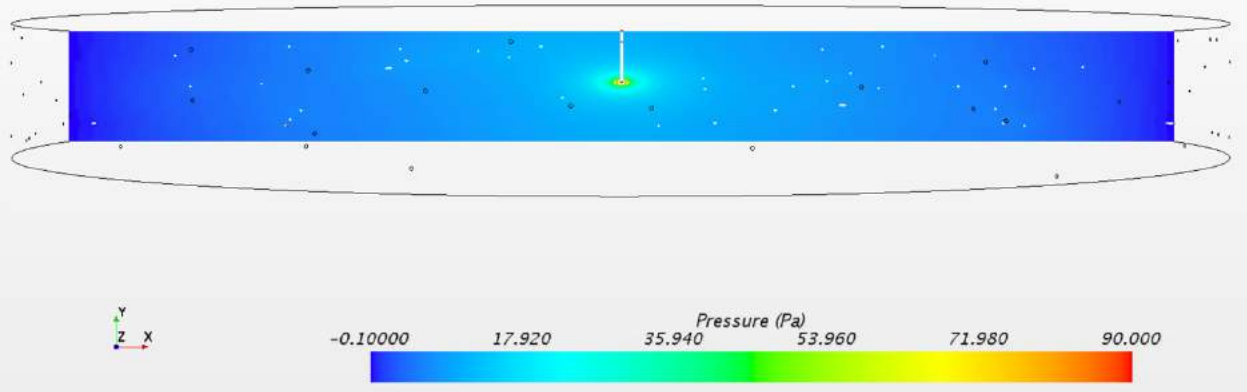

Figure 44. 12 mm tissue thickness CFD pressure gradient with 90° cannula.

The largest difference observed in considering the insulin deposition shape was between the 6 mm tissue and the other tissue thicknesses. The 12 mm, 18 mm, 24 mm, and 30 mm tissues did not have any significant difference that could be observed between them. In regards to comparing these depots with the 6 mm tissue though, there was a drastic difference in deposition size. It can be seen in Figure 43 that the deposition area was over three times larger transversly and two times taller than the other tissue thickness depots. The deposition area in the 6 mm tissue was also only half the elliptical shape observed in the other tissue thicknesses.

8.3 45° x 13 mm Lg. Cannula

The cannula geometry consisting of an insertion angle of 45° and cannula length of 13 mm yield insulin deposits as represented in Figures 45 and 46. The additional tissue domain insulin depot results are shown in Appendix E.

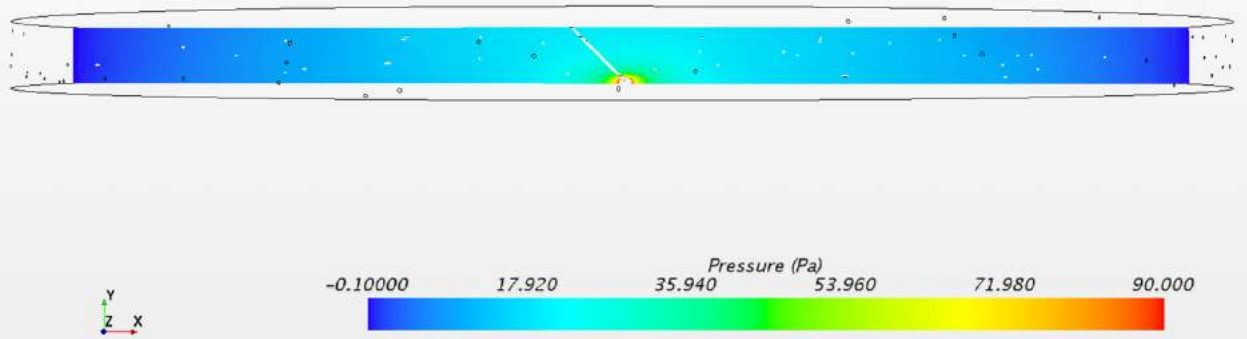

Figure 45. 6 mm tissue thickness CFD pressure gradient with 45° cannula.

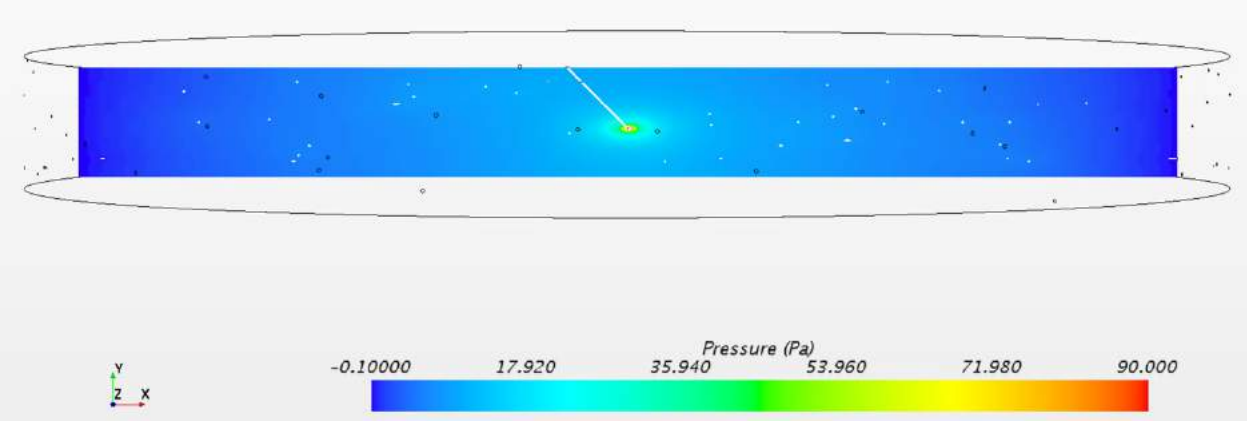

Figure 46. 12 mm tissue thickness CFD pressure gradient with 45° cannula.

Just as was observed in the previous case set, the only noticeable difference in the insulin deposits in the simulations of set 2 was between the depot of the 6 mm tissue compared to the other tissue thicknesses. The depot in the 6 mm thick adipose tissue was again noted to be over three times larger in the transverse direction and two times larger in height than the depots found in the thicker adipose tissue domains. Also, only about half of the elliptical depot shape was observed again in the 6 mm tissue domain.

8.4 30° x 13 mm Lg. Cannula

The resulting insulin depot formed from infusion through a 13 mm long cannula inserted at 30° are represented in Figures 47 and 48. The addition insulin depot formation results for this case set can be found in the additional figures of Appendix E.

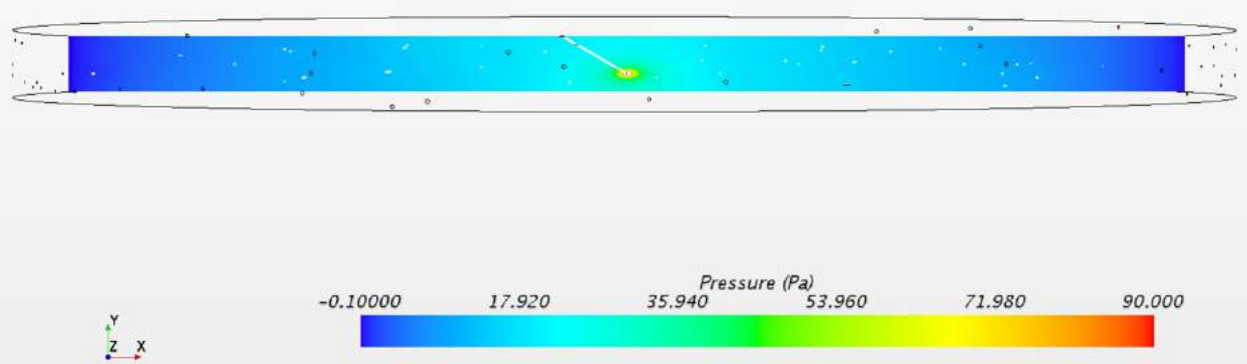

Figure 47. 6 mm tissue thickness CFD pressure gradient with 30° cannula.

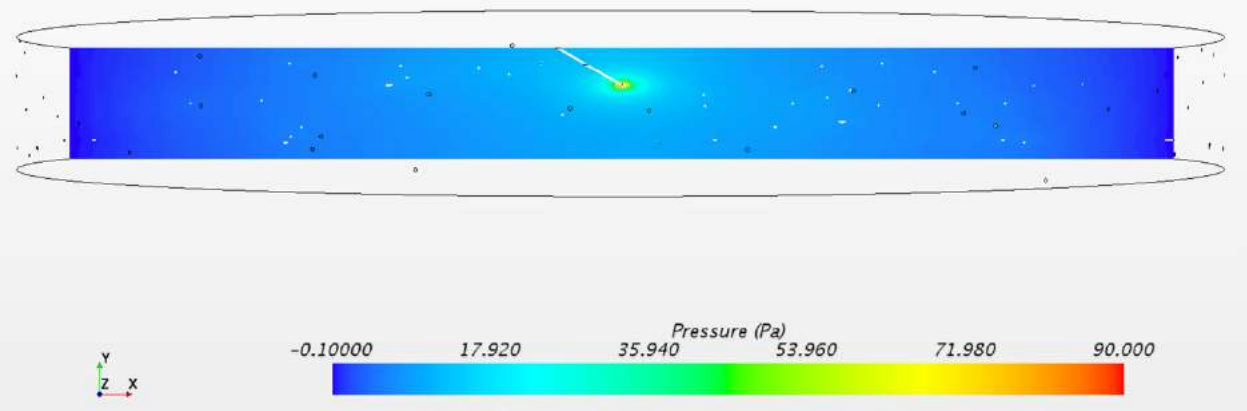

Figure 48. 12 mm tissue thickness CFD pressure gradient with 30° cannula.

Again, as in the previous cases, the only noticeable difference in the insulin depots formed during the insulin delivery through a 13 mm cannula inserted at 30° was between the depot of the 6 mm tissue compared to the thicker tissue domains. The depot in the 6 mm thick adipose tissue was just under three times larger in the transverse and height directions than the depots found in the thicker adipose tissue domains. The majority of the elliptical depot shape was observed in the 6 mm tissue domain with the 30° cannula insertion angle.

8.5 20° x 13 mm Lg. Cannula

The cannula geometry consisting of an insertion angle of 20° and cannula length of 13 mm resulted in insulin deposits as represented by Figures 49 and 50. The additional tissue domain insulin depot results are found in Appendix E.

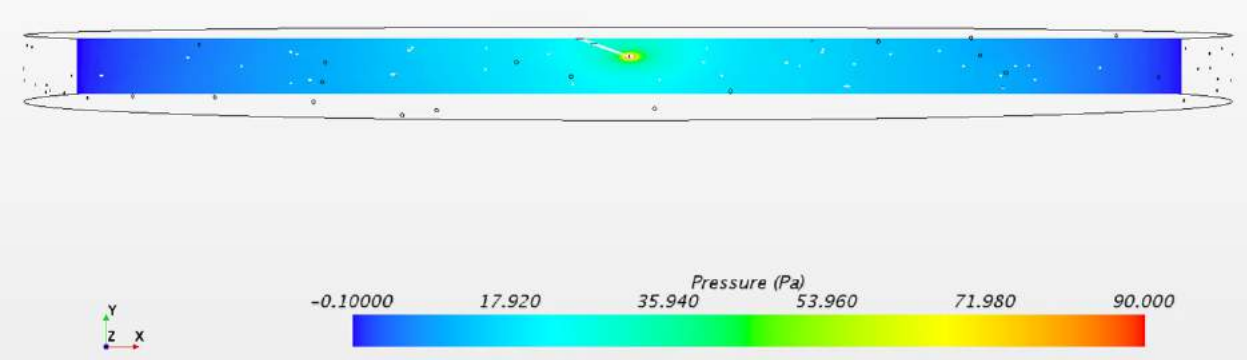

Figure 49. 6 mm tissue thickness CFD pressure gradient with 20° x 13 mm Lg. cannula.

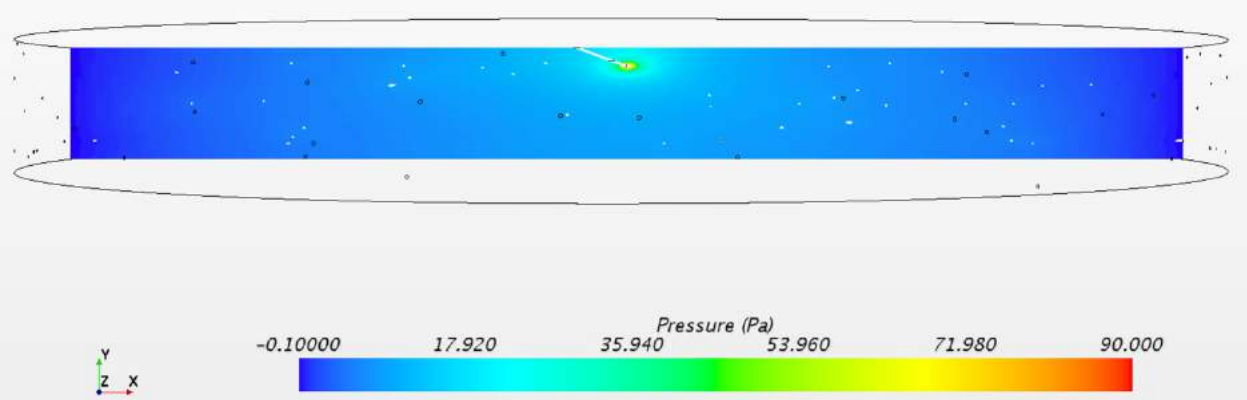

Figure 50. 12 mm tissue thickness CFD pressure gradient with 20° x 13 mm Lg. cannula.

As previously observed, the only noticeable difference in the insulin deposits after delivery through a 20° x 13 mm long cannula was between the depot of the 6 mm tissue compared to the thicker tissue domains. The depot in the 6 mm thick adipose tissue was just over 2.5 times larger in the transverse and height directions than the depots found in the thicker adipose tissue domains. The majority of the elliptical depot shape was observed in the 6 mm tissue domain, with the absent portion of the shape being at the dermis boundary of the domain rather that the muscular boundary.

8.6 20° x 17 mm Lg. Cannula

The resulting insulin depot formed from infusion through a 17 mm long cannula inserted at 20° are represented in Figures 51 and 52. The addition insulin depot formation results for the rest of the tissue domains in this case set can be found in Appendix E.

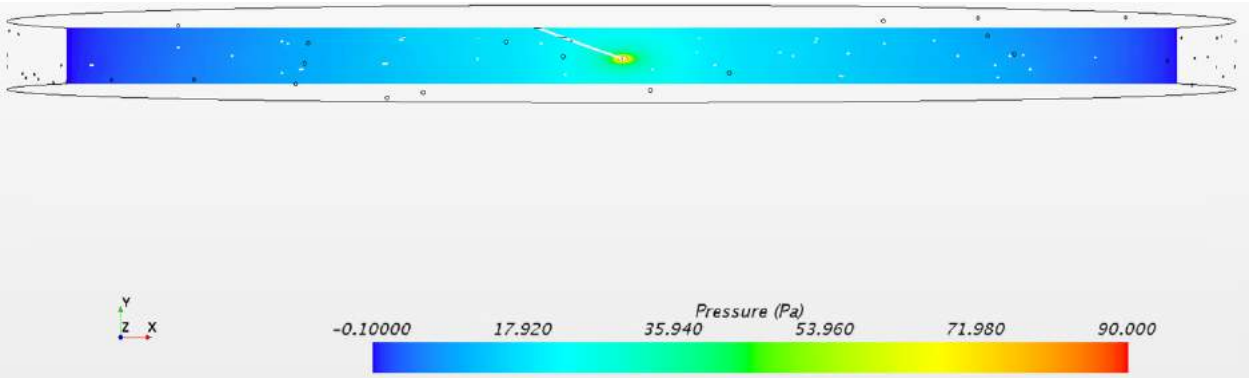

Figure 51. 6 mm tissue thickness CFD pressure gradient with 20° x 17 mm Lg. cannula.

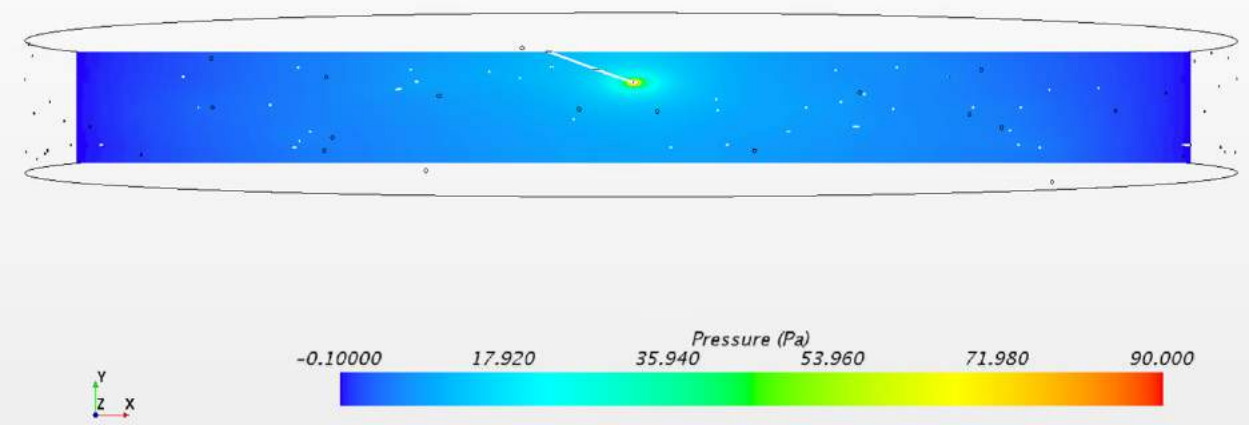

Figure 52. 12 mm tissue thickness CFD pressure gradient with 20° x 17 mm Lg. cannula.

Finally, the only noticeable difference in the insulin deposits formed after infusion through a 20° x 17 mm long cannula was between the depot of the 6 mm adipose tissue model compared to the thicker tissue domains. The depot in the 6 mm thick adipose tissue was again over 2.5 times larger in the transverse and height directions than the depots found in the thicker adipose tissue domains. The majority of the elliptical depot shape was observed in the 6 mm tissue domain, with the depot being about centered in the height of the tissue domain.

8.7 Cross Case Set Analysis

There were differences observed in each of the sets between the 6 mm tissue insulin depots and the depots in the thicker tissue domains. This trend can be more clearly seen in the insulin deposit radial length and height measurements across each of the case sets and tissue thicknesses as found in Figure 53 and 54. The depot shape being measured for each of the cases can be seen in Appendix E. It can be noted the insulin depot was measured in the same manner as the steady state validation case, as shown in Figure 35. It was clearly seen that the 6 mm tissue sample results in a much larger deposit of insulin in both length and height compared to the other tissue thickness in each of the case sets.

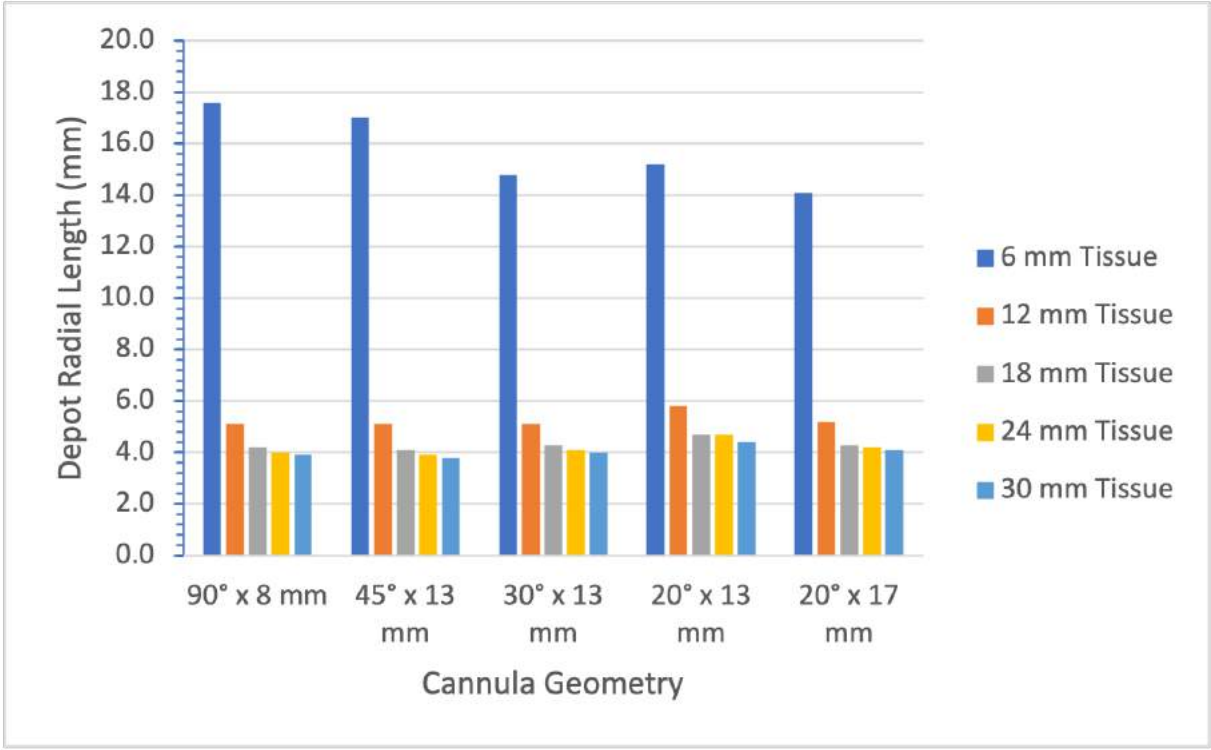

Figure 53. Insulin depot radial length vs. cannula geometry and tissue thickness.

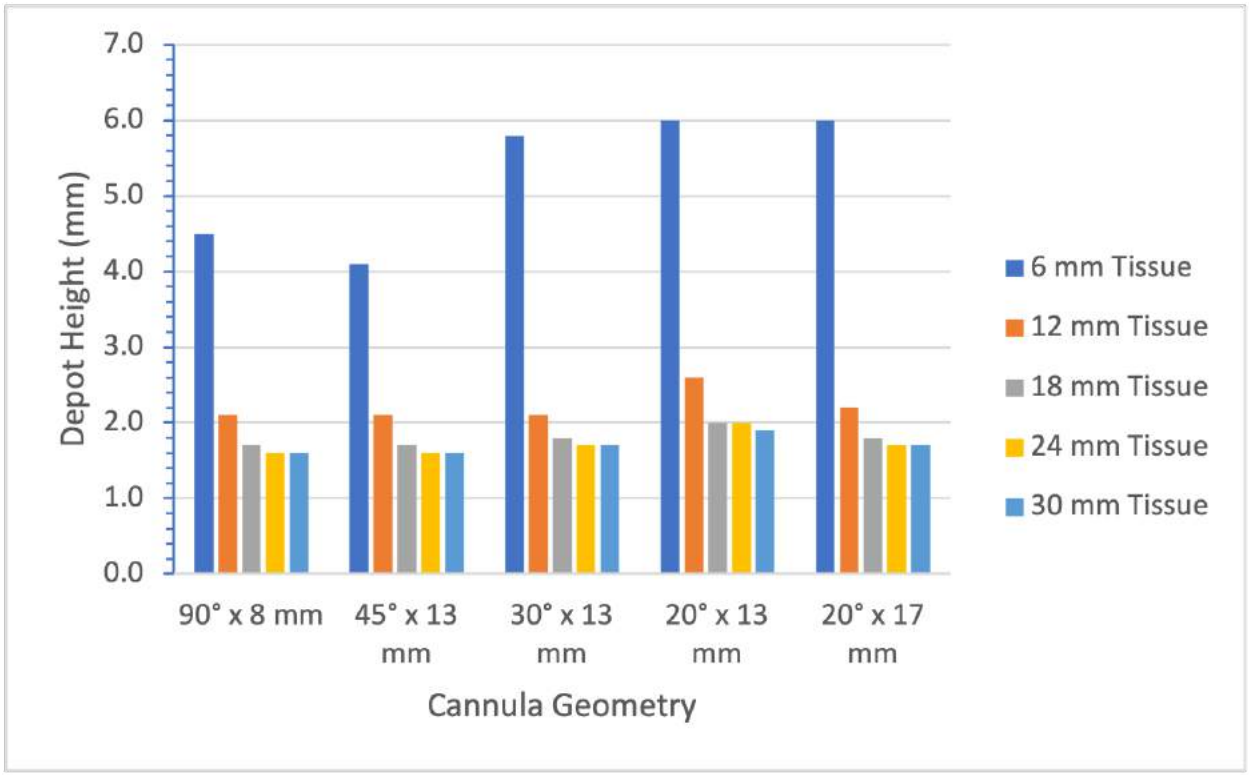

Figure 54. Insulin depot height vs. cannula geometry and tissue thickness.

What was noted when looking at how the different case set compare to each other though was that overall, in the case of the 6 mm adipose tissue domains, the length of the depot trended downward across the sample sets, while the height trended upward. In the thicker tissue samples, the insulin deposition length and height stayed relatively constant across the case sets, with a notable increase in both dimensions only in the case of a cannula geometry of length 13 mm and insertion angle of 20° respectively.

To further quantify these results, a two-factor analysis of variance (ANOVA) statistical analysis was completed for both the length and height measurements of the simulated insulin depots for each case. Assuming a significance level of 0.05, it was shown that across all of the case sets and tissue thicknesses, the tissue thickness was a factor of significance, while the cannula geometry was not of significance in the insulin depot measurements, as shown by the P-values of the analysis found in Table 19.

Given the difference that was able to be seen between 6 mm tissue thickness and thicker tissue domain depot results in each of the case sets, a single factor ANOVA was completed on the

6 mm tissue cases considering each of the five cannula geometries considered for both the length and height of the insulin depot. This was done in order to examine whether the cannula geometry

Table 19. Two-factor ANOVA without replication results.

Factor	Deposition Length P-value	Deposition Height P-value
Cannula Geometry	0.602	0.0535
Tissue Thickness	4.677×10^{-14}	1.0267×10^{-10}

was a significant factor across the thin 6 mm tissue on its own. It was found that the cannula geometry was significant in both the case of the length and height of the insulin deposit, as shown by the P-values in Table 20 below.

Table 20. One-factor ANOVA without replication results for 6 mm tissue thickness.

Factor	Deposition Length P-value	Deposition Height P-value
Cannula Geometry	1.095×10^{-6}	0.0234

Similarly, a two-factor ANOVA was completed for all of the length and height measurements excluding the 6 mm tissue simulations. This isolated the more similar thick tissue depot formations to analyze the significant factors in this similar grouping. The ANOVA, as shown in Table 21, indicated that when considering the depot results without the 6 mm samples, both the cannula geometries and tissue thicknesses were significant factors for both the length and height of the insulin depot.

Table 21. Two-factor ANOVA without replication results excluding 6 mm tissue thickness.

Factor	Deposition Length P-value	Deposition Height P-value
Cannula Geometry	6.891×10^{-8}	1.626×10^{-6}
Tissue Thickness	8.252×10^{-12}	5.953×10^{-9}

Further, looking at just the two sets of cases using the 20° insertion angle with an either 13 mm or 20 mm cannula, it was found that there was not statistical significance between these two

case sets across the different tissue thicknesses. This was done using a t-test assuming unequal variance with a significance level of 0.05, which resulted in the P-values as shown below in Table 22.

Table 22. T-test assuming unequal variance for 20° insertion angle cannula with different cannula lengths.

Factor	P-value (one-tail)	P-value (two-tail)
Cannula Length	0.42163093	0.84326185

Even with the small sample sizes, which could be accounted for assuming unequal variance, the P-value was found to be much higher than the confidence level of 0.05, and therefore the hypothesis that there was no difference between the mean values of the two data sets was upheld. This indicated therefore that there was not a statistically significant difference in the deposition of insulin due the depth the cannula was placed into the adipose tissue domain at a 20° insertion angle. Further detailed analysis of these results obtained from the developed CFD model can be found in Chapter 10.

9. Average Drug Dispersion Pattern

A large component of the drug delivery in adipose tissue is the drug flow away from the cannula after deposition. The manner in which the largest density of the drug flows away from depot and the direction in which it does could largely be affected by the cannula geometry, tissue thickness, as well as tissue vascularization. This dispersion plays directly into drug uptake from the adipose tissue extracellular space. Therefore, simulating the flow pattern away from the cannula outlet in the steady state model through the use of streamlines gives a visual representation of what this average drug dispersion would look like given the designed CFD domain.

9.1 90° x 8 mm Lg. Cannula

In the case of the CFD models with a 90° insertion angle and 8 mm long cannula, it was shown that the overall drug dispersion pattern across the simulations was a very symmetric and planar circular pattern. This can be seen in Figures 55 and 56 as well as the additional figures

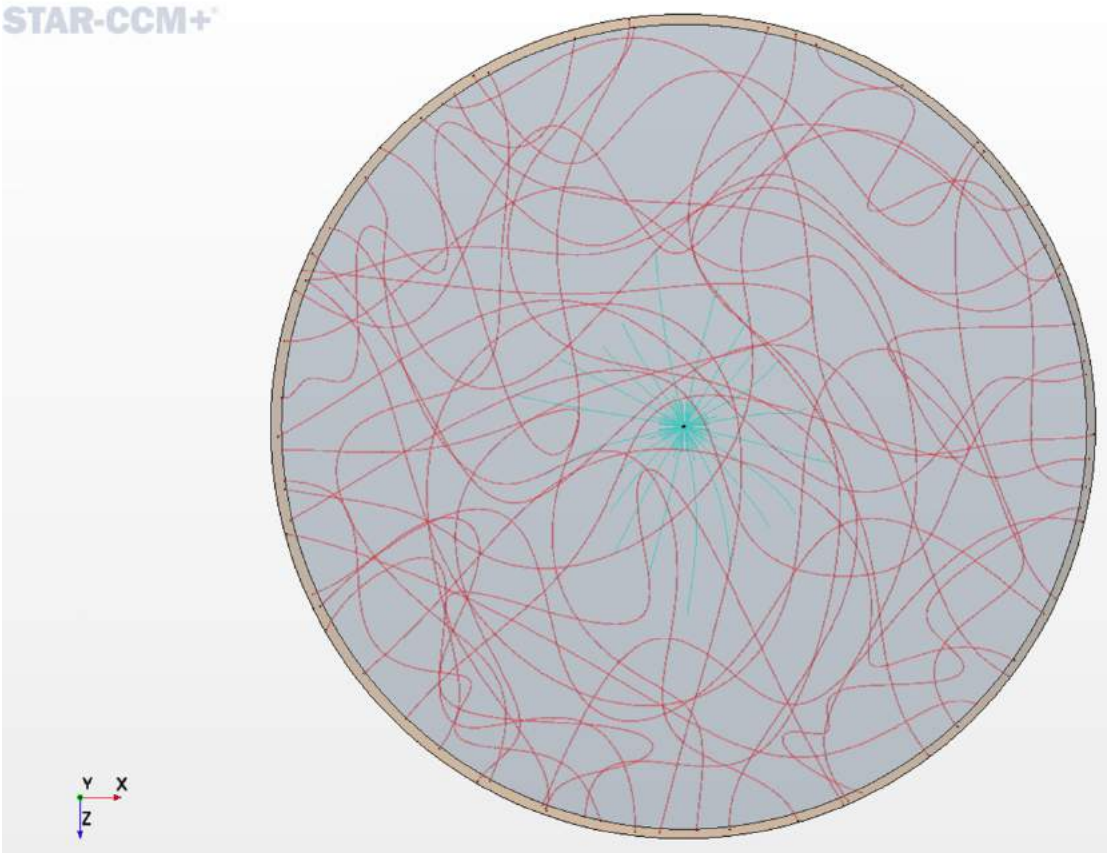

(a)

Figure 55. Average drug dispersion from cannula for 6 mm tissue and 90° cannula (a) top view.

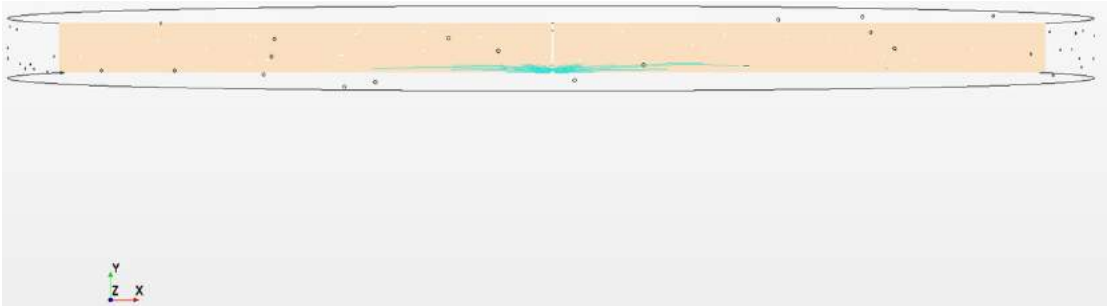

(b)

Figure 55 cont. Average drug dispersion from cannula for 6 mm tissue and 90° cannula (b) side view.

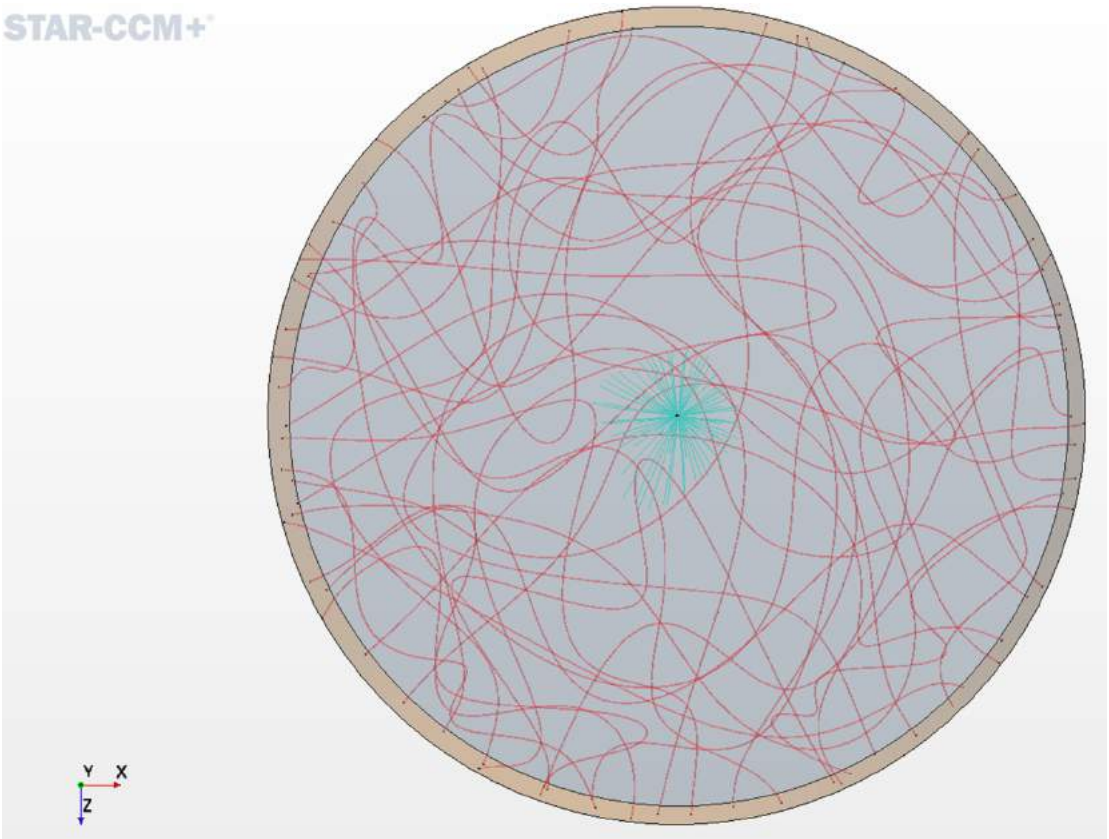

(a)

Figure 56. Average drug dispersion from cannula for 12 mm tissue and 90° cannula (a) top view.

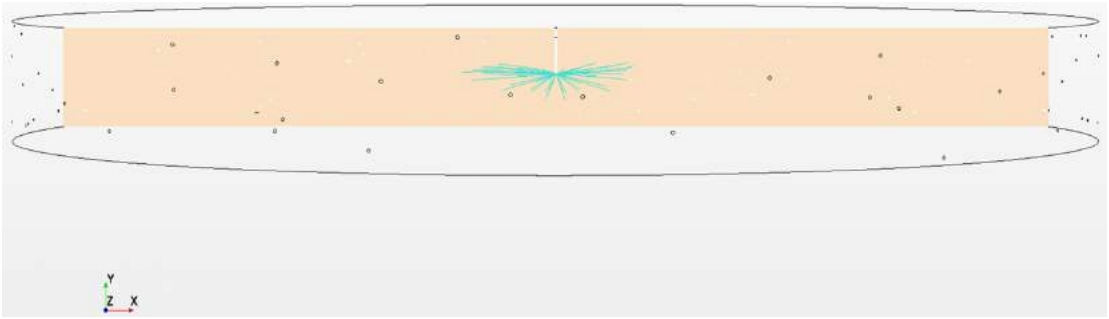

(b)

Figure 56 cont. Average drug dispersion from cannula for 12 mm tissue and 90° cannula (b) side view.

in Appendix F. It can be seen that the 6 mm tissue thickness resulted in a larger diameter dispersion outreach as well as a much more planar distribution than the thicker tissue domains. The overall distribution in the 6 mm tissue appears to rise in the domain slightly after injection. The thicker tissue domains also do rise slightly as the dispersion moves outward, but directly under the cannula outlet there is noted to be dispersion downward into the tissue as well.

In comparing the thicker tissue domains, it can be seen that the 12 mm tissue thickness has a smaller diameter outreach than the thicker adipose tissues, and the 30 mm thick tissue has the widest outreach diameter of the thicker tissue domains.

9.2 45° x 13 mm Lg. Cannula

The observed insulin drug dispersion pattern across the models with a cannula insertion angle of 45° and 13 mm length was a planar elliptical shape with a longitudinal axis running in the z-direction in the 6 mm tissue thickness as shown in Figure 57 respectively. In contrast, as shown by Figure 58 as well as the additional figures in Appendix F, there was symmetry observed across the x-axis in the top view, but the depth dispersion differed greatly from the thinner 6 mm tissue domain. The insulin was noted to disperse deeper into the tissue then follow a parallel path to the muscular boundary of the domain in the case of the 12 mm and 18 mm tissue domains, while in the 6 mm domain the dispersion went upward due to the close proximity to the muscular boundary of the cannula outlet.

The 24 mm and 30 mm tissue domain simulations showed that the dispersion of the drug would have a larger outreach than the 12 mm and 18 mm adipose tissue thicknesses, as well as

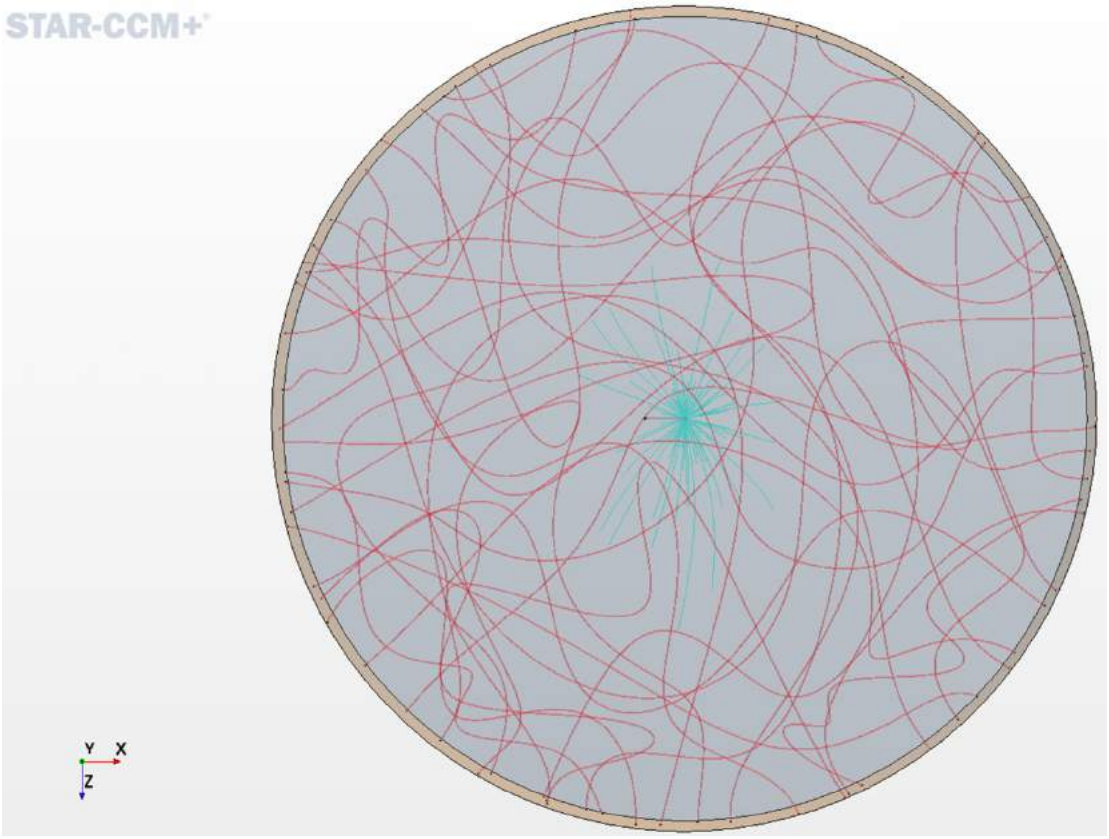

(a)

(b)

Figure 57. Average drug dispersion from cannula for 6 mm tissue and 45° cannula (a) top view (b) side view.

have a more broad and straight path dispersion into the adipose tissue. The drug dispersion was noted to not reach a point in which the muscular layer influences the dispersion pattern to flow parallel to the lower tissue boundary in these thicker tissue domains.

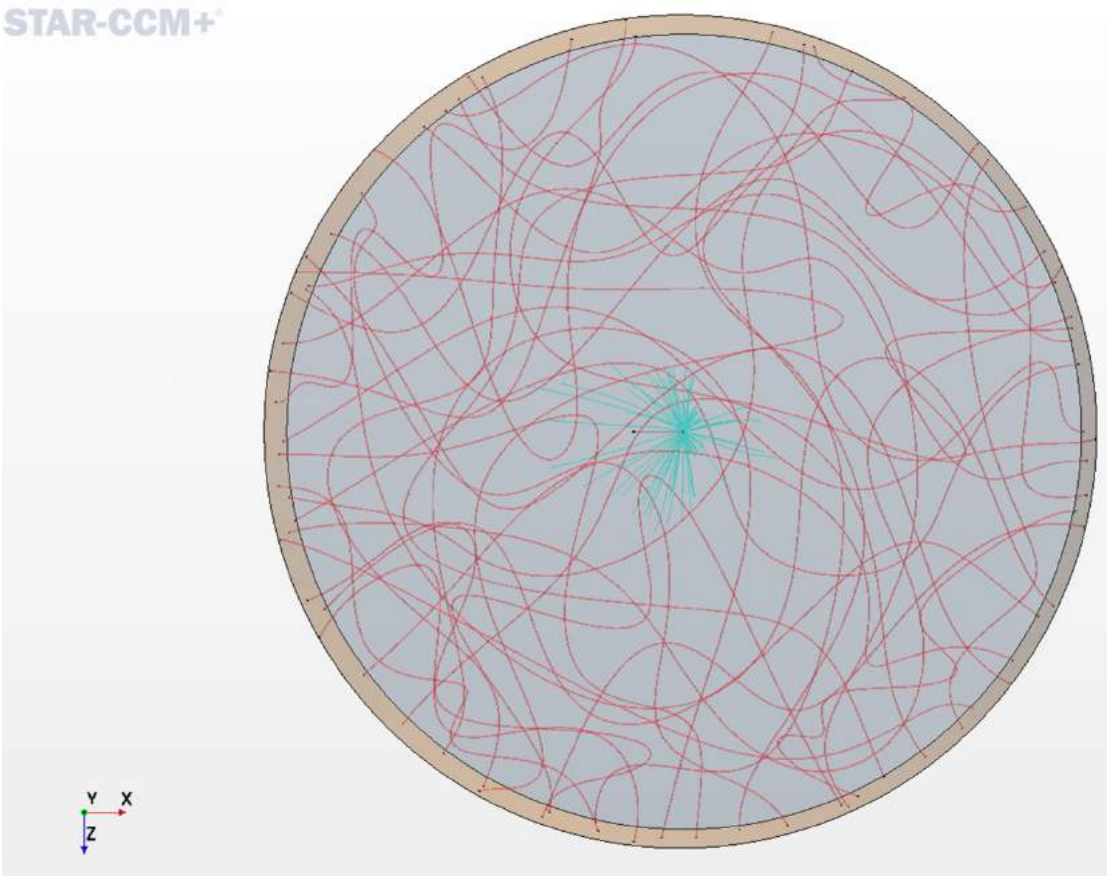

(a)

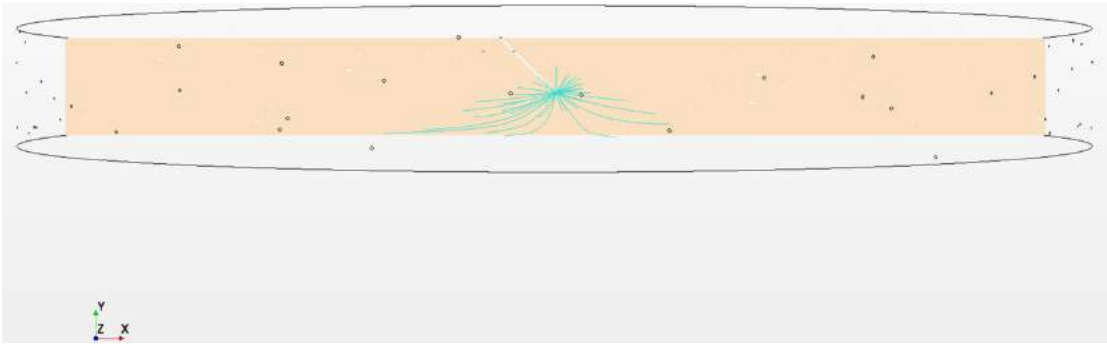

(b)

Figure 58. Average drug dispersion from cannula for 12 mm tissue and 45° cannula (a) top view (b) side view.

9.3 30° x 13 mm Lg. Cannula

Considering the cases in which the cannula was inserted at 30° and had a length of 13 mm, the observed insulin dispersion pattern across each of the tissue thickness domain was very similar.

From the top view, it could be seen that each of dispersion patterns was semi elliptical in shape with its major axis in the z-direction, as shown by Figure 59 and 60 as well as the additional figures in Appendix F.

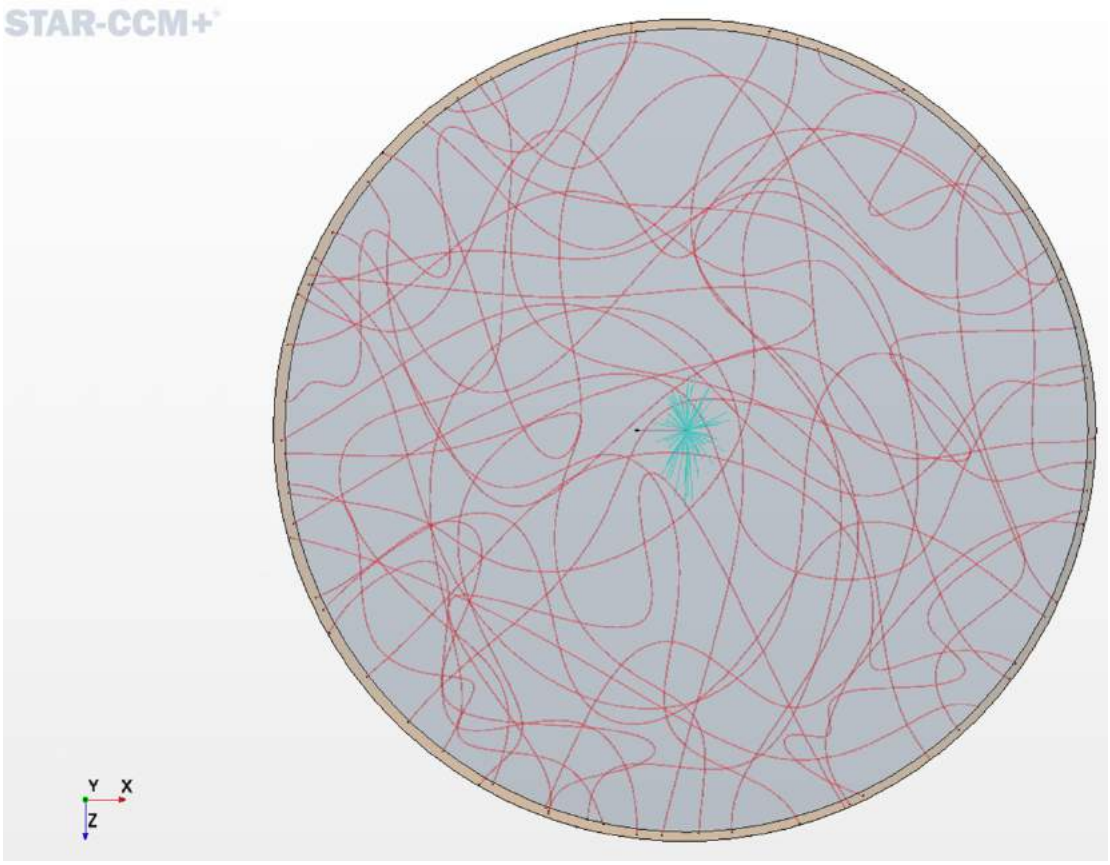

(a)

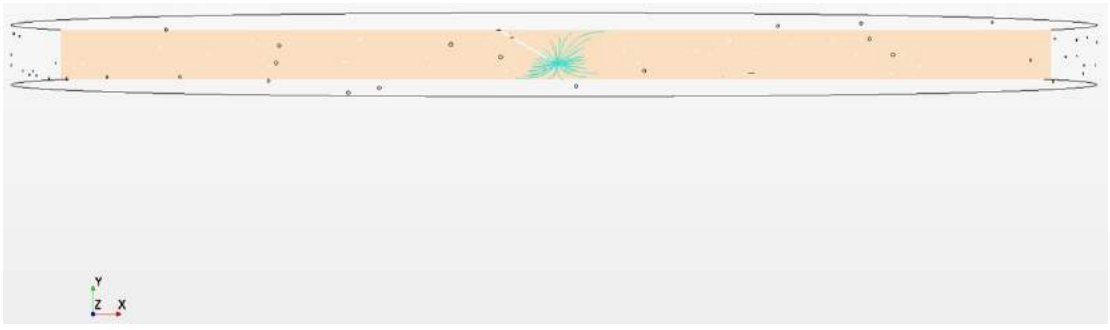

(b)

Figure 59. Average drug dispersion from cannula for 6 mm tissue and 30° cannula (a) top view (b) side view.

(a)

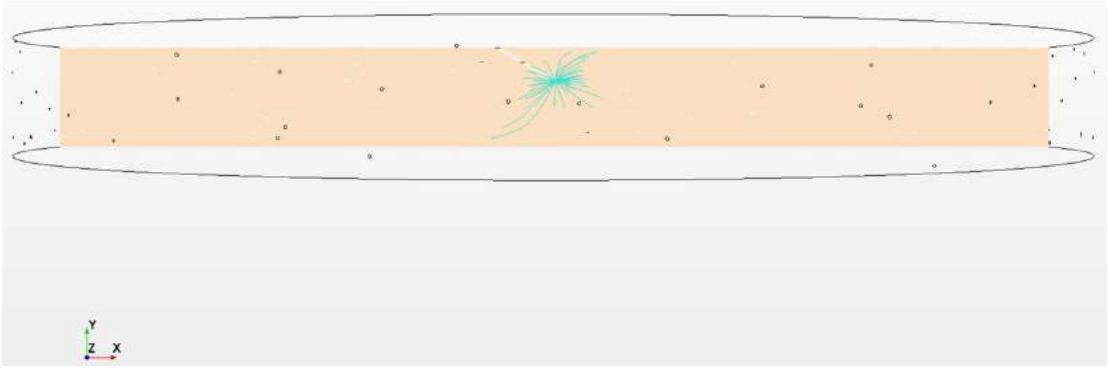

(b)

Figure 60. Average drug dispersion from cannula for 12 mm tissue and 30° cannula (a) top view (b) side view.

In the side view, the x-y plane the dispersion pattern was very similar in each of the tissue thickness domains also. The 6 mm domain did show a slight variance with a larger segment of insulin dispersion going above the cannula outlet compared to below, but this could be attributed to the domain thickness constraint on the dispersion, as seen in Figure 59. A smaller planer area of

dispersion was also observed in the 6 mm tissue domain compared to the thicker adipose tissue models, as shown in the top views of the figures above.

9.4 20° x 13 mm Lg. Cannula

The modeled insulin dispersion after delivery through a 20° x 13 mm long cannula matched each other even more closely across the five tissue domains than previous case sets. It can be seen in Figure 60, 62, and the additional figures in Appendix F that the insulin dispersion pattern in the transverse plane was not notably different from one tissue domain to the next. A semi-elliptical dispersion pattern was again noticed in the top view with a longitudinal axis in the z-direction. The side profile of the dispersion pattern also had a circular shape to it and extends toward both the upper dermis layer and the lower muscular layer of the domain in each of the tissue thicknesses.

(a)

Figure 61. Average drug dispersion from cannula for 6 mm tissue and 20° x 13 mm Lg. cannula (a) top view.

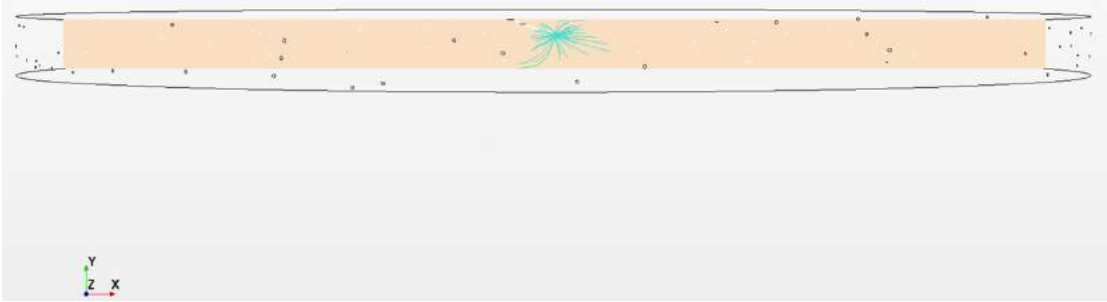

(b)

Figure 61 cont. Average drug dispersion from cannula for 6 mm tissue and 20° x 13 mm Lg. cannula (b) side view.

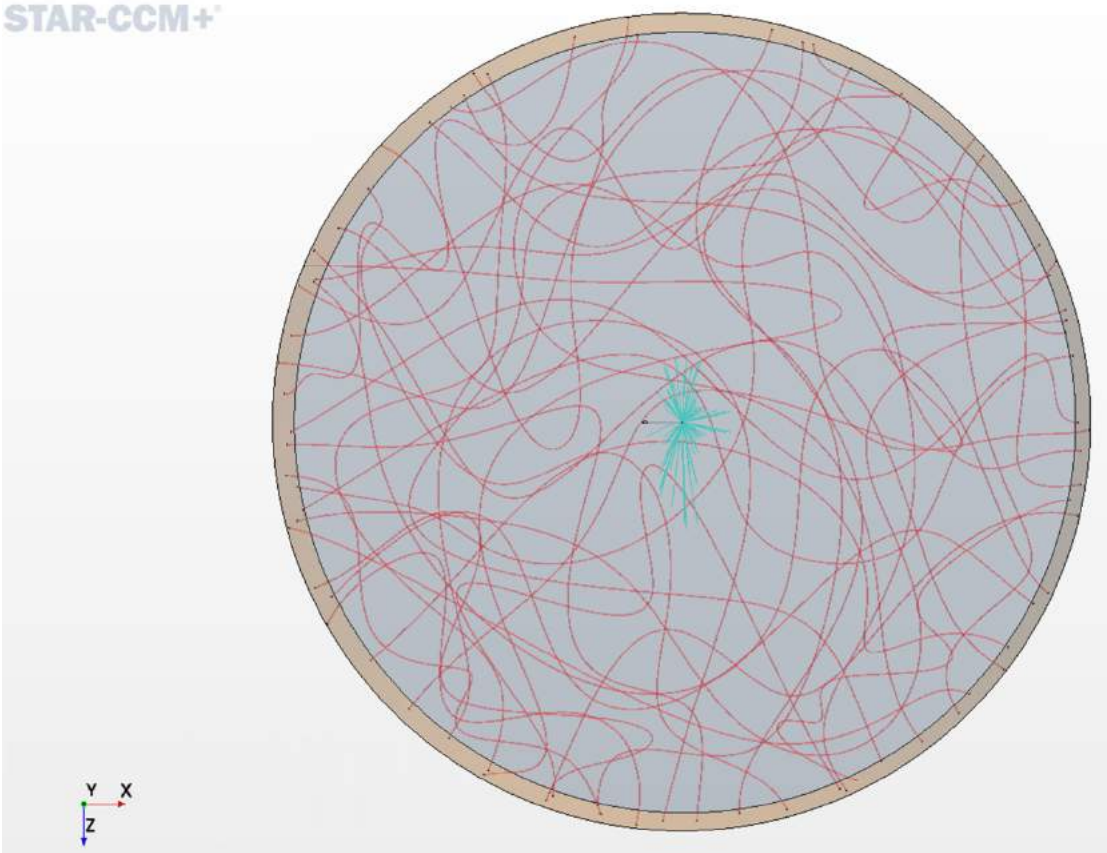

(a)

Figure 62. Average drug dispersion from cannula for 12 mm tissue and 20° x 13 mm Lg. cannula (a) top view.

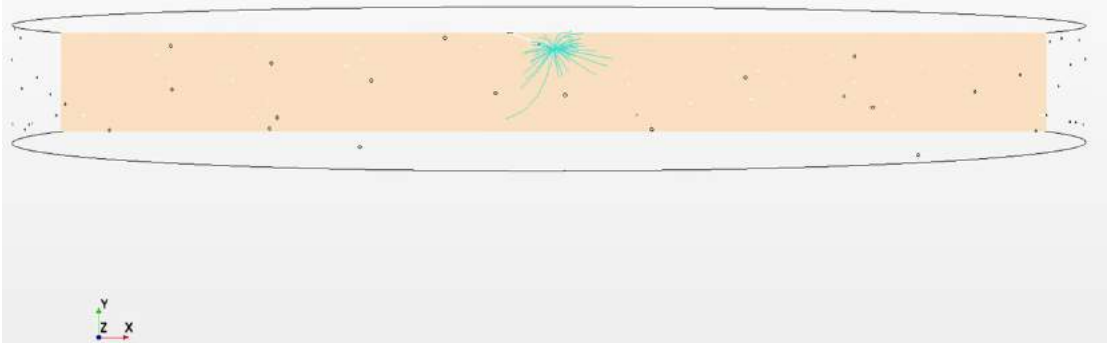

(b)

Figure 62 cont. Average drug dispersion from cannula for 12 mm tissue and 20° x 13 mm Lg. cannula (b) side view.

9.5 20° x 17 mm Lg. Cannula

The modeled insulin dispersion for the cases in which a cannula of 17 mm long and insertion angle of 20° was used also had a very similar dispersion pattern to each other in each tissue thickness considered. It can be seen in Figure 63, 64, and the additional figures in Appendix F that the insulin dispersion pattern was observed to be very similar in shape with respect to the transverse direction of the domains, with the 6 mm tissue domain having a slightly smaller longitudinal elliptical axis length than the thicker tissue domains. the different tissue domains. The side profile of the dispersion pattern also was very similar, with a slight variation noted in the 6 mm tissue thickness as it reached the muscular layer of the domain while the thicker adipose tissue models were unobstructed by this boundary.

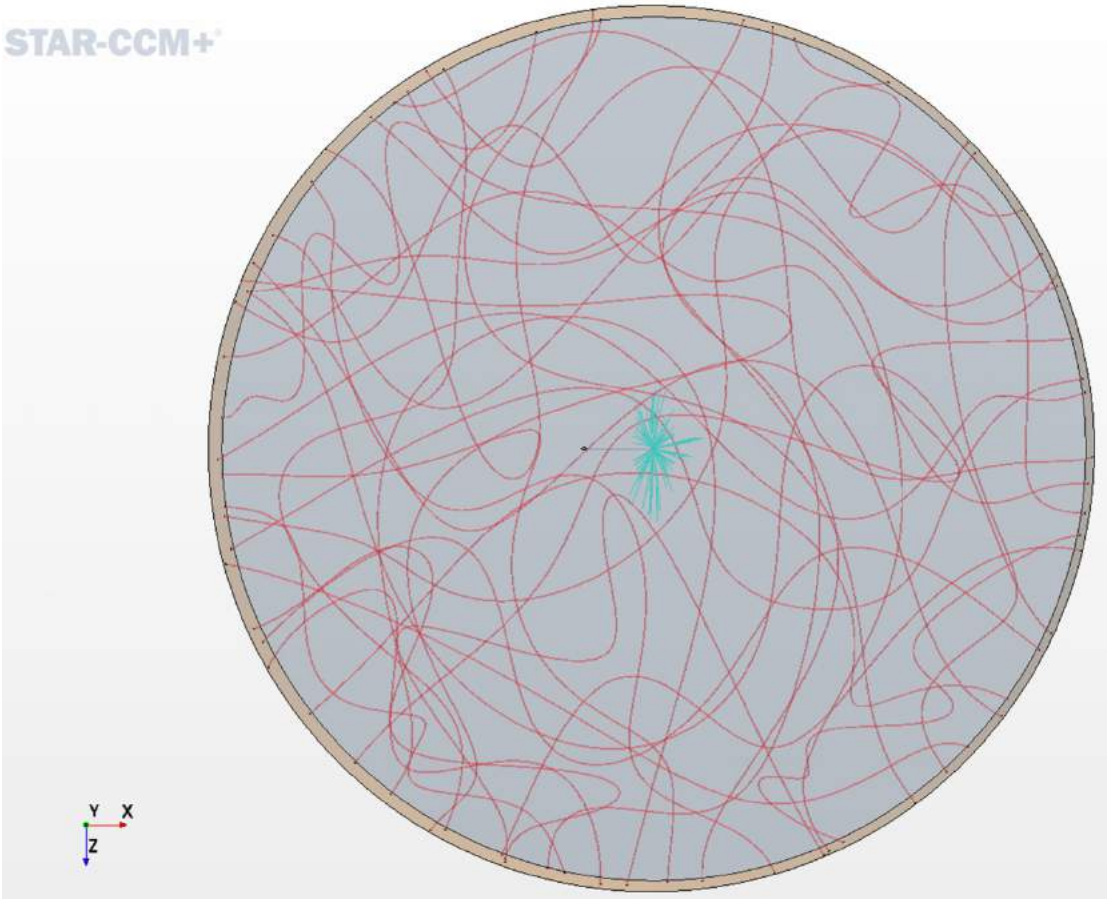

(a)

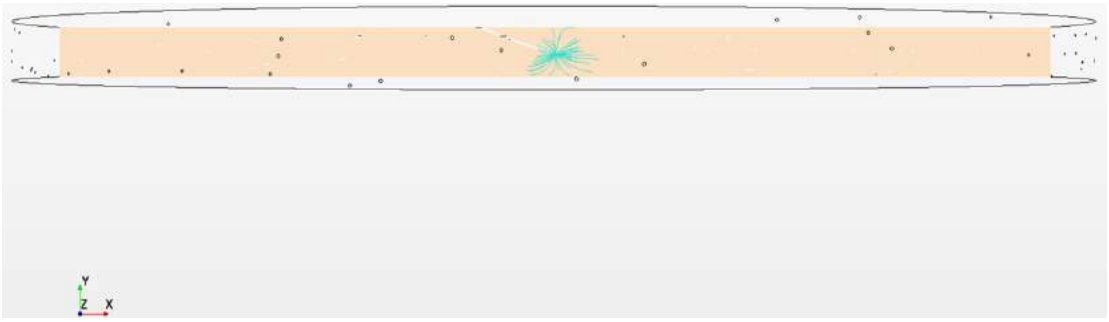

(b)

Figure 63. Average drug dispersion from cannula for 6 mm tissue and 20° x 17 mm Lg. cannula (a) top view (b) side view.

(a)

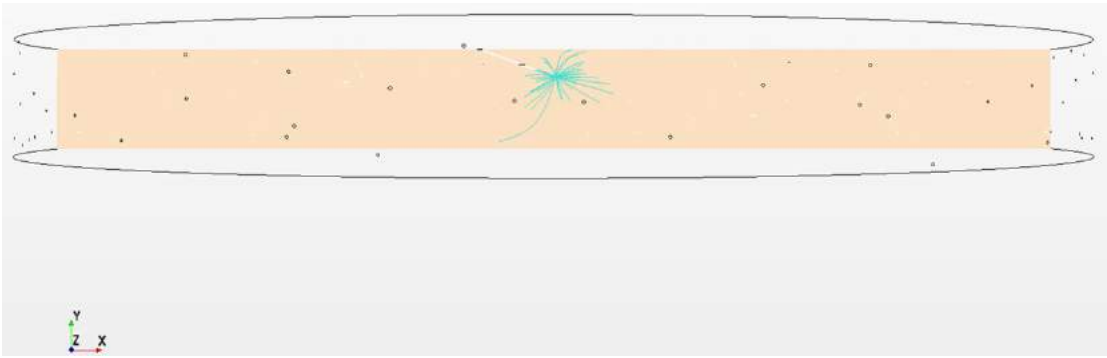

(b)

Figure 64. Average drug dispersion from cannula for 12 mm tissue and 20° x 17 mm Lg. cannula (a) top view (b) side view.

9.6 Cross Case Set Analysis

Considering the dispersion patterns observed across the five case sets of cannula geometries, several noted insulin dispersion differences across the domains were a direct result of the cannula geometry and the tissue thickness. First, it was generally seen that the lower the

insertion angle of the cannula, the lower the dispersion in the x-z plane of the tissue. Adding to this, as the insertion angle decreased the density of the flow in the x-direction of the domain decreased as well. These dispersion trends were observed from the 45° insertion angle proceeding down to the 20° insertion angle.

It was observed when comparing across the cannula geometry sets that the 90° and 45° insertion angles resulted in unique insulin dispersion, but once the cannula had an insertion angle of 30° or below, the insulin dispersion was very similar between the angles of insertion. This can be seen by how closely the 30° and 20° insertion angle results match each other, being almost indiscernible when compared, such as in Figures 60 and 62 respectively. The 90° insertion cannula and 45° insertion cannula both were shown to have a more uniform distribution of insulin dispersion around the cannula as well as greater outreach of the dispersion.

It was also noted when comparing the two cannula lengths of 13 mm and 17 mm inserted at an angle of 20°, the 17 mm cannula was found to generate a greater insulin distribution compared to the 13 mm cannula. This can be seen by comparing Figure 62 and 64, where the 13 mm cannula dispersion appears to be limited by its close proximity to the dermis boundary of the adipose tissue region. Further detailed analysis of these results obtained from the developed CFD model can be found in Chapter 10.

10. Research Outcome Analysis

From the observations made as the flow of insulin moves from the end for the infusion cannula to dispersing in the tissue, there were various larger trends that were found that can be applied to current understanding of insulin pump therapy. Further, these trends can be applied to current insulin therapy methods to indicate what further developments could improve treatment as well as standardize insulin delivery across the various anatomical conditions faced by patients.

10.1 Thin Adipose Tissue

The biggest observation through this study was that the constant case that had the largest effect on the insulin delivery as well as the greatest variability from cannula geometry to cannula geometry was the thin 6 mm adipose tissue domain. One of the notable causes of this due to the infusion set cannula geometry was the proximity of the outlet to the muscular boundary. This was largely displayed in the results of the 90° x 8 mm long cannula and 45° x 13 mm long cannula delivery insulin into the 6 mm tissue domain. With the insulin being infused very close to a solid boundary, there was little volume in the negative y-direction to be filled. Therefore, the only volume for the insulin to disperse to after leaving the cannula was out around the point of infusion in the x-z plane and above the point of infusion.

Throughout the study the thin adipose region was shown to affect even the flow directly out of the cannula at the micro scale. It was also largely observed in the formation of the insulin depot, and further by the large dispersion area of the insulin. Previous research in insulin delivery suggested that the hydraulic pressure dictated how insulin dispersed in the transverse direction before the interstitial pressure was great enough for the insulin to permeate the extracellular layer [26]. The case of the 6 mm tissue domain presented an extreme example of this phenomenon with the injection area being so close to the upper and lower boundaries of the adipose subcutaneous space that hydraulic pressure required for fluid particle move vertically in the tissue subspace was very large, resulting in a more transverse dispersion.

10.2 Deposition and Dispersion

In addition to the noted observations of the thin tissue domain, the same hydraulic pressure induced distribution could be attributed as the cause for the pattern of deposition and dispersion

noted in comparing the different cannula geometry cases. Even though the transverse direction had a greater porosity, as the cannula insertion angle decreased, the insulin diffusion trended to penetrate deeper into the tissue and not radiate out as much transversely. This would likely come from the fact that although the x and z directions had a greater porosity, when the cannula was directing insulin primarily in the positive x-direction of the domain, a greater flow resistance was induced within the medium in this direction compared to the other directions. The localized hydraulic pressure induced by the continuous flux of insulin in the x-direction could have resulted in the path of least resistance for the insulin to spread in the tissue to be the positive or negative z-direction and even down in the less porous y-direction over the higher-resistant positive x-direction. This phenomenon was even observed in the flow development directly out of the cannula end, as shown in Chapter 7. This observation would agree with previous subcutaneous infusion research that attributed the higher transverse spread of the drug to the medium flow resistance and porosity of the tissue around the site [26].

What should be noted here though is that although this trend was observed in this study, this would have to be confirmed with further study in tissue porosity and permeability and how the different cannula angles would affect ex vivo insulin deposition and dispersion. The previous studies only considered variations of a 90° insertion angle cannula, and therefore, the modeled directionally varied porosity of the tissue was based off these results [26, 46]. The way in which the current study modeled the anisotropic nature of the adipose tissue due to the extracellular matrix was most accurate manner based upon the very minimal information about this region available. Therefore, it is unclear how a lower angled infusion cannula effects the overall deposition and dispersion of the insulin in actual biologic adipose tissue. The observed results are viable though by the current understanding of porous media modeling, the hydraulic nature of drug diffusion previously observed in studies, as well as the verification of the model as discussed in Chapter 6 [3, 5, 11, 21, 23, 25, 26, 54].

Another factor not previously discussed was the observation that in the thin tissue samples, such as the 6 mm and often the 12 mm domain, the delivery was near the bottom or center of the tissue depth. In the case of the thicker tissues though, this deposition area was very high in the adipose region, especially when considering the low insertion angle cannulas. The overall dispersion pattern was similar to thinner adipose tissue domains being considered, but there was a drastic difference in the relative location within the tissue where the depot and dispersion fell.

Although this did not have significance in the case of how the deposition and dispersion occurred, this would likely have greater implications for actual insulin absorption.

10.3 Applications for Understanding Insulin Delivery

Based on these results, several applications concerning current insulin delivery dynamics using pump therapy were able to be drawn. First, concerning insulin delivery in lean patients, it could be concluded that the cannula geometry has a significant effect on insulin deposition and dispersion in the adipose tissue. One indication of this would be the impact observed on the insulin depot size as well as dispersion out into the adipose subspace when the cannula geometry was varied in the study. As the drug requires contact with capillaries to be absorbed into the blood stream and ultimately used by the body physiologically, the shape and size the insulin flows during infusion would be crucial to delivery effectiveness. Therefore, applying this practically, being able to achieve a larger volume of insulin deposition and a larger area of dispersion would ultimately result in more effective administration of the insulin as the drug would be in contact with a greater number of these capillaries. Further, as previously stated in published research, the longer the drug is in the extracellular area of the adipose tissue, the higher the chance of localized factors that impact the drug molecules and tissue itself, resulting in variable kinetics of the insulin [5, 16, 23].

A further application related insulin absorption from the current study results would be related to the fact that thicker tissue has been found to be a less vascularly dense tissue [53]. Therefore, this would be of great significance, as the lower infusion angle cannulas produced an almost identical diffusion pattern across each of the tissue thicknesses considered. If the thicker tissue had a lower vascular density, as was assumed by the model, but the same diffusion of insulin as a thinner adipose tissue sample, the kinetics of absorption for the insulin would be drastically different between the two tissues. This would add additional significance to the fact that cannula geometry plays a significant role in insulin deposition and dispersion. It does also facilitate that the cannula geometry and the tissue thickness do have a dependent relationship, as was able to be shown in the statistical metrics of the lean tissue in this study.

This application relating the dispersion characteristics of insulin due to low insertion angle cannulas and vascularization in different thickness adipose regions could be applied to a single patient's anatomy also. Previous research showed that the regions of the body suitable for insulin delivery could have varied thickness even within an individual [48-50]. Therefore, applying the

previous discussion about the absorption in different tissue thickness related to diffusion and vascularization, and overal insulin absorption, it could be concluded that using one cannula geometry in different anatomical regions could result in variable insulin kinematics within a single patient. This application is critical, because the treatment of Type 1 Diabetes relies upon the observations of blood glucose trends over time, whether manually adjusting insulin rates or using an autonomous system to maintain blood glucose homeostasis. The implication of this on autonomous pump therapy would be that precise insulin requirements for even an individual patient would not be easily achieved due to varied insulin kinematics from day to day due to infusion site rotation. Autonomous pump systems base insulin requirements off days to even weeks of average insulin use and the resulting blood glucose control. This indicates blood glucose homeostatic balance would be greatly affected by varied insulin kinetics across the anatomic tissue regions across the patient varied insulin kinetics within the adipose tissue, even when using a close loop pump system. A further factor of this also would be that the thinner tissue and different anatomical regions would be more likely to have dispersion affected by a "massaging" effect due to the movement of the muscle below the adipose tissue. Based on the previous ex vivo research, this would affect the insulin depot and dispersion causing the drug to spread farther out transversely in the tissue, in turn being an additional factor affecting the absorption kinetics [26]. Therefore, it would be necessary to develop a system to limit absorption variable across single patient anatomical regions, whether that be using specific cannula geometries employed in specific regions or another method.

Finally, in relation to observation made throughout this study and the actual insulin absorption kinetics into the capillaries, it could be concluded there may be an effect on how the different cannula geometries and tissue thicknesses affect this physiological function. As previously described, the interstitial fluid is always flowing, as driven by capillary exchange into and out of the extracellular space around the adipocytes [27-35]. The exchange is facilitated through the oncotic pressure differential between the intra-capillary region and the extracellular adipose regions [27, 28]. Understanding this, there is a possibility that this kinetic exchange would be affected by the pressure induced through the injection of insulin into the region that is already saturated with fluid. Further, the combination of the different cannula geometries and tissue thicknesses was shown to induce a different localized pressure area (noted as the insulin depot) depending on the cannula and tissue combination, as shown Chapter 8. Therefore, further research

to study if this localized pressure disturbance in the tissue due to insulin delivery affects this physiologic interchange, and what implication that may have for insulin delivery would be a warranted area of research.

Overall, the development of the CFD model of insulin delivery into the adipose region and the results obtained through this study in conjunction with previous research indicated there is a need for further research in this area subcutaneous drug delivery. It was shown that the cannula design in relation to the anatomical variations of adipose tissue did produce significantly different results, that would, even based on a simplified understanding of insulin kinetics, have a large effect on insulin delivery in the treatment of Type 1 Diabetes. These results further validated previous research studies that also called for an action to better understand infusion set delivery and insulin kinetics, indicating it was one of the weak points of current pump delivery systems [8, 14, 20]. Considering autonomous insulin pumps are already used in insulin therapy, this study provided evidence that a further understanding the delivery mechanics of insulin in relation to the pump cannula and tissue interface should be a priority in order to improve individualized Type 1 Diabetes management.

11. Conclusion

Drug delivery could be said to be one of the most important components of medical treatments, as it requires the ability to achieve the desired target response, but at the same time reduce the possibility for any adverse ramifications. An additional component to this is the patient quality of life during treatment, which has a large importance in chronic conditions such as Type 1 Diabetes. The current state of the art systems for insulin administration includes insulin infusion pumps continuously into the adipose tissue between the dermis and muscular layers used in conjunction with continuous glucose monitors to achieve a closed loop insulin infusion system for more precise control of patient blood glucose levels by delivery the drug.

Given the importance of the nature of especially accurate and predicable drug delivery, high variability of insulin delivery even within a single patient has been identified in research. Influential factors such as physiologic and biologic functions, adipose tissue anatomy, and the infusion set design have all been factors identified as creating this variability. Little research has indicated the effect each of these factors may have on insulin delivery though. Utilization of technology such as computational fluid dynamics (CFD) model can lead the way in the study of these factors' effects on the kinetics of insulin within the adipose tissue domain.

In studying previously published research in the areas around subcutaneous drug delivery, insulin and other drug kinetics, fluid flow in biologic tissue, and other areas relating to subcutaneous biology, it was evident there has been a large chasm between in vivo type research and computational models when it comes to drug delivery, especially regarding insulin infusion. The literary research indicated a CFD model could be designed to simulate the interstitial fluid flow in adipose tissue induced by capillary exchange. Further, previously developed models provided useful insight into modeling biological tissue as a porous medium and obtain accurate results from this assumption about biological tissue. Additionally, other published research provided crucial insight into the unique characteristics of adipose tissue, such as its extracellular matrix, required to create such a model. From this research, a study using computational models in the area of insulin delivery was able to be designed.

A porous media CFD model was able to be developed to model the adipose tissue environment with its interstitial fluid flow induced by capillary fluid exchange within the subspace. The anisotropic nature of the domain was modeled using previously published observations from biologic tissue through the application of the Ergun equation. Insulin delivery was incorporated

into the model, and its accuracy was verified using previously published ex vivo research on insulin infusion in both a time-dependent and steady state scenario. The recreation of this published ex vivo insulin delivery study using the developed CFD model yielded very similar results to the original published study insulin depot.

The current study was designed to analyze the effect of both cannula geometry and tissue thickness on the deposition and dispersion of insulin within the adipose tissue subcutaneous space. The five most common cannula geometry currently used in pump therapy and a range of adipose tissue thicknesses that encompasses the range from lean to obese patients were considered as the design variables. The cannula geometry varied in insertion angle from 90° to 20° and in length from 8 mm to 17 mm. The adipose tissue domains were the range of 6 mm to 30 mm. Each cannula design was studied in each tissue thickness to analyze the effect of these factors on insulin deposition and dispersion.

The results and analysis of these CFD models indicated that both the cannula geometry and the tissue thickness have a significant influence insulin deposition and dispersion. The cannula geometry was observed to impact the flow development directly from the cannula end. Further, in considering the insulin depot formation in the regards to the different tissue thickness and cannula geometries, it was found using an ANOVA two-factor statistical test, the tissue thickness and cannula geometry were of significance, in both the case of lean and obese adipose tissue. It was also observed that the length was not a significant factor in insulin depot development at a low insertion angle using a statistical t-test.

In addition, through graphical comparison of the dispersion pattern of the insulin in the adipose tissue using streamlines it was further shown that 6 mm adipose tissue thickness resulted in a much different dispersion pattern regarding higher insertion angle cannula geometries compared to the thicker tissue domains. It was observed for the lower insertion angles though the dispersion pattern of the insulin infused from the cannula was very similar between the different tissue thickness, only different according to the exact cannula design. Also, the results indicated that the shallower angle of insertion resulted in a lower level of dispersion in x-direction as well as a lower transverse propagation from the cannula outlet.

Therefore, through the analysis of these results coupled with the current understanding of adipose tissue physiology and adipose drug delivery kinetics, the conclusion first could be made that a CFD model is not only a viable way to study drug delivery, but also a valuable tool for

studying the delivery of drugs such as insulin. Further it was observed that both the tissue thickness and cannula design have a significant impact insulin deposition and dispersion in adipose tissue. It was also shown that a great variation in drug kinetic would be found in lean patients because of differing cannula designs on insulin delivery. Similarly, the results indicated a drastic difference would be observed in insulin absorption kinetics due to the variation of vascularization in lean versus thick adipose tissue with a low angle of infusion cannula.

Overall, the yielded results indicated that further research into the effect of two significant factors impacting delivery, cannula geometry and tissue thickness, is warranted. This is especially true considering new autonomous infusion pump require very predictable day to day insulin kinetics to improve blood glucose control rather than increase risk for dangerous blood glucose levels. Therefore, the CFD model was able to be used as a tool to better understand insulin kinetics, but this was just a first step in the direction of understanding and simulating insulin delivery to be able to predict individual patient kinetics. To reach such a level of individualize patient care though, this study proved a significant amount of research in both the parameterization of biological tissue anatomy and flow as well as further factors that influence insulin delivery must be studied. Through this additional research, the treatment of Type 1 Diabetes, and other treatments utilizing subcutaneous delivery could be greatly improved.

12. Future Work

Several areas of further study were able to be indicated by the results of this study. First, the completion of a singular case in the time dependent domain and simulate the delivery of insulin over an entire day period. This would include at least several insulin boluses as well as a continual basal insulin rate throughout the day. This type of study would be a first step in the direction of an individual patient simulator model that could better be used to tailor treatment plans to patients. This study would be also able to indicate how continuous infusion causes the infused drug concentration to grow and shrink depending on infusion rate and bolus size.

Further, characteristic parameters of adipose tissue require more study to increase the understanding of the biological environment and the computational modeling of such environments. The interstitial flow, for instance, could be studied as a factor that may influence the dispersion of the insulin within the tissue, especially in a time dependent domain. Another parameter that could be further investigated and quantified to improve CFD modeling would be the anisotropic effect of the adipose tissue on true biological tissue using different cannula geometries. This would allow for the anisotropic properties of the adipose tissue that influence insulin delivery to be more accurately modeled in the computational model domain for further insulin deposition study.

Additionally, another element of study would be the addition of muscular motion to the model, in order the better simulate the dynamic nature of the anatomic region the insulin is being delivered to. This would especially hold true in tissue on the legs where the muscle is constant motion during walking and physical activity. A study looking into this phenomenon would help to understand the kinetics of insulin in different anatomic regions of the body due to the tissue movement around the infusion site.

Finally, a similar CFD model or the refined CFD model could be used in the design of new cannula geometries. It could be used as a tool to prove the deposition and dispersion pattern, allowing for the ability to better predict the insulin deposition for ideal and consistent insulin kinetics. This allows for a very efficient way to trial new cannula designs as well as visualize how it may compare to another design in a very controlled tissue sample.

Appendix A: Mathematical Calculations

Unit conversion for IU/min to kg/s:

First, noting that 100 units of insulin (IU) are in 1 mL of drug solution, therefore one IU is:

$$1\ IU = \left(\frac{1\ mL}{100\ IU}\right) = 0.01\ mL$$

Then, converting this to time dependance, the unit of IU/min converted to mL/s would be:

$$1\frac{IU}{min} = \left(\frac{1\ mL}{100\ IU}\right)\left(\frac{1\ min}{60\ sec}\right) = 1.6667\ \times\ 10^{-4}\frac{mL}{s}$$

The density of the insulin drug solution is 1.005 g/mL [83], making the conversion from mL/s to kg/s as follows:

$$1.6667 \times\ 10^{-4}\frac{mL}{s} = \left(\frac{1.005\ g}{1\ mL}\right)\left(\frac{1\ kg}{1000\ g}\right) = 1.675 \times\ 10^{-7}\frac{kg}{s}$$

Therefore, 1 IU/min is $1.675 \times\ 10^{-7}$ kg/s.

Appendix B: Additional Model Development Figures

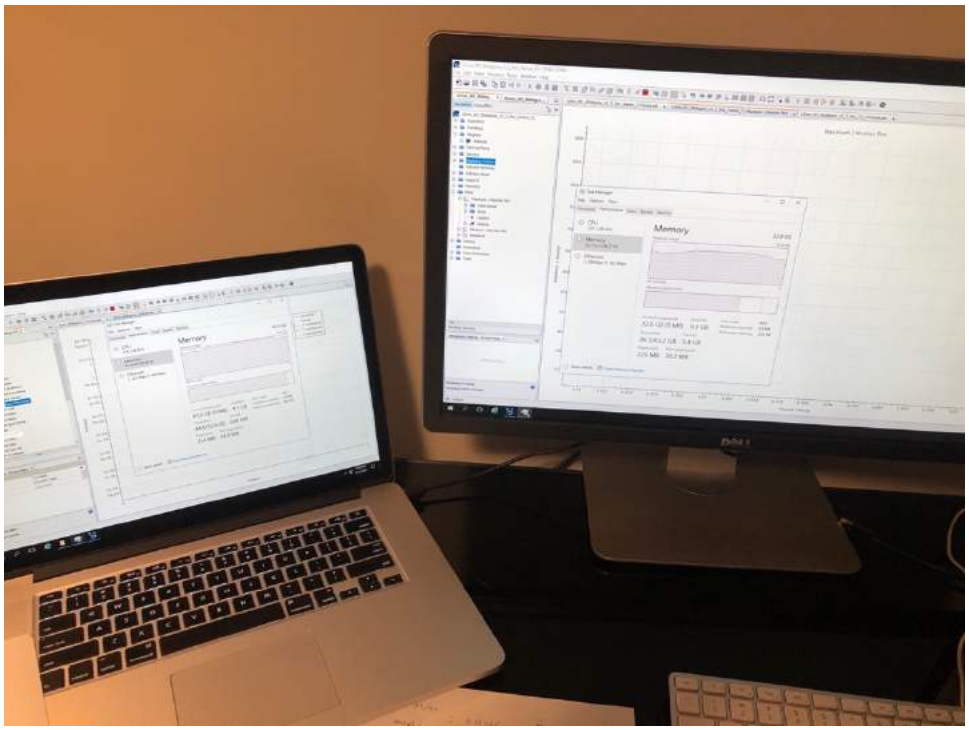

Figure B-1. Use case of maximum server power during case trial running (total of 64 GB of ram).

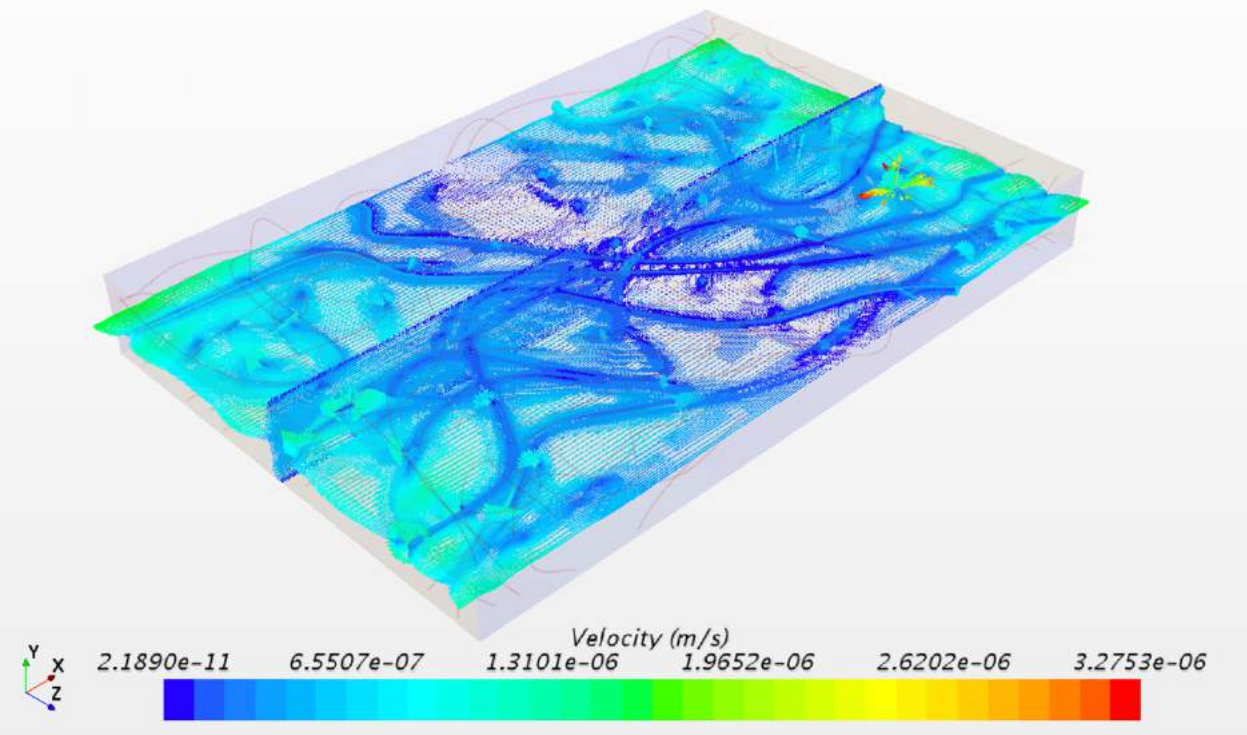

Figure B-1. Noted stagnation velocities created by capillary exchange linearized velocities.

Table B-2. Model cases requiring smaller relative minimum cell size.

Case (tissue thickness /cannula geometry)	Relative Minimum Size (% base)
18 mm/90° x 8 mm	0.3235
30 mm/90° x 8 mm	0.0324
30 mm/45° x 13 mm	0.0322
30 mm/30° x 13 mm	0.0324
18 mm/20° x 13 mm	0.0324
30 mm/20° x 17 mm	0.0323

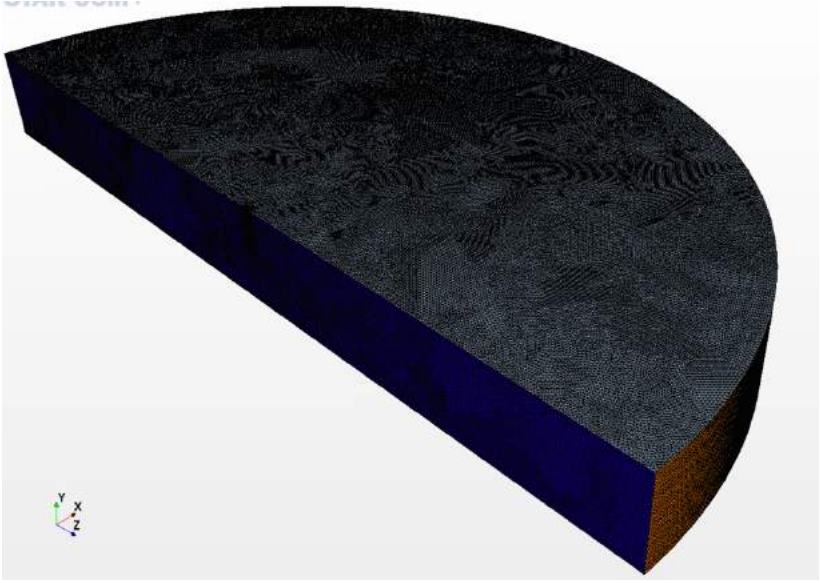

Figure B-2. Unsteady validation case domain surface mesh.

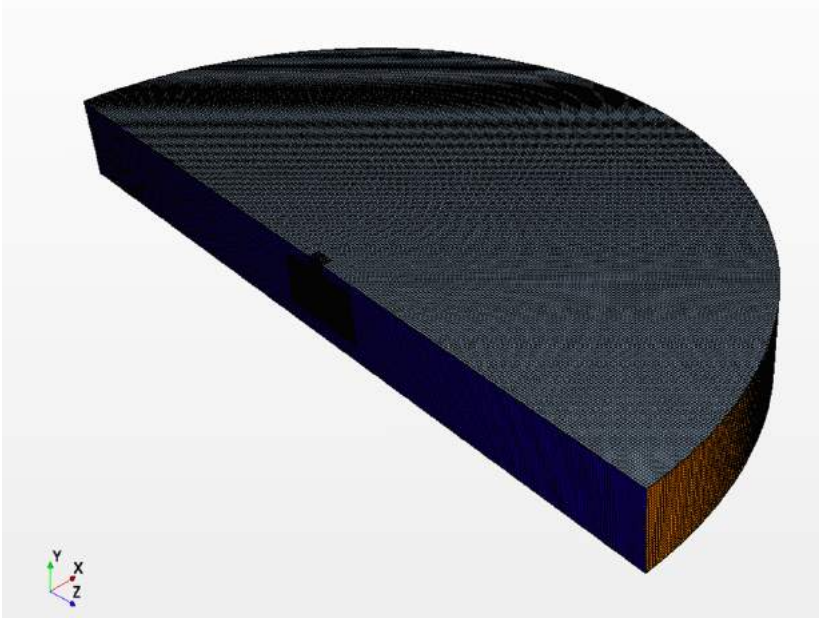

Figure B-3. Unsteady validation case domain outer volume mesh.

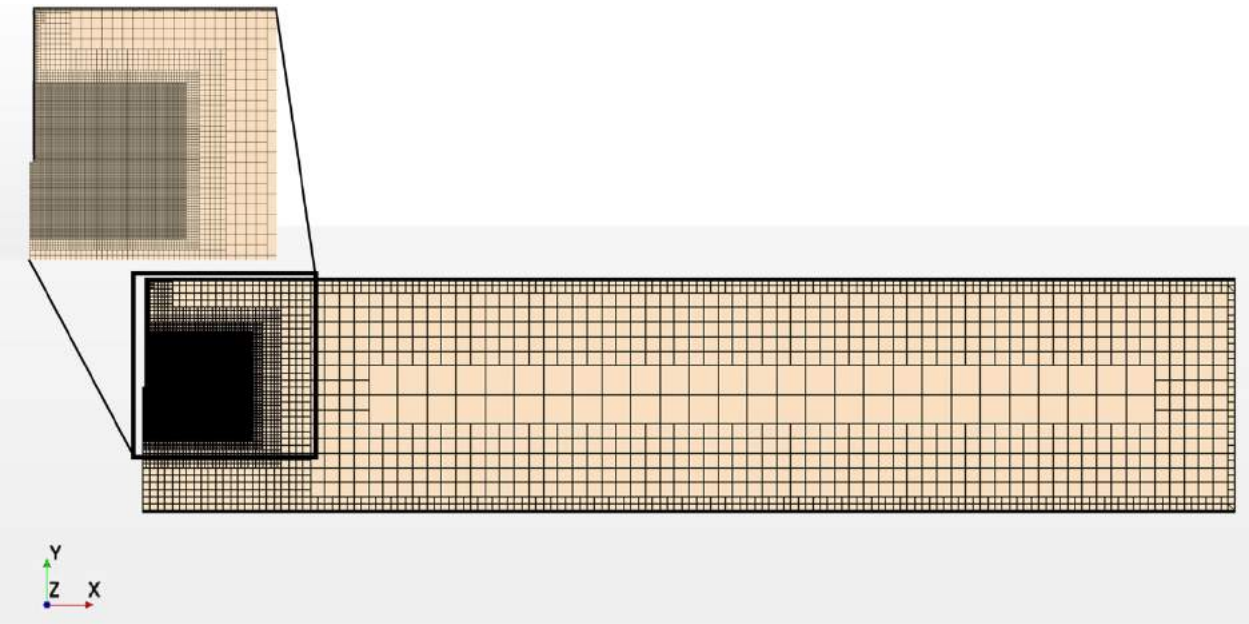

Figure B-4. Unsteady validation case domain interior volume mesh.

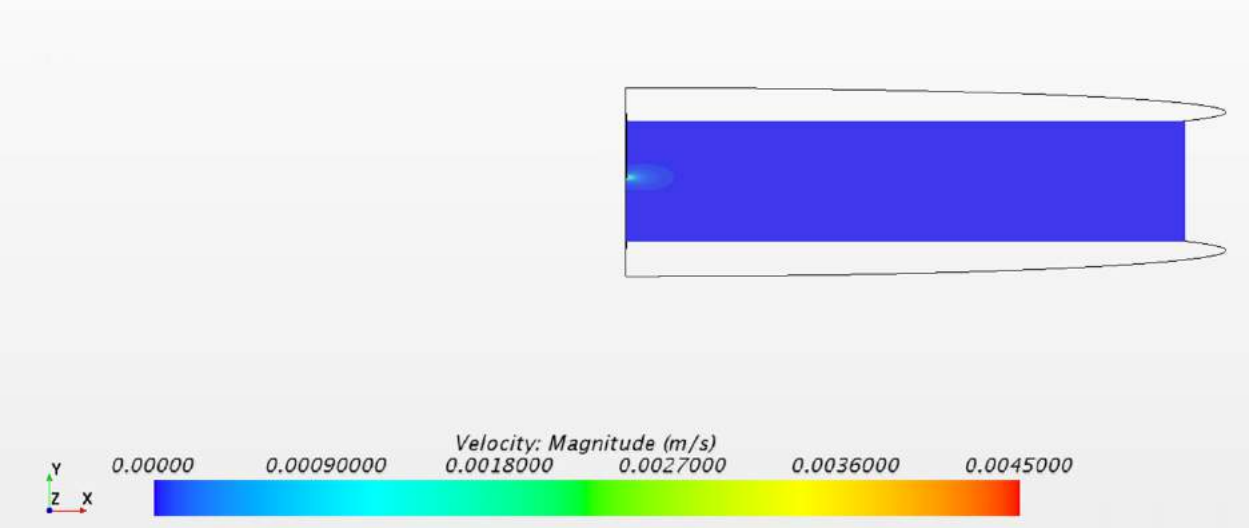

Figure B-5. Unsteady validation case domain interior volume mesh.

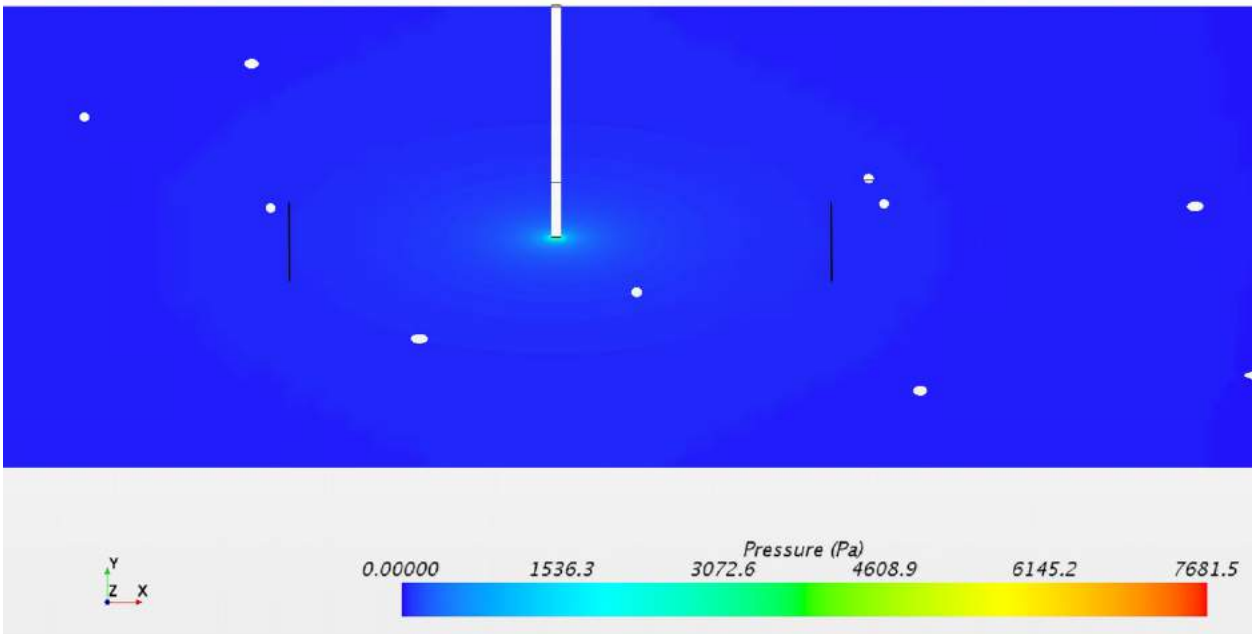

Figure B-6. Steady state validation case showing pressure contours around cannula outlet marking insulin depot.

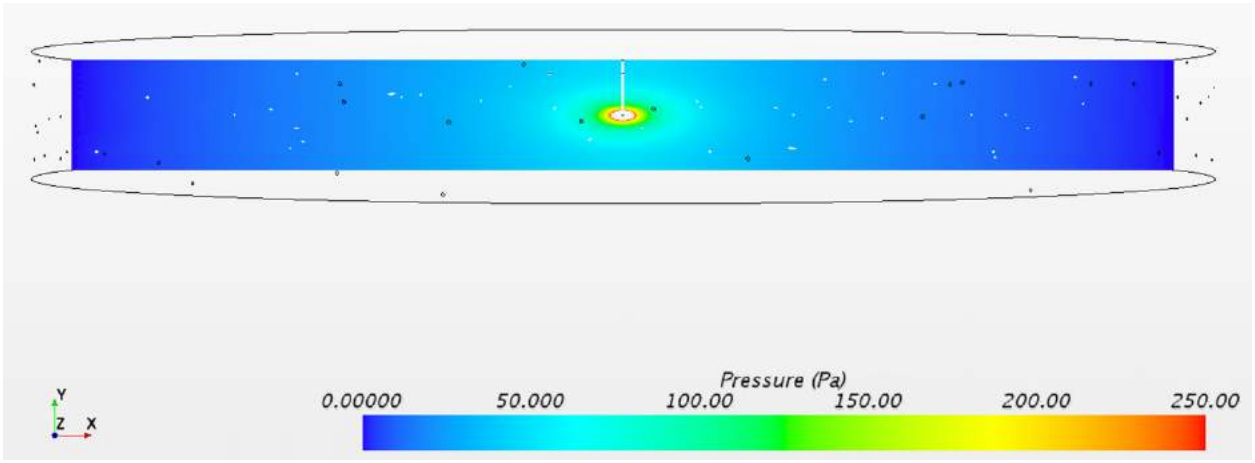

Figure B-7. Steady state validation case full domain side view.

Appendix C: Error Residuals for Cases

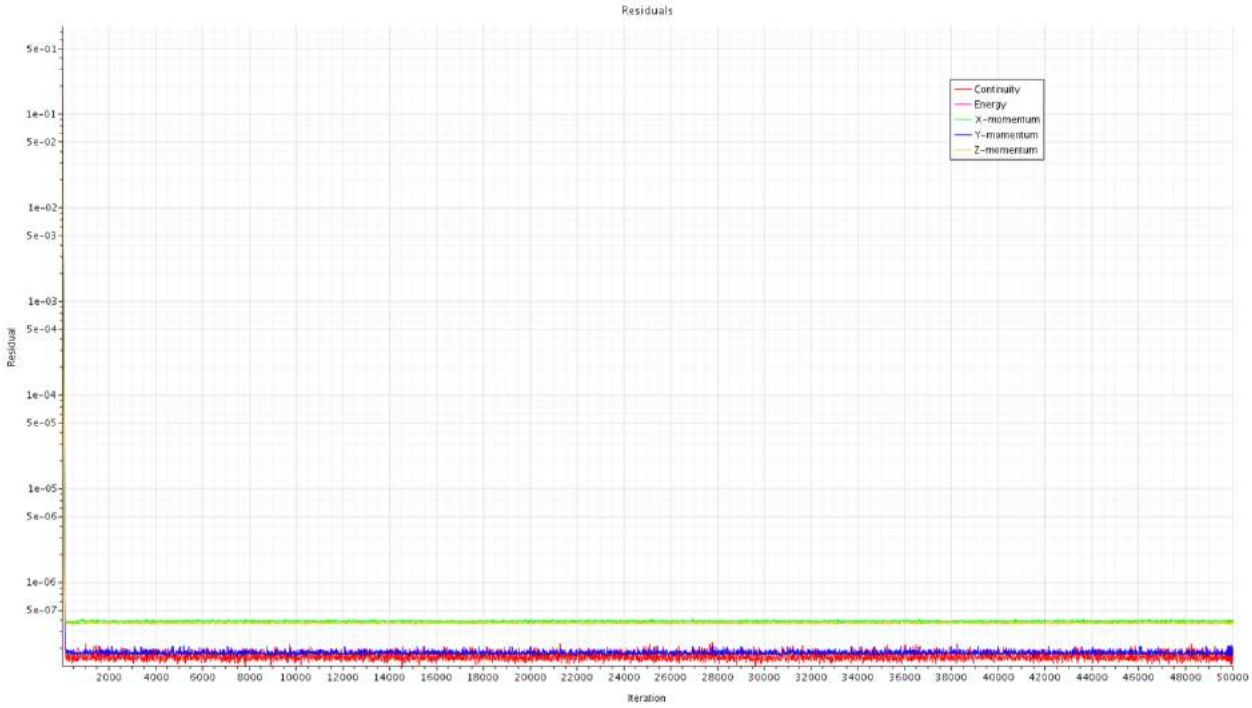

Figure C-1. Residuals error plot for implicit unsteady verification case.

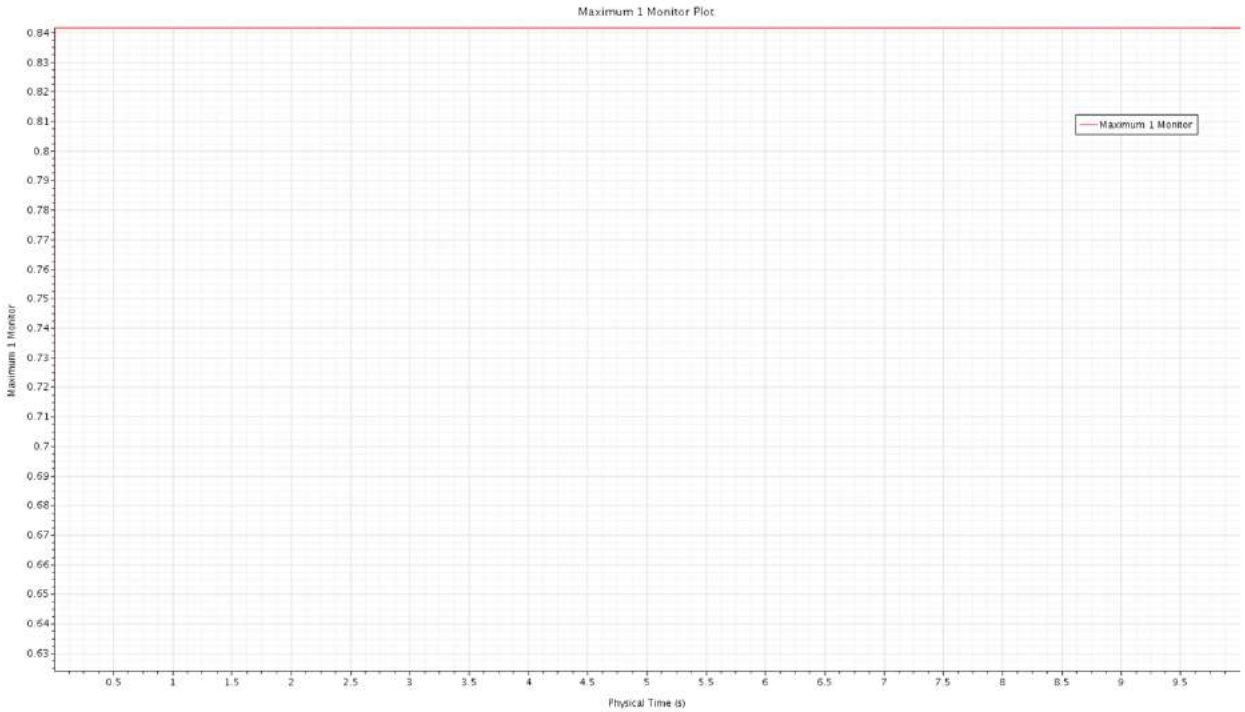

Figure C-2. Maximum Courant number plot for implicit unsteady verification case.

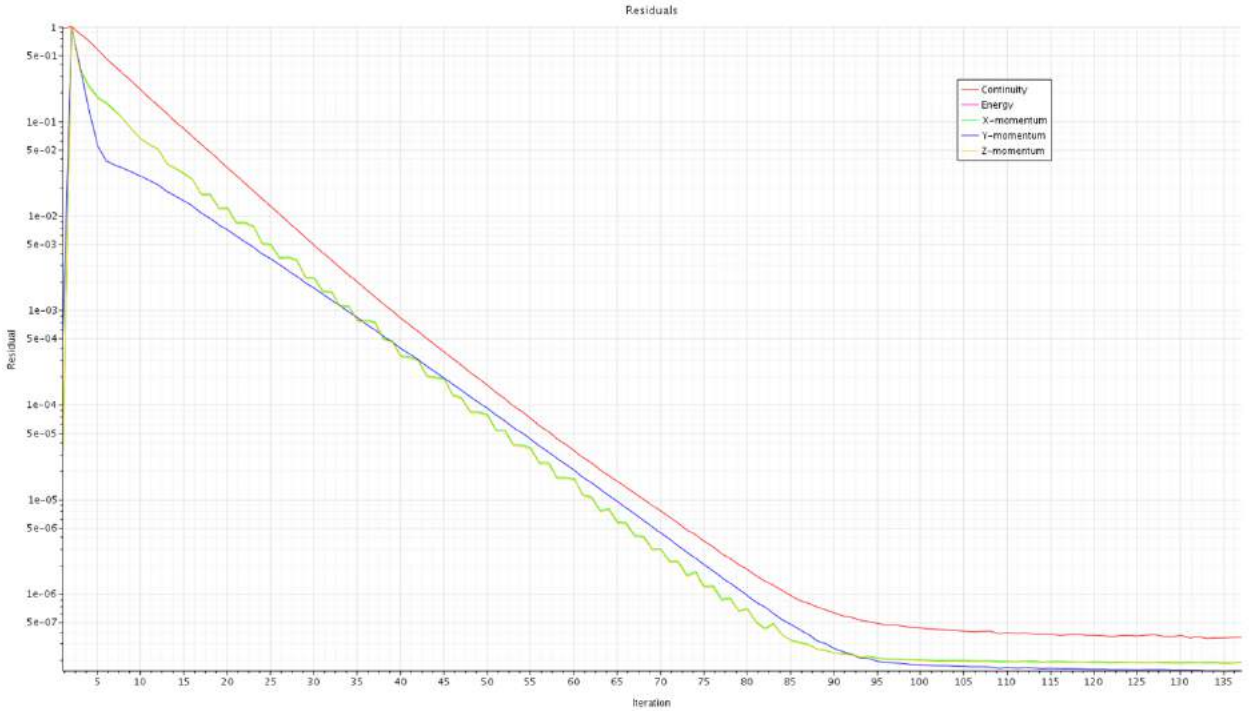

Figure C-3. Residuals error plot for steady state verification case.

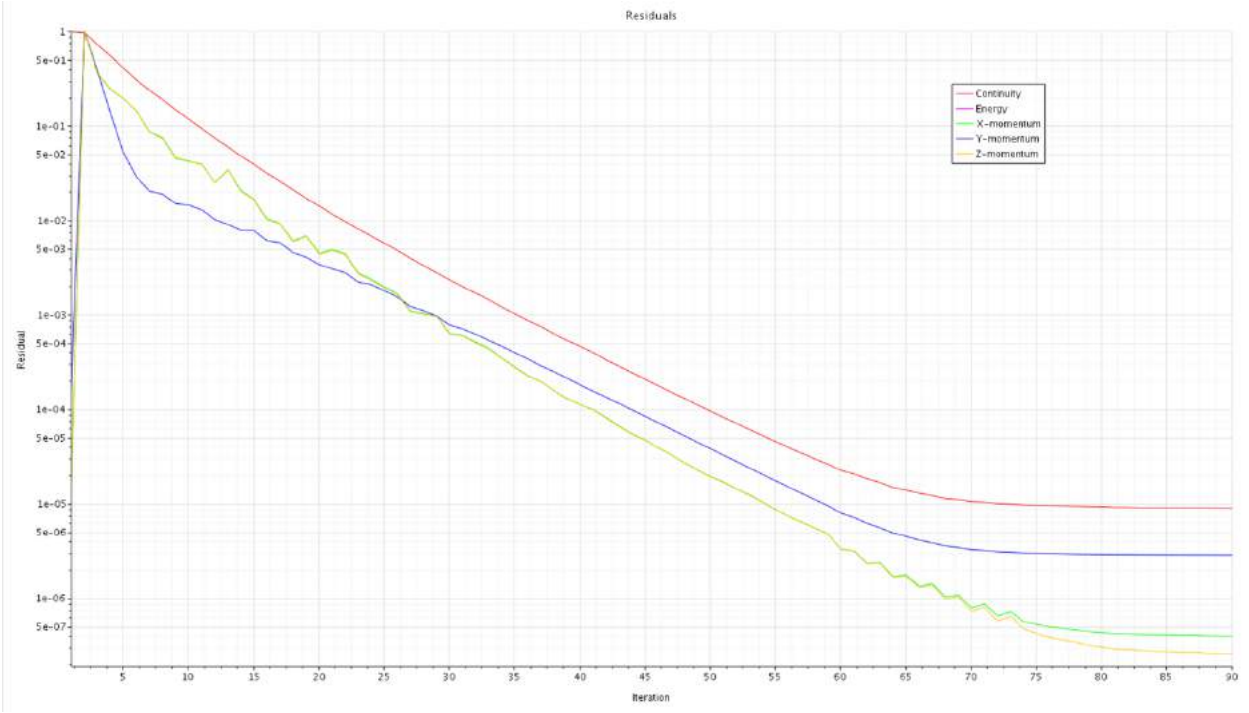

Figure C-4. Residuals error plot of 6 mm tissue with 90° x 8 mm Lg. cannula.

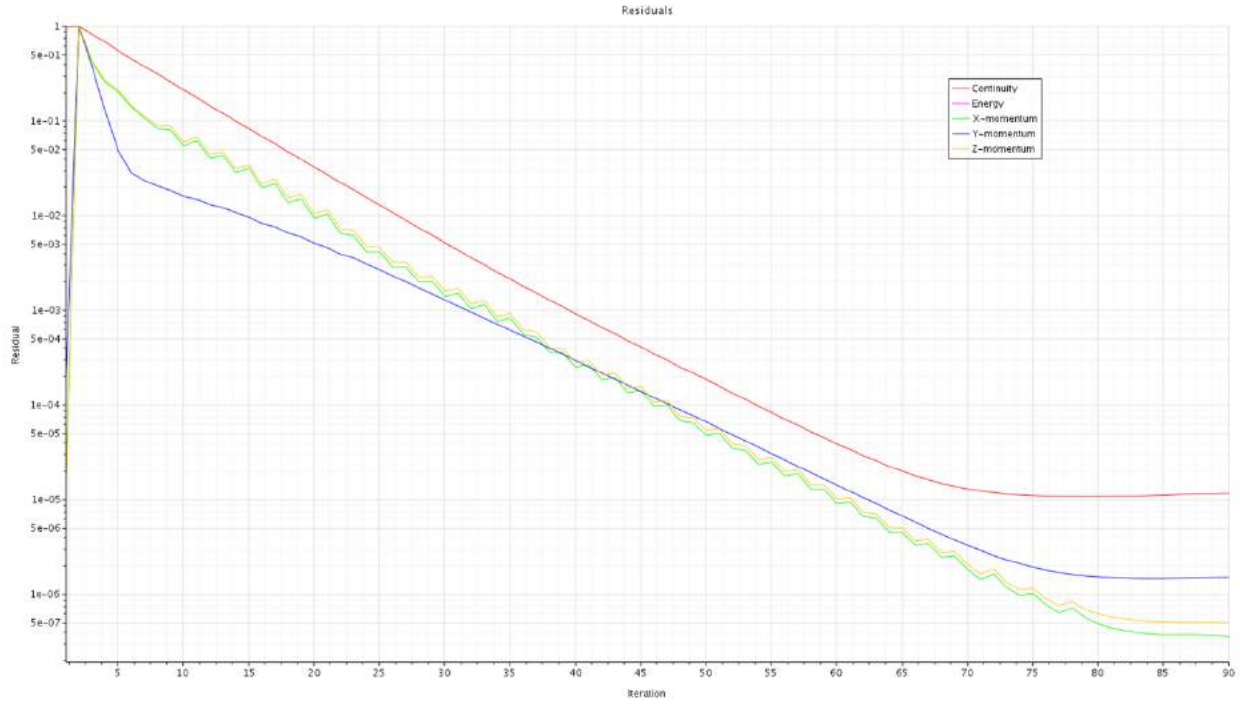

Figure C-5. Residuals error plot of 12 mm tissue with 90° x 8 mm Lg. cannula.

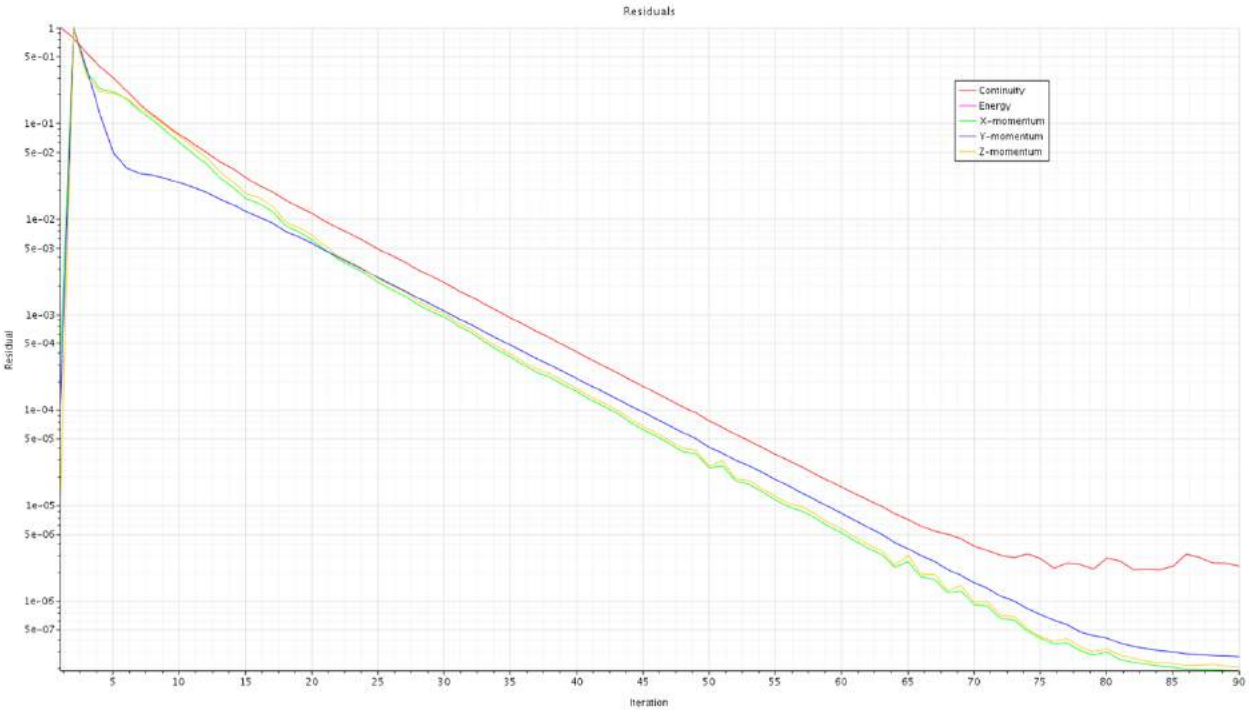

Figure C-6. Residuals error plot of 18 mm tissue with 90° x 8 mm Lg. cannula.

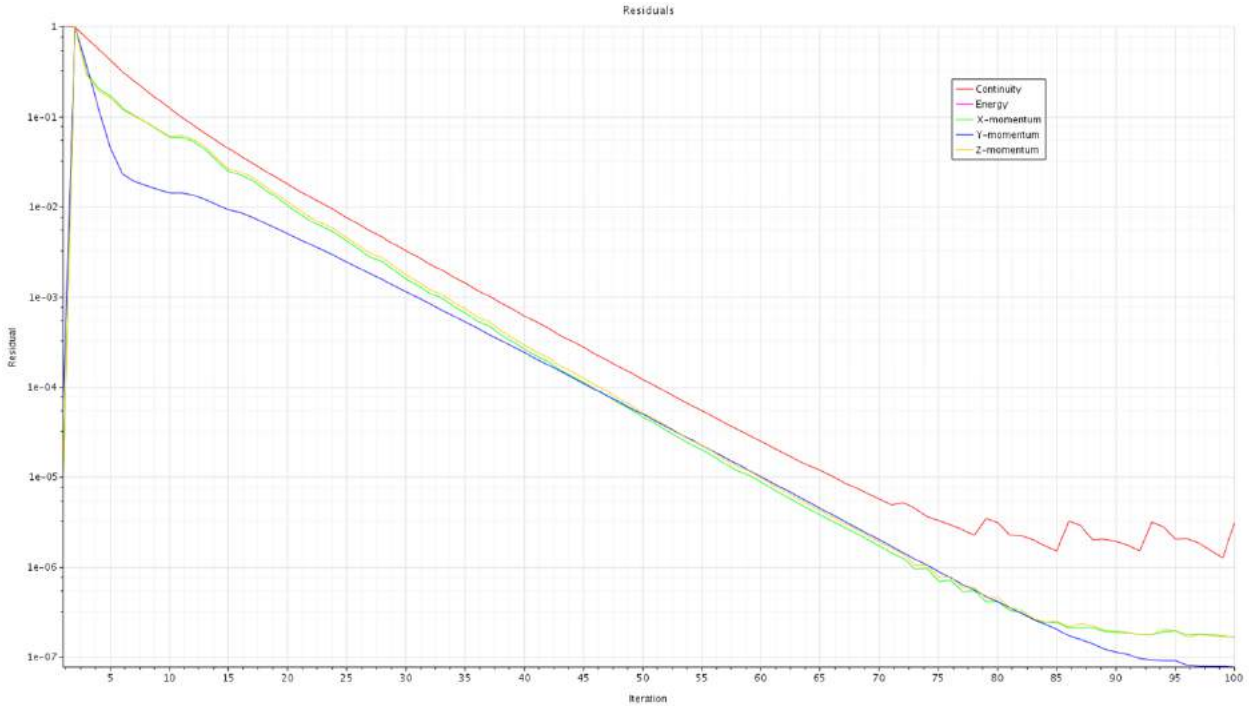

Figure C-7. Residuals error plot of 24 mm tissue with 90° x 8 mm Lg. cannula.

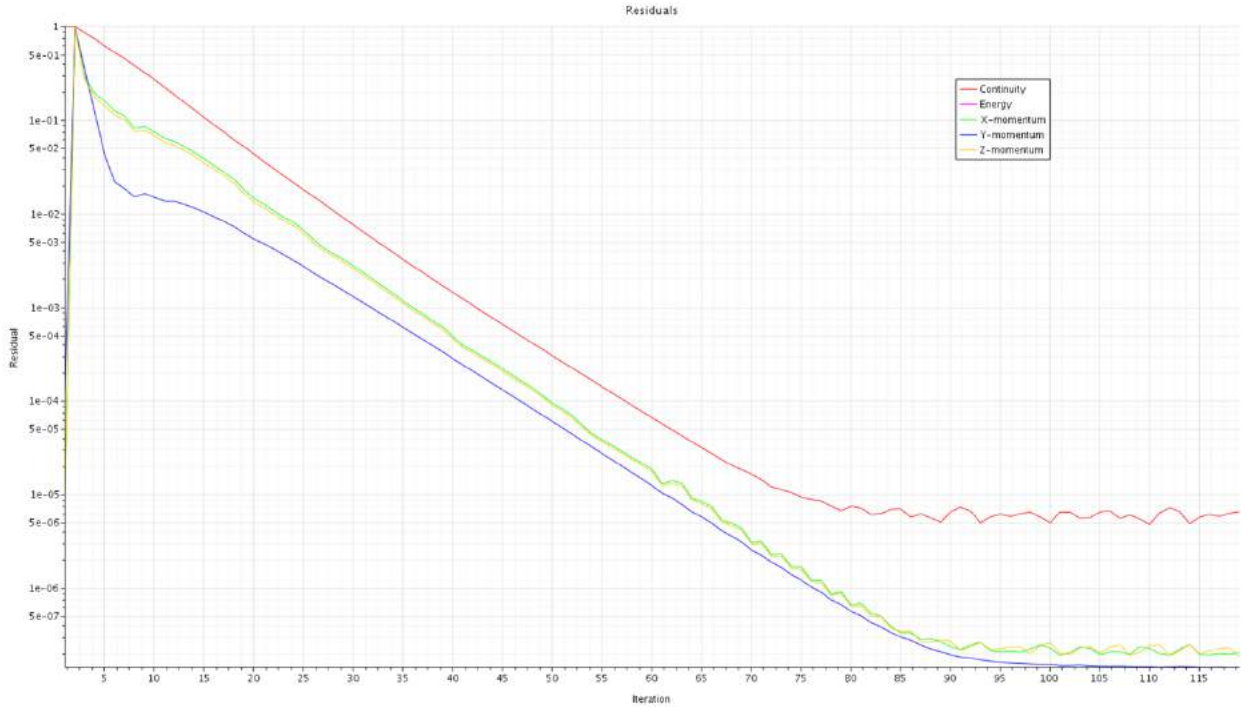

Figure C-8. Residuals error plot of 30 mm tissue with 90° x 8 mm Lg. cannula.

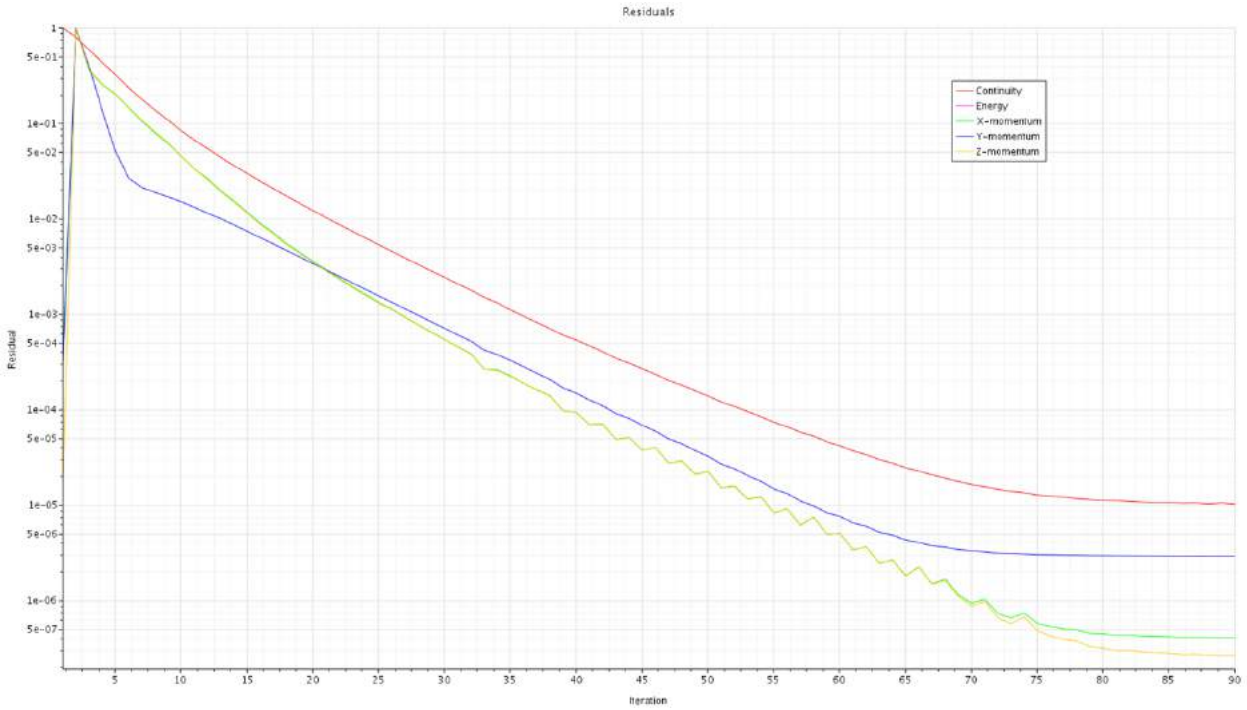

Figure C-9. Residuals error plot of 6 mm tissue with 45° x 13 mm Lg. cannula.

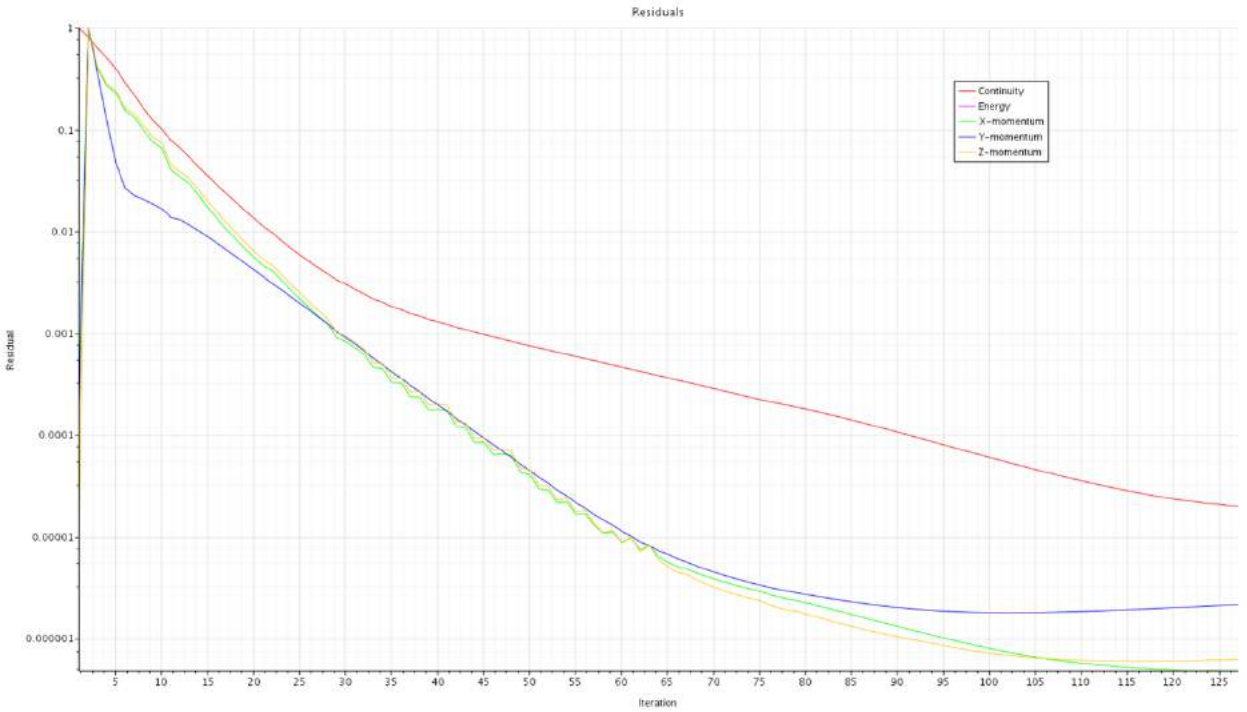

Figure C-10. Residuals error plot of 12 mm tissue with 45° x 13 mm Lg. cannula.

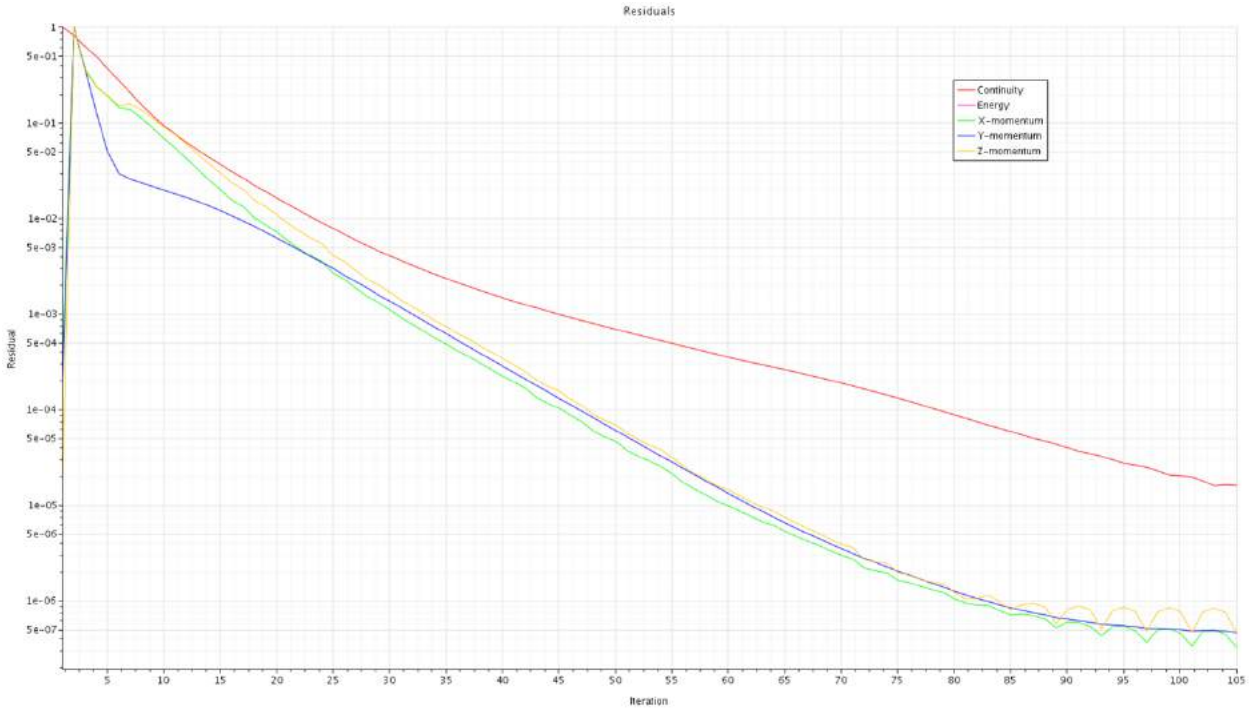

Figure C-11. Residuals error plot of 18 mm tissue with 45° x 13 mm Lg. cannula.

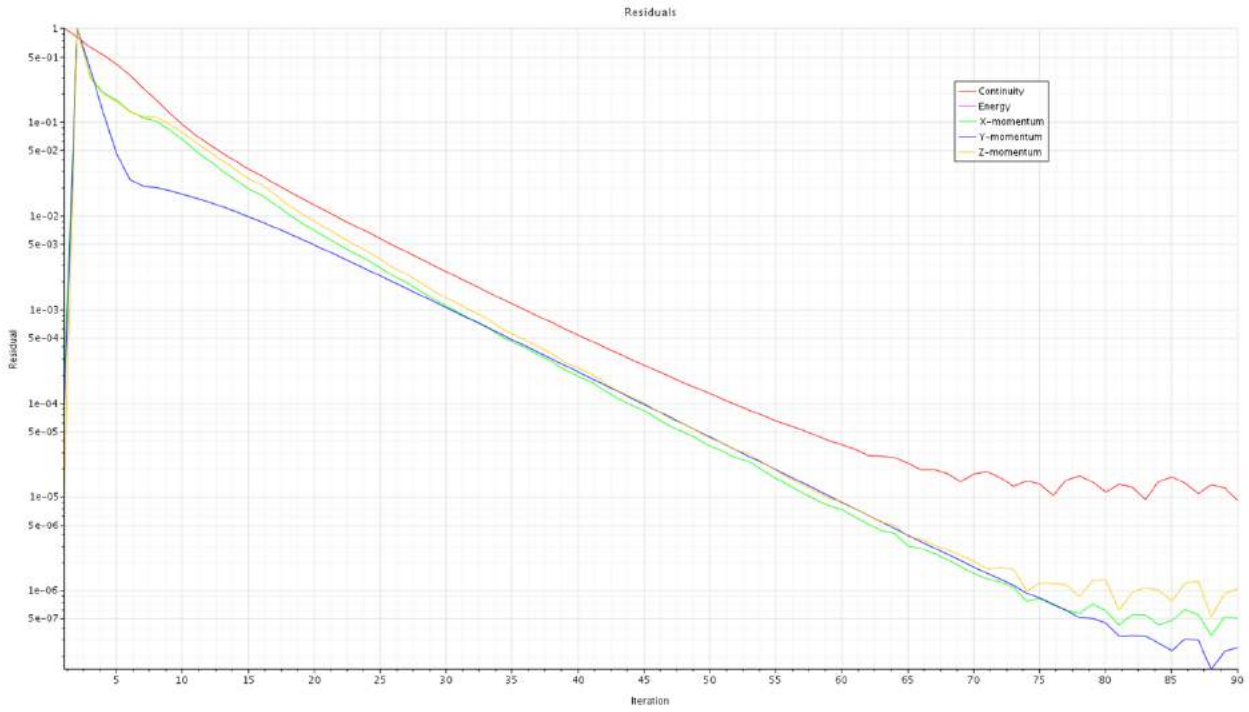

Figure C-12. Residuals error plot of 24 mm tissue with 45° x 13 mm Lg. cannula.

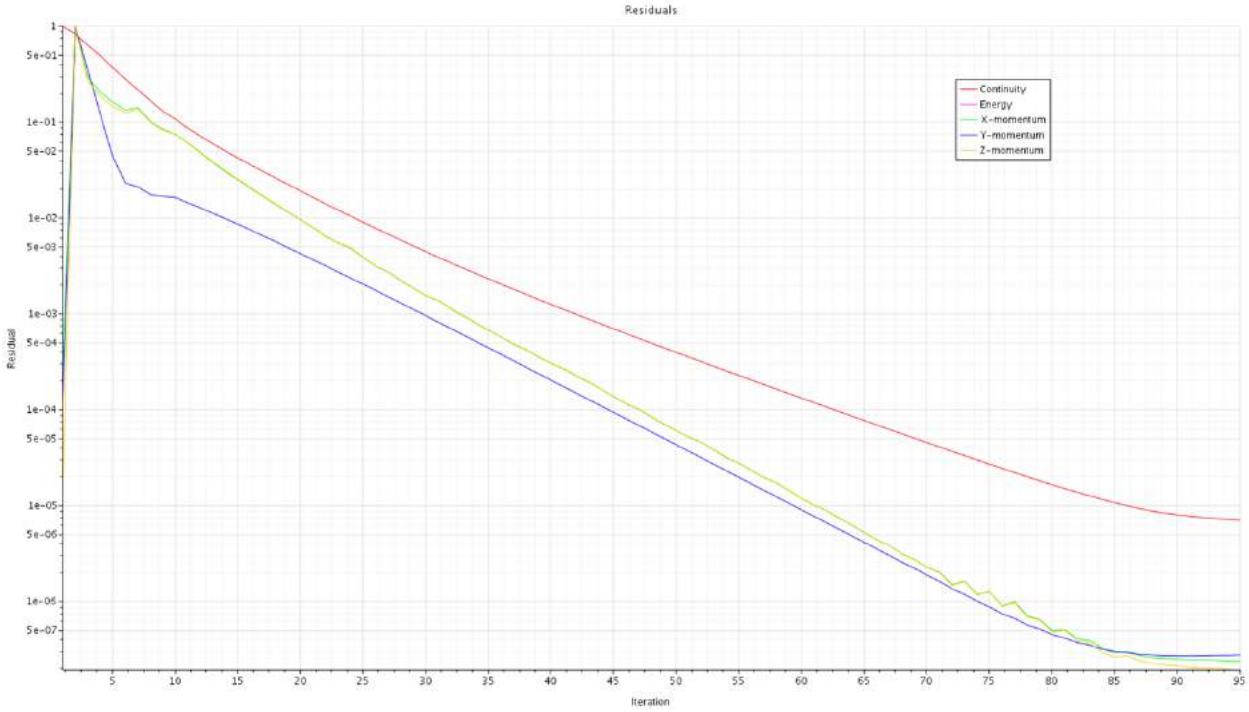

Figure C-13. Residuals error plot of 30 mm tissue with 45° x 13 mm Lg. cannula.

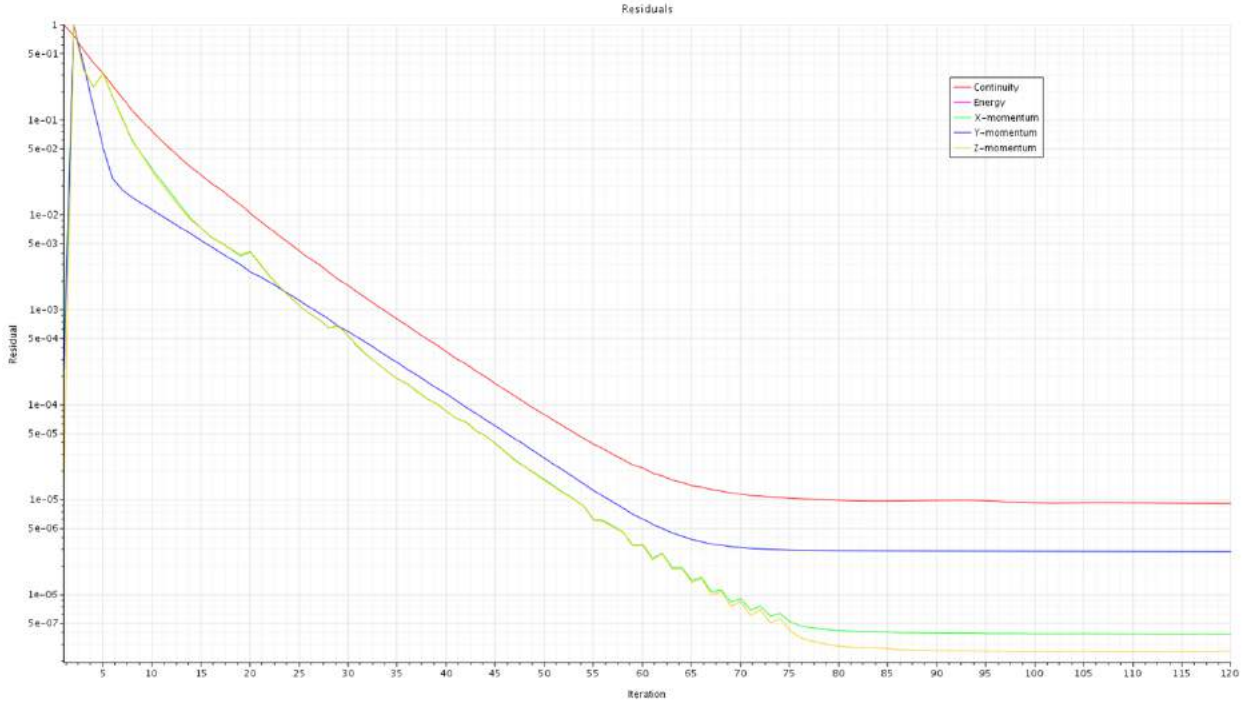

Figure C-14. Residuals error plot of 6 mm tissue with 30° x 13 mm Lg. cannula.

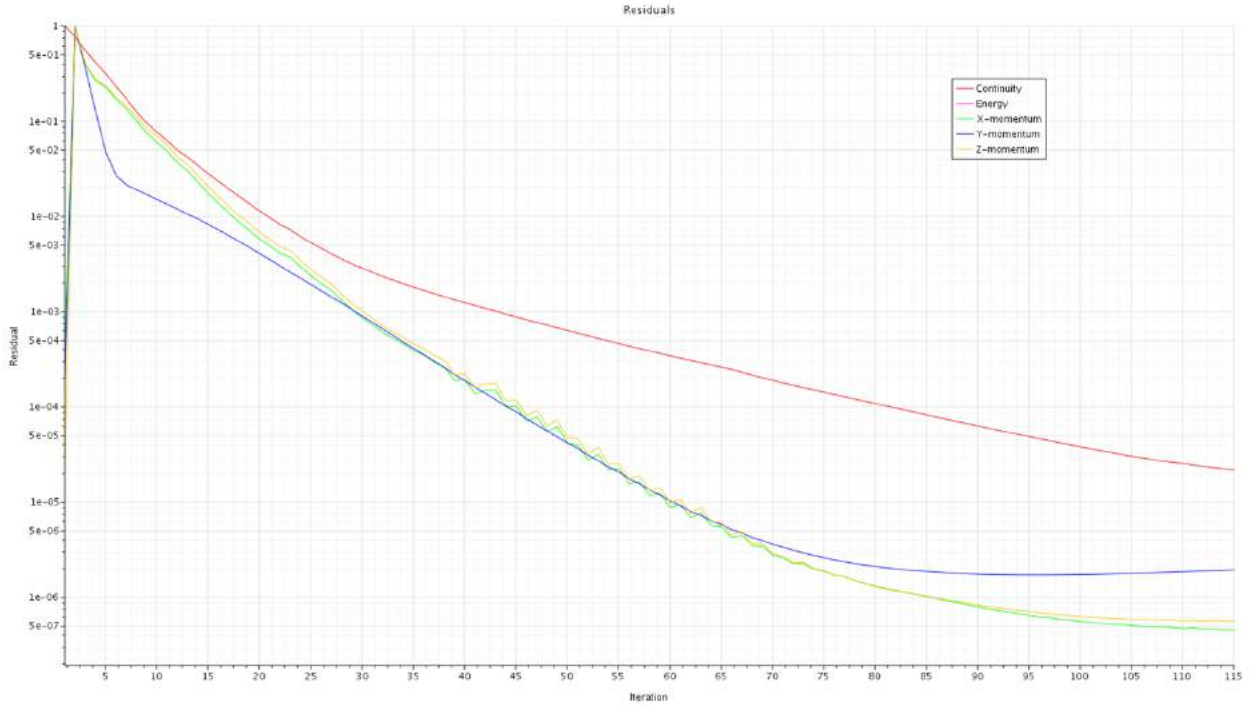

Figure C-15. Residuals error plot of 12 mm tissue with 30° x 13 mm Lg. cannula.

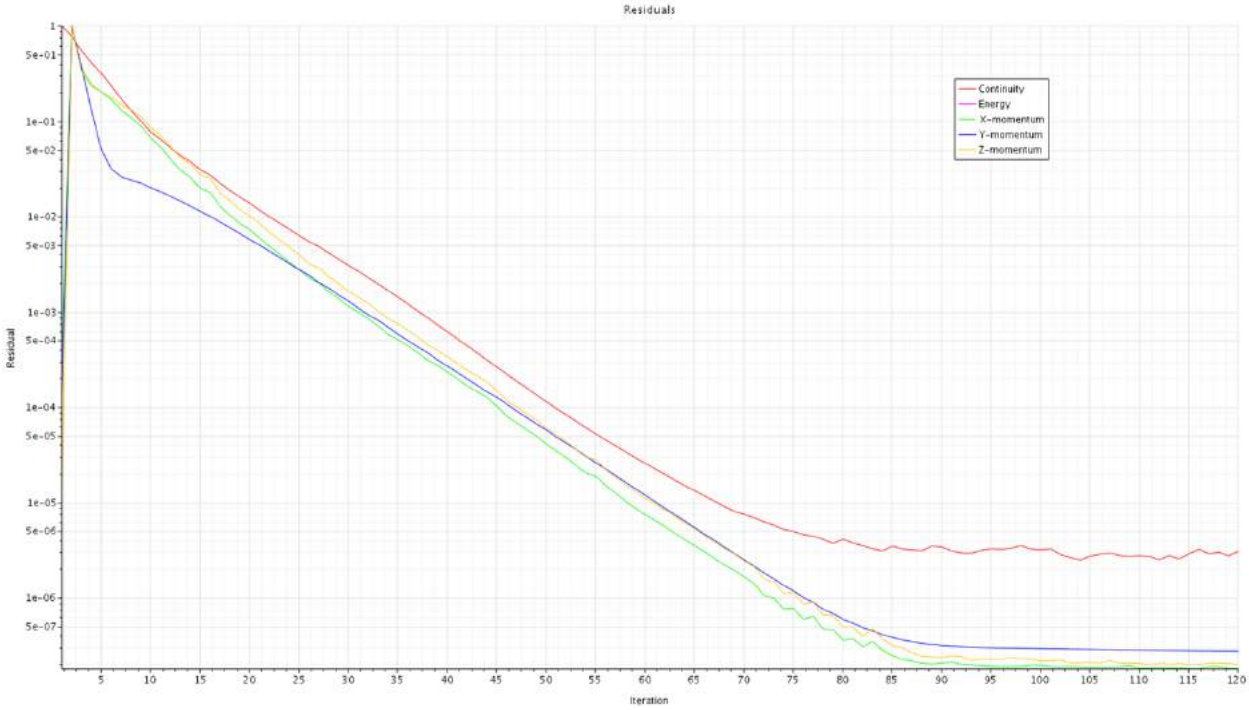

Figure C-16. Residuals error plot of 18 mm tissue with 30° x 13 mm Lg. cannula.

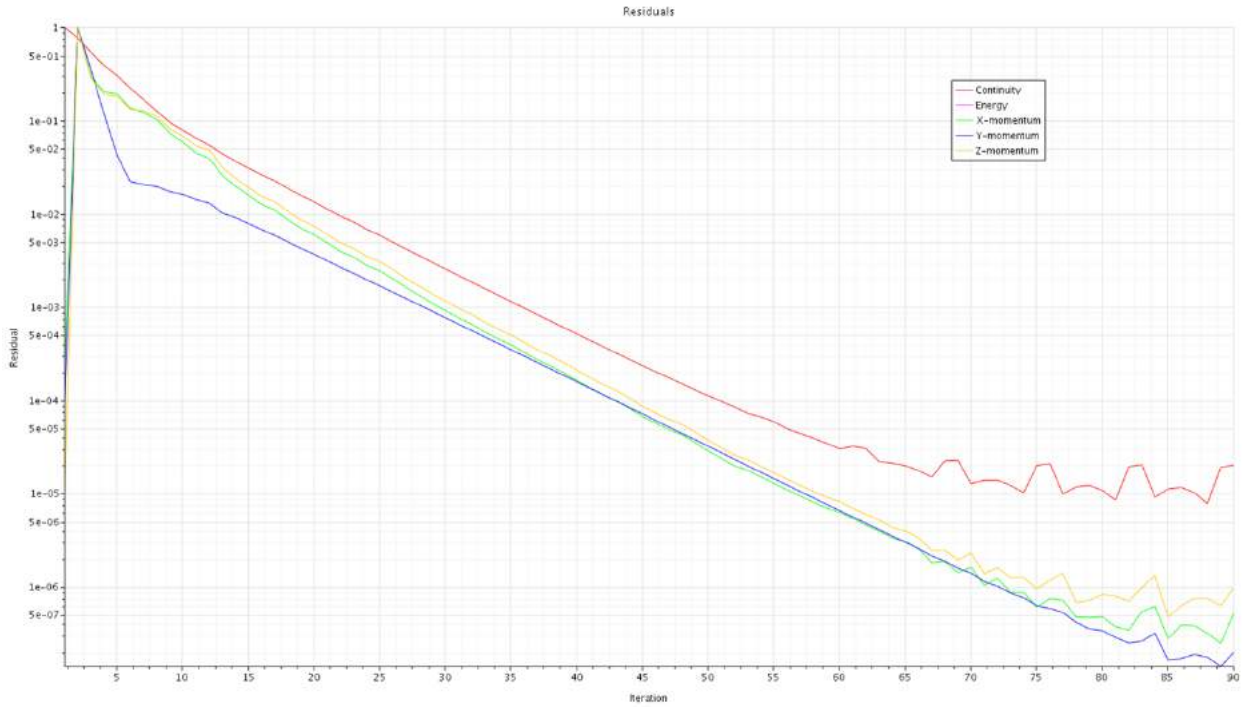

Figure C-17. Residuals error plot of 24 mm tissue with 30° x 13 mm Lg. cannula.

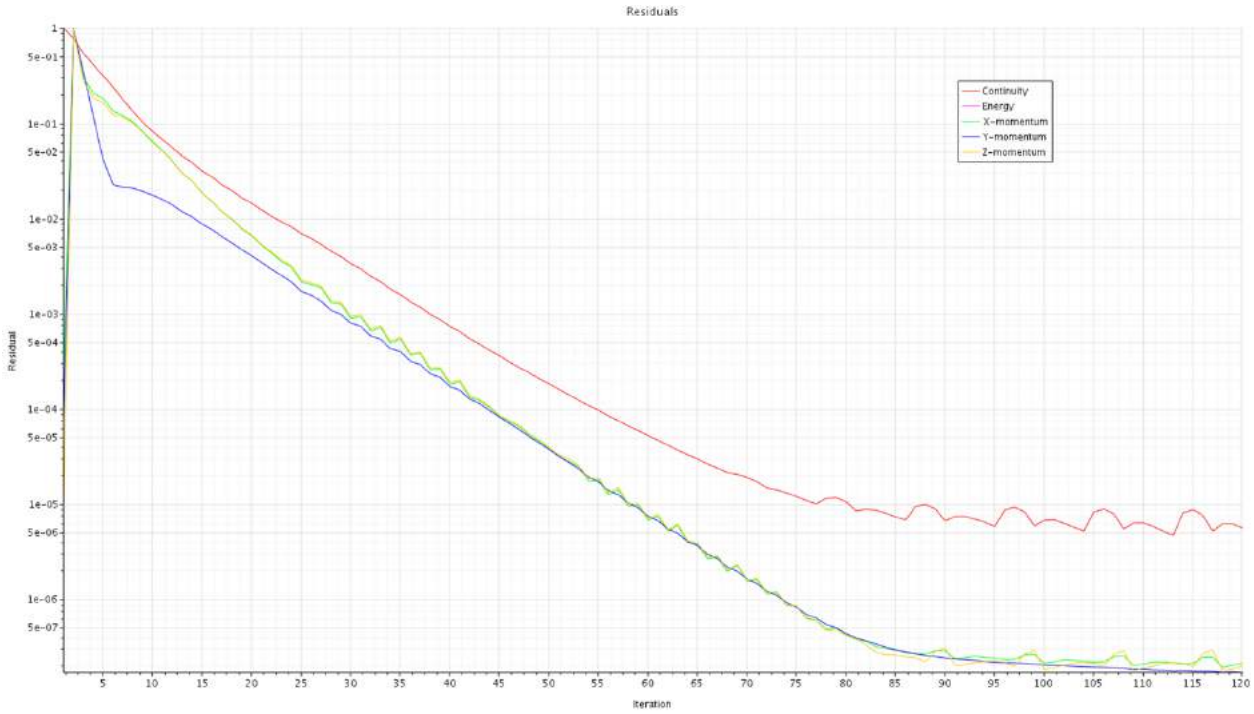

Figure C-18. Residuals error plot of 30 mm tissue with 30° x 13 mm Lg. cannula.

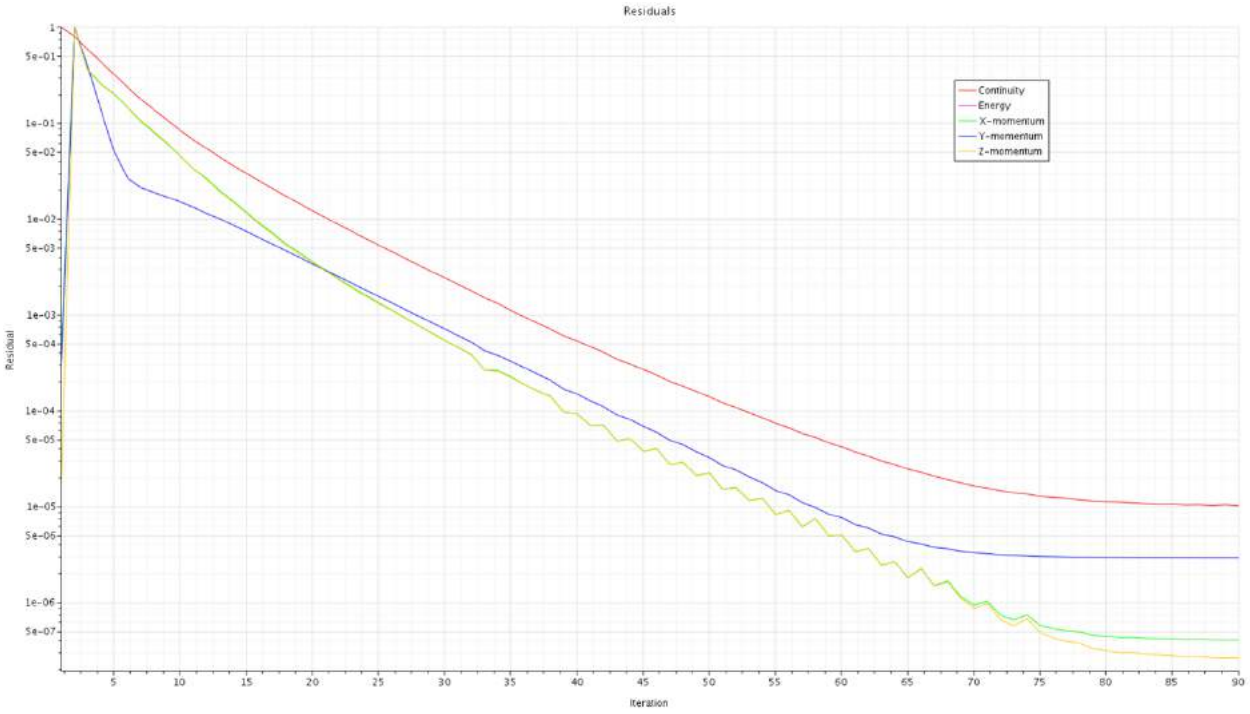

Figure C-19. Residuals error plot of 6 mm tissue with 20° x 13 mm Lg. cannula.

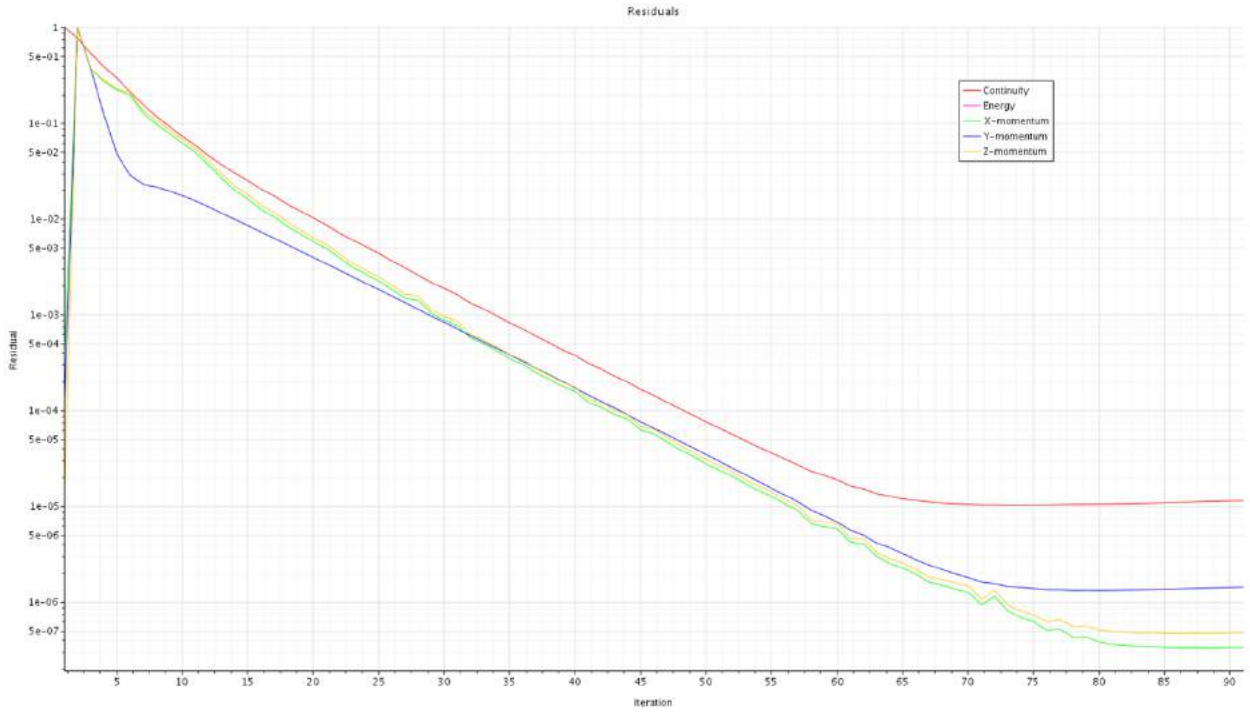

Figure C-20. Residuals error plot of 12 mm tissue with 20° x 13 mm Lg. cannula.

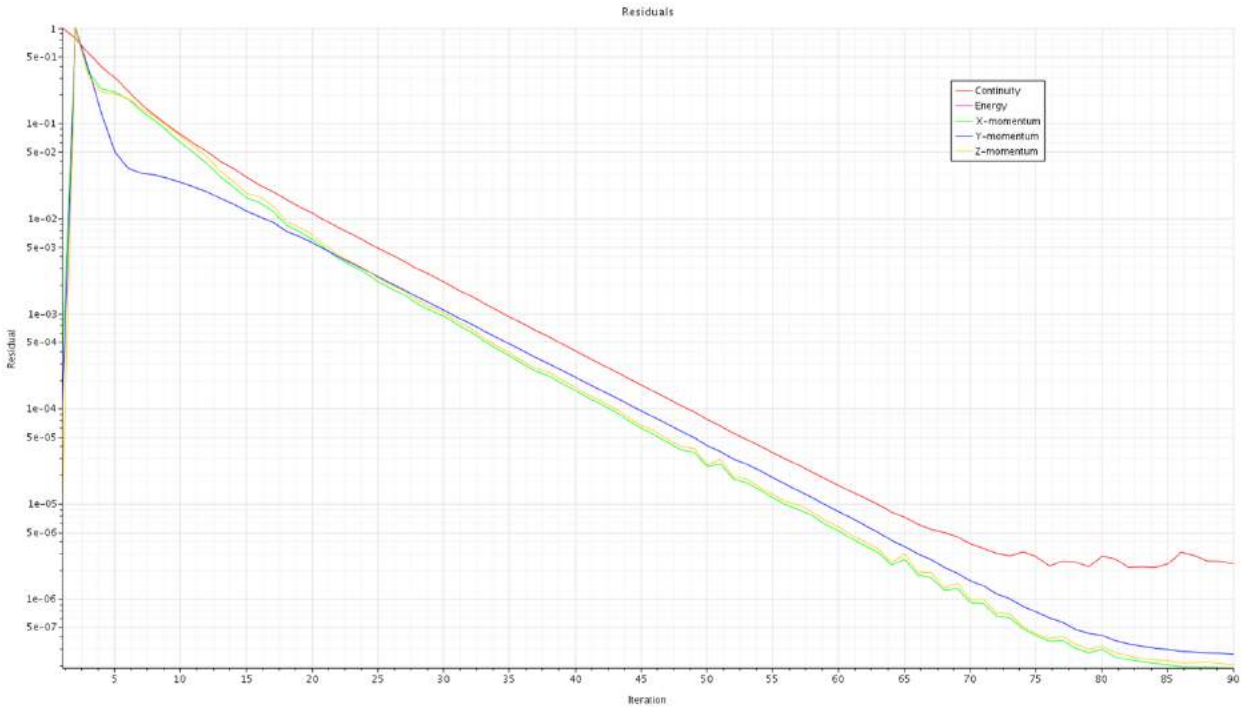

Figure C-21. Residuals error plot of 18 mm tissue with 20° x 13 mm Lg. cannula.

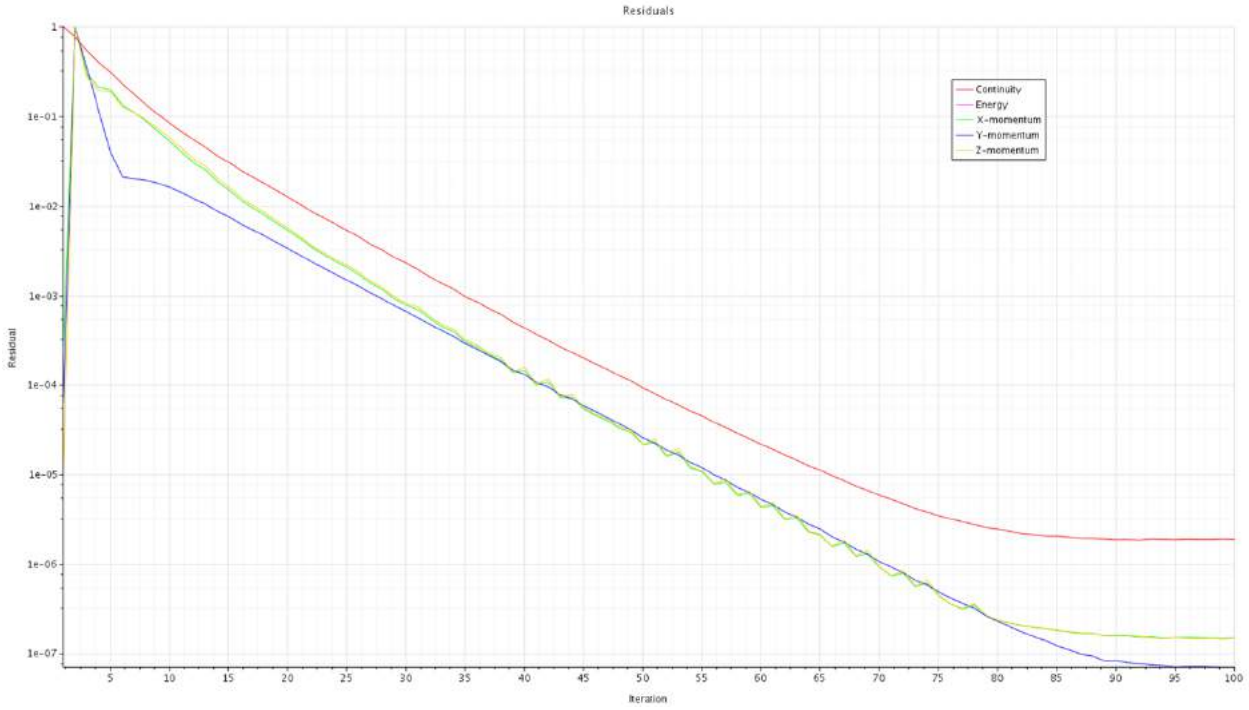

Figure C-22. Residuals error plot of 24 mm tissue with 20° x 13 mm Lg. cannula.

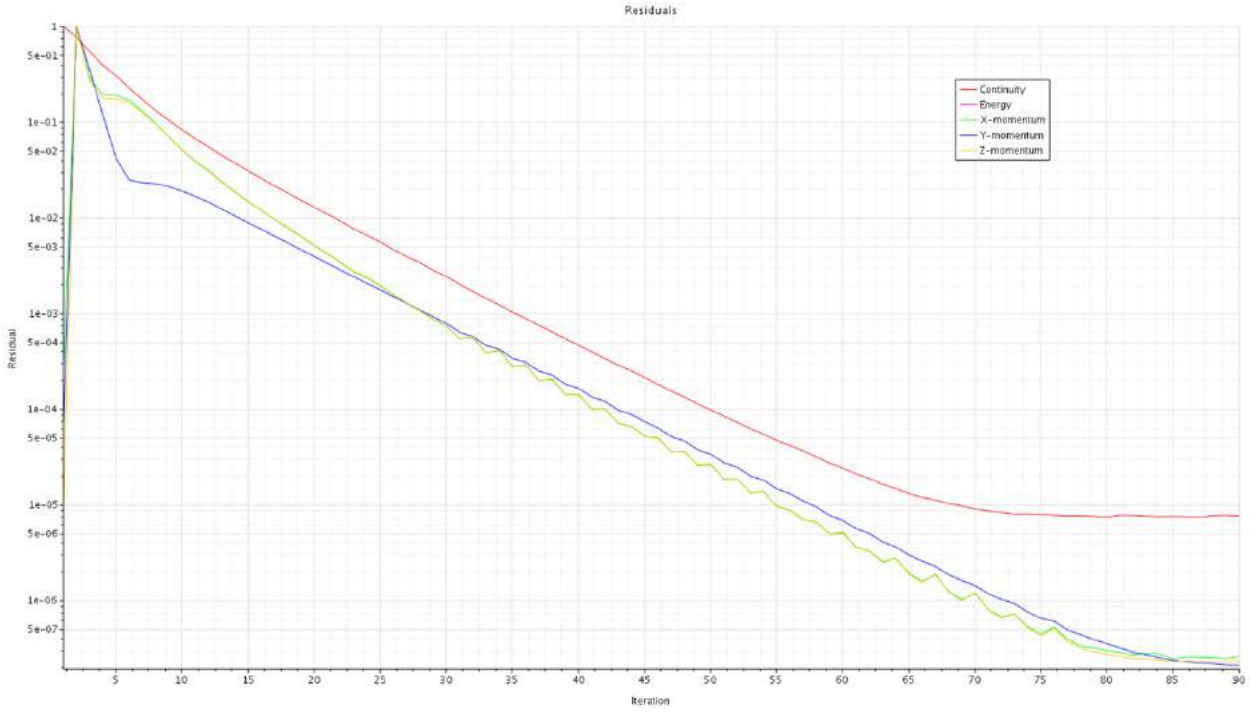

Figure C-23. Residuals error plot of 30 mm tissue with 20° x 13 mm Lg. cannula.

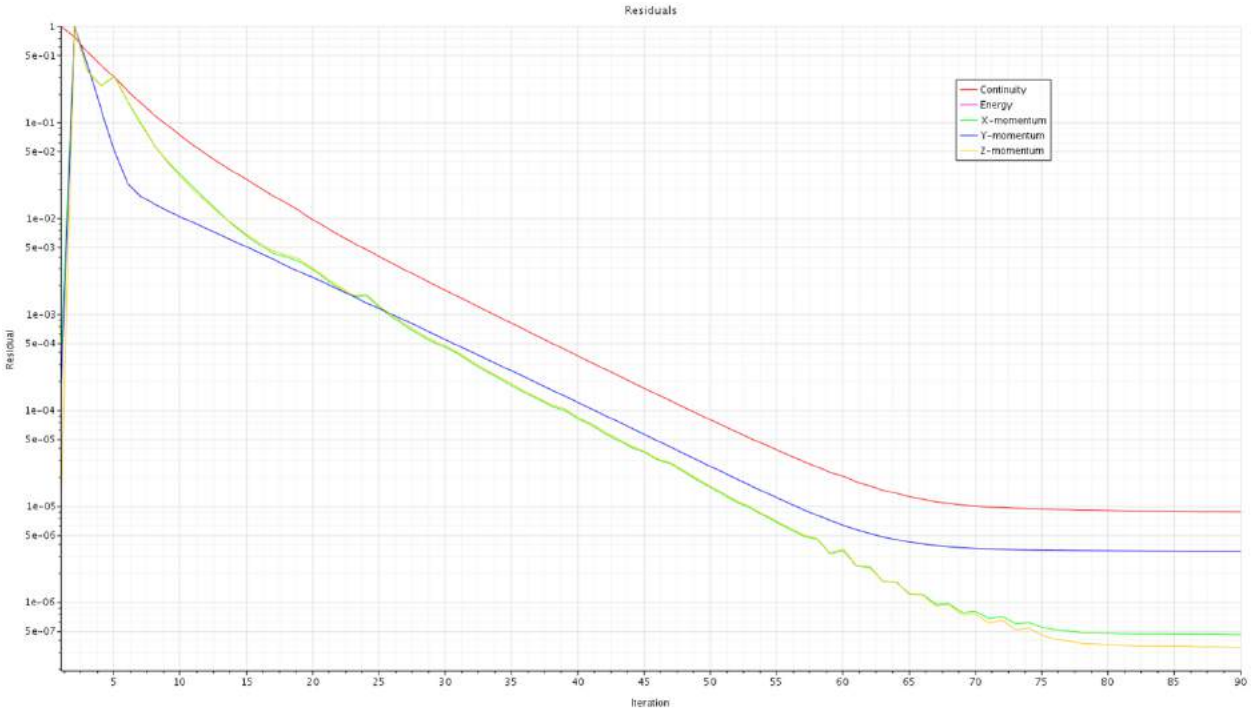

Figure C-24. Residuals error plot of 6 mm tissue with 20° x 17 mm Lg. cannula.

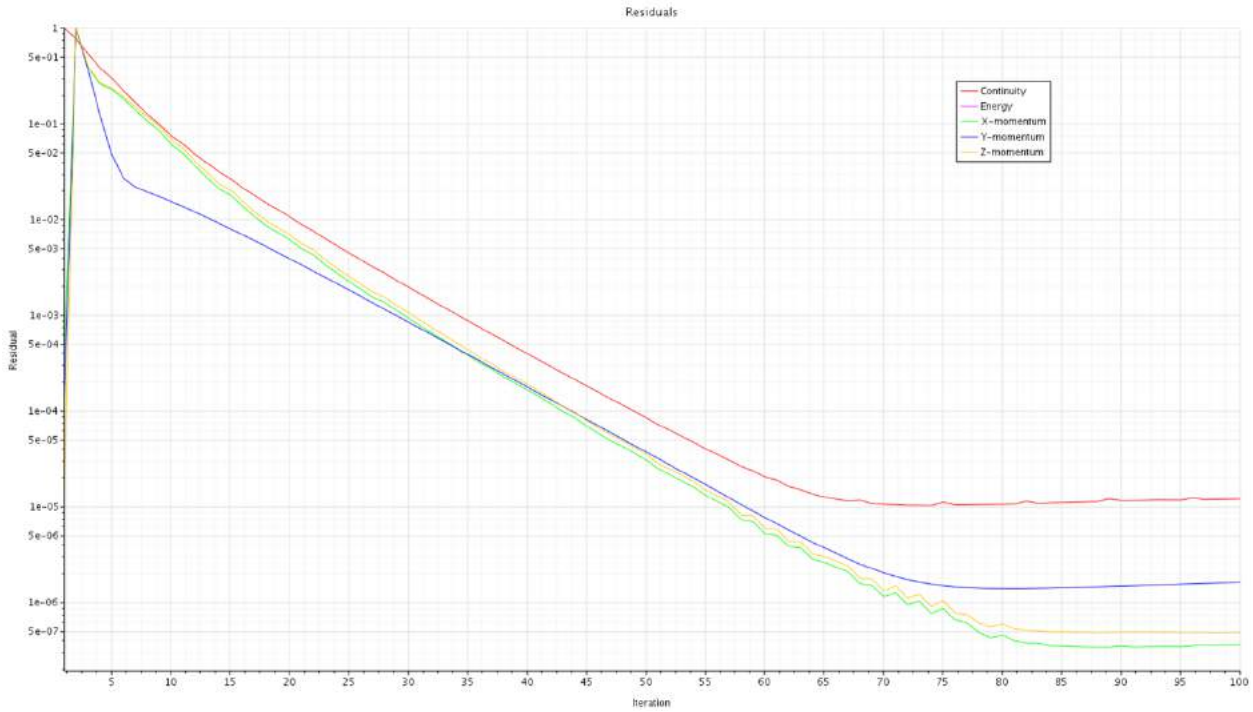

Figure C-25. Residuals error plot of 12 mm tissue with 20° x 17 mm Lg. cannula.

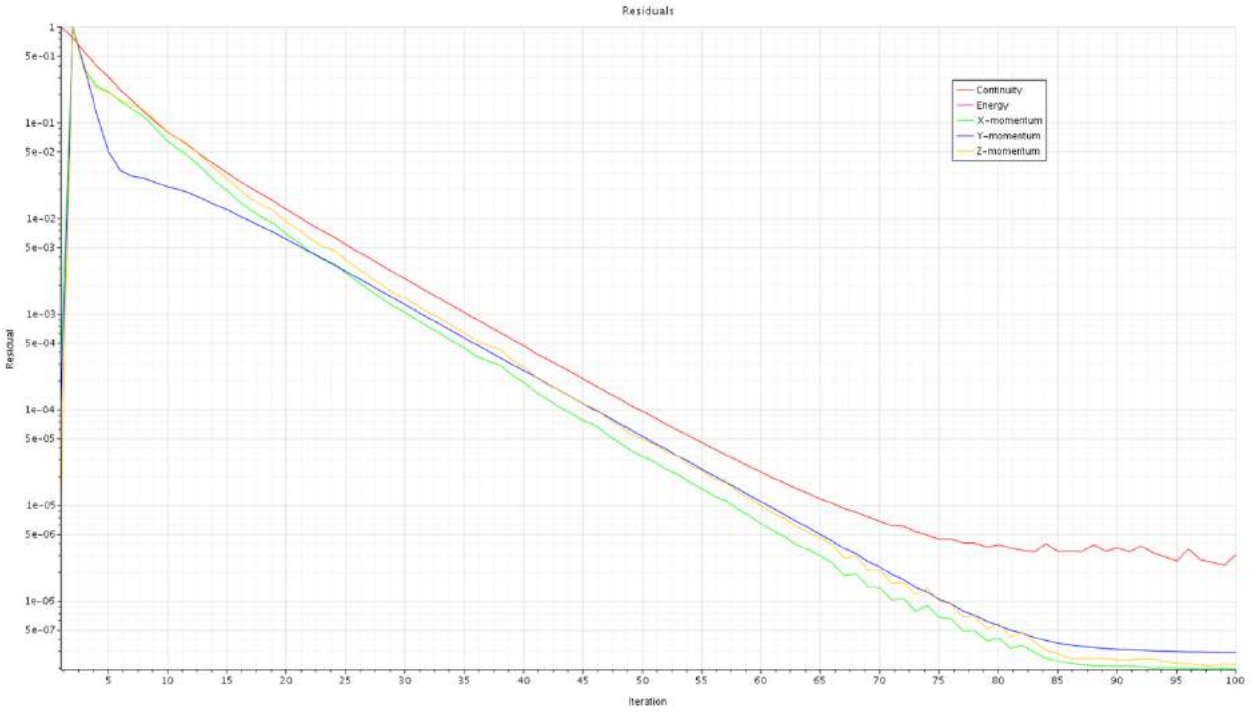

Figure C-26. Residuals error plot of 18 mm tissue with 20° x 17 mm Lg. cannula.

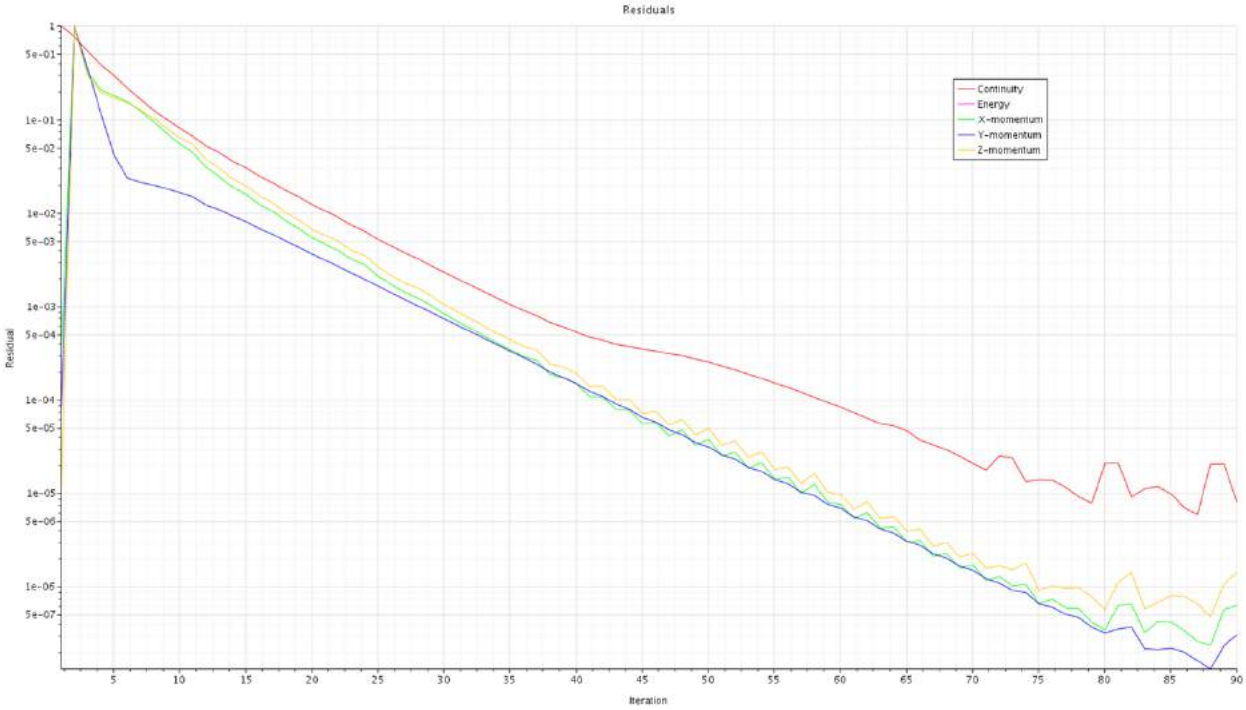

Figure C-27. Residuals error plot of 24 mm tissue with 20° x 17 mm Lg. cannula.

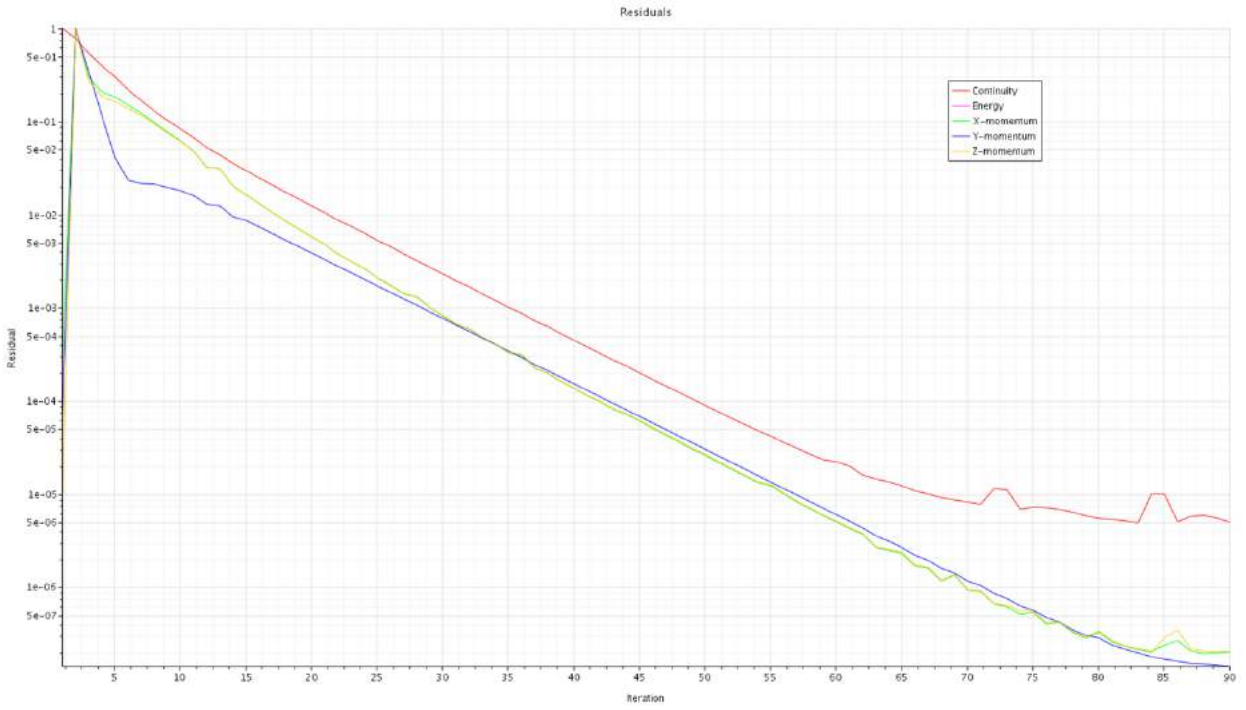

Figure C-28. Residuals error plot of 30 mm tissue with 20° x 17 mm Lg. cannula.

Appendix D: Chapter 7 Additional Figures

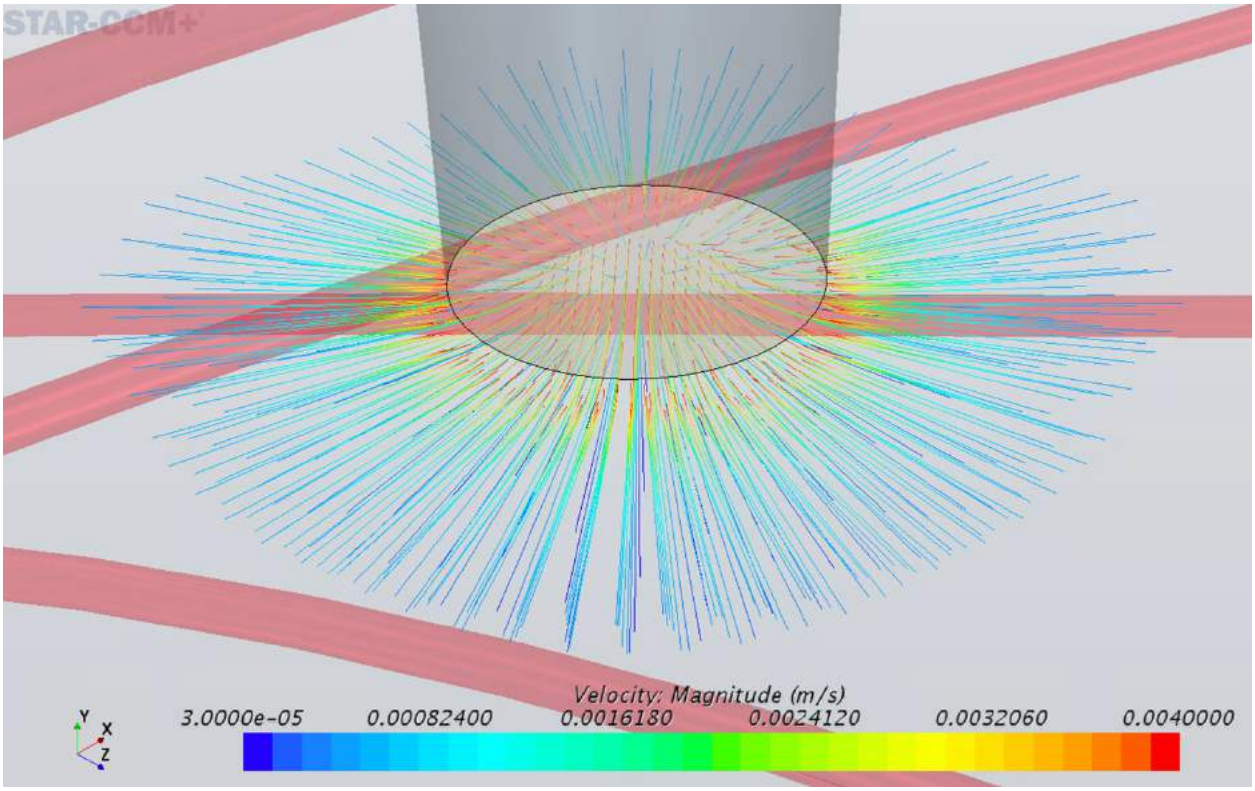

(a)

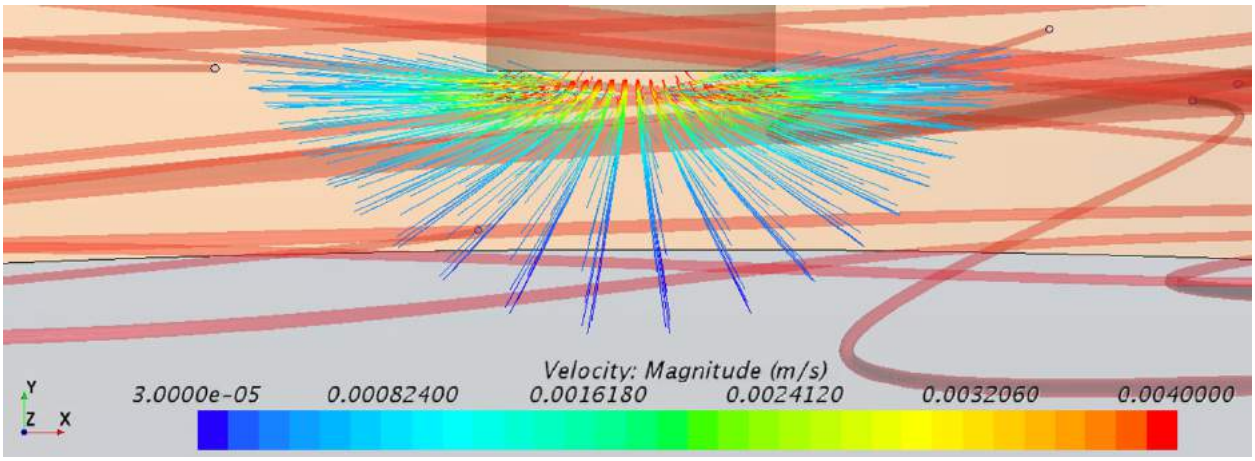

(b)

Figure D-1. Outflow pattern and velocity at cannula outlet in 12 mm tissue with 90° x 8 mm Lg. cannula geometry (a) isometric view (b) side view.

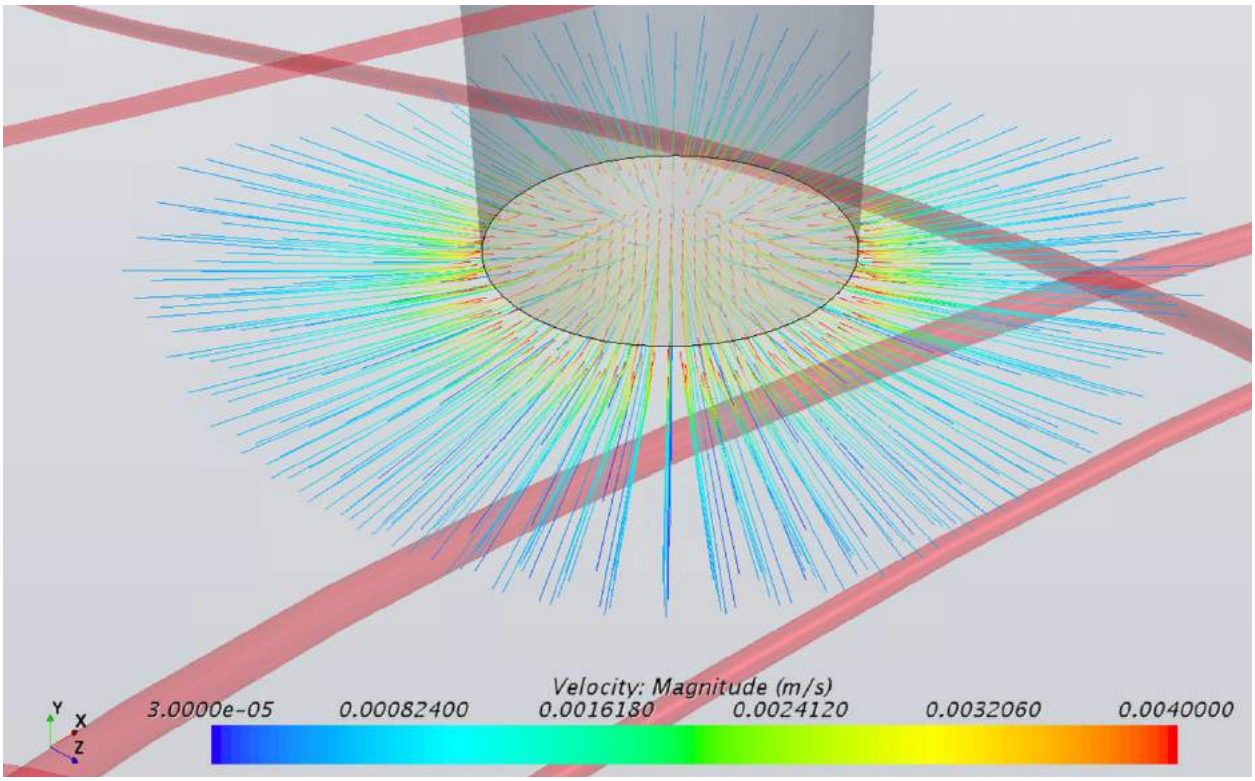

(a)

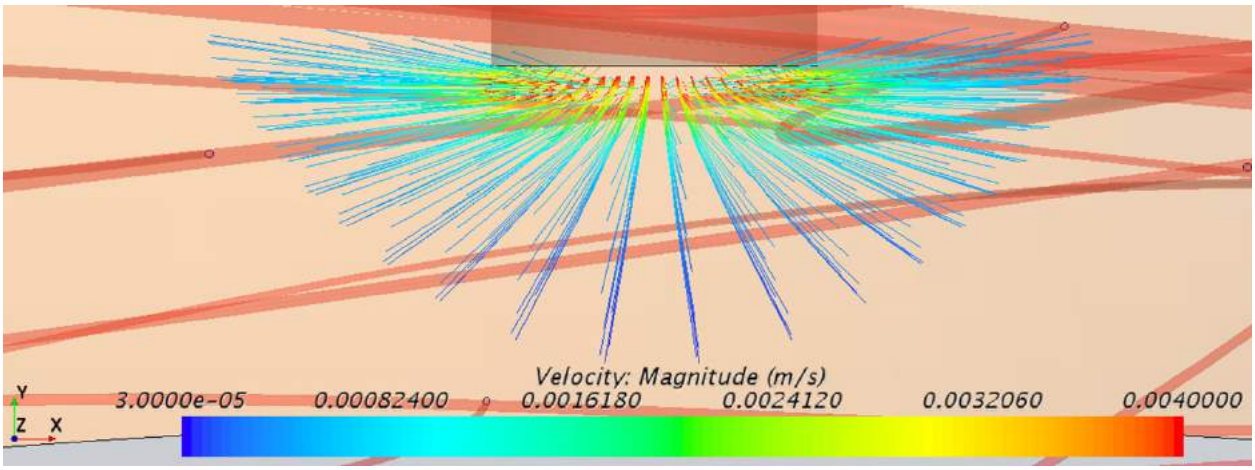

(b)

Figure D-2. Outflow pattern and velocity at cannula outlet in 18 mm tissue with 90° x 8 mm Lg. cannula geometry (a) isometric view (b) side view.

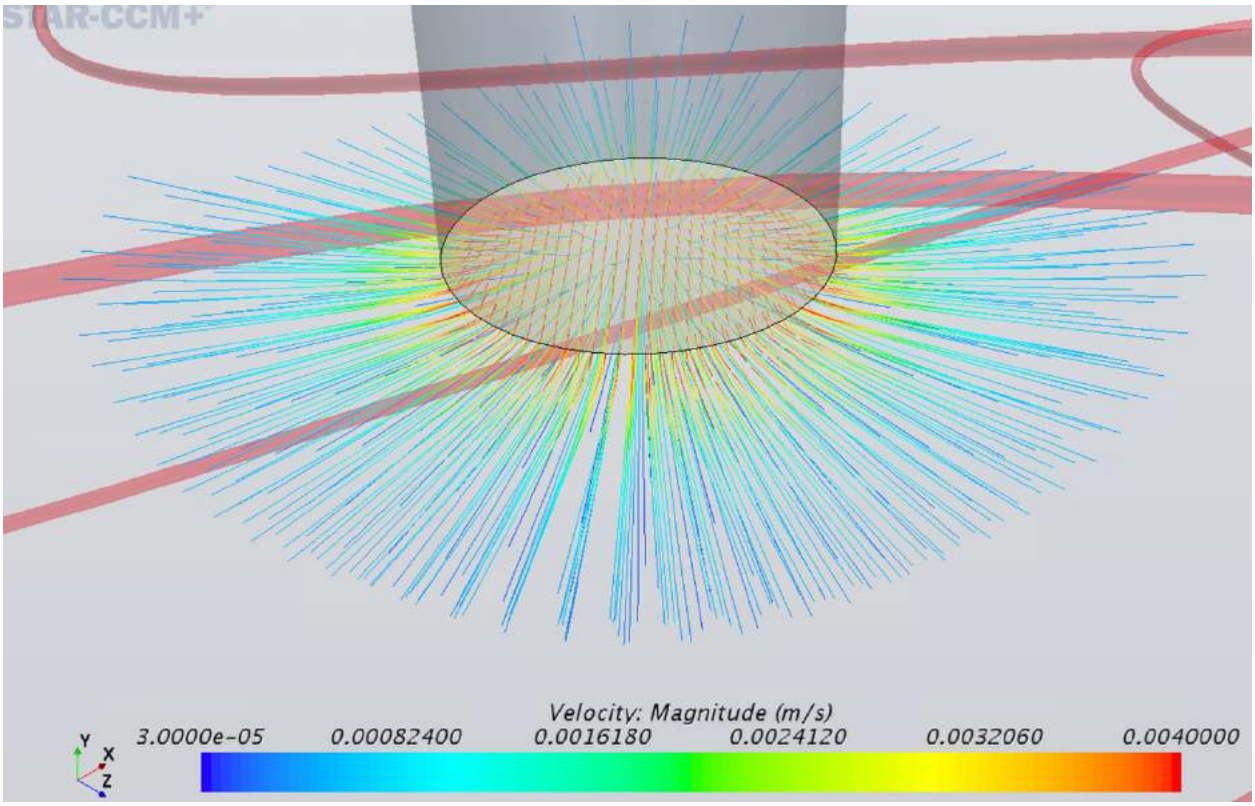

(a)

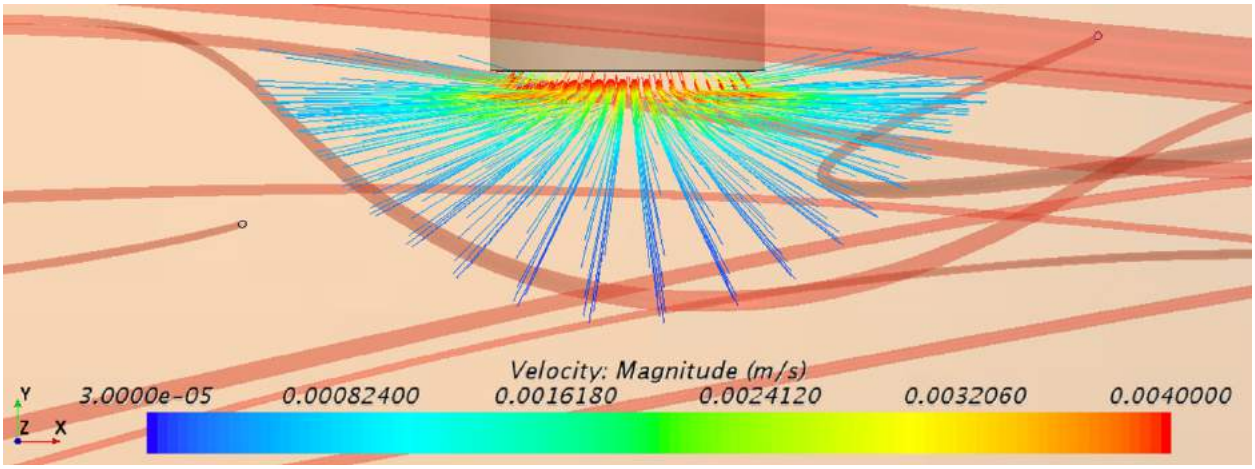

(b)

Figure D-3. Outflow pattern and velocity at cannula outlet in 24 mm tissue with 90° x 8 mm Lg. cannula geometry (a) isometric view (b) side view.

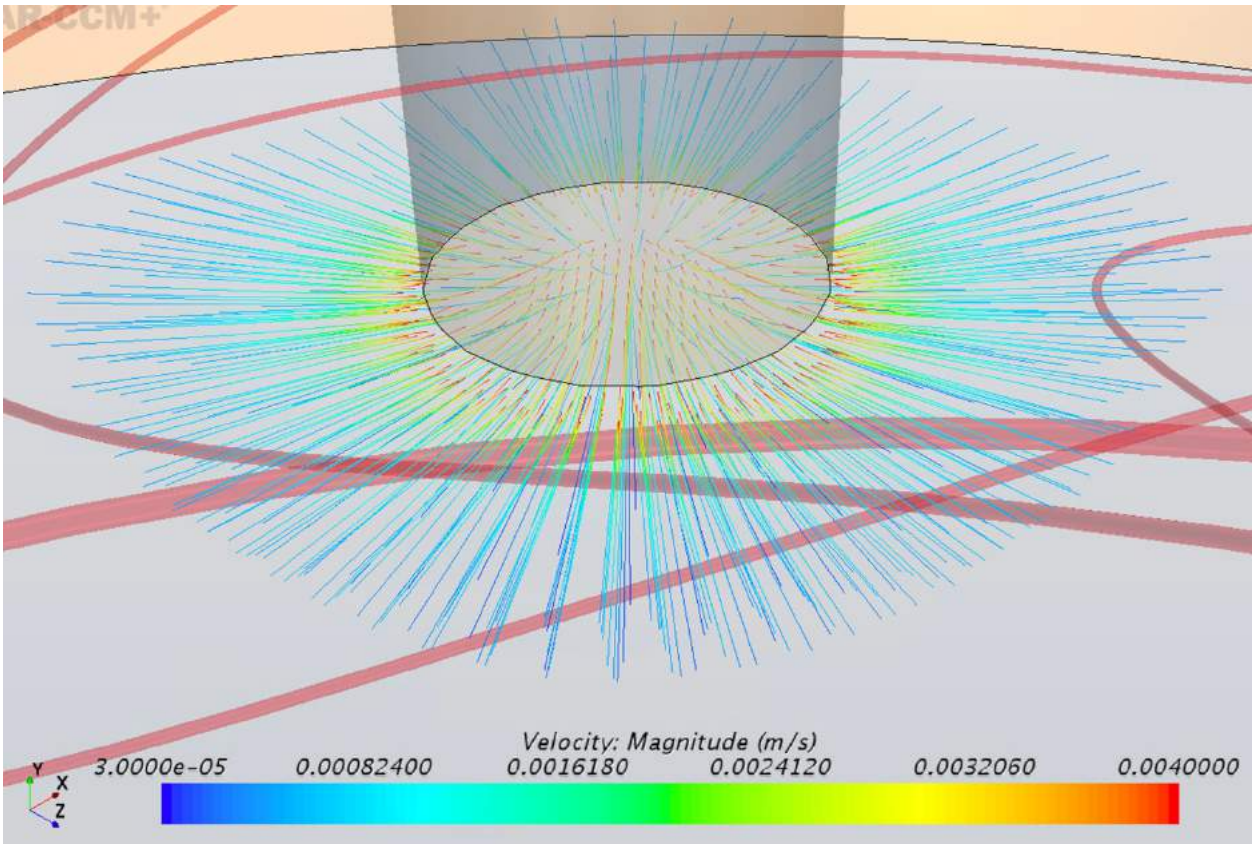

(a)

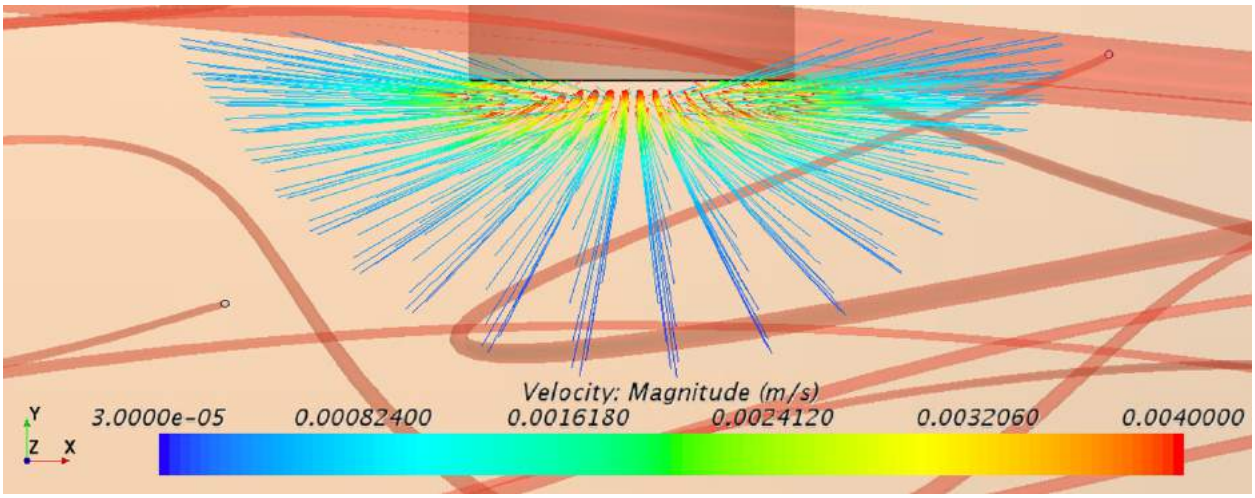

(b)

Figure D-4. Outflow pattern and velocity at cannula outlet in 30 mm tissue with 90° x 8 mm Lg. cannula geometry (a) isometric view (b) side view.

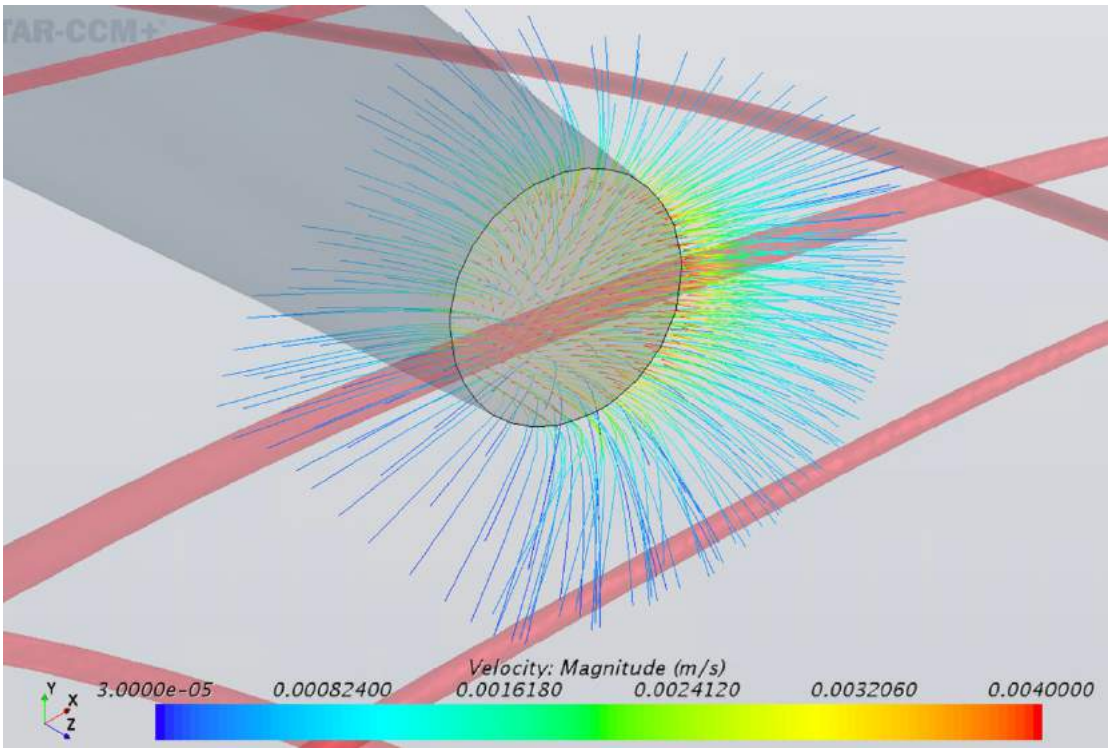

(a)

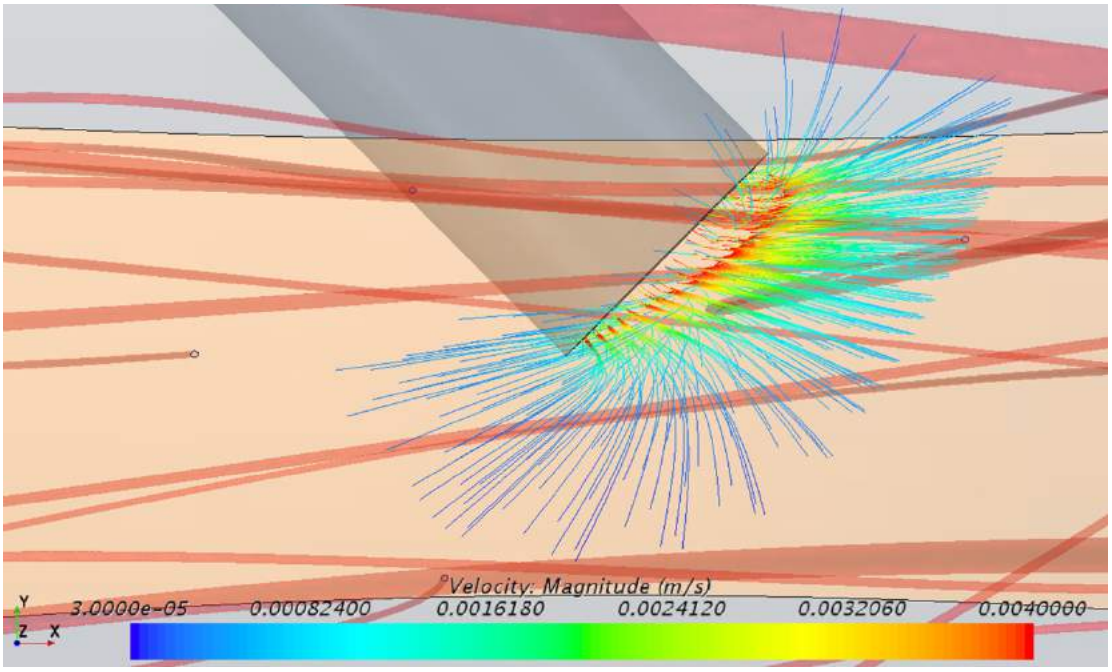

(b)

Figure D-5. Outflow pattern and velocity at cannula outlet in 18 mm tissue with 45° x 13 mm Lg. cannula geometry (a) isometric view (b) side view.

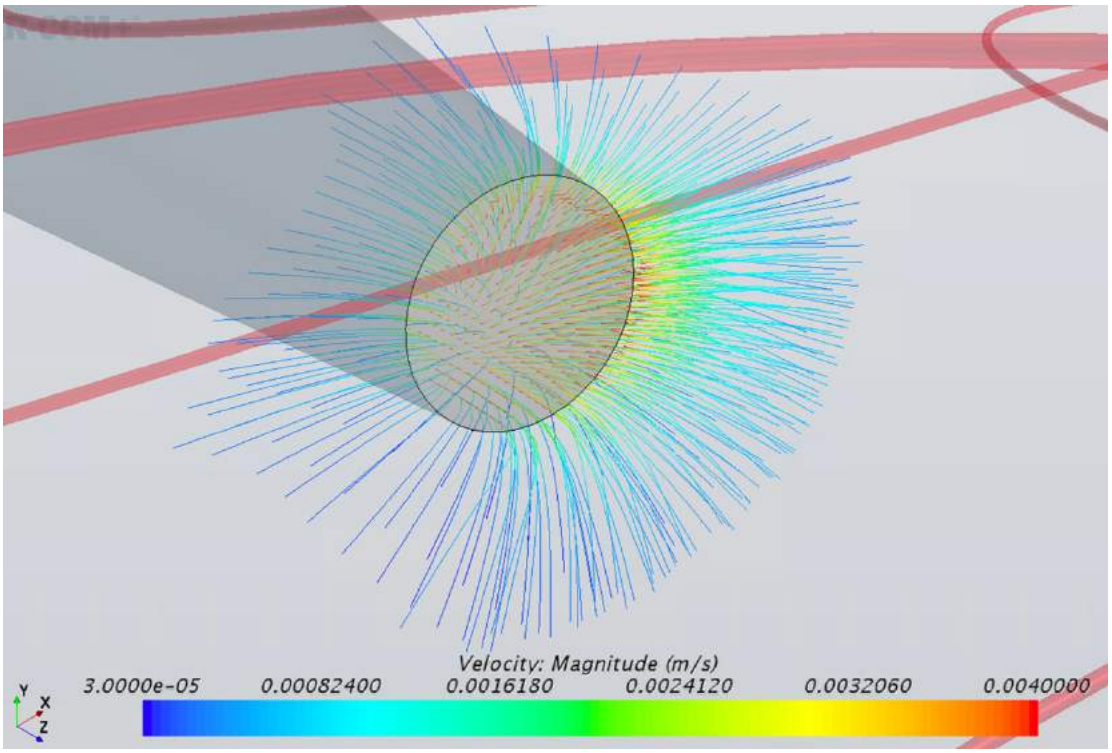

(a)

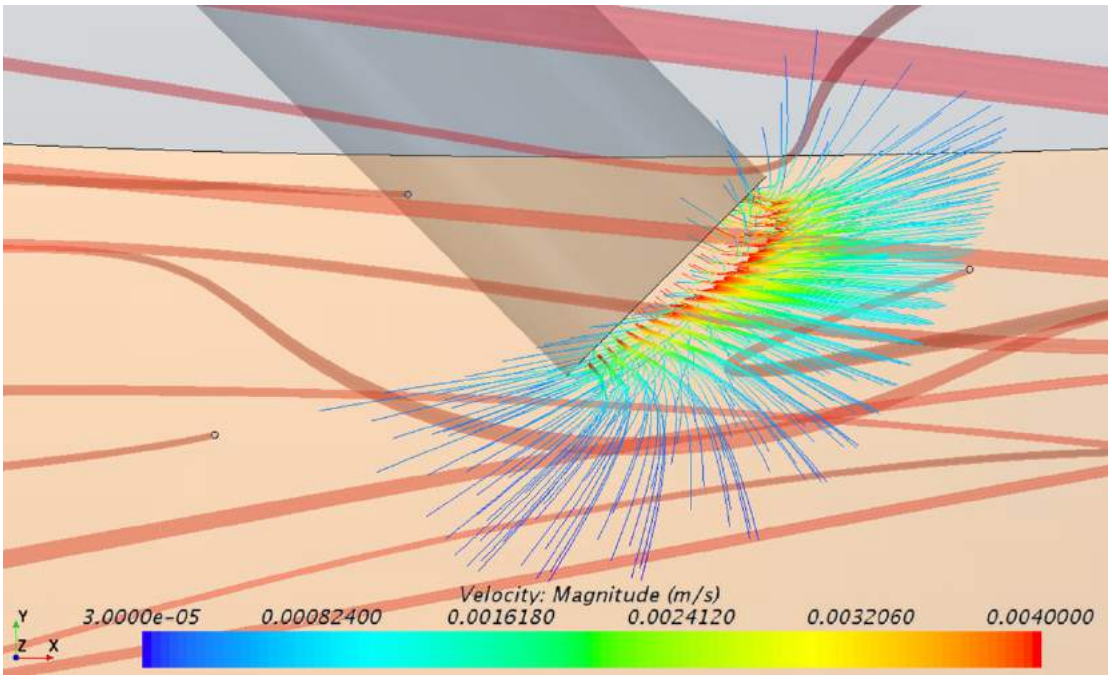

(b)

Figure D-6. Outflow pattern and velocity at cannula outlet in 24 mm tissue with 45° x 13 mm Lg. cannula geometry (a) isometric view (b) side view.

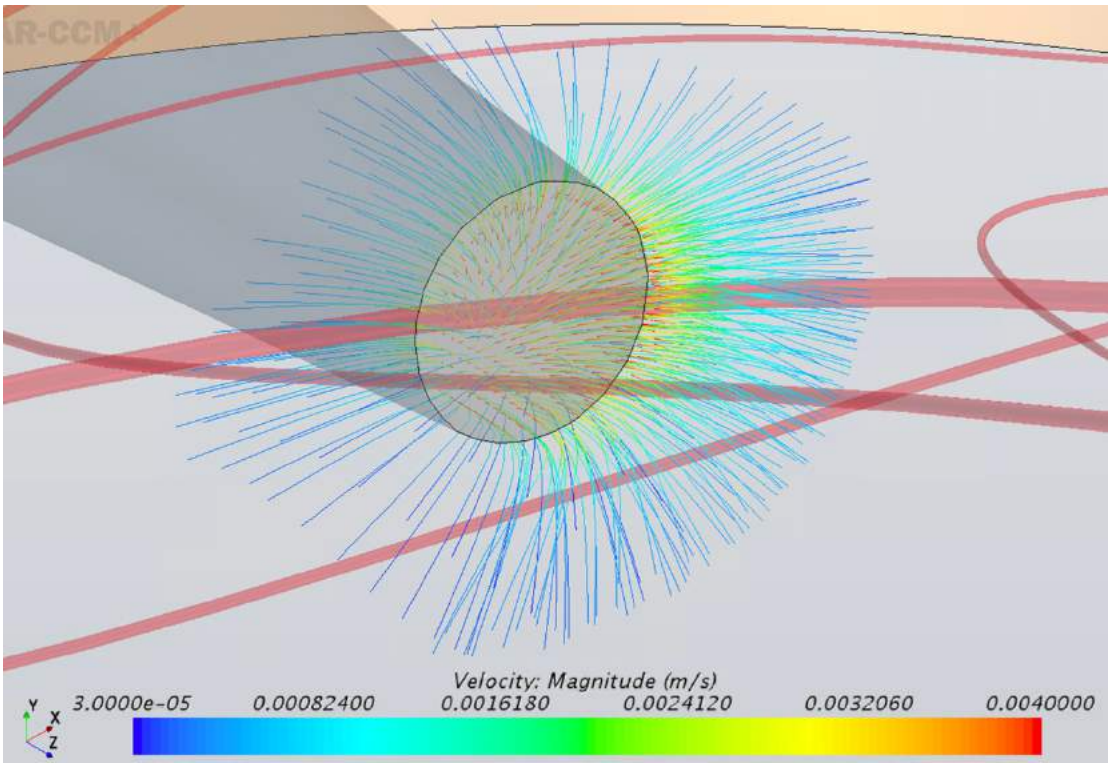

(a)

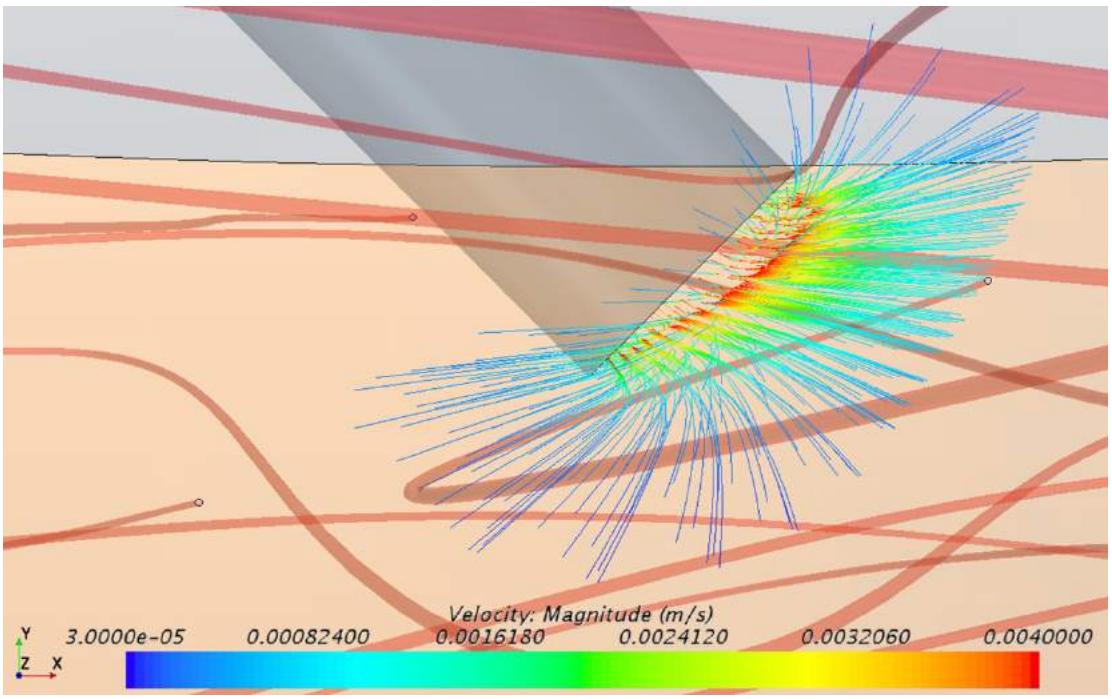

(b)

Figure D-7. Outflow pattern and velocity at cannula outlet in 30 mm tissue with 45° x 13 mm Lg. cannula geometry (a) isometric view (b) side view.

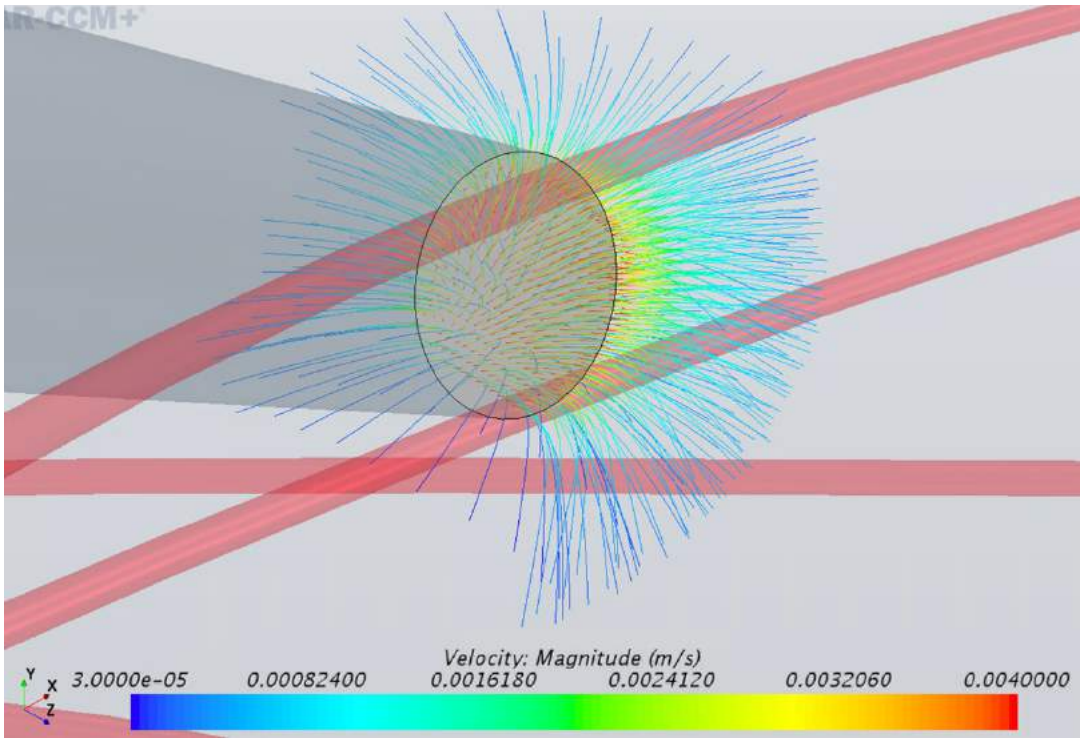

(a)

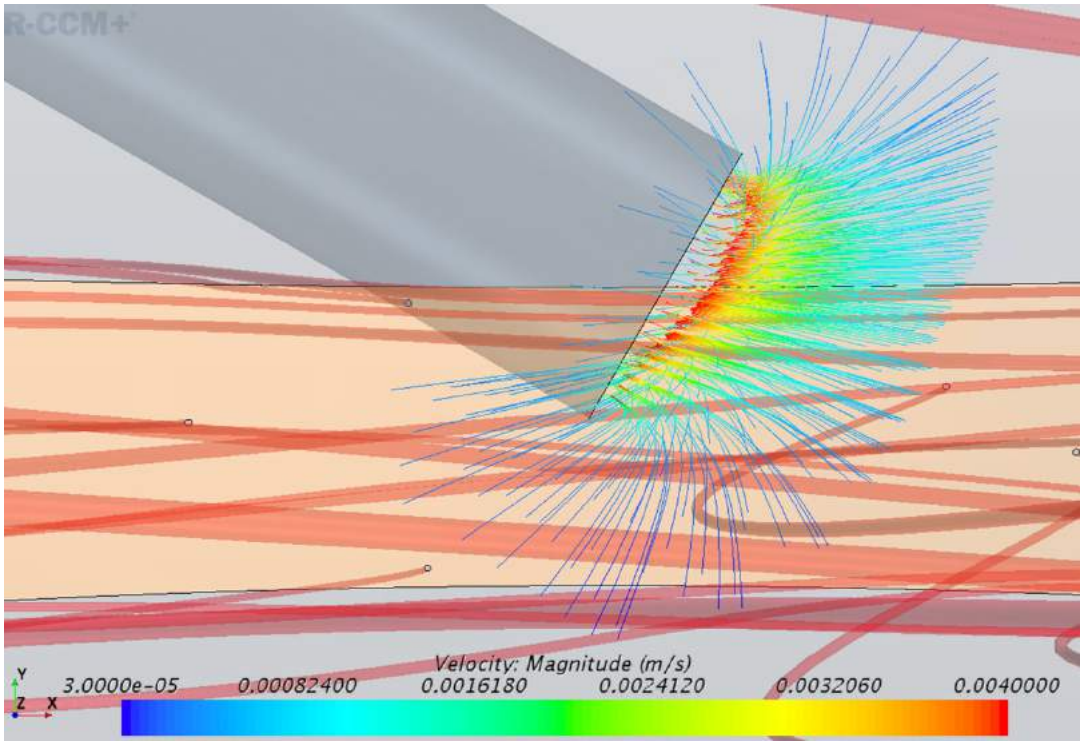

(b)

Figure D-8. Outflow pattern and velocity at cannula outlet in 12 mm tissue with 30° x 13 mm Lg. cannula geometry (a) isometric view (b) side view.

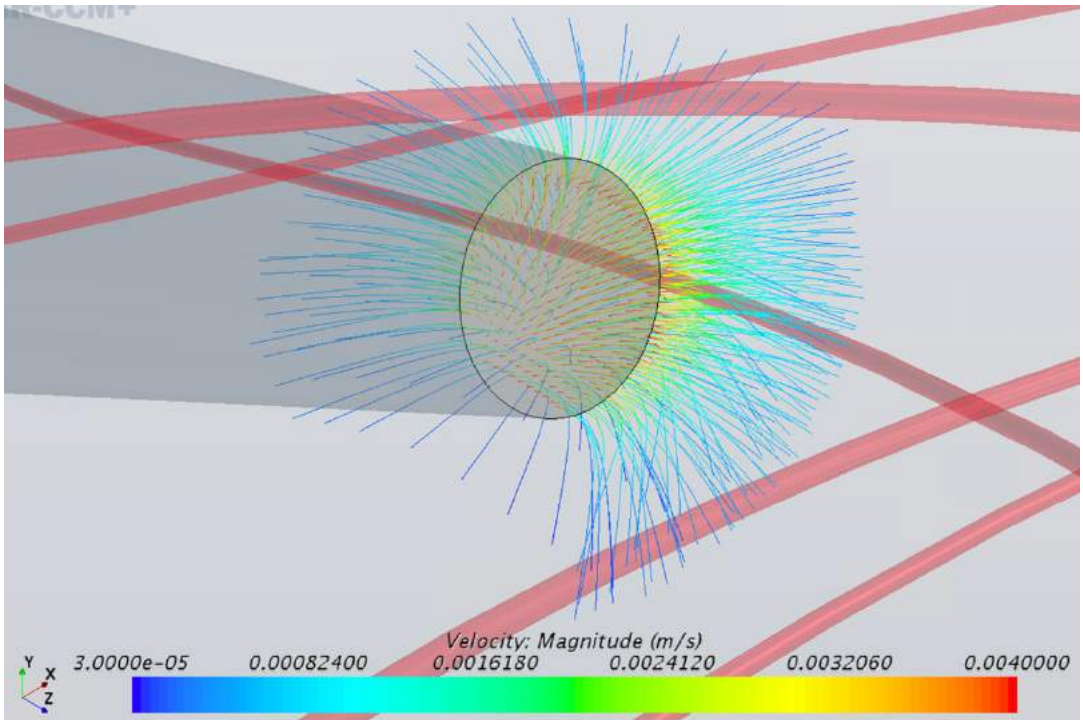

(a)

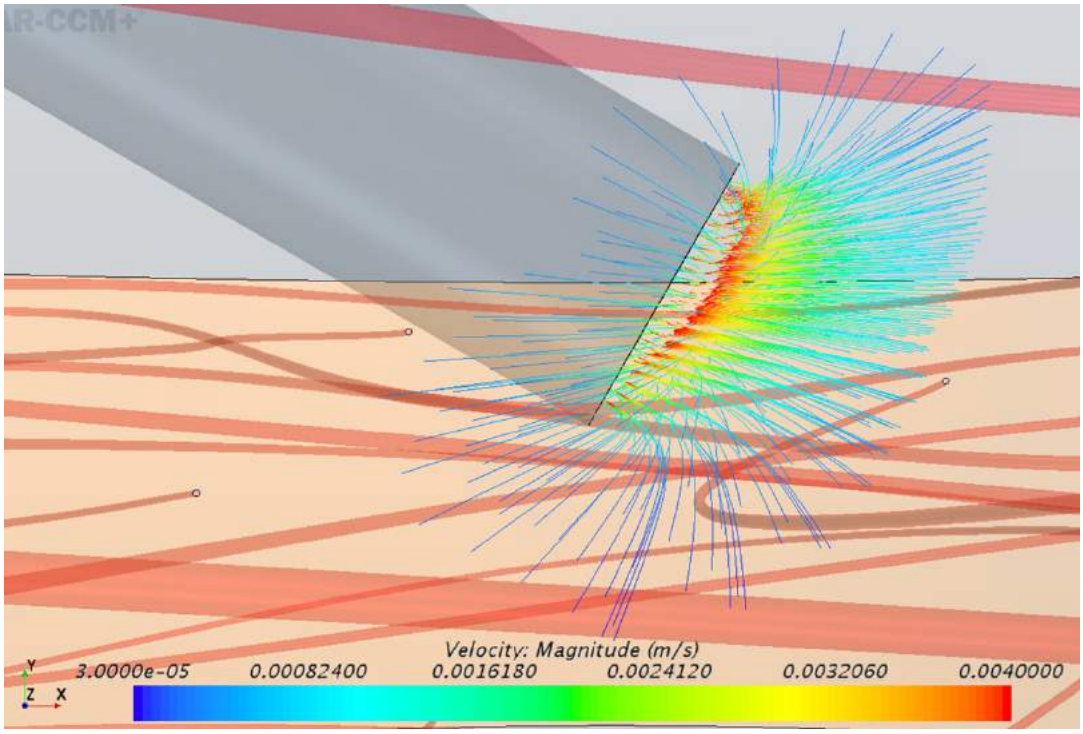

(b)

Figure D-9. Outflow pattern and velocity at cannula outlet in 18 mm tissue with 30° x 13 mm Lg. cannula geometry (a) isometric view (b) side view.

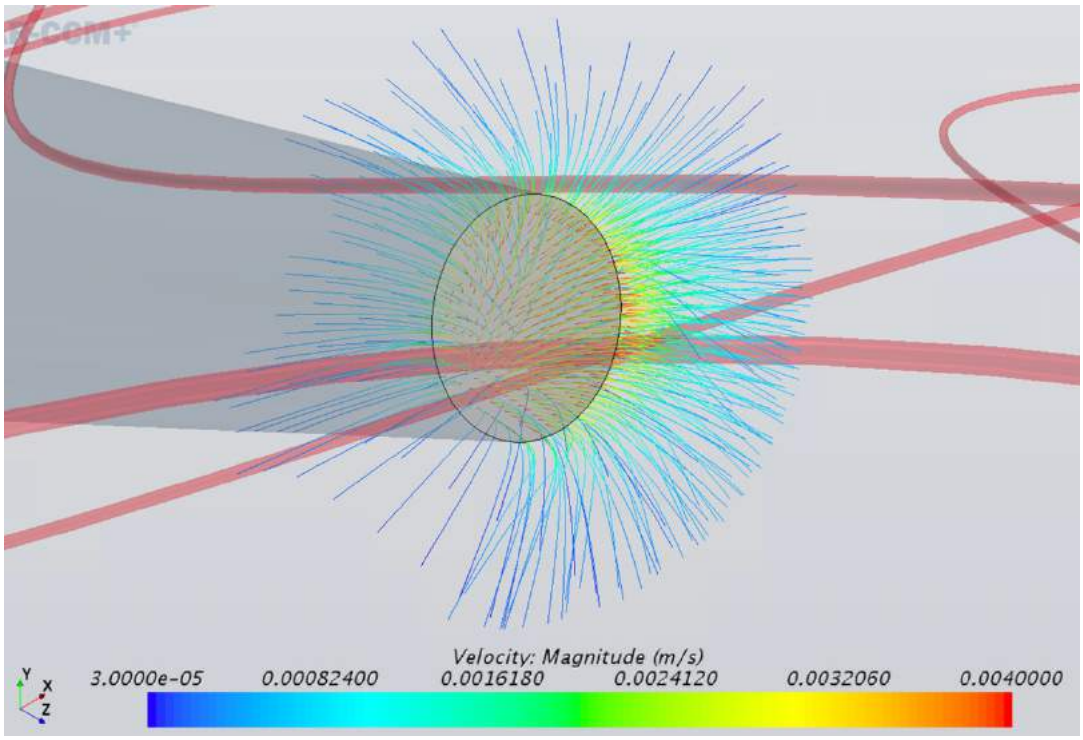

(a)

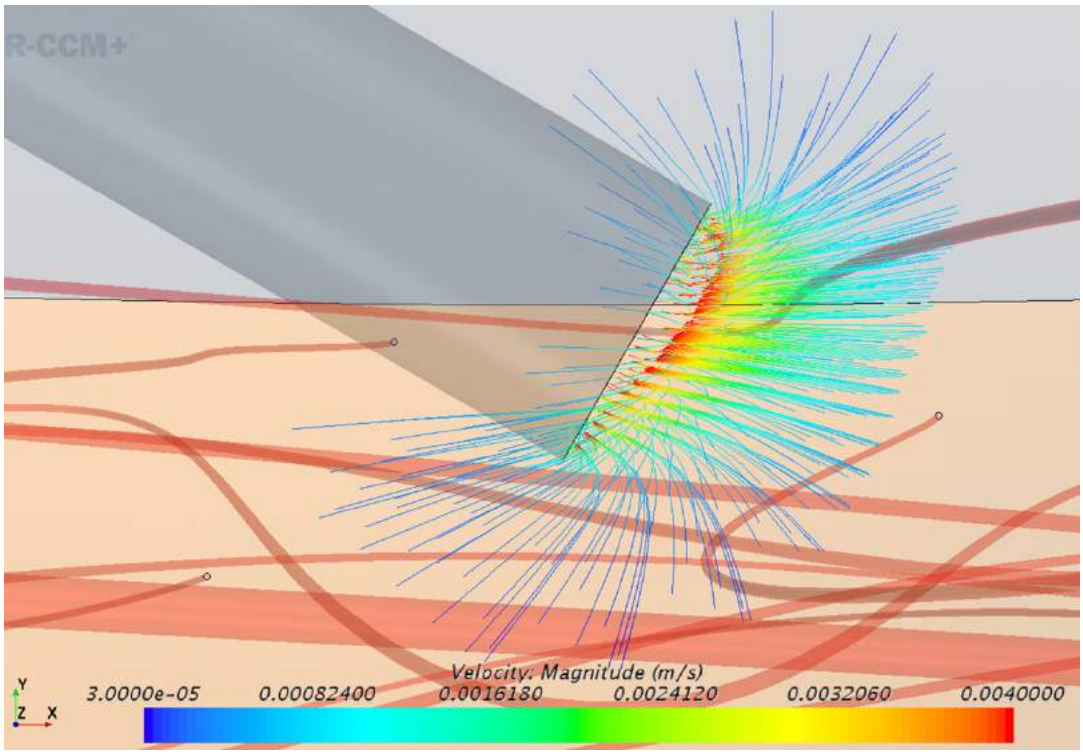

(b)

Figure D-10. Outflow pattern and velocity at cannula outlet in 24 mm tissue with 30° x 13 mm Lg. cannula geometry (a) isometric view (b) side view.

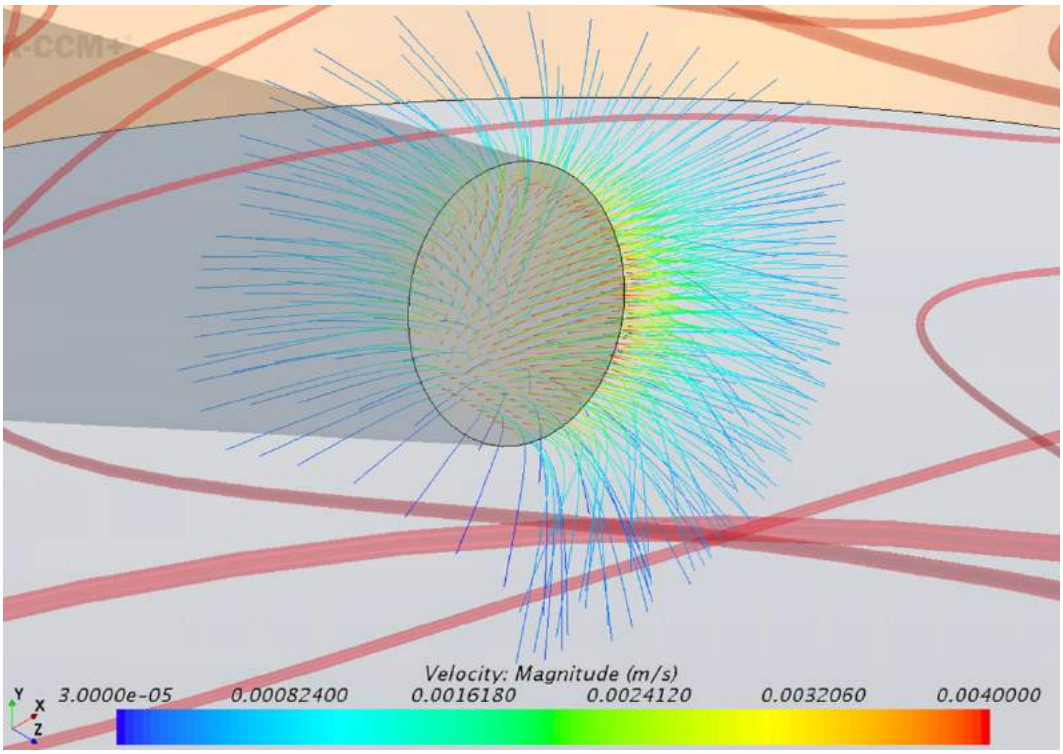

(a)

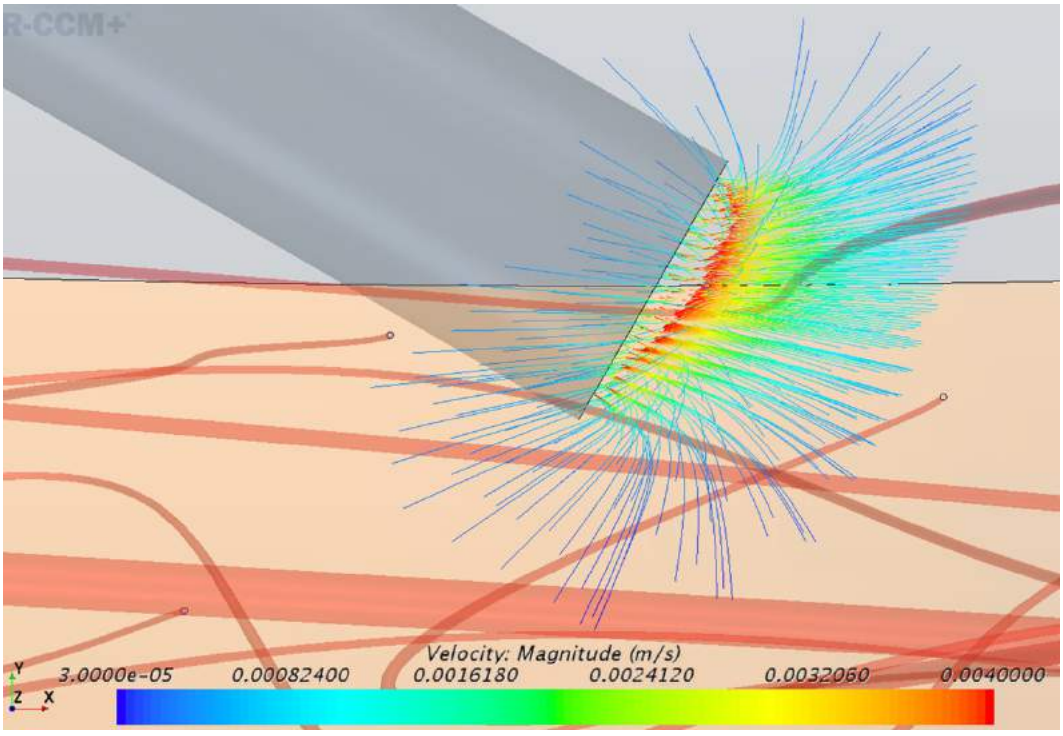

(b)

Figure D-11. Outflow pattern and velocity at cannula outlet in 30 mm tissue with 30° x 13 mm Lg. cannula geometry (a) isometric view (b) side view.

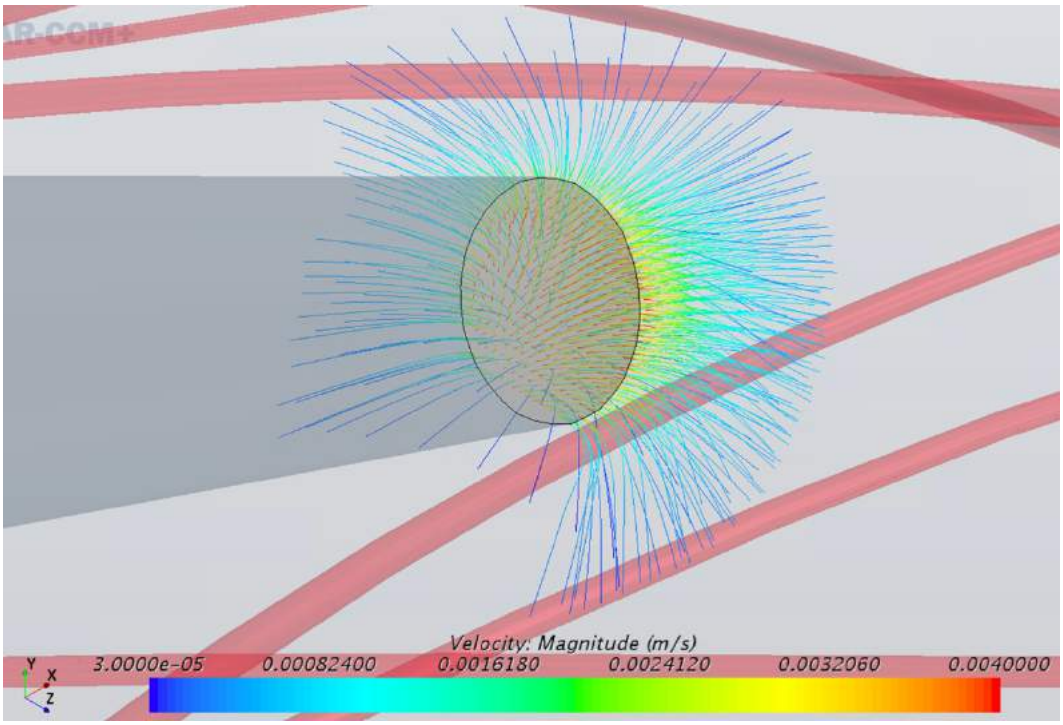

(a)

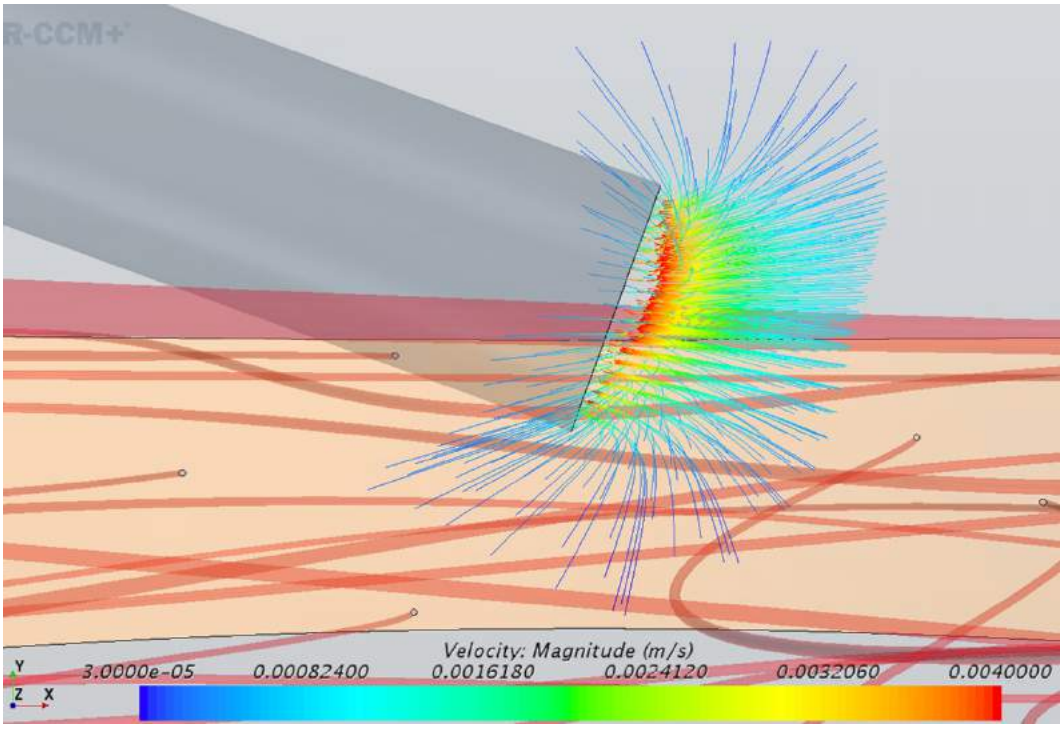

(b)

Figure D-12. Outflow pattern and velocity at cannula outlet in 12 mm tissue with 20° x 13 mm Lg. cannula geometry (a) isometric view (b) side view.

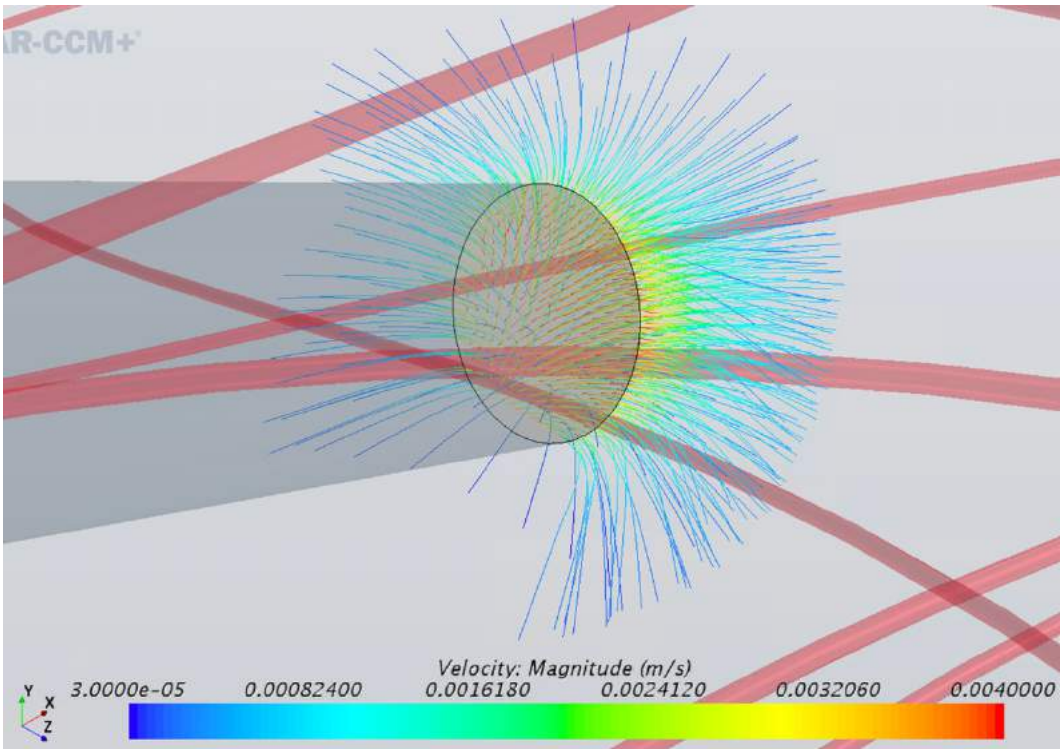

(a)

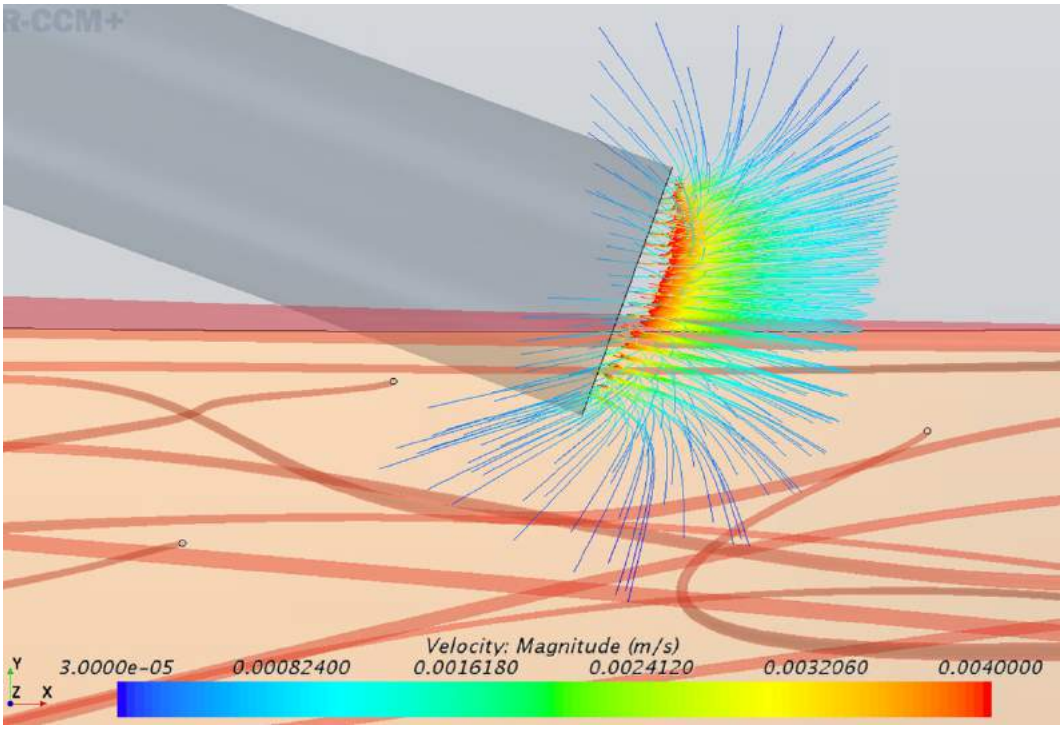

(b)

Figure D-13. Outflow pattern and velocity at cannula outlet in 18 mm tissue with 20° x 13 mm Lg. cannula geometry (a) isometric view (b) side view.

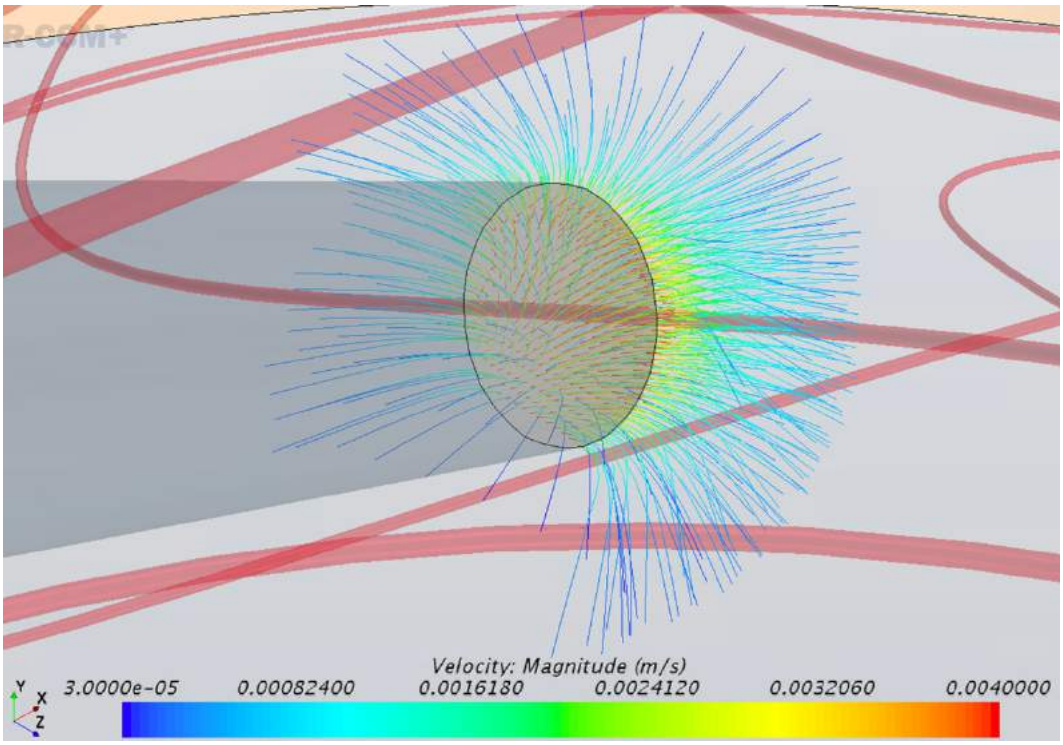

(a)

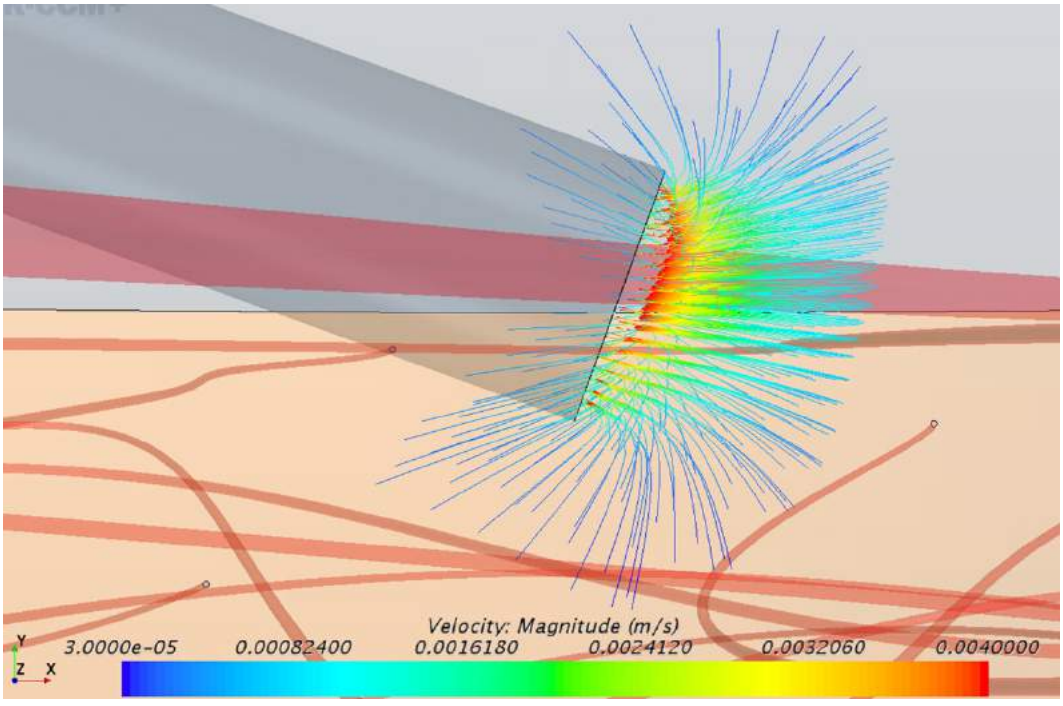

(b)

Figure D-14. Outflow pattern and velocity at cannula outlet in 24 mm tissue with 20° x 13 mm Lg. cannula geometry (a) isometric view (b) side view.

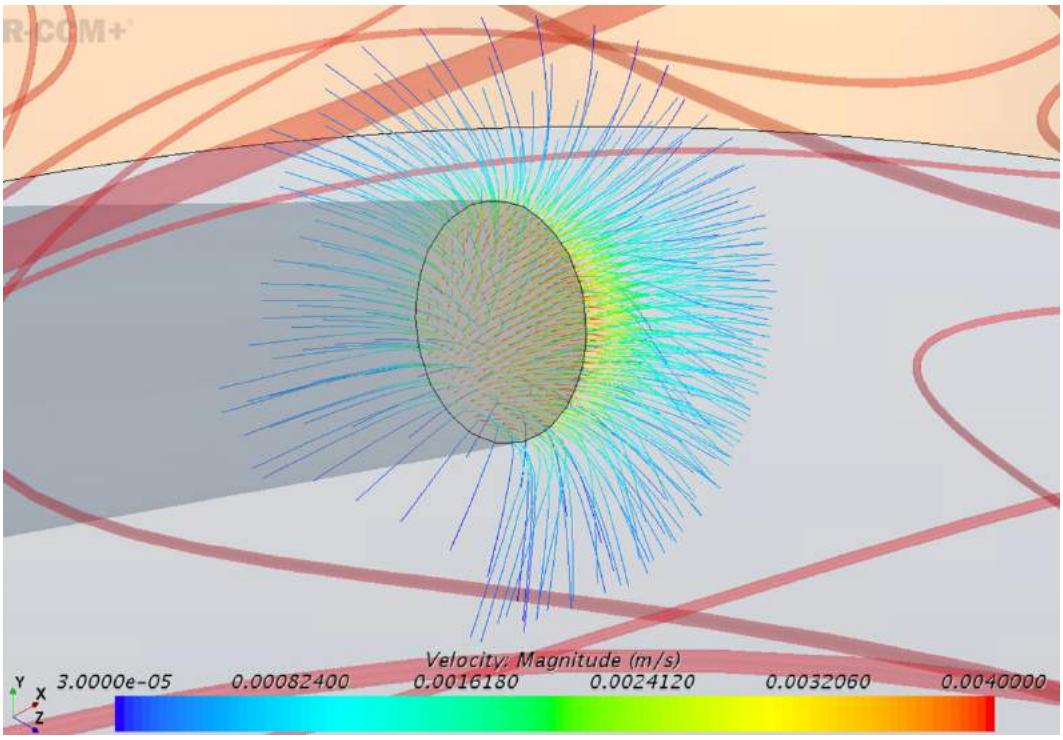

(a)

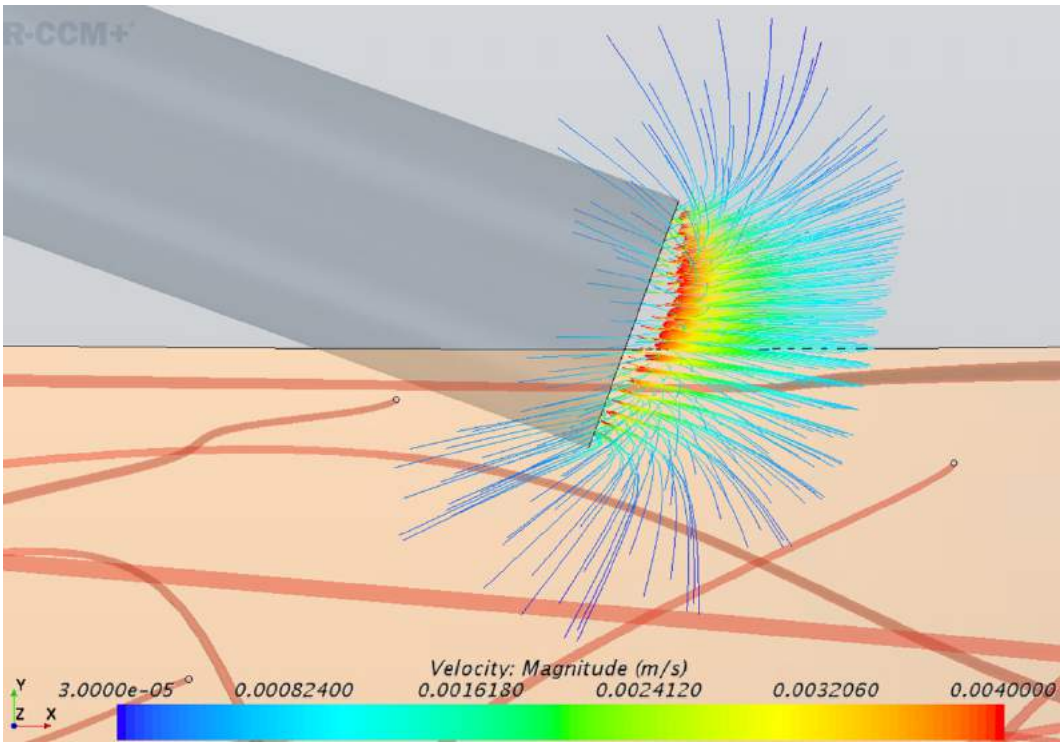

(b)

Figure D-15. Outflow pattern and velocity at cannula outlet in 30 mm tissue with 20° x 13 mm Lg. cannula geometry (a) isometric view (b) side view.

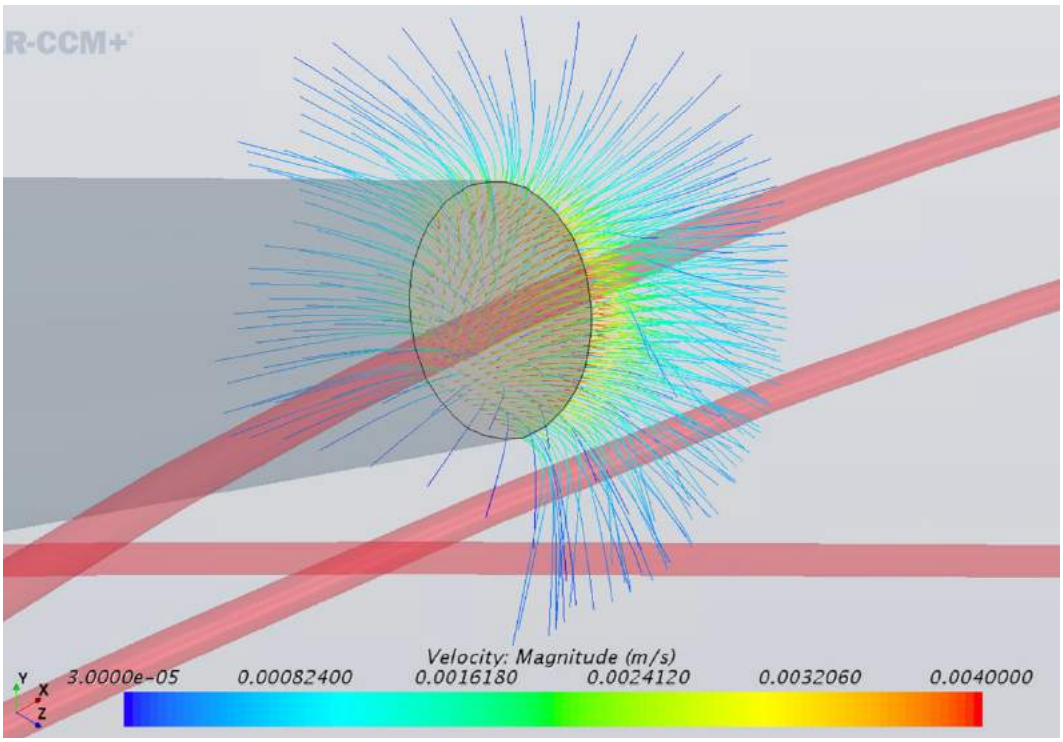

(a)

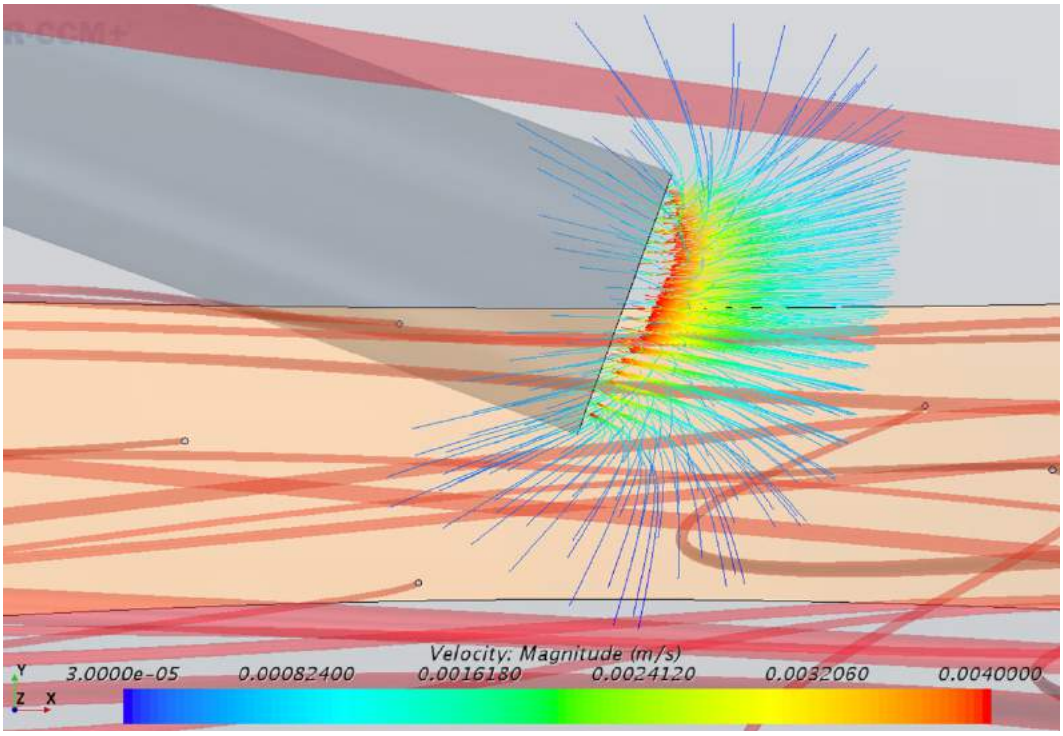

(b)

Figure D-16. Outflow pattern and velocity at cannula outlet in 12 mm tissue with 20° x 17 mm Lg. cannula geometry (a) isometric view (b) side view.

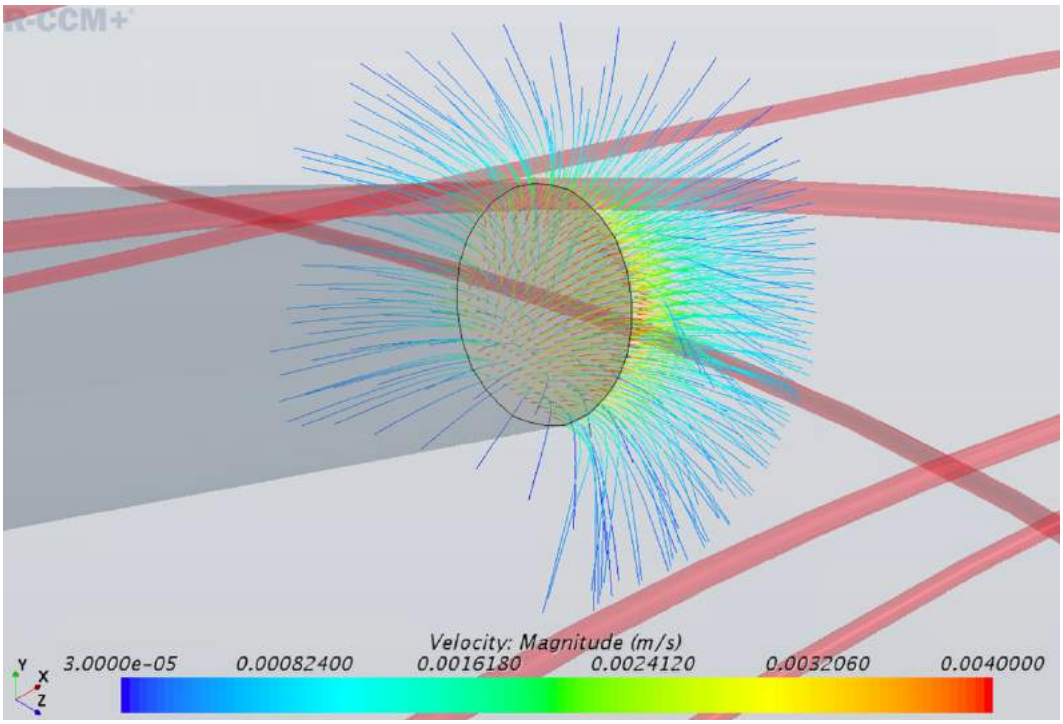

(a)

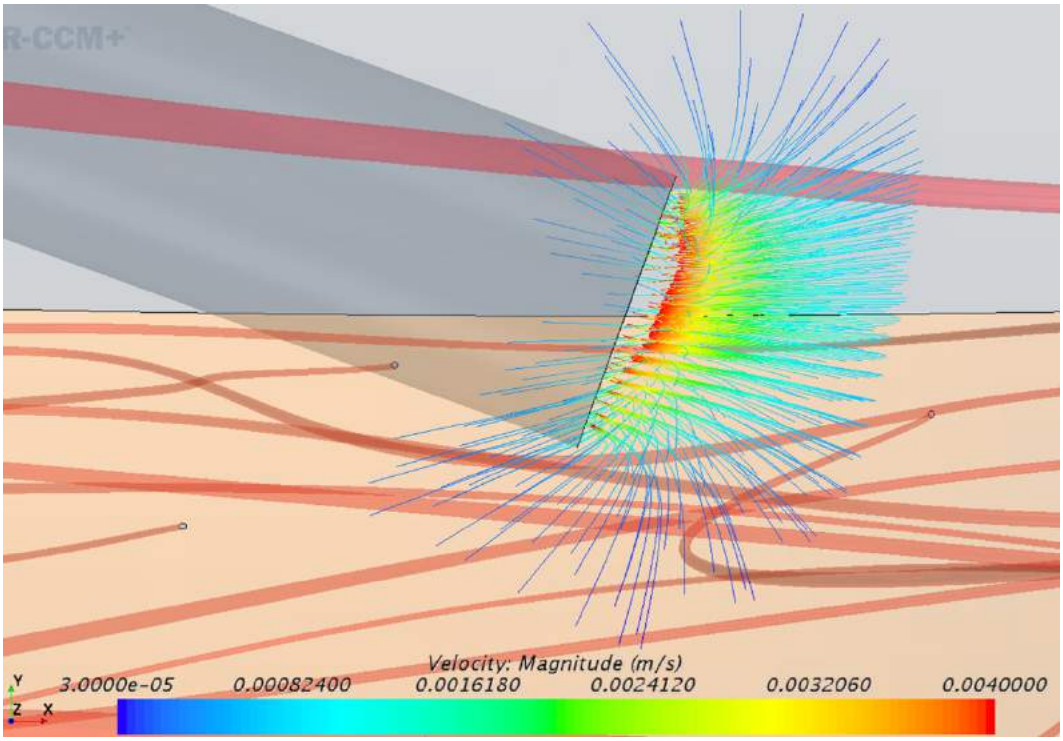

(b)

Figure D-17. Outflow pattern and velocity at cannula outlet in 18 mm tissue with 20° x 17 mm Lg. cannula geometry (a) isometric view (b) side view.

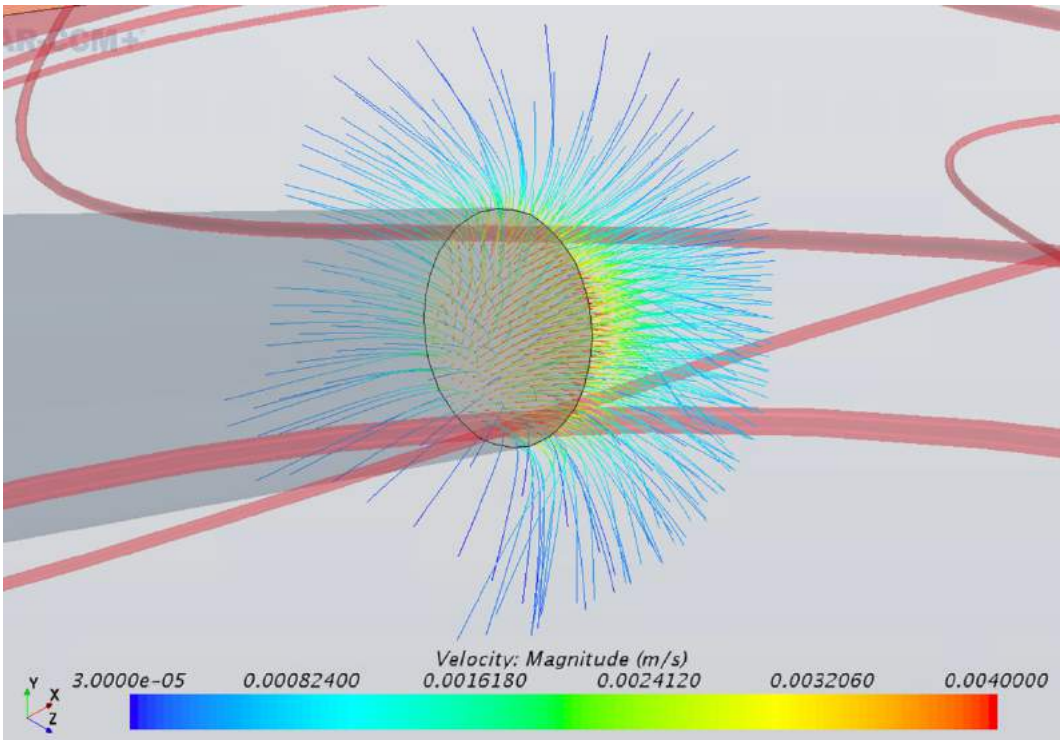

(a)

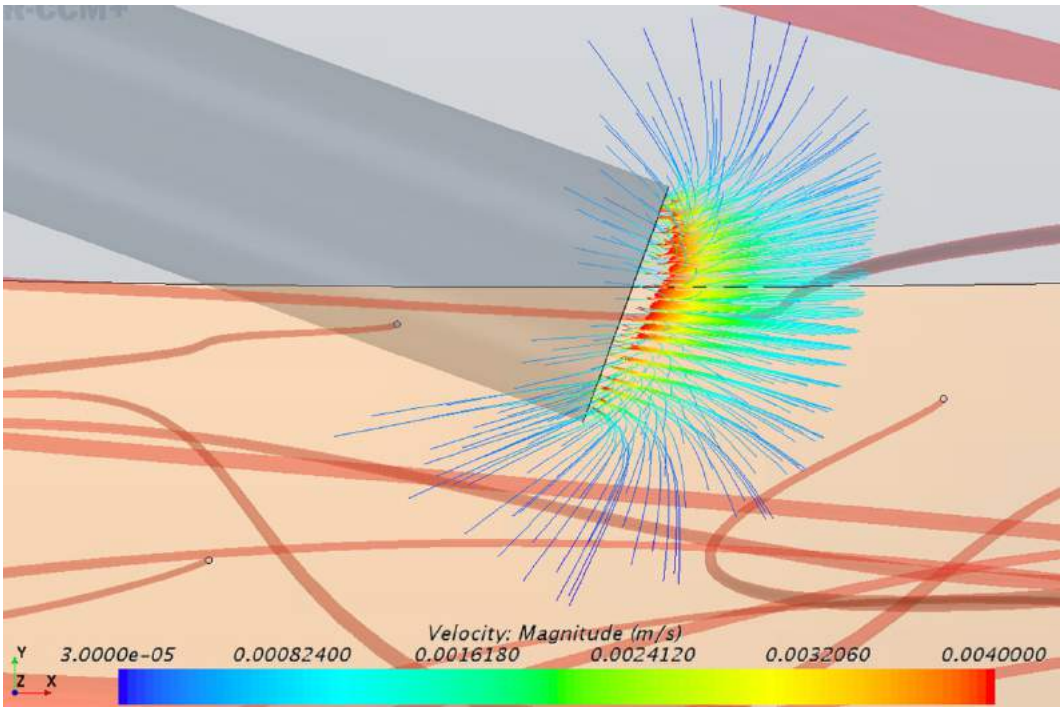

(b)

Figure D-18. Outflow pattern and velocity at cannula outlet in 24 mm tissue with 20° x 17 mm Lg. cannula geometry (a) isometric view (b) side view.

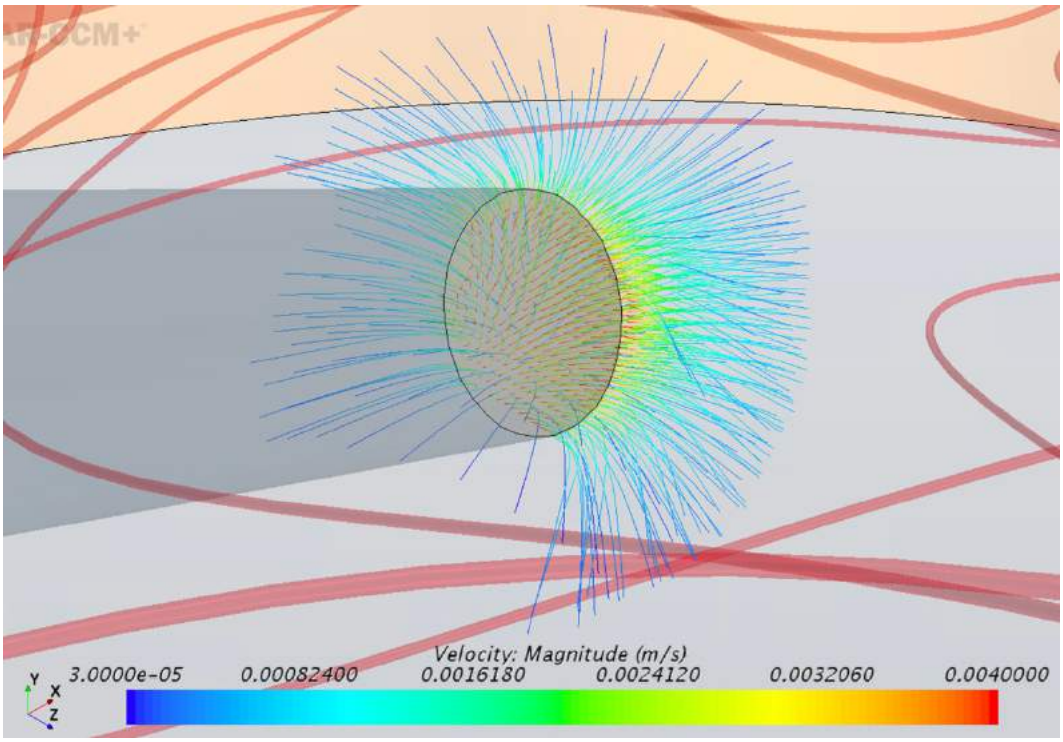

(a)

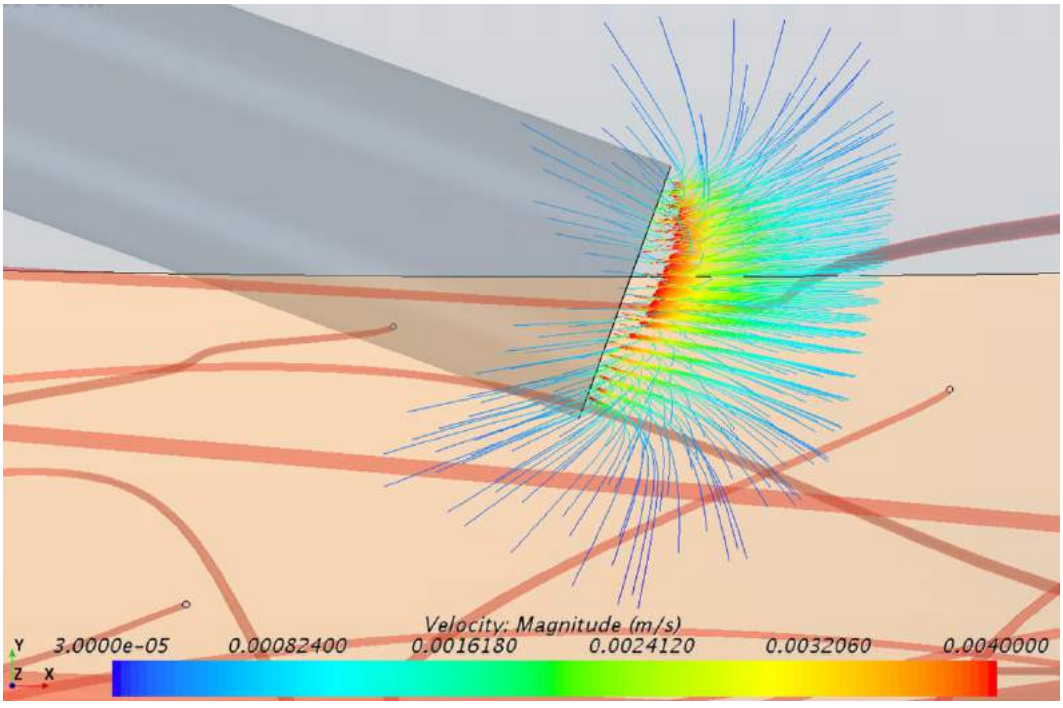

(b)

Figure D-19. Outflow pattern and velocity at cannula outlet in 30 mm tissue with 20° x 17 mm Lg. cannula geometry (a) isometric view (b) side view.

Appendix E: Chapter 8 Additional Figures

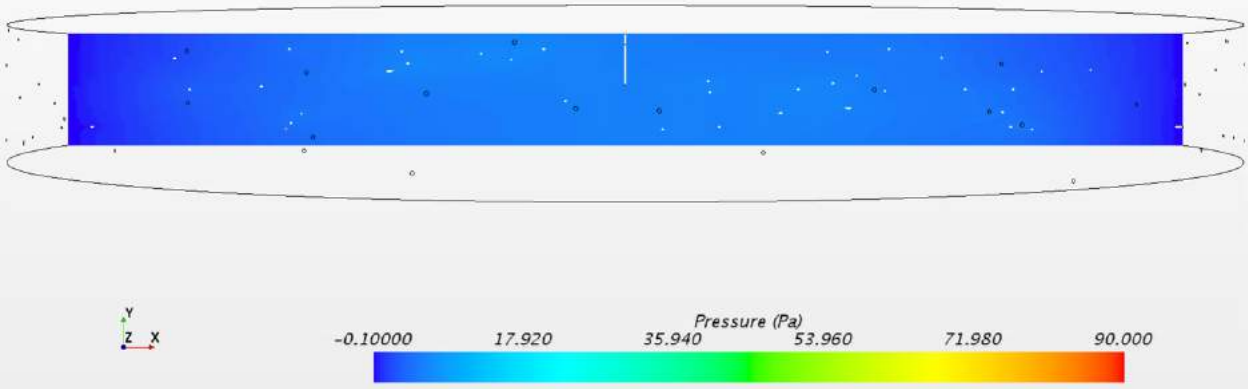

Figure E-1. 12 mm tissue thickness CFD pressure gradient with no insulin delivery.

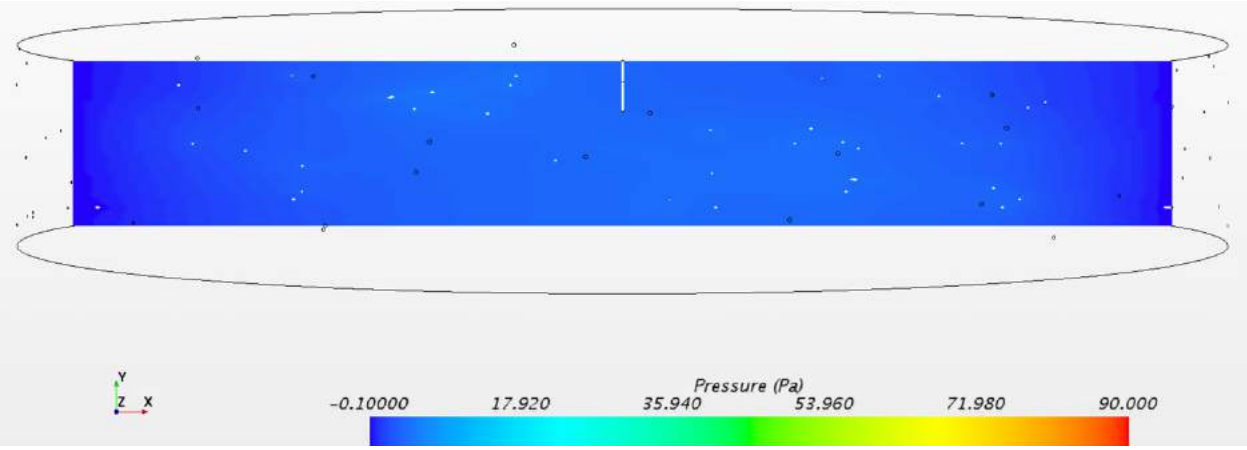

Figure E-2. 18 mm tissue thickness CFD pressure gradient with no insulin delivery.

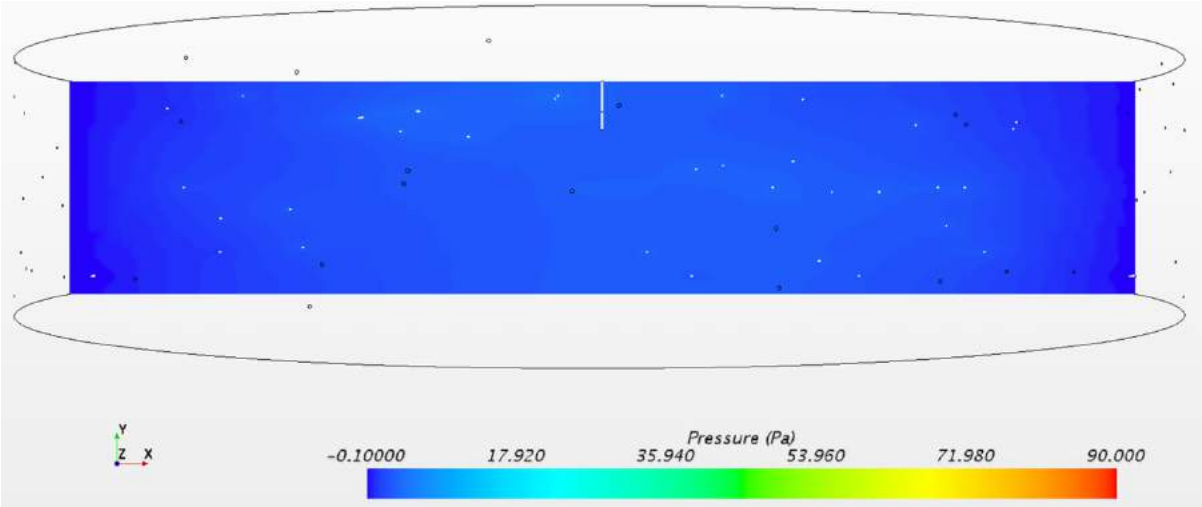

Figure E-3. 24 mm tissue thickness CFD pressure gradient with no insulin delivery.

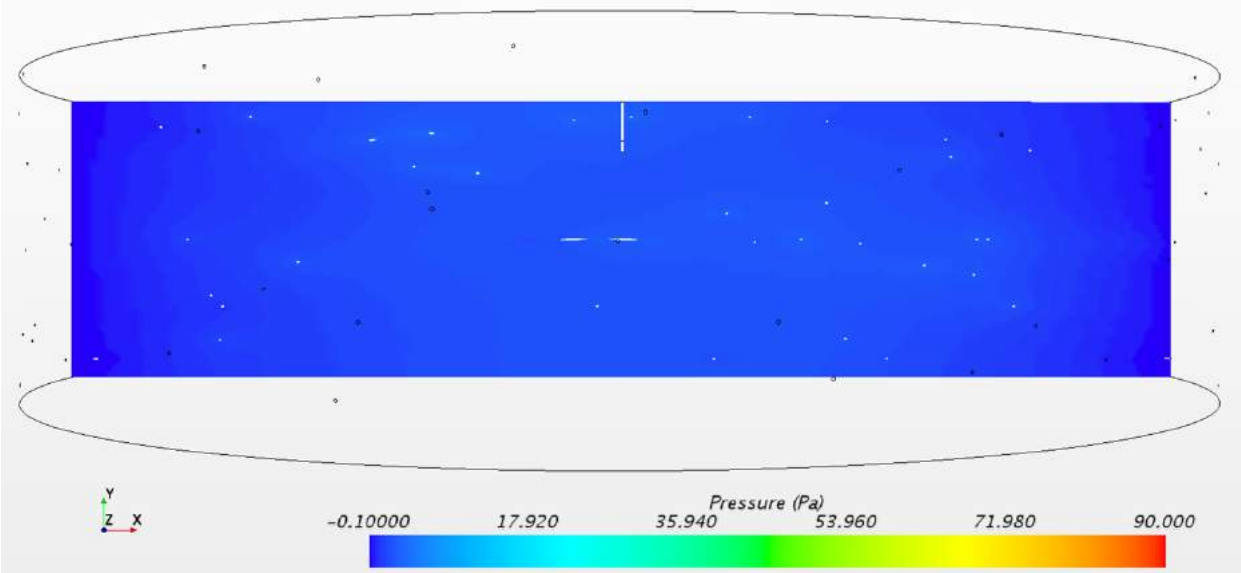

Figure E-4. 30 mm tissue thickness CFD pressure gradient with no insulin delivery.

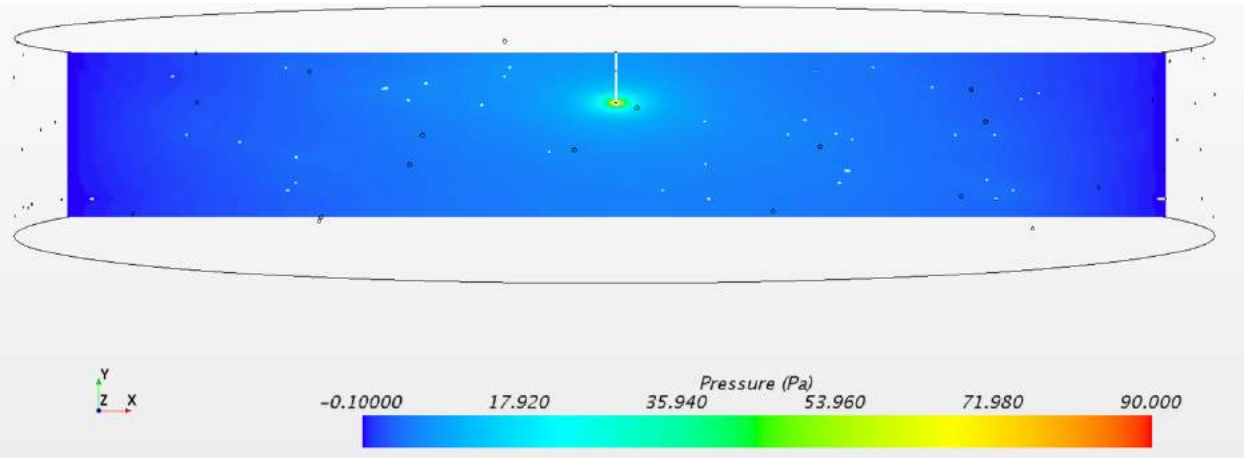

Figure E-5. 18 mm tissue thickness CFD pressure gradient with 90° cannula.

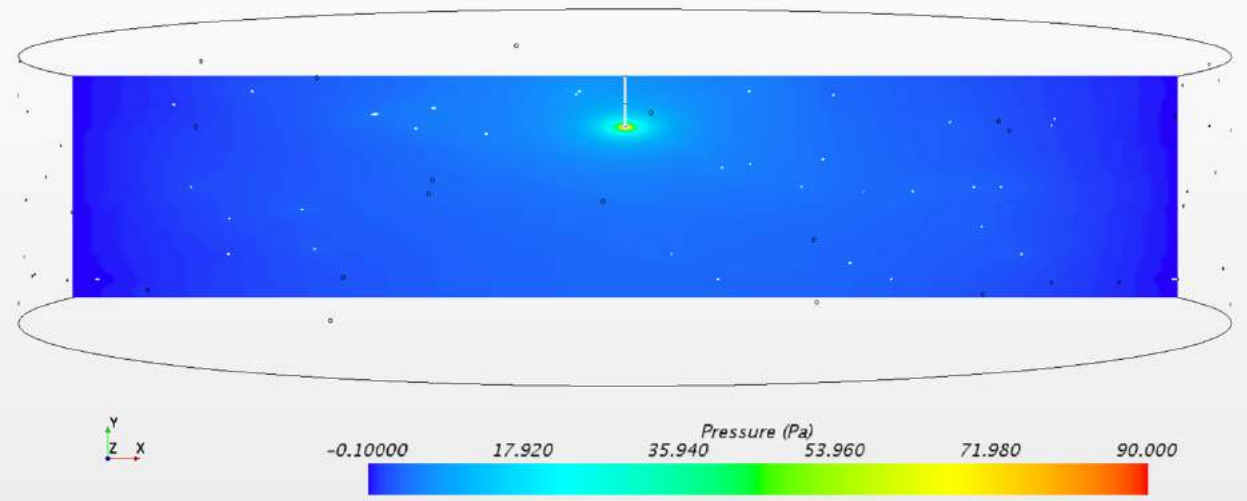

Figure E-6. 24 mm tissue thickness CFD pressure gradient with 90° cannula.

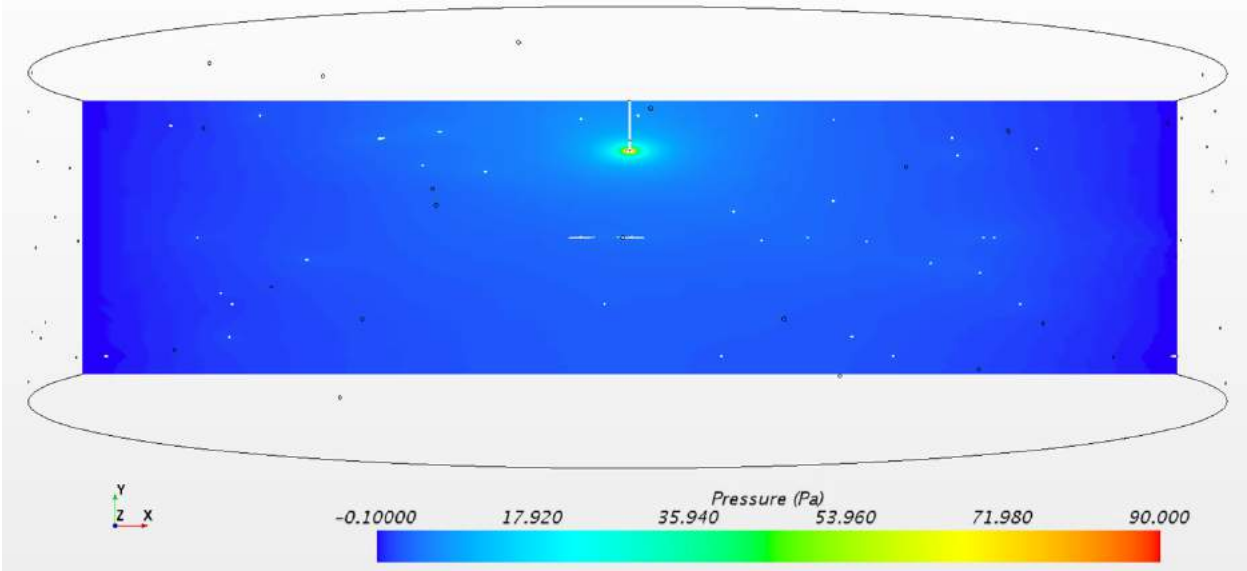

Figure E-7. 30 mm tissue thickness CFD pressure gradient with 90° cannula.

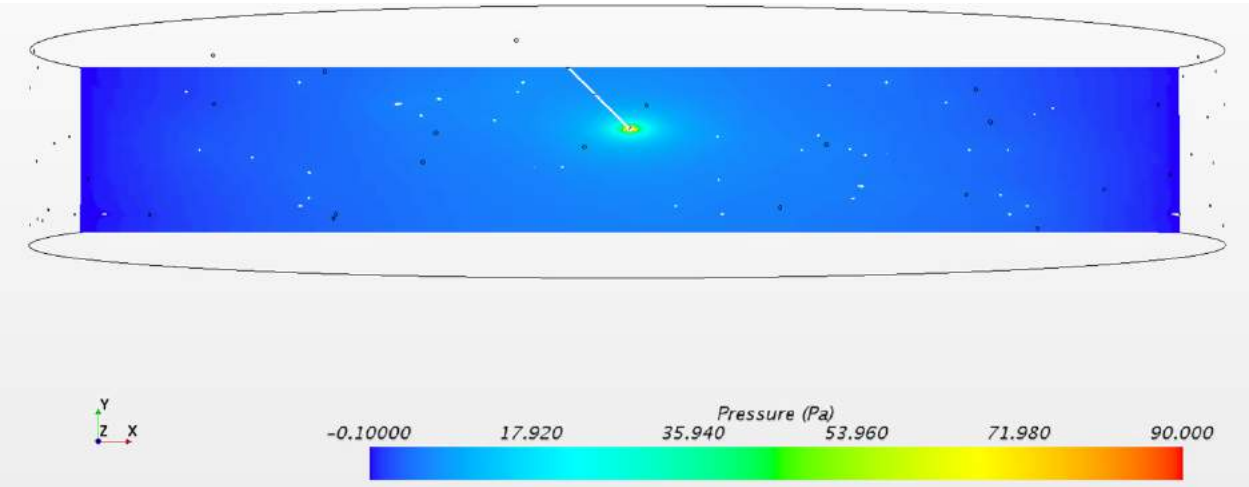

Figure E-8. 18 mm tissue thickness CFD pressure gradient with 45° cannula.

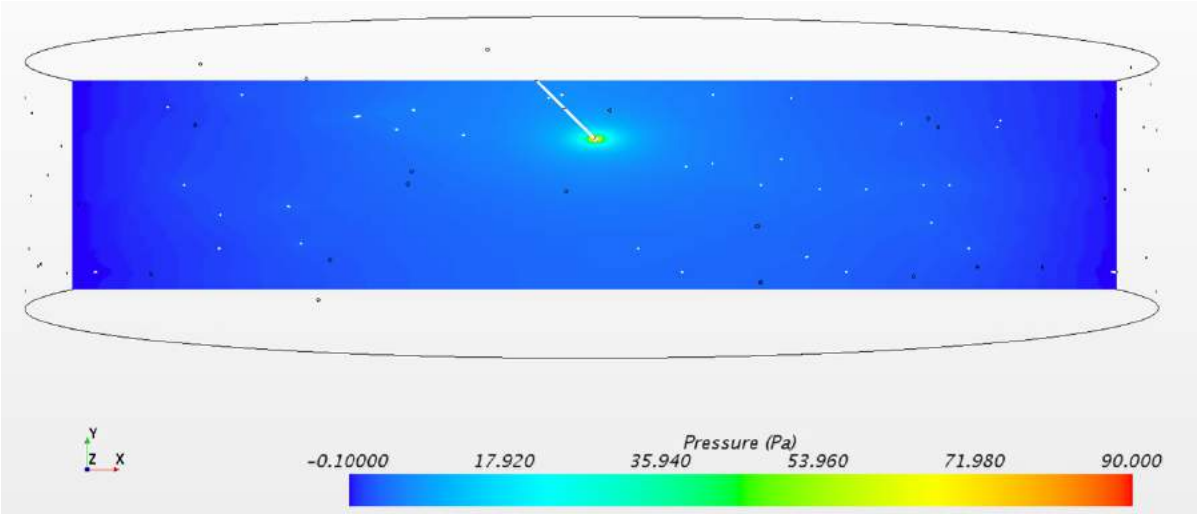

Figure E-9. 24 mm tissue thickness CFD pressure gradient with 45° cannula.

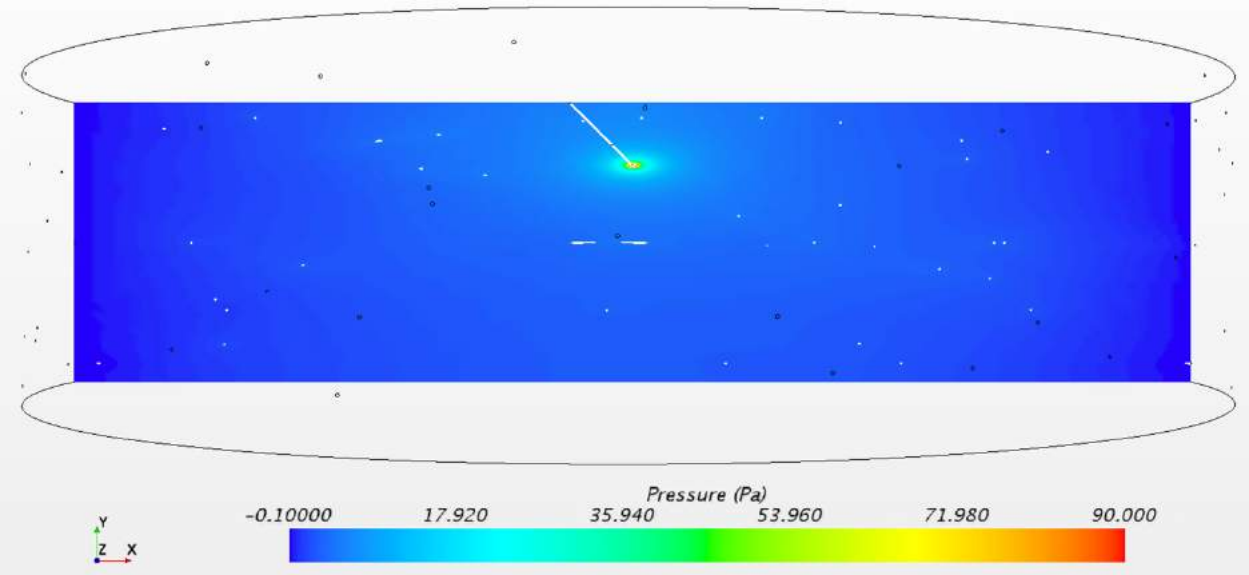

Figure E-10. 30 mm tissue thickness CFD pressure gradient with 45° cannula.

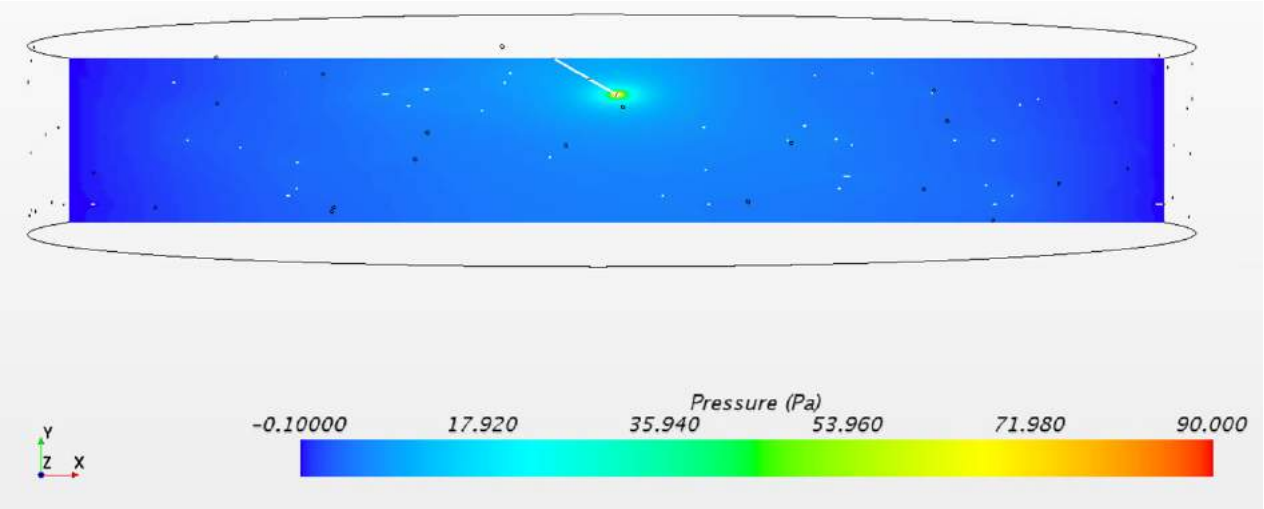

Figure E-11. 18 mm tissue thickness CFD pressure gradient with 30° cannula.

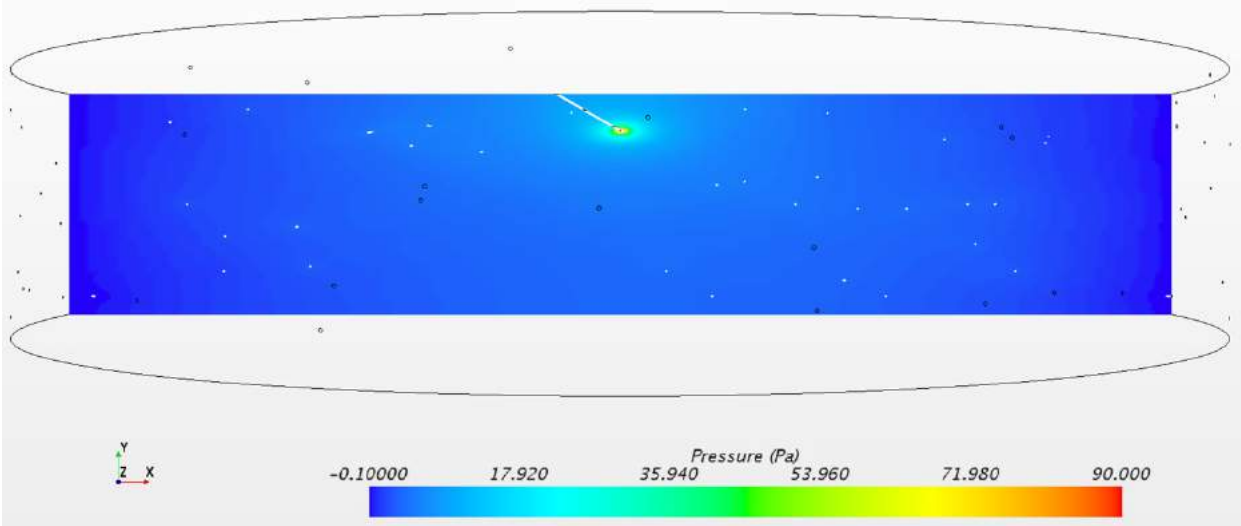

Figure E-12. 24 mm tissue thickness CFD pressure gradient with 30° cannula.

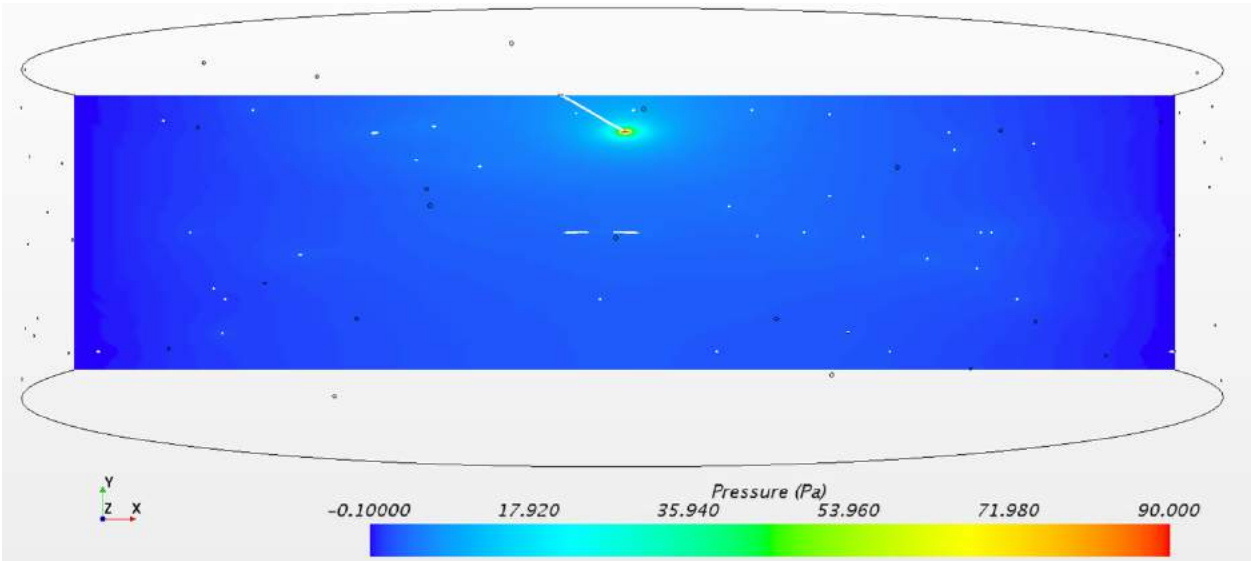

Figure E-13. 30 mm tissue thickness CFD pressure gradient with 30° cannula.

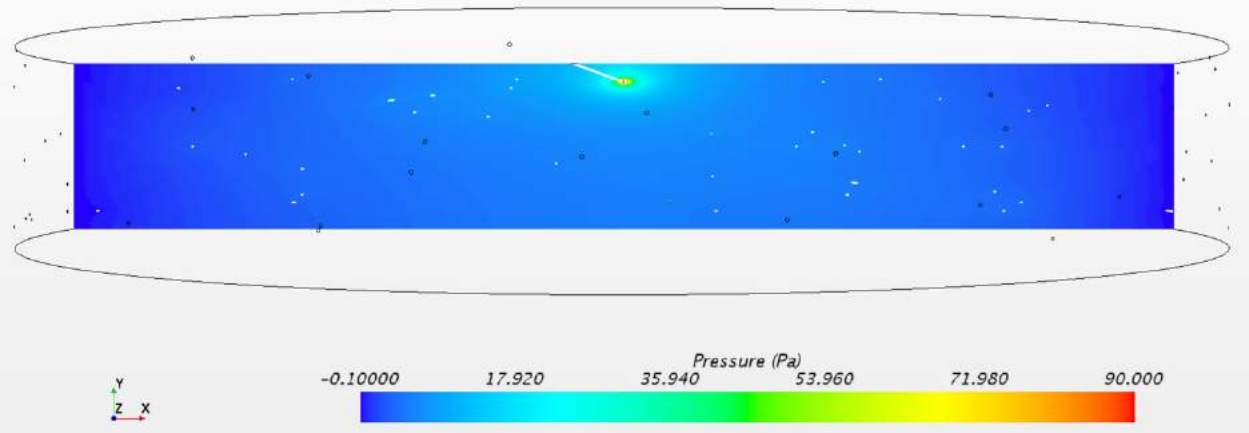

Figure E-14. 18 mm tissue thickness CFD pressure gradient with 20° 13 mm long cannula.

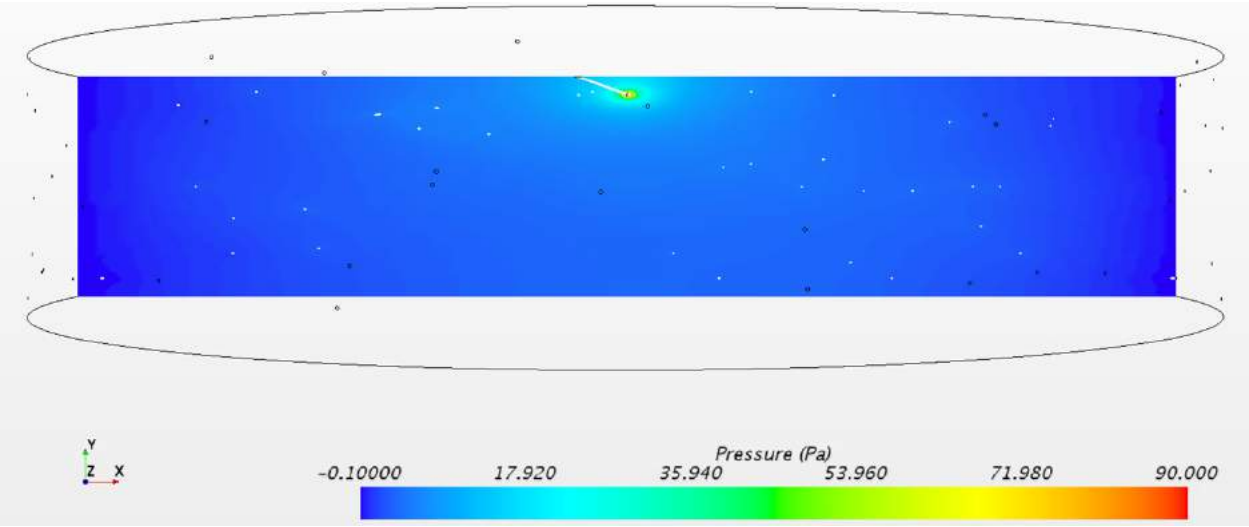

Figure E-15. 24 mm tissue thickness CFD pressure gradient with 20° 13 mm long cannula.

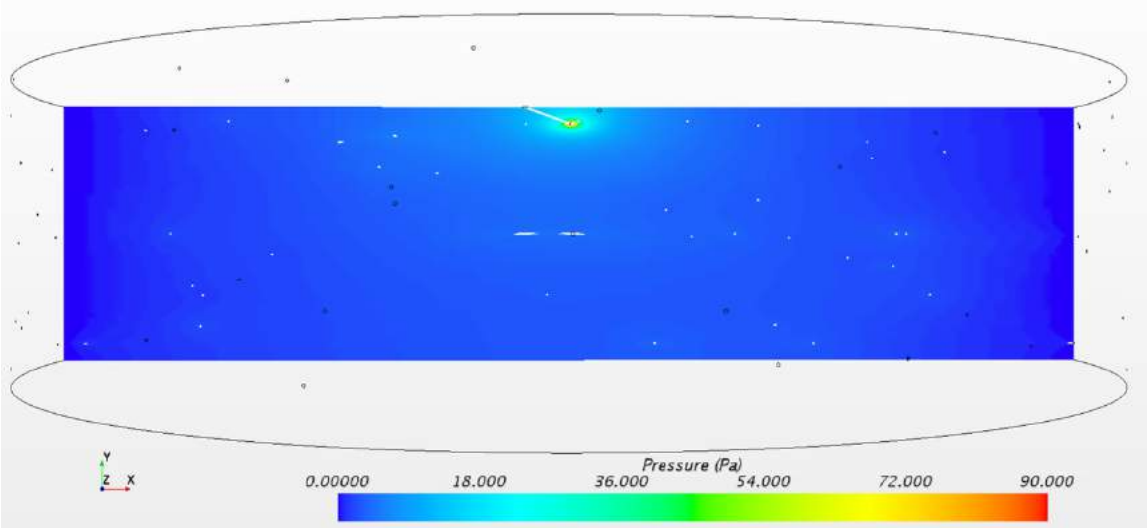

Figure E-16. 30 mm tissue thickness CFD pressure gradient with 20° 13 mm long cannula.

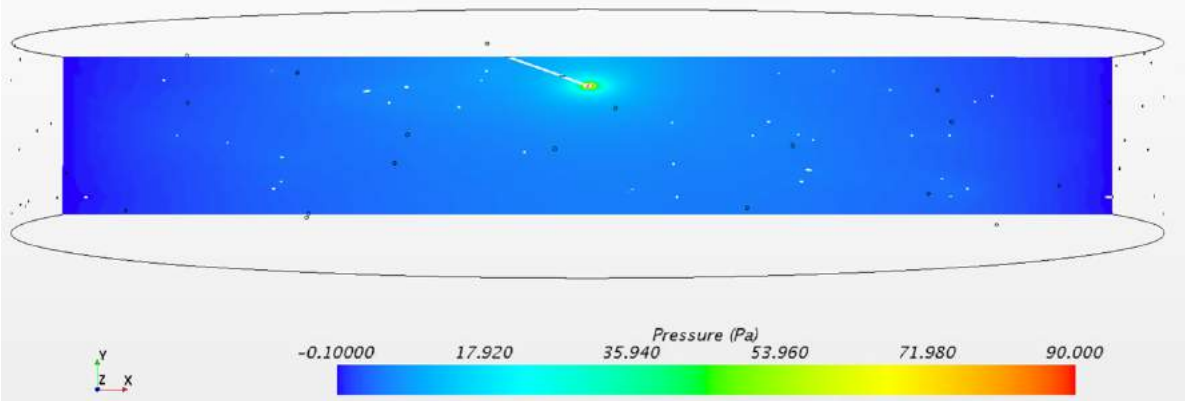

Figure E-17. 18 mm tissue thickness CFD pressure gradient with 20° 13 mm long cannula.

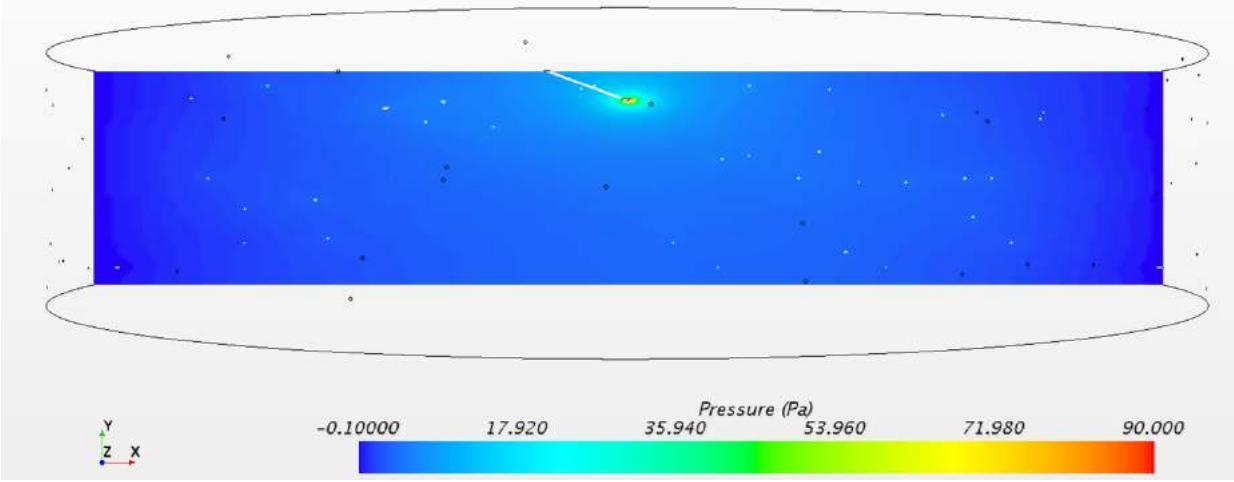

Figure E-18. 24 mm tissue thickness CFD pressure gradient with 20° 13 mm long cannula.

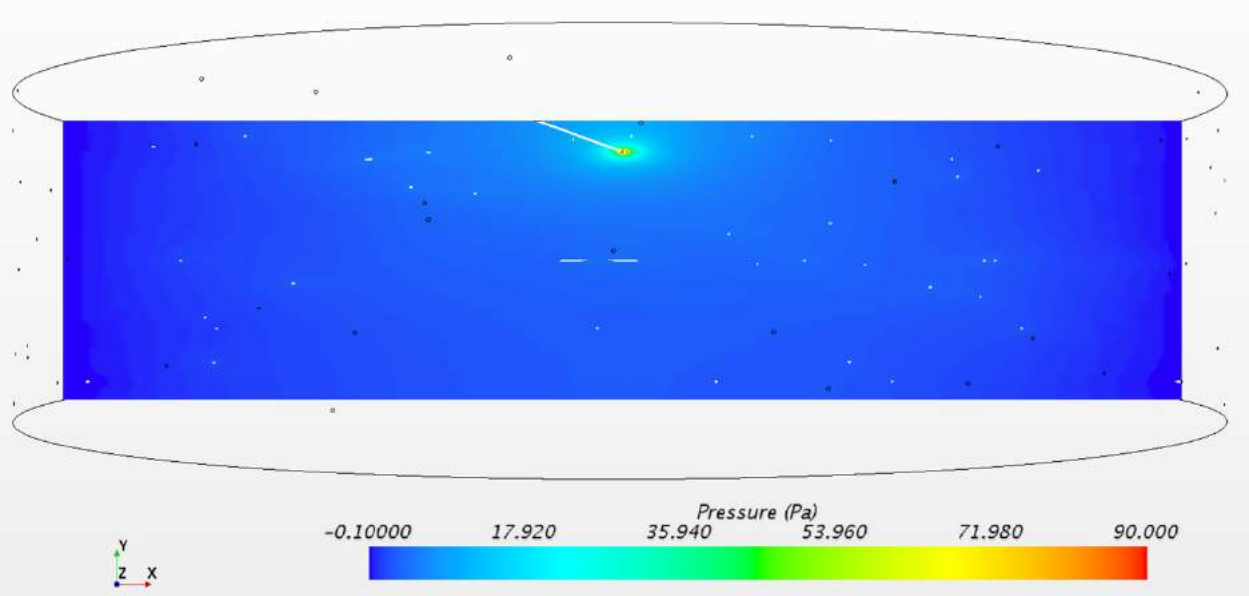

Figure E-19. 30 mm tissue thickness CFD pressure gradient with 20° 13 mm long cannula.

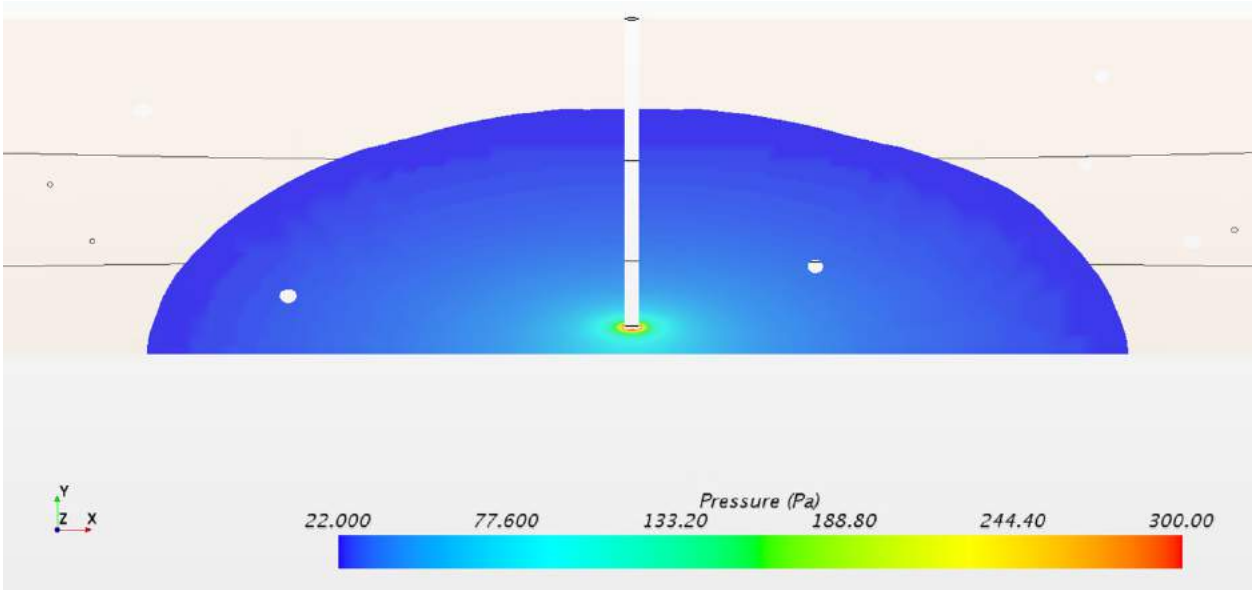

Figure E-20. 6 mm tissue thickness CFD pressure gradient of insulin depot at cannula tip with 90° cannula.

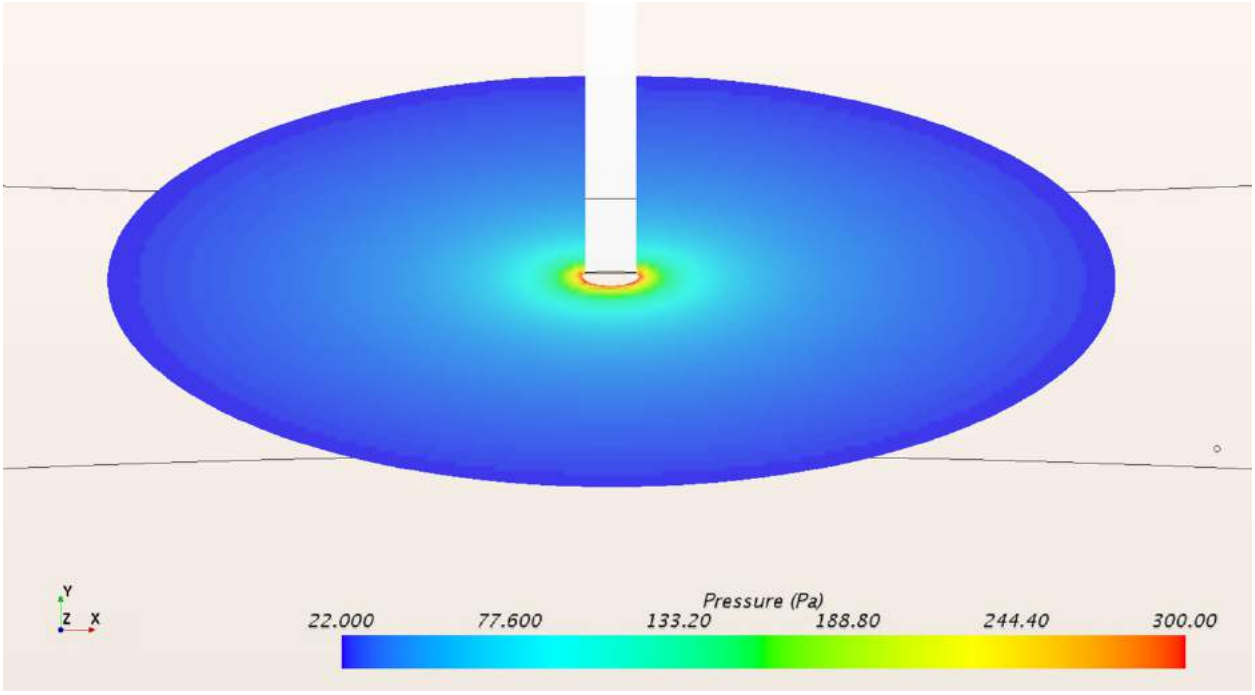

Figure E-21. 12 mm tissue thickness CFD pressure gradient of insulin depot at cannula tip with 90° cannula.

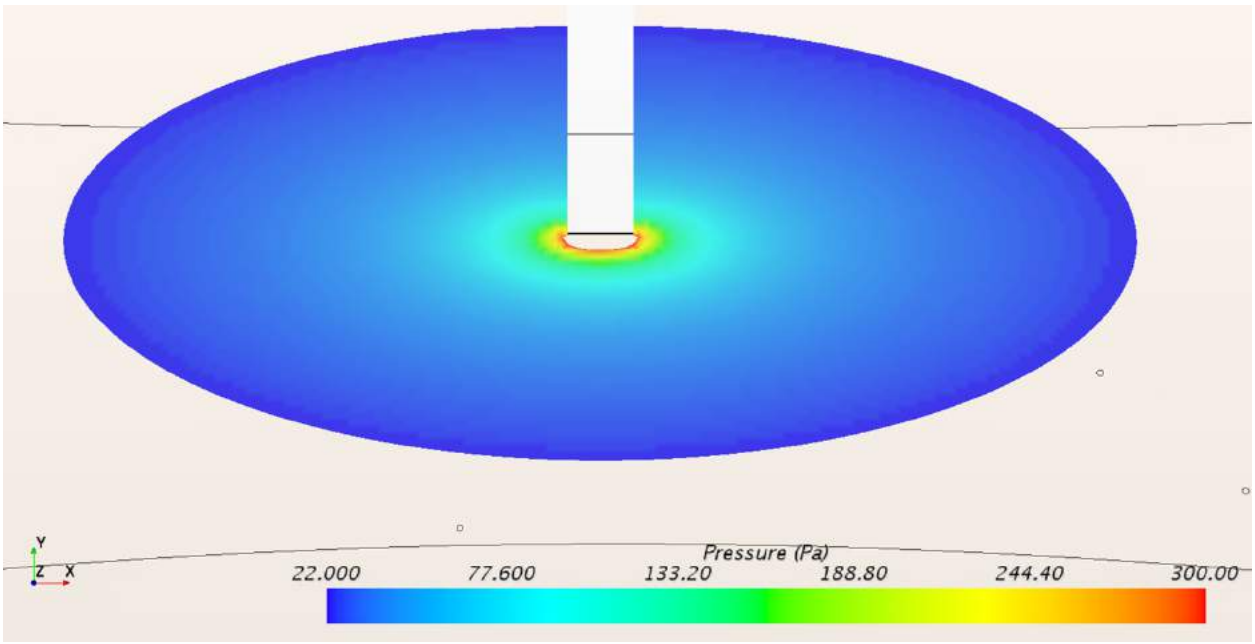

Figure E-22. 18 mm tissue thickness CFD pressure gradient of insulin depot at cannula tip with 90° cannula.

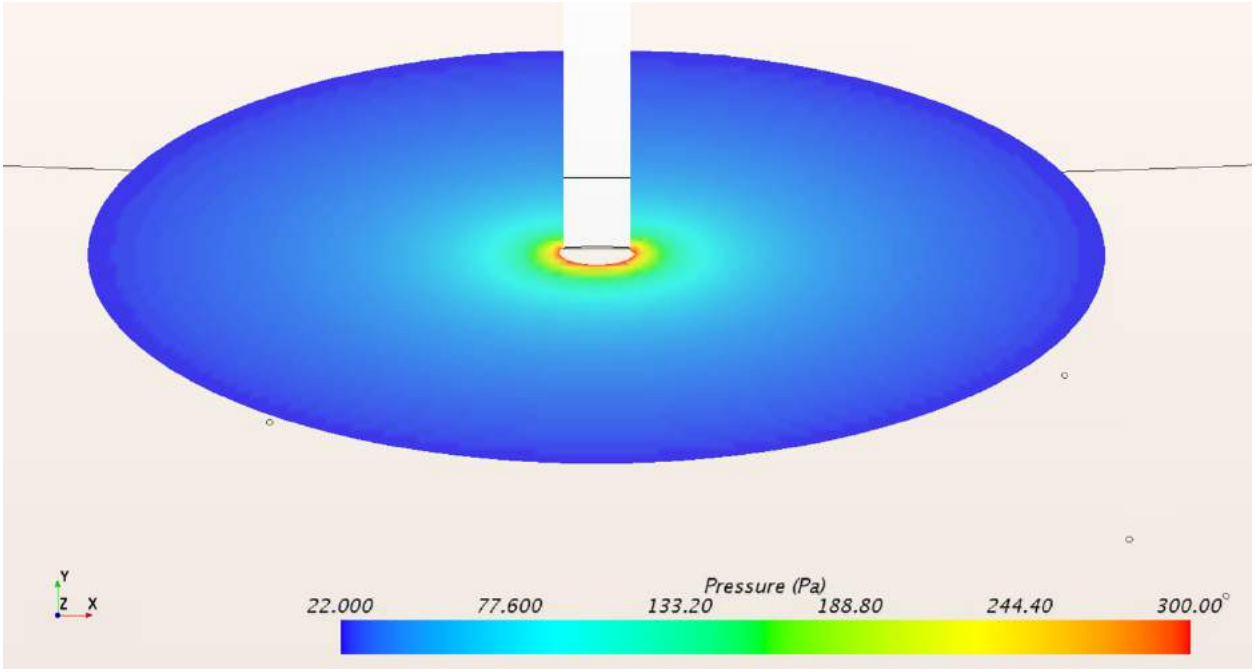

Figure E-23. 24 mm tissue thickness CFD pressure gradient of insulin depot at cannula tip with 90° cannula.

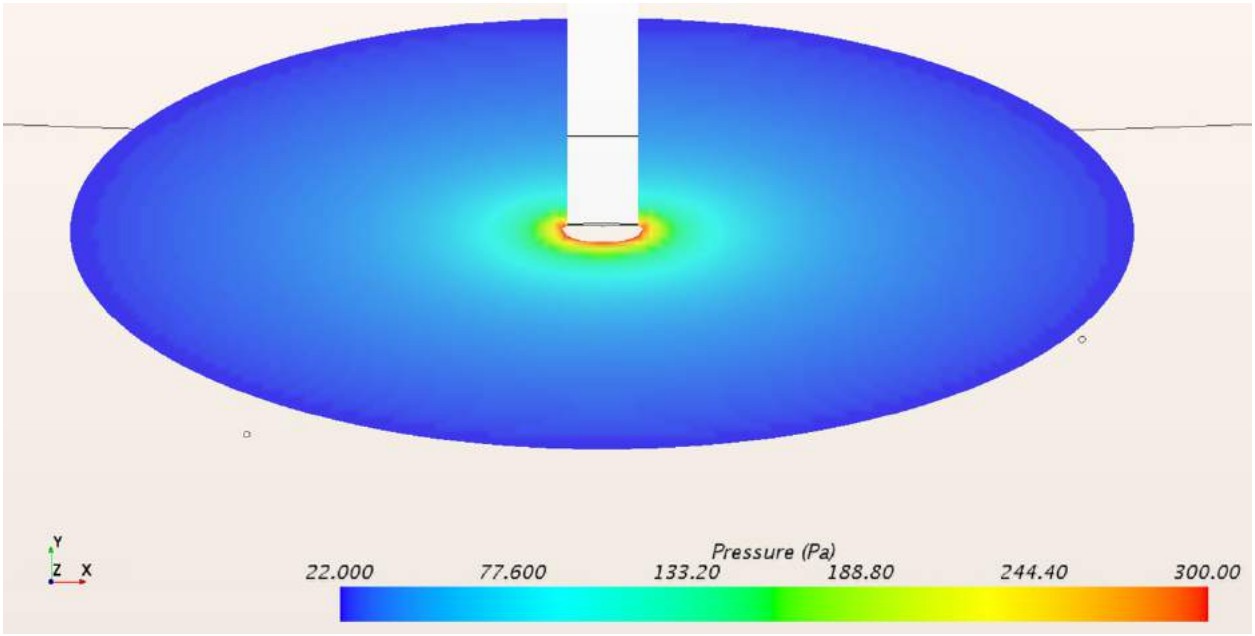

Figure E-24. 30 mm tissue thickness CFD pressure gradient of insulin depot at cannula tip with 90° cannula.

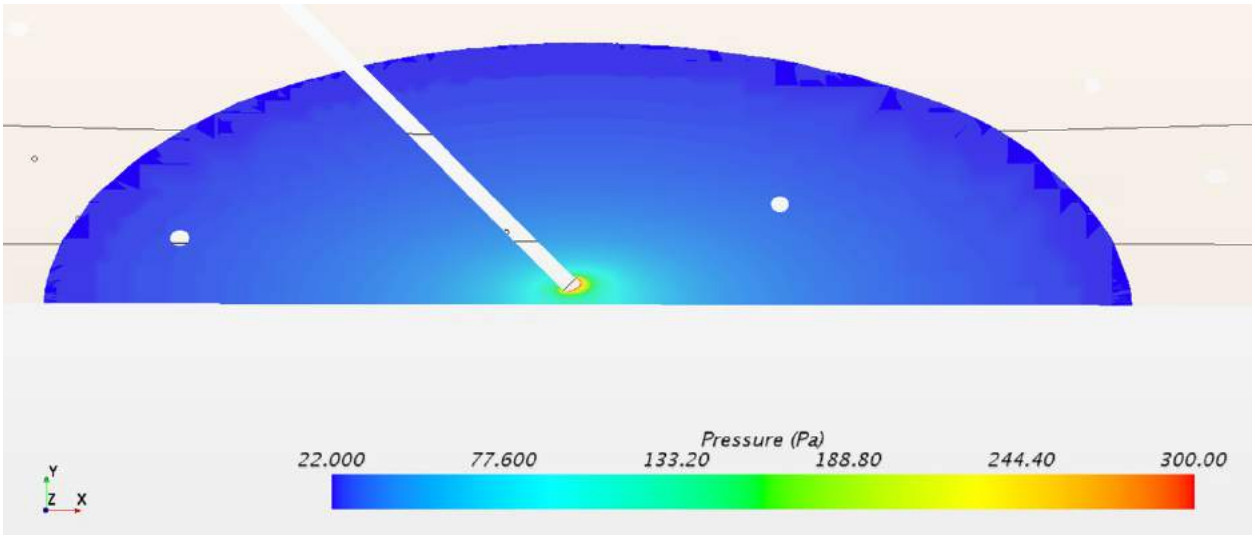

Figure E-25. 6 mm tissue thickness CFD pressure gradient of insulin depot at cannula tip with 45° cannula.

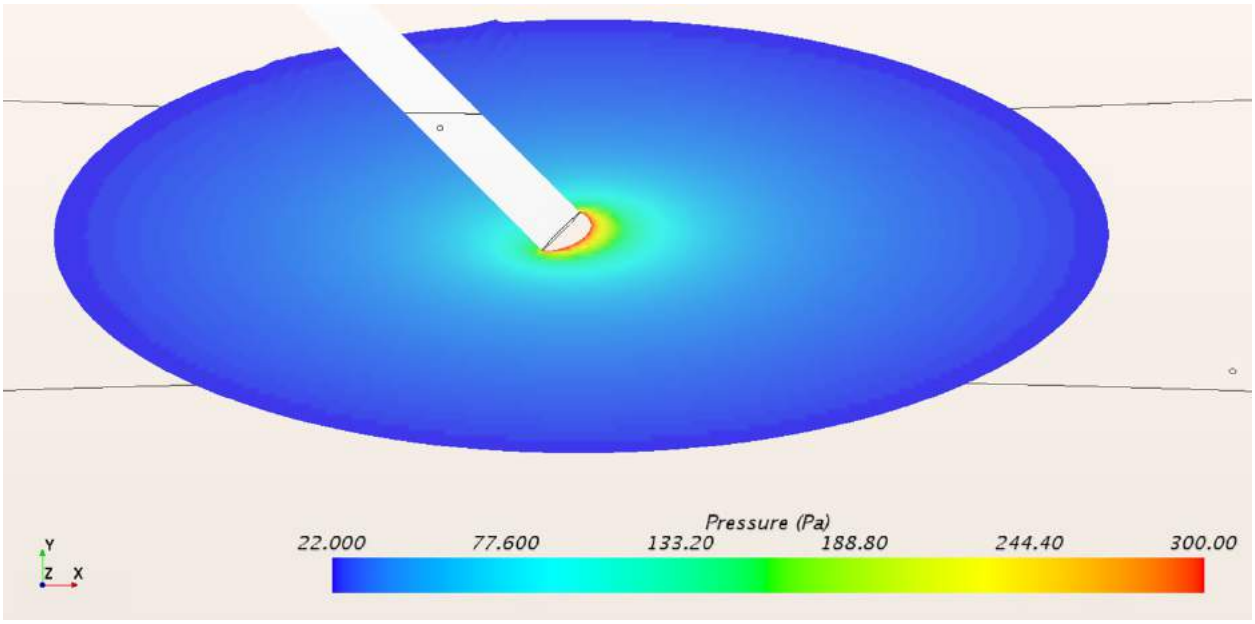

Figure E-26. 12 mm tissue thickness CFD pressure gradient of insulin depot at cannula tip with 45° cannula.

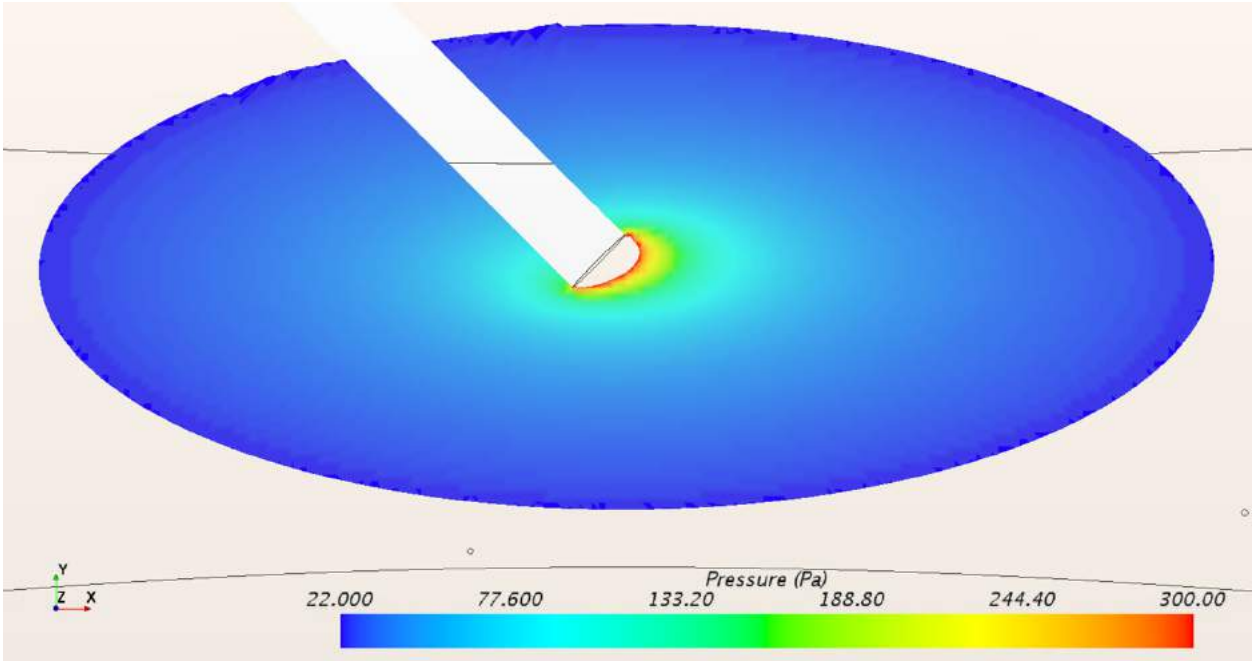

Figure E-27. 18 mm tissue thickness CFD pressure gradient of insulin depot at cannula tip with 45° cannula.

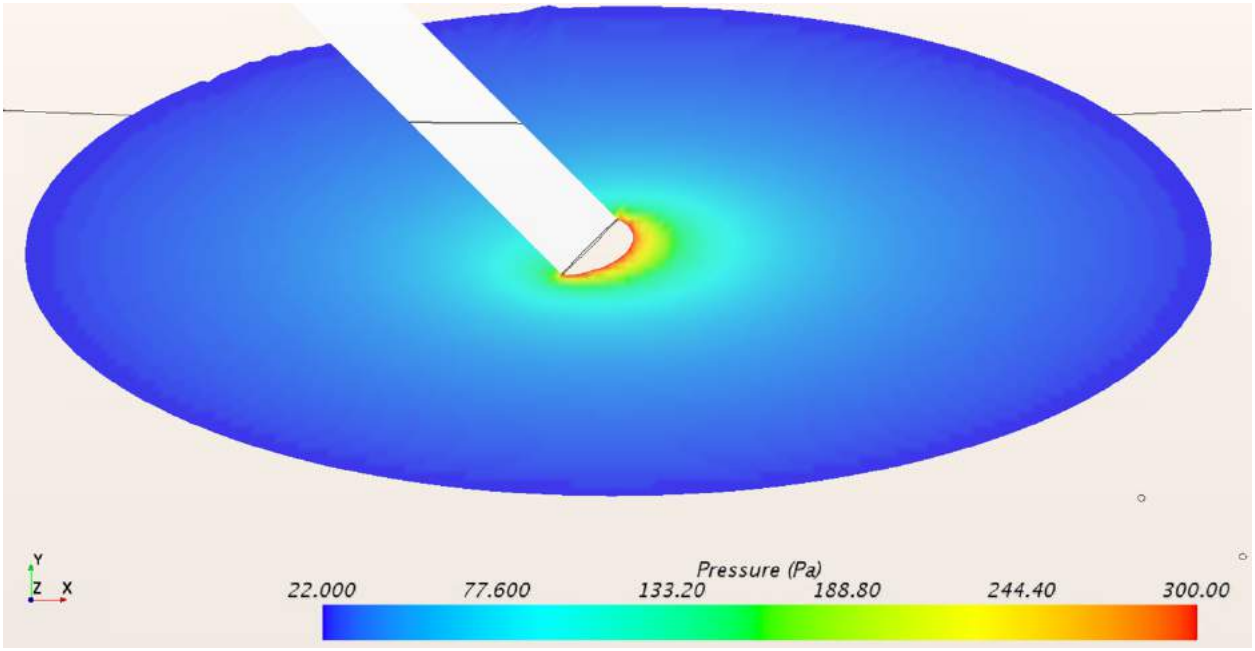

Figure E-28. 24 mm tissue thickness CFD pressure gradient of insulin depot at cannula tip with 45° cannula.

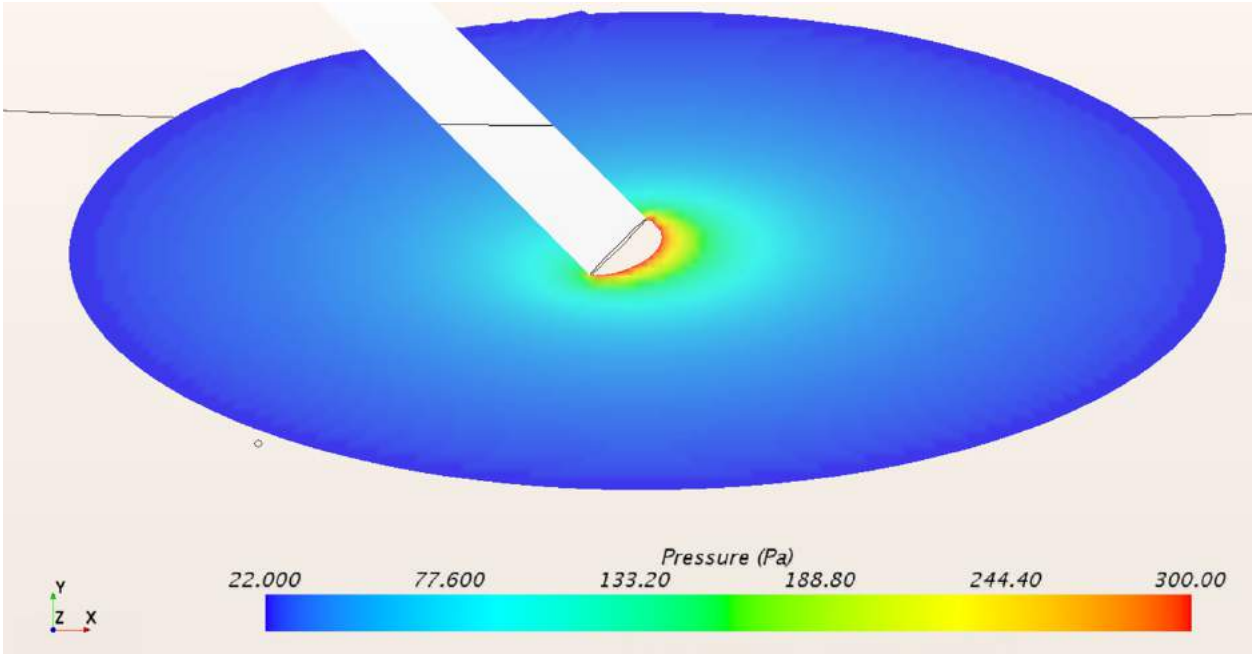

Figure E-29. 30 mm tissue thickness CFD pressure gradient of insulin depot at cannula tip with 45° cannula.

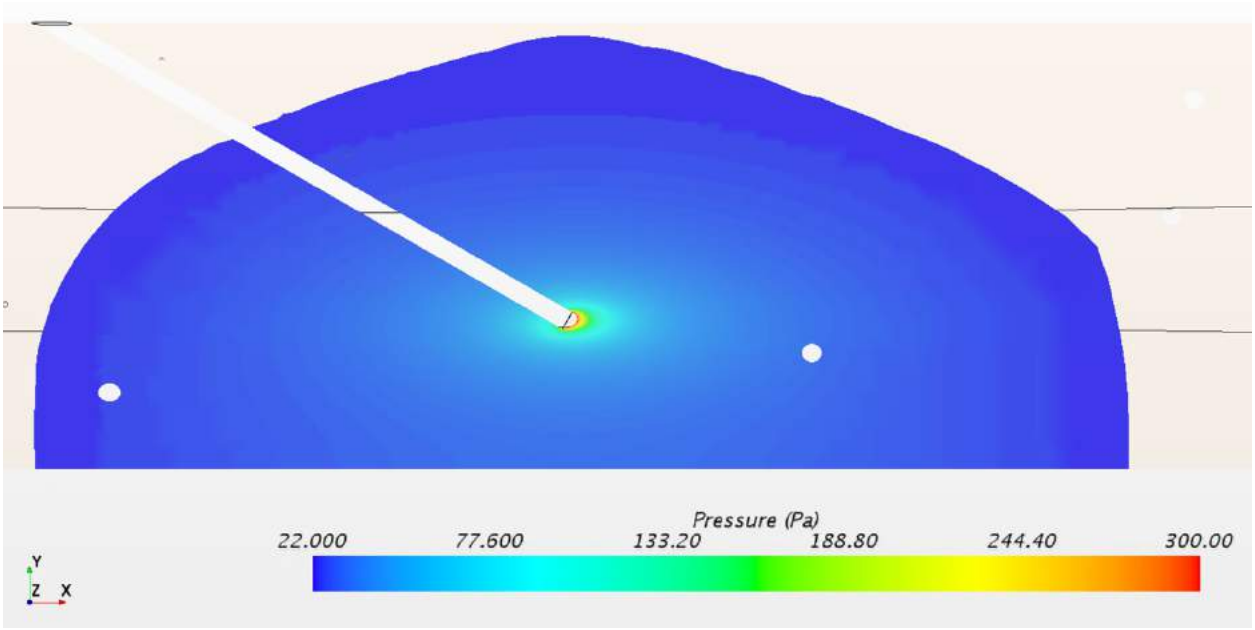

Figure E-30. 6 mm tissue thickness CFD pressure gradient of insulin depot at cannula tip with 30° cannula.

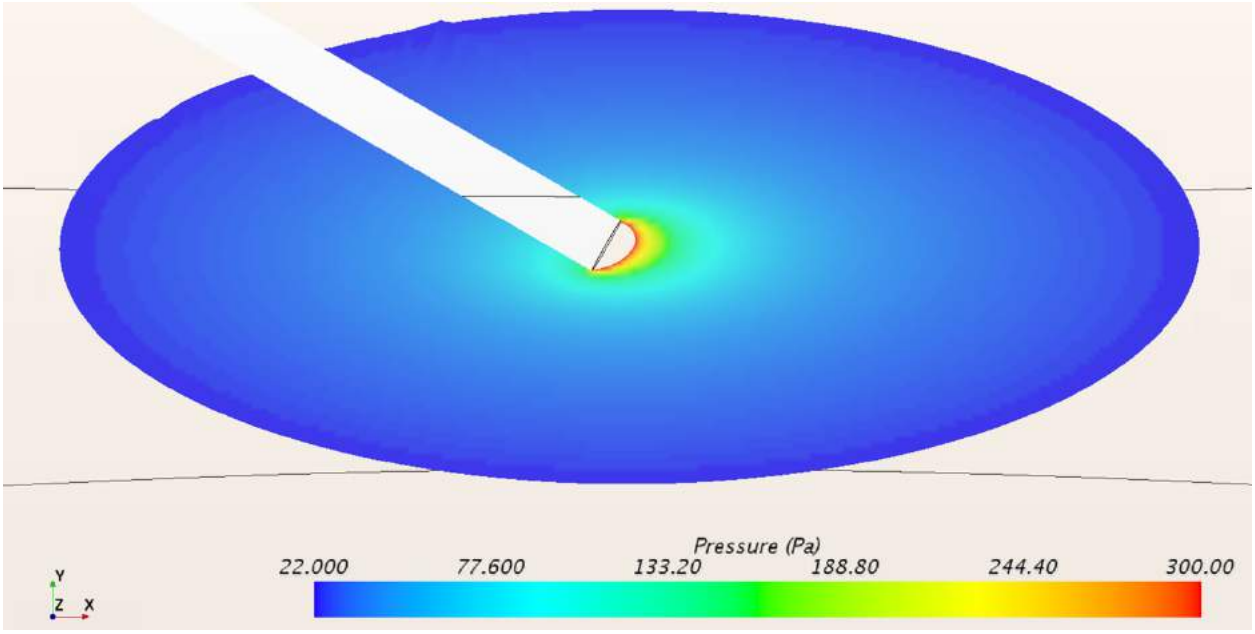

Figure E-31. 12 mm tissue thickness CFD pressure gradient of insulin depot at cannula tip with 30° cannula.

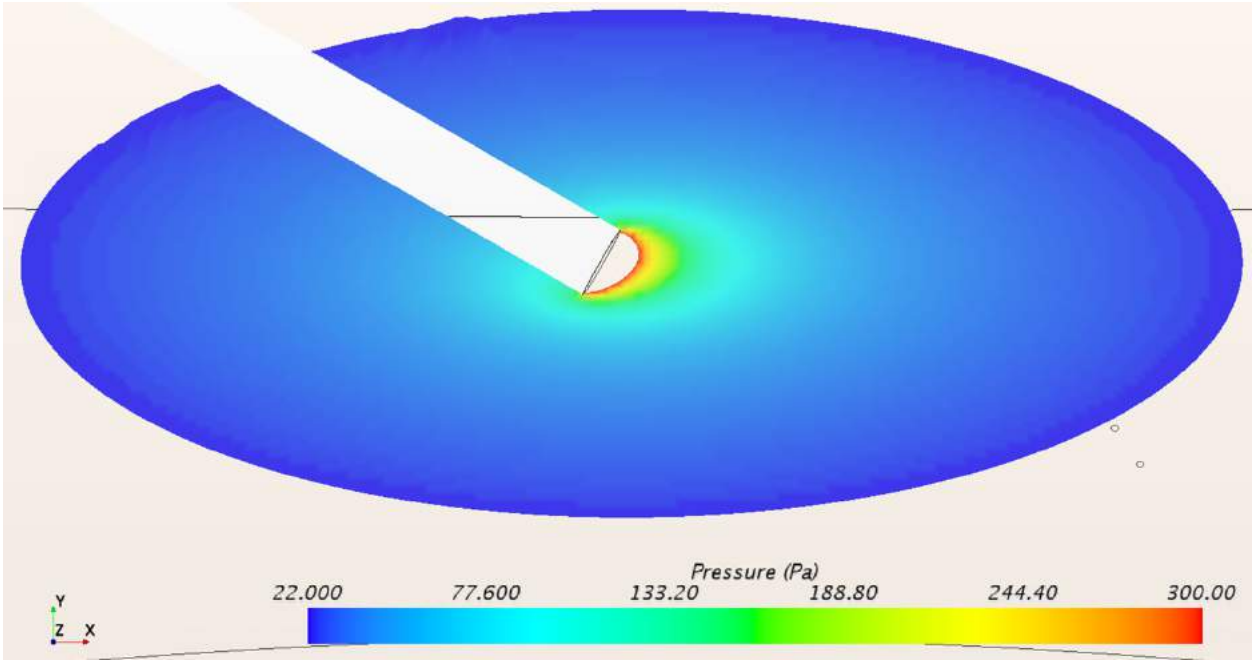

Figure E-32. 18 mm tissue thickness CFD pressure gradient of insulin depot at cannula tip with 30° cannula.

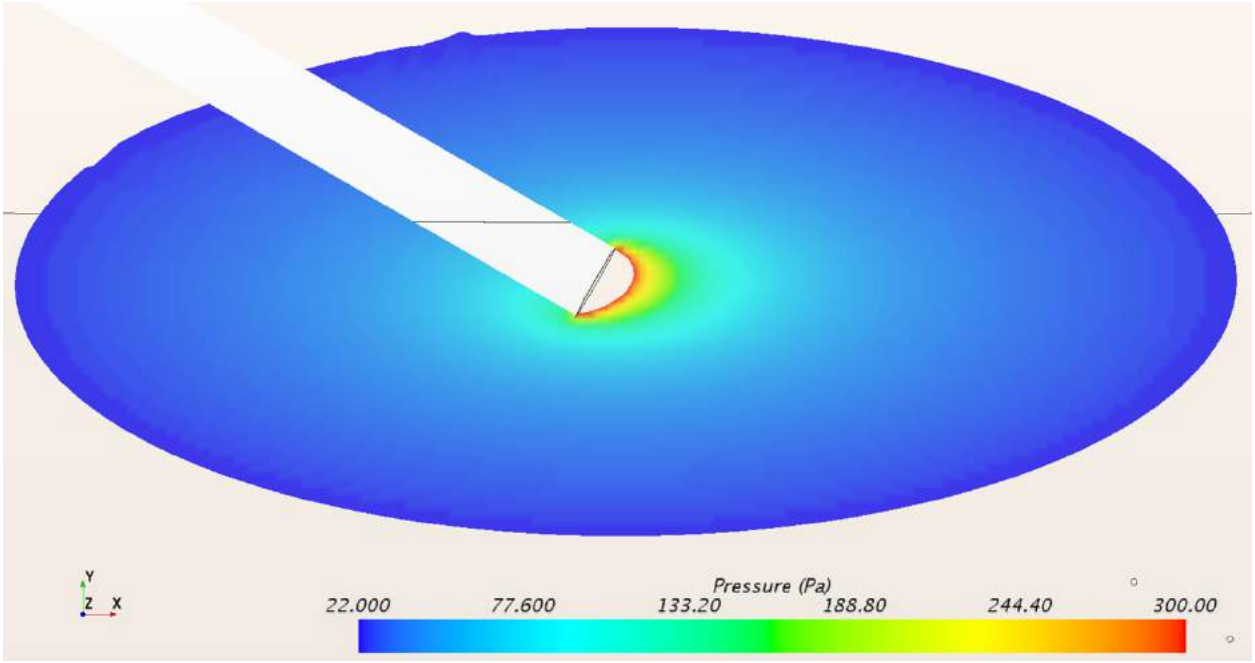

Figure E-33. 24 mm tissue thickness CFD pressure gradient of insulin depot at cannula tip with 30° cannula.

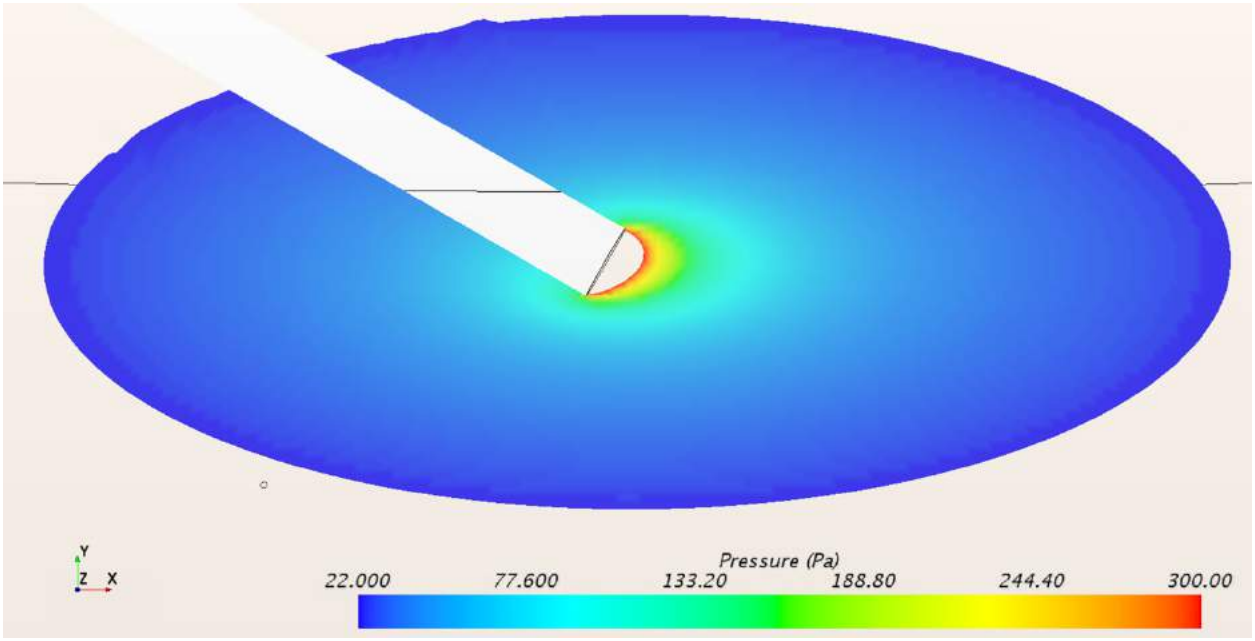

Figure E-34. 30 mm tissue thickness CFD pressure gradient of insulin depot at cannula tip with 30° cannula.

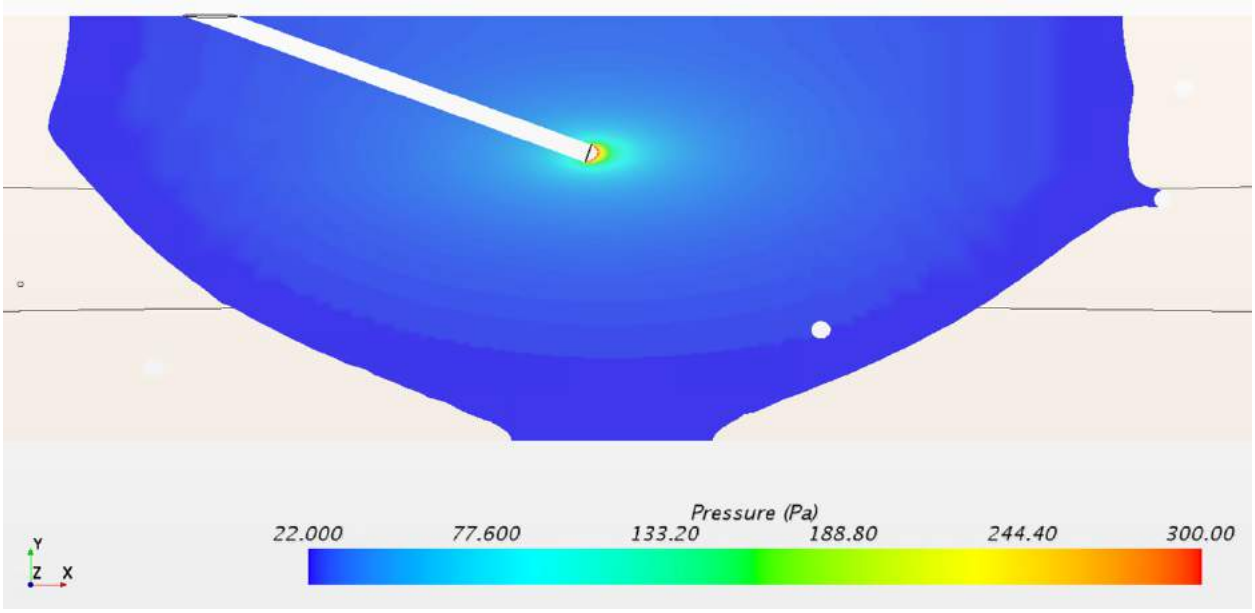

Figure E-35. 6 mm tissue thickness CFD pressure gradient of insulin depot at cannula tip with 20° x 13 mm long cannula.

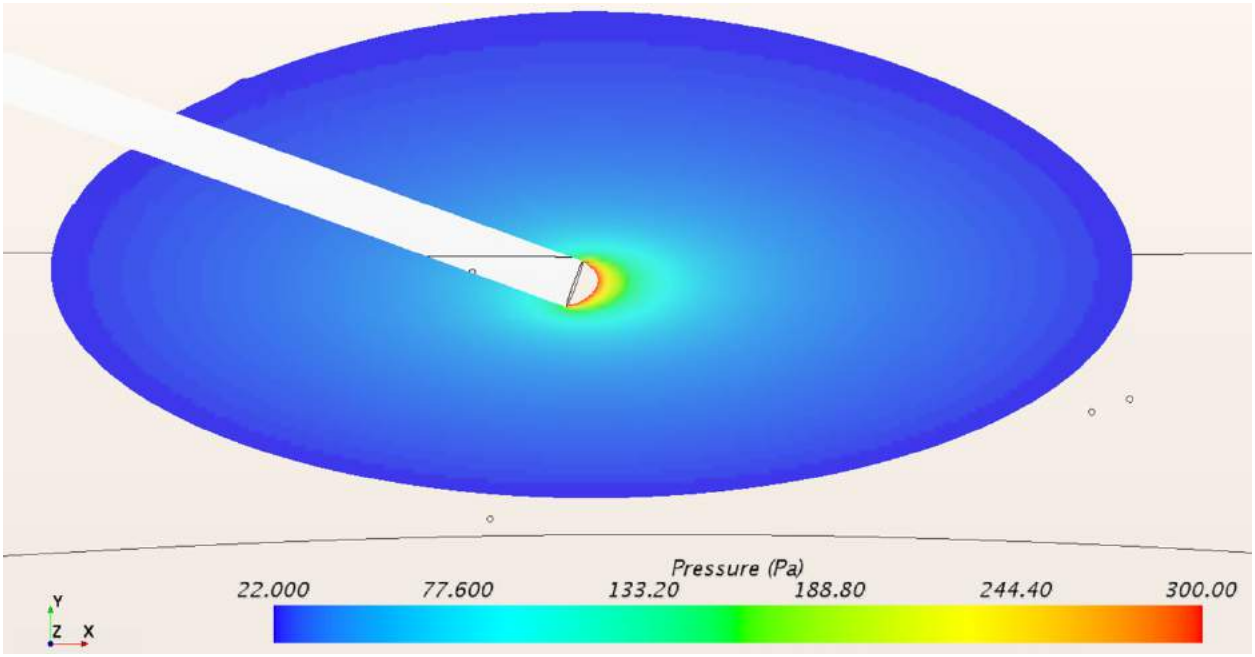

Figure E-36. 12 mm tissue thickness CFD pressure gradient of insulin depot at cannula tip with 20° x 13 mm long cannula.

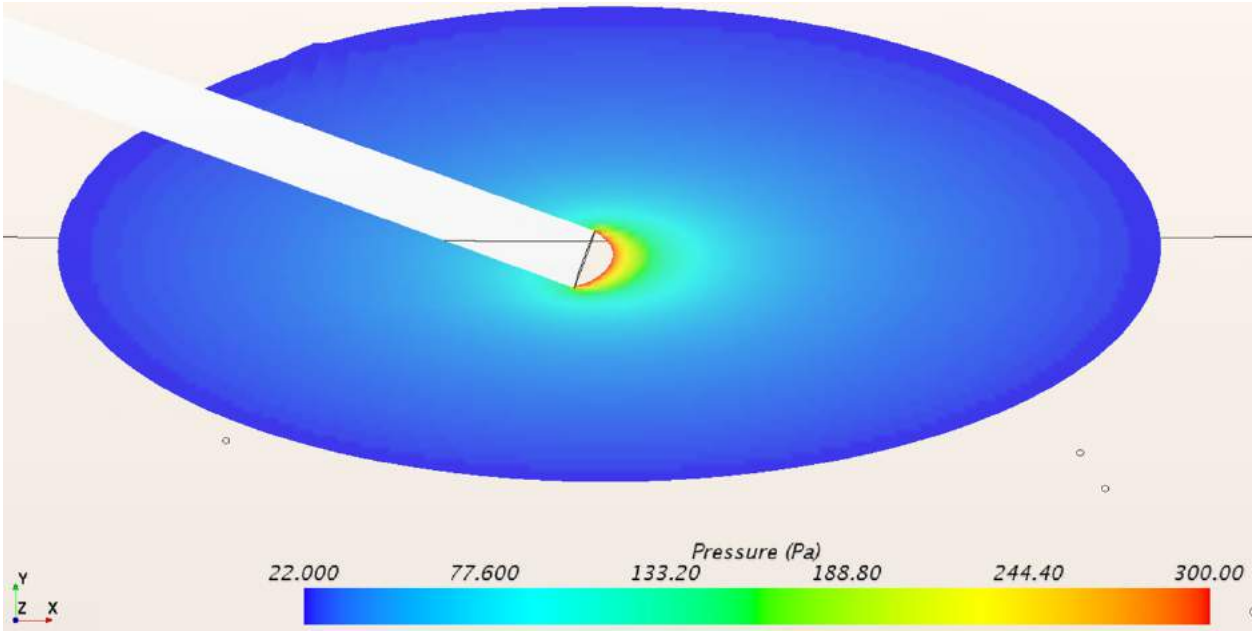

Figure E-37. 18 mm tissue thickness CFD pressure gradient of insulin depot at cannula tip with 20° x 13 mm long cannula.

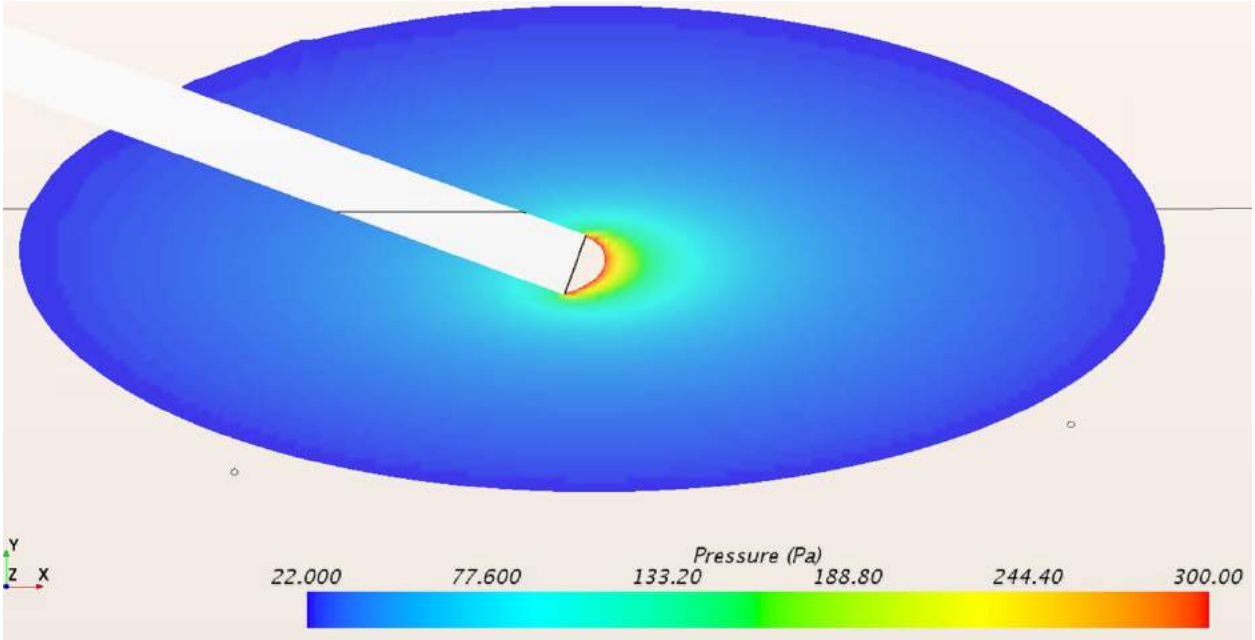

Figure E-38. 24 mm tissue thickness CFD pressure gradient of insulin depot at cannula tip with 20° x 13 mm long cannula.

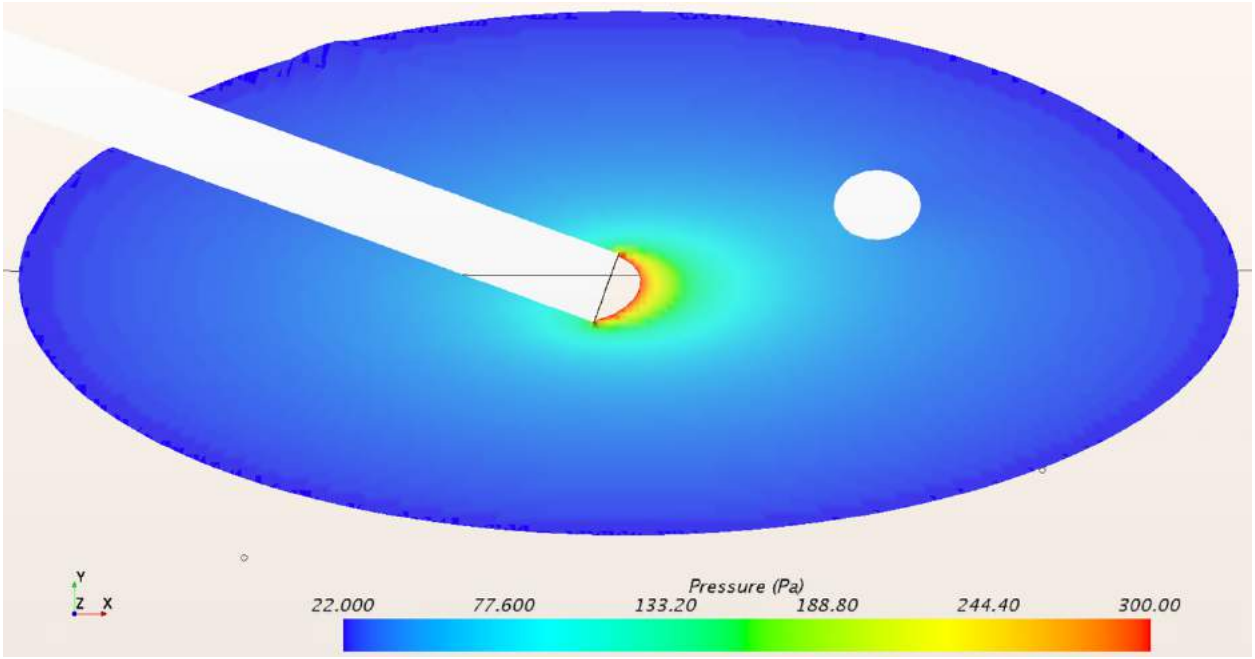

Figure E-39. 30 mm tissue thickness CFD pressure gradient of insulin depot at cannula tip with 20° x 13 mm long cannula.

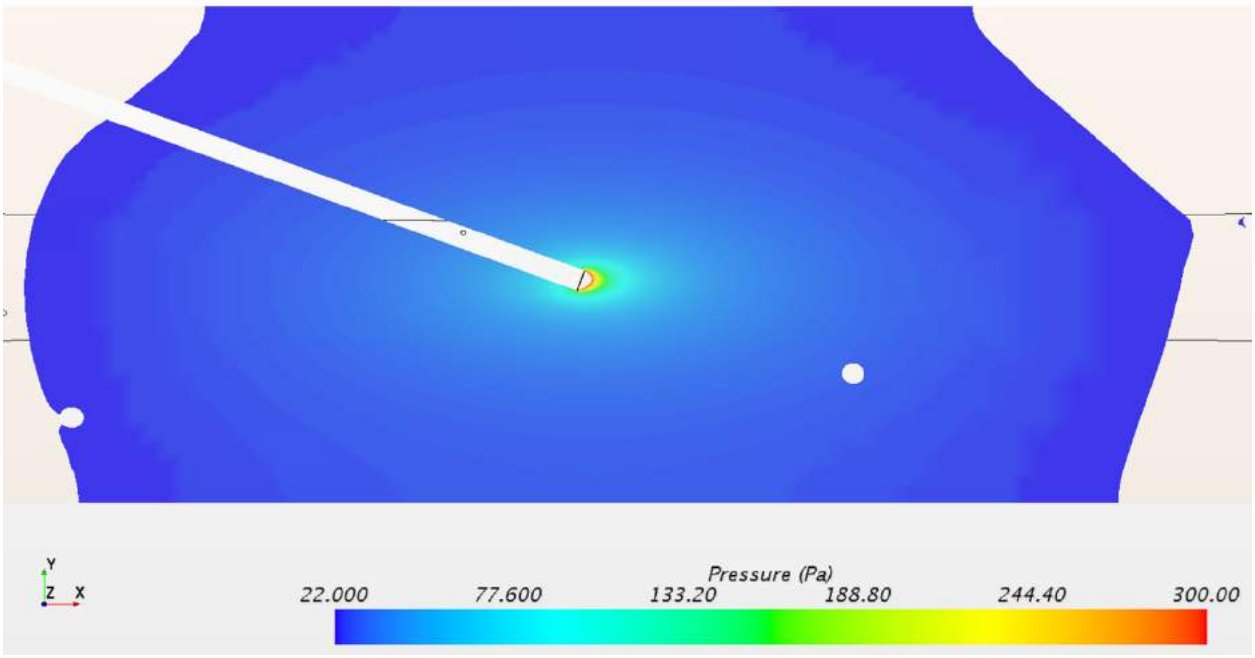

Figure E-40. 6 mm tissue thickness CFD pressure gradient of insulin depot at cannula tip with 20° x 17 mm long cannula.

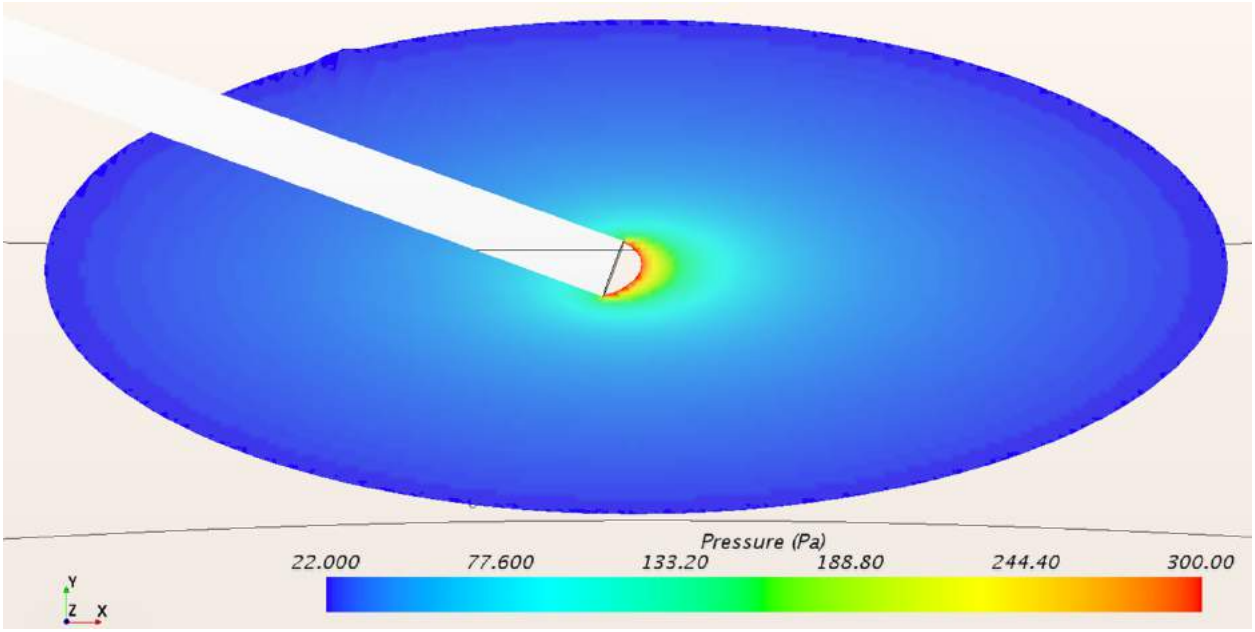

Figure E-41. 12 mm tissue thickness CFD pressure gradient of insulin depot at cannula tip with 20° x 17 mm long cannula.

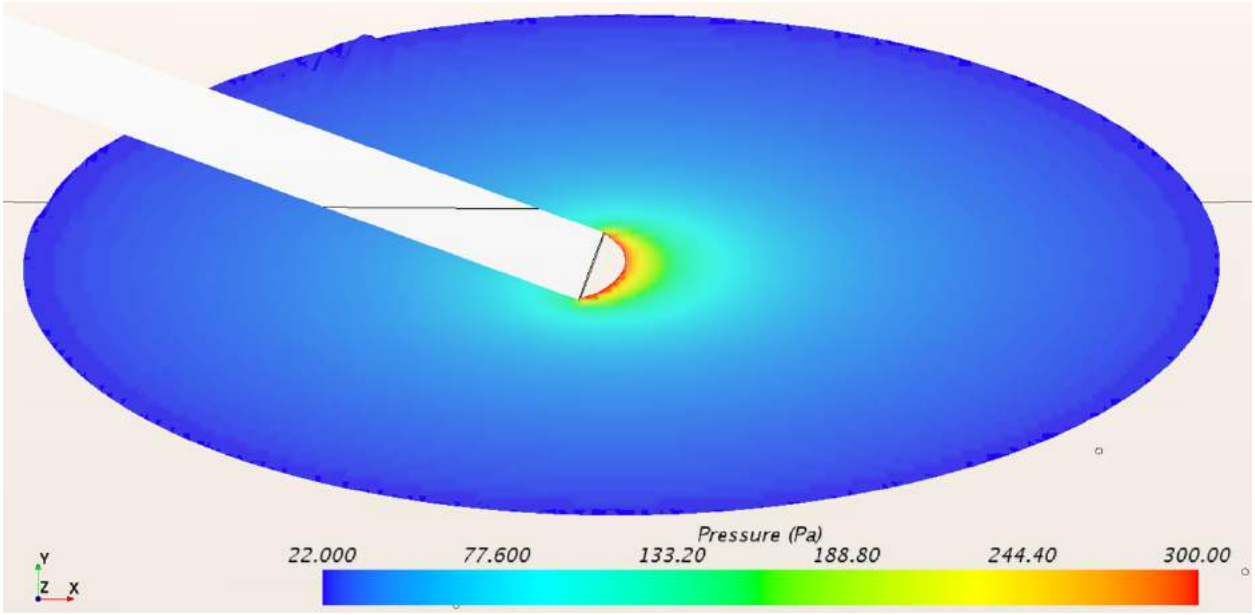

Figure E-42. 18 mm tissue thickness CFD pressure gradient of insulin depot at cannula tip with 20° x 17 mm long cannula.

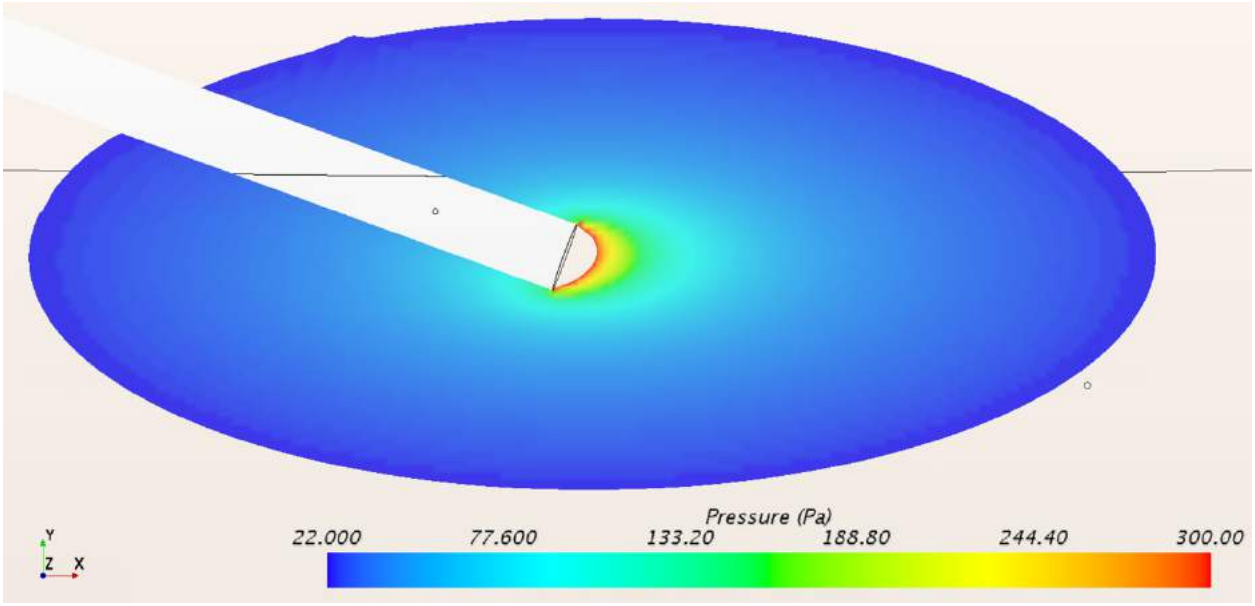

Figure E-43. 24 mm tissue thickness CFD pressure gradient of insulin depot at cannula tip with 20° x 17 mm long cannula.

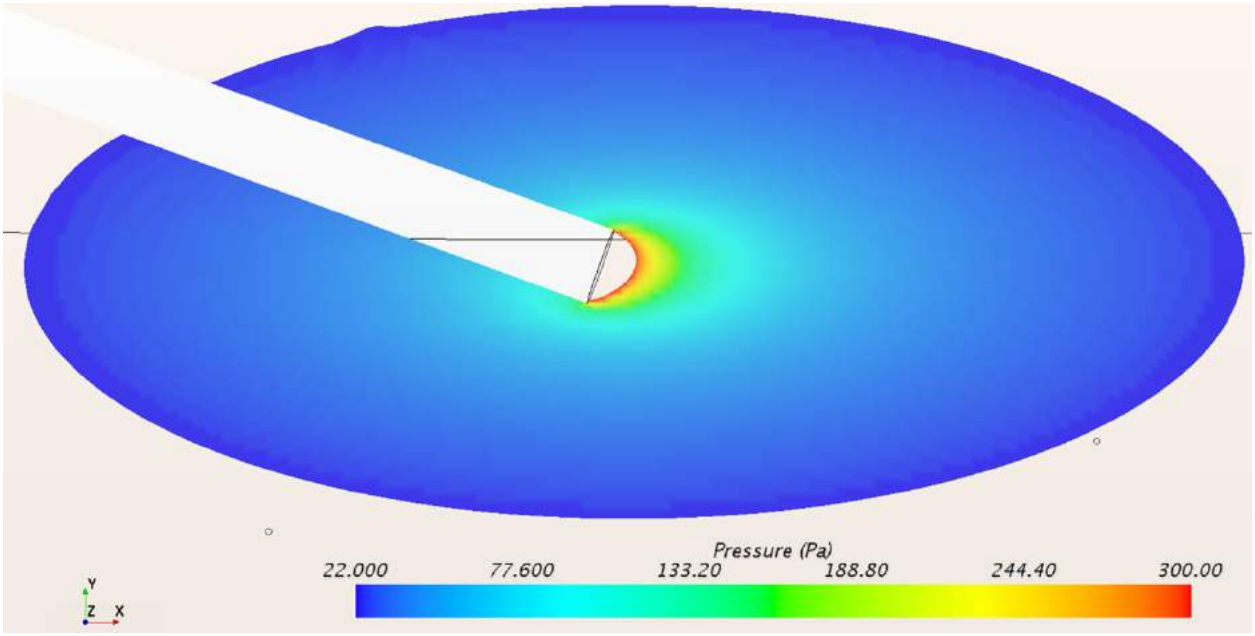

Figure E-44. 30 mm tissue thickness CFD pressure gradient of insulin depot at cannula tip with 20° x 17 mm long cannula.

Appendix F: Chapter 9 Additional Figures

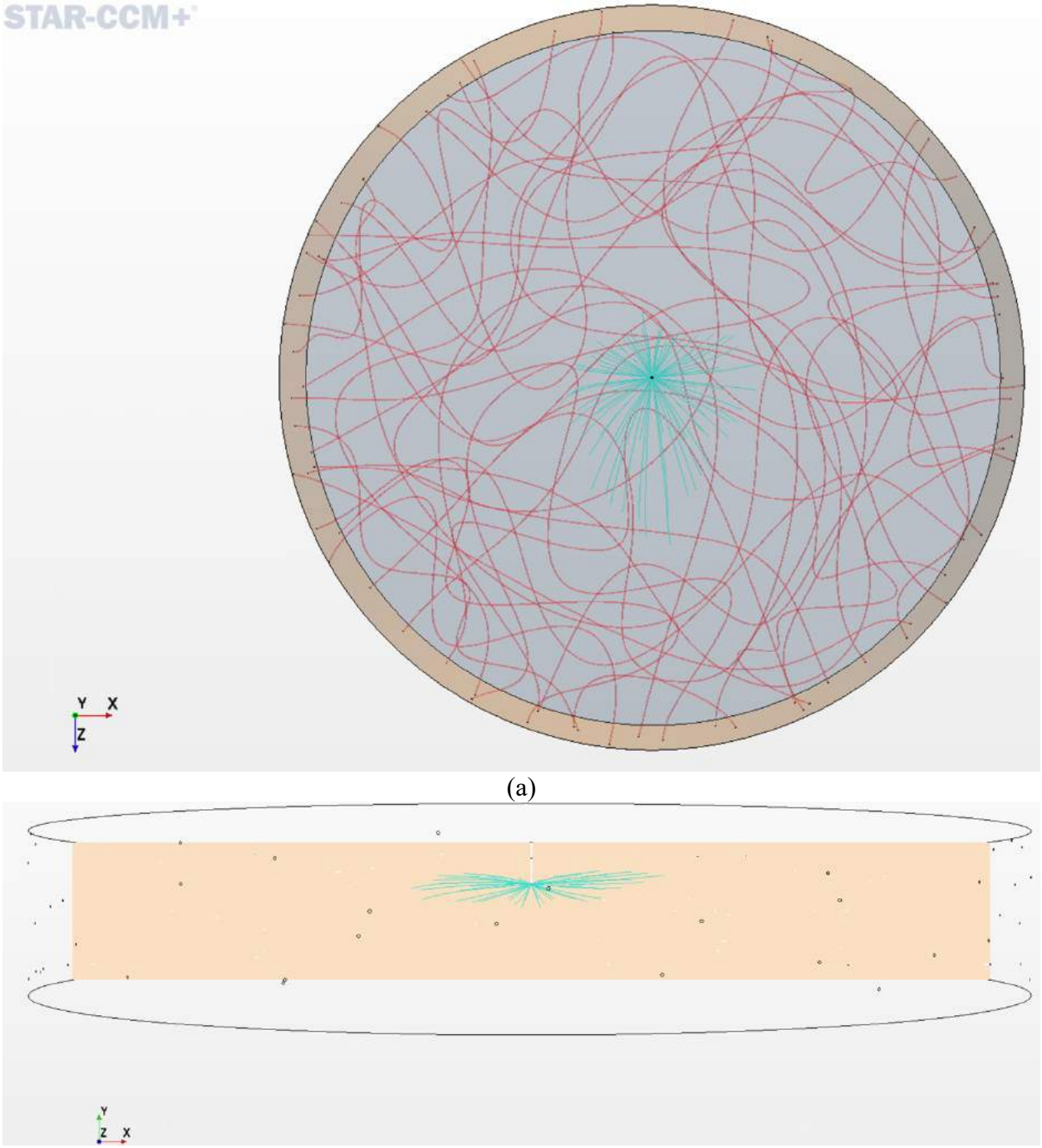

(a)

(b)

Figure F-1. Average drug dispersion from cannula for 18 mm tissue and 90° cannula (a) top view (b) side view.

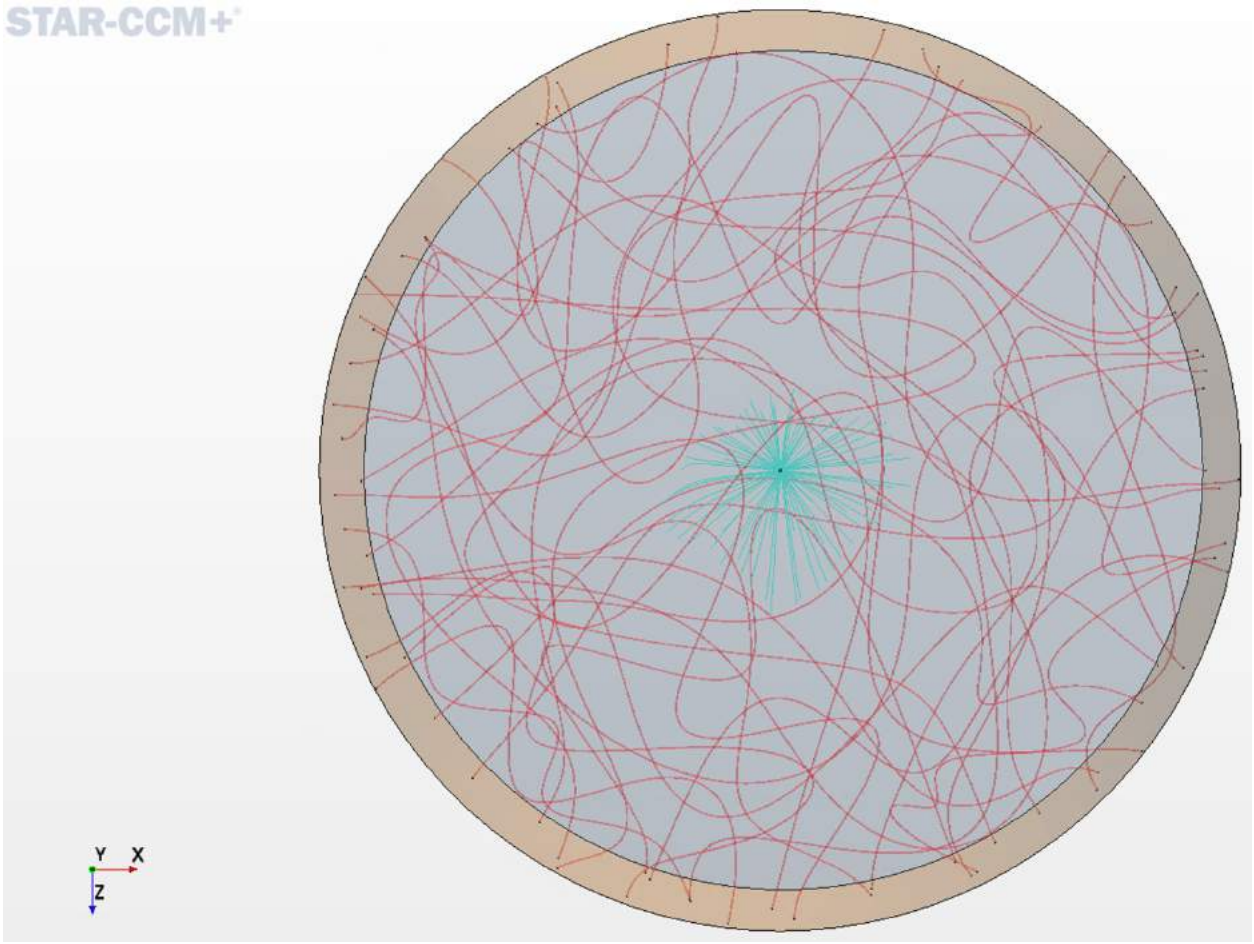

(a)

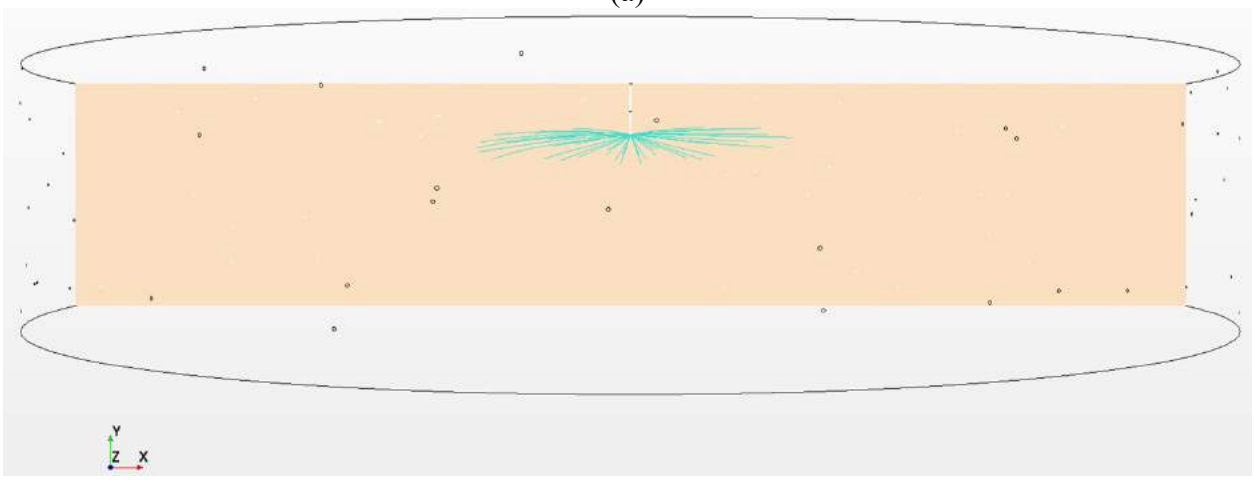

(b)

Figure F-2. Average drug dispersion from cannula for 24 mm tissue and 90° cannula (a) top view (b) side view.

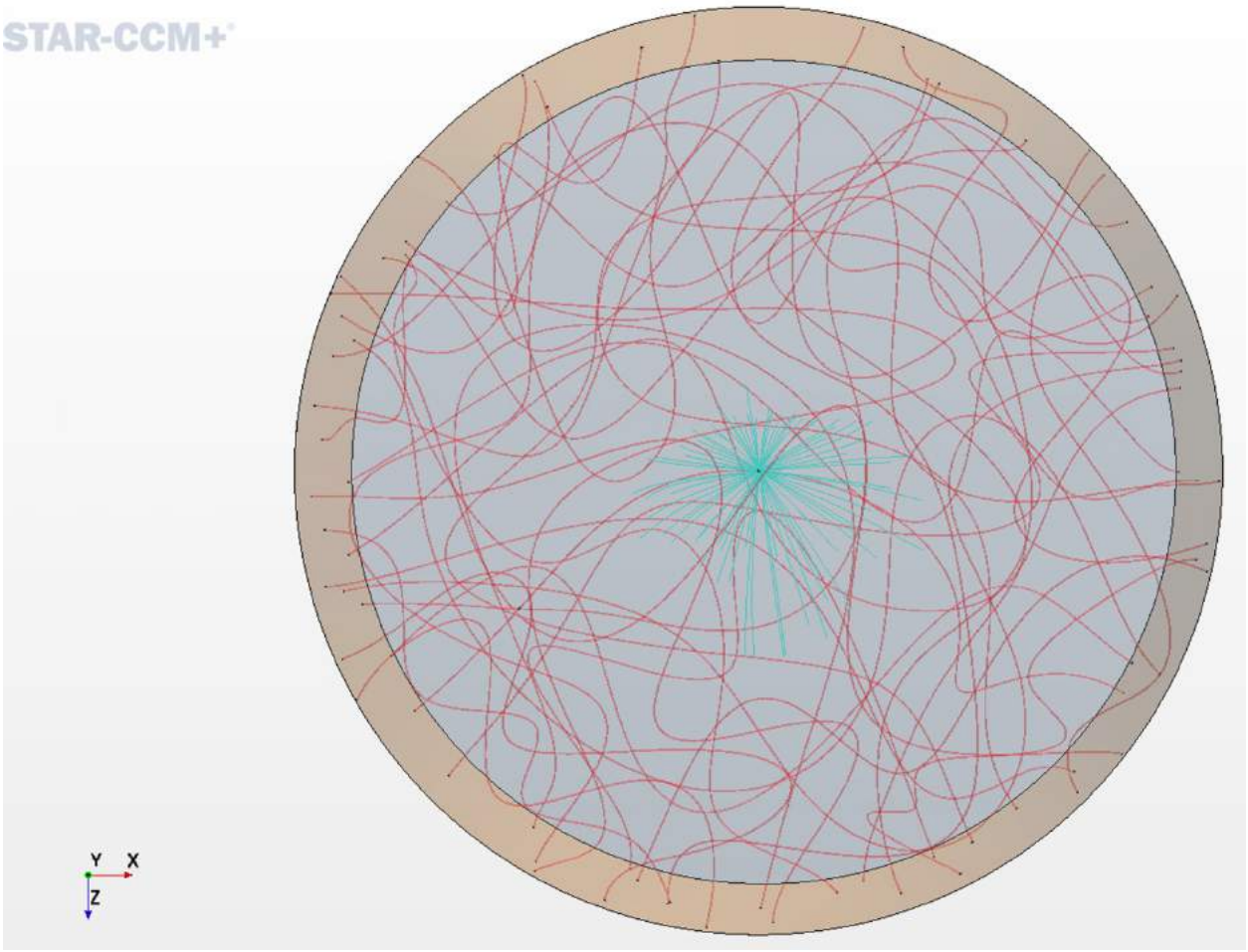

(a)

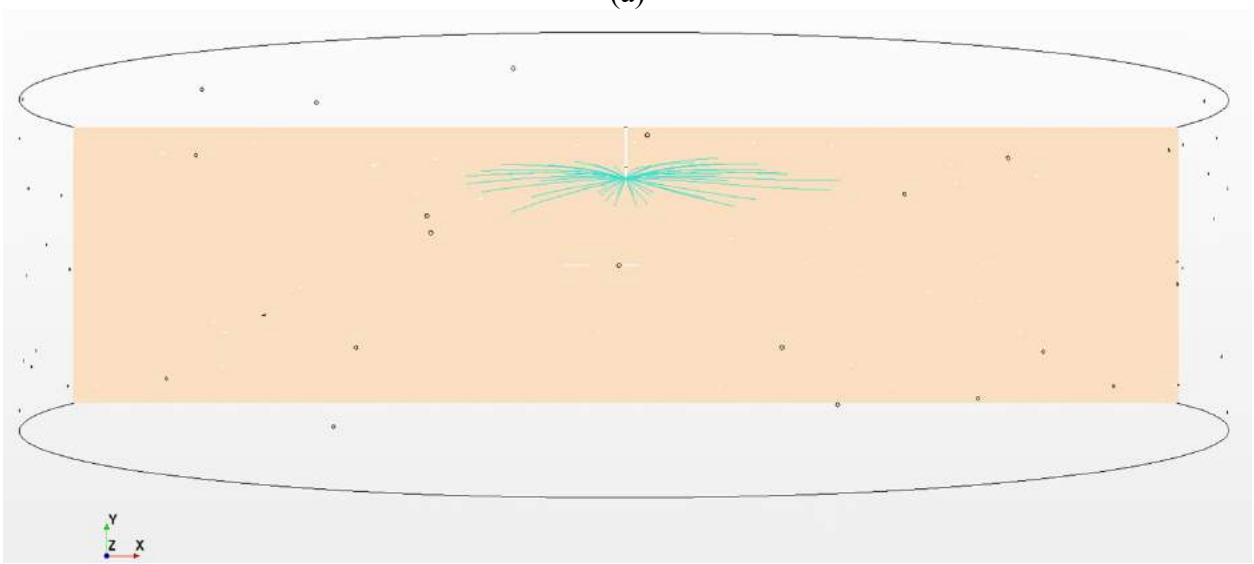

(b)

Figure F-3. Average drug dispersion from cannula for 30 mm tissue and 90° cannula (a) top view (b) side view.

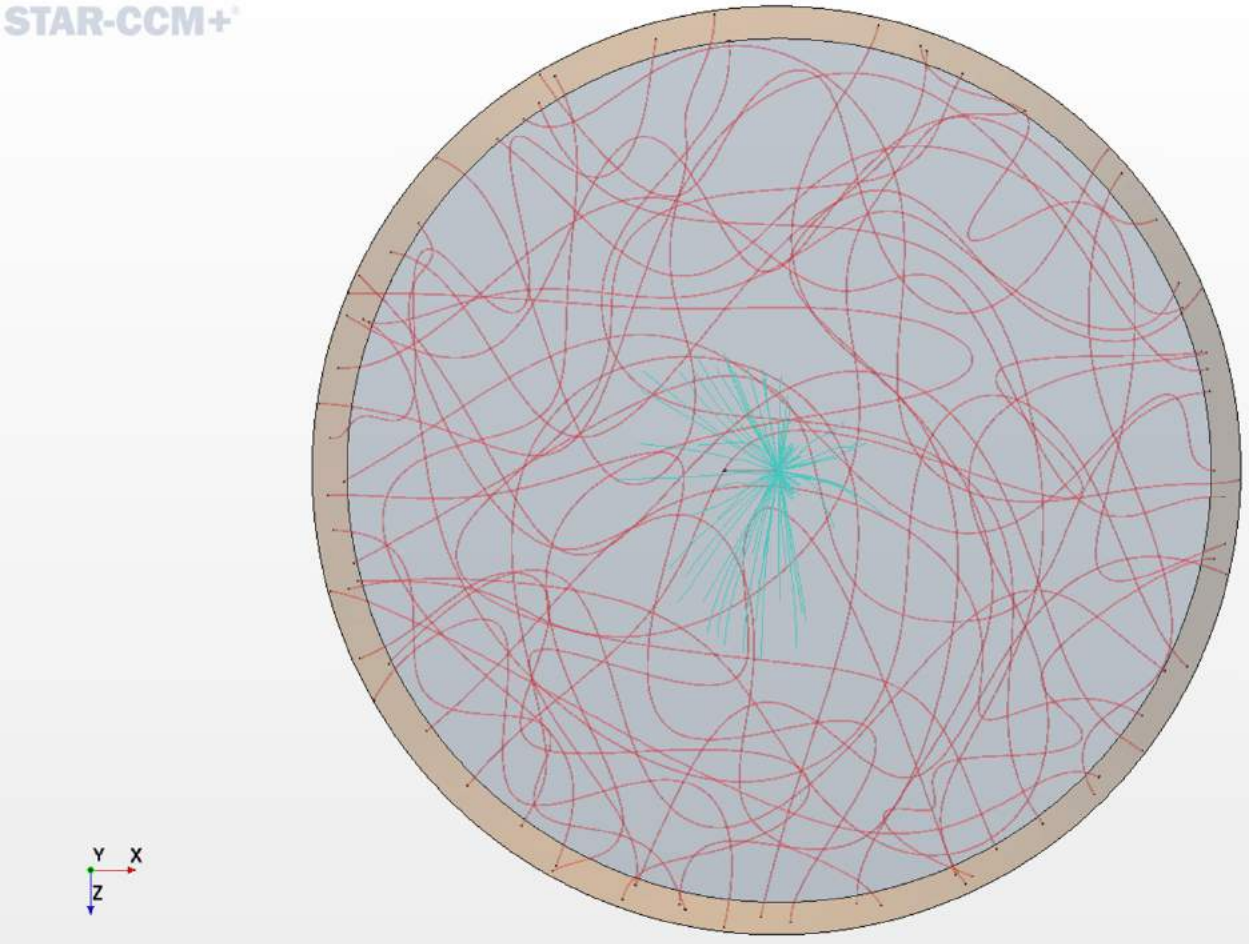

(a)

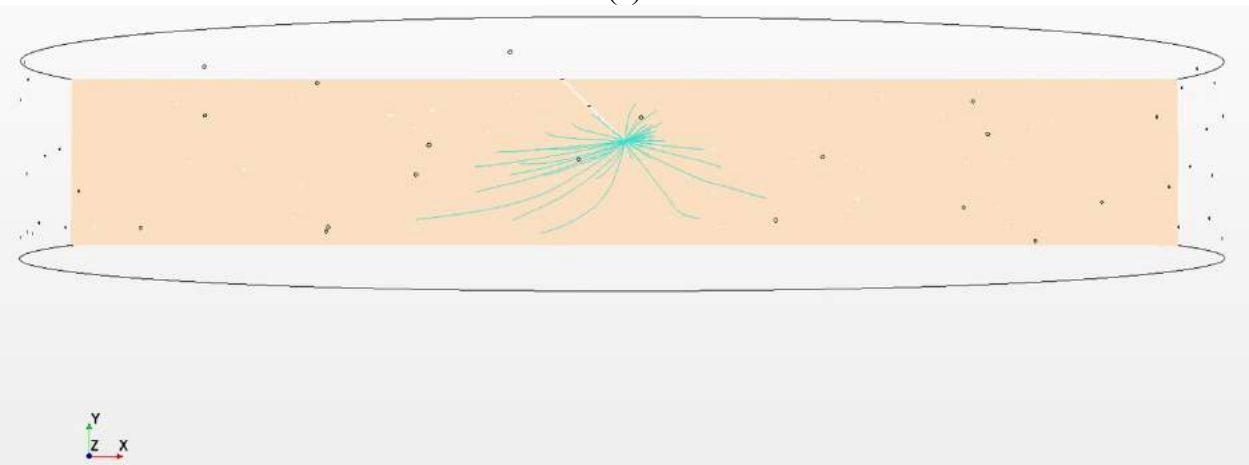

(b)

Figure F-4. Average drug dispersion from cannula for 18 mm tissue and 45° cannula (a) top view (b) side view.

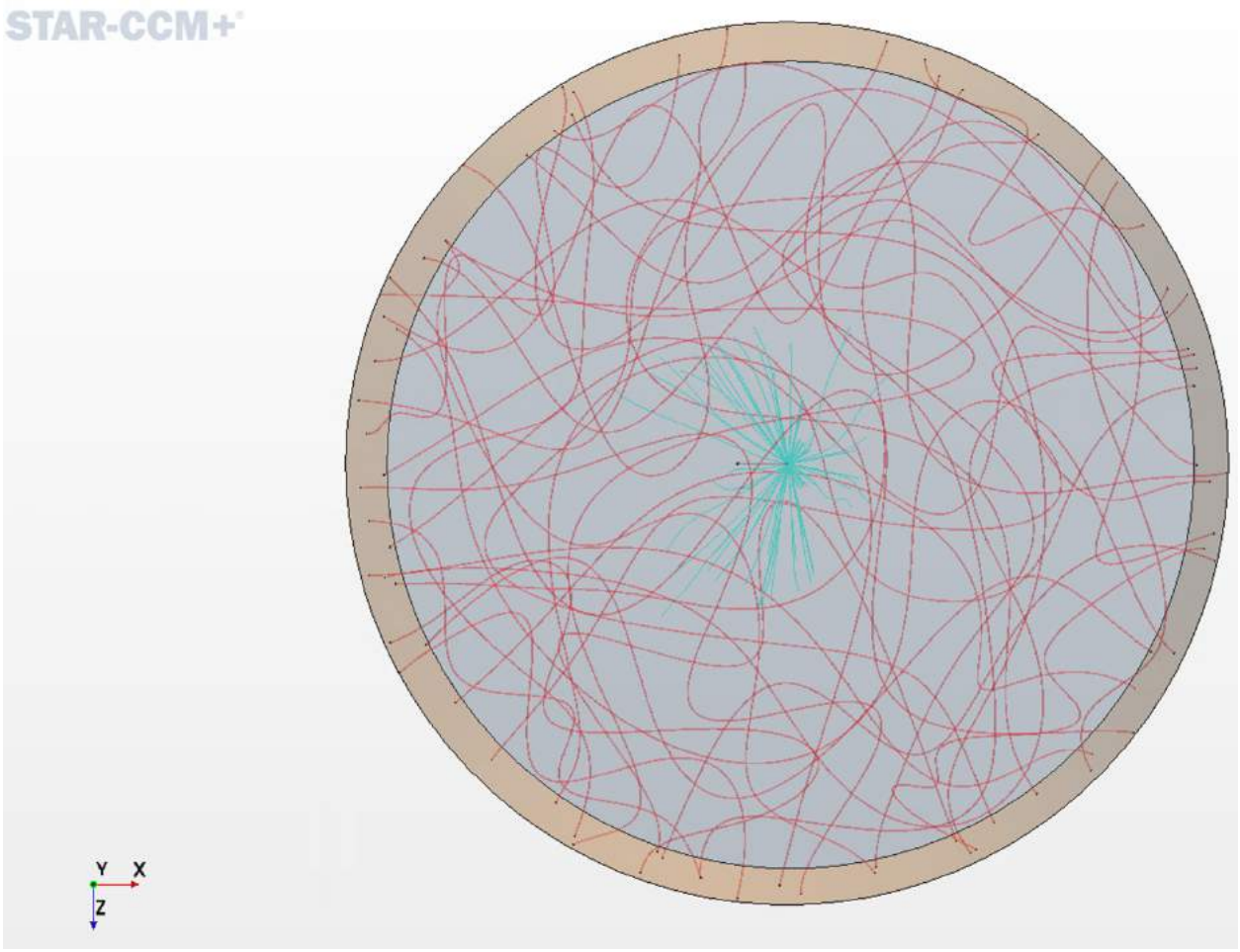

(a)

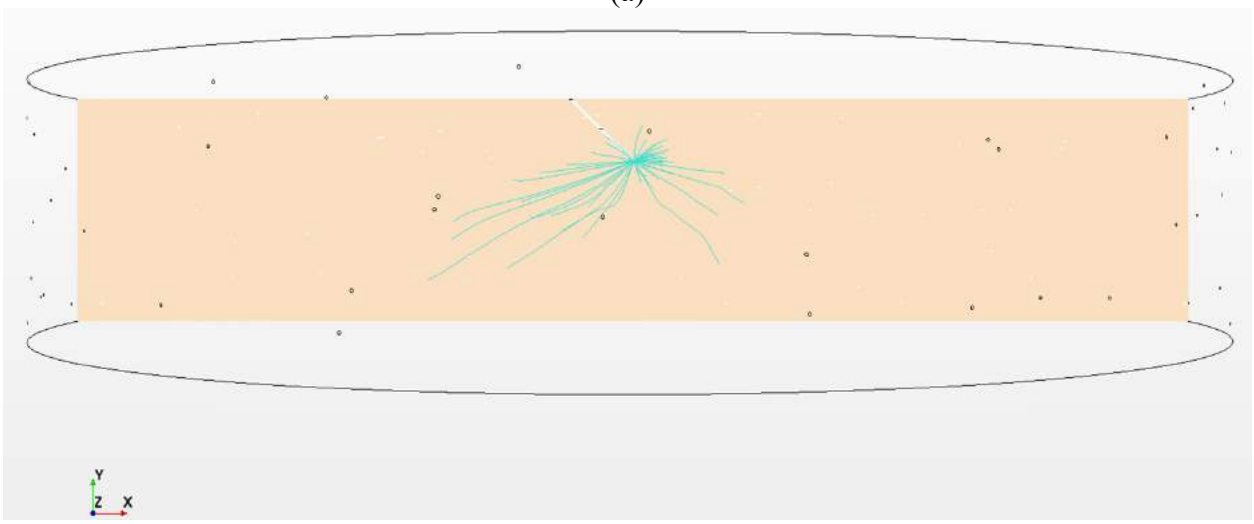

(b)

Figure F-5. Average drug dispersion from cannula for 24 mm tissue and 45° cannula (a) top view (b) side view.

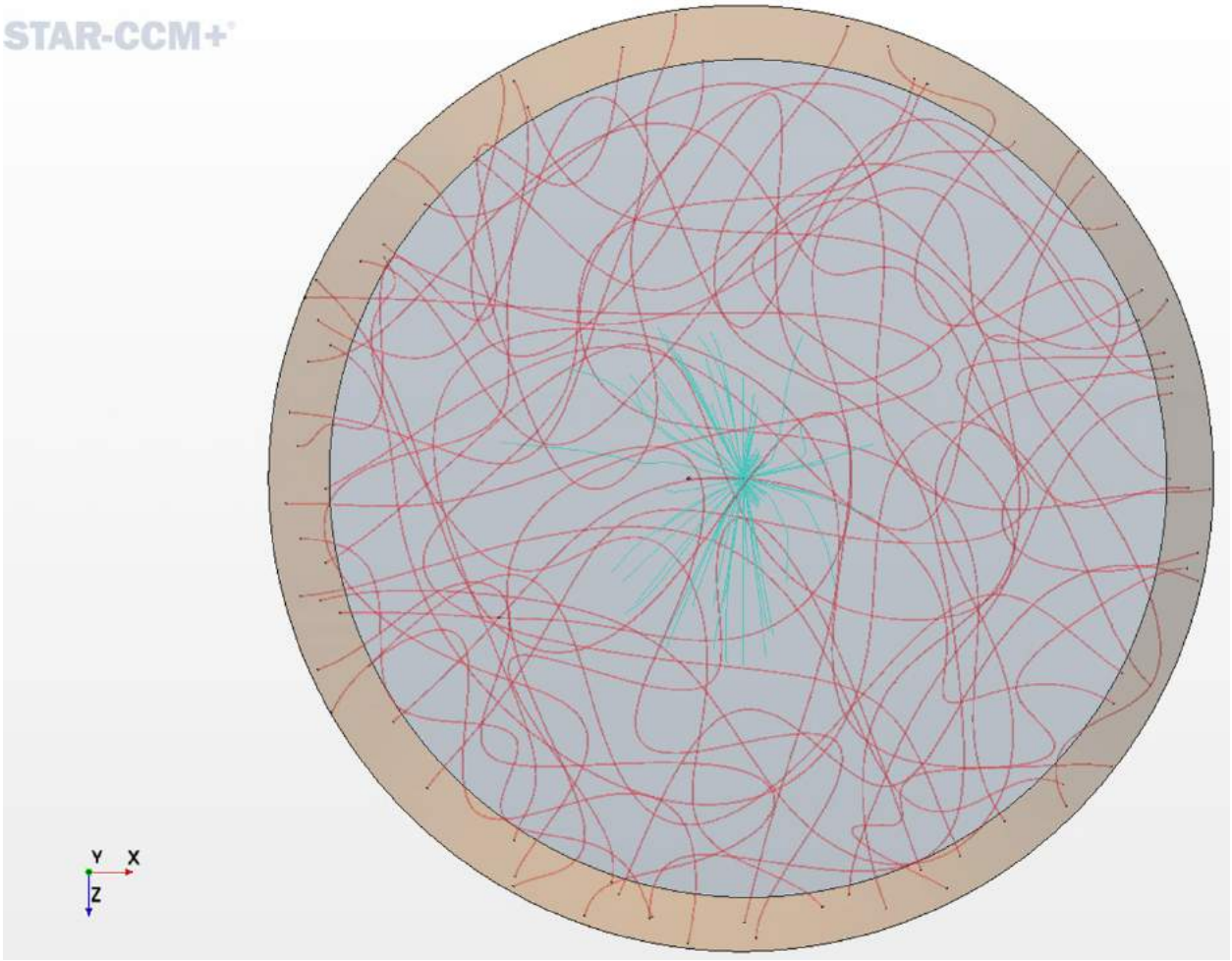

(a)

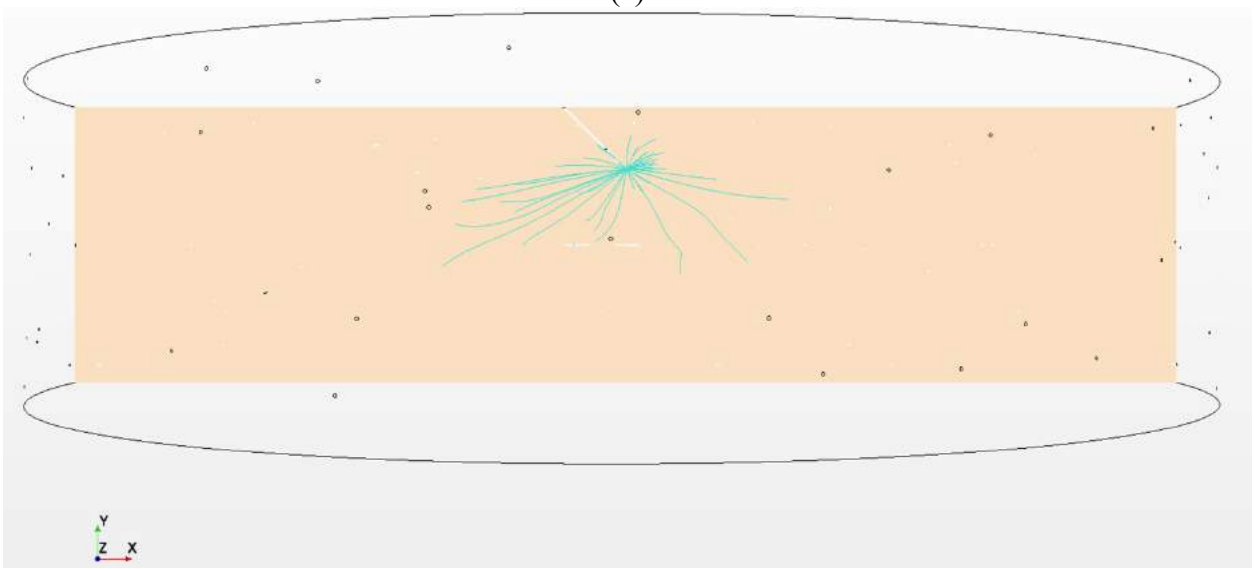

(b)

Figure F-6. Average drug dispersion from cannula for 30 mm tissue and 45° cannula (a) top view (b) side view.

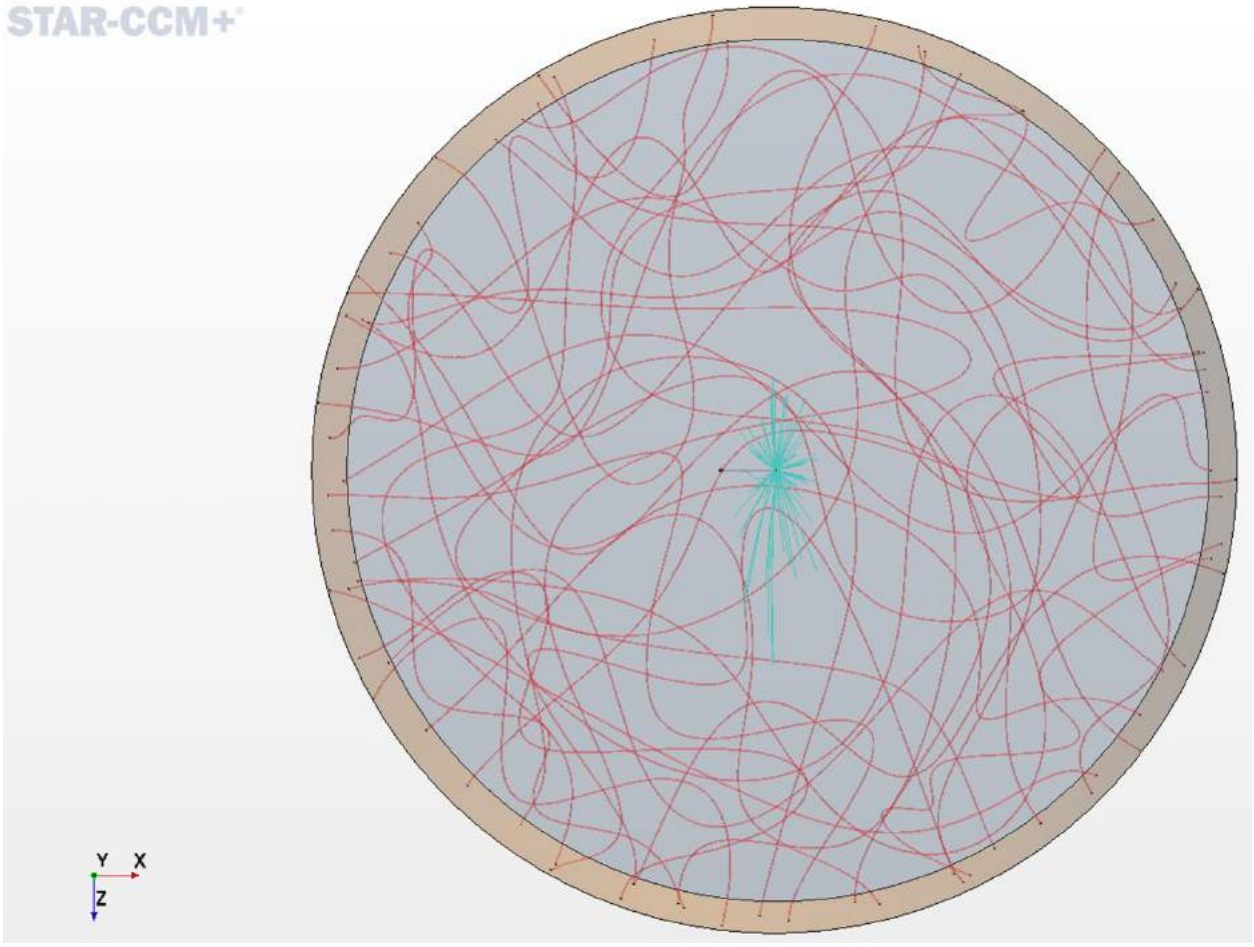

(a)

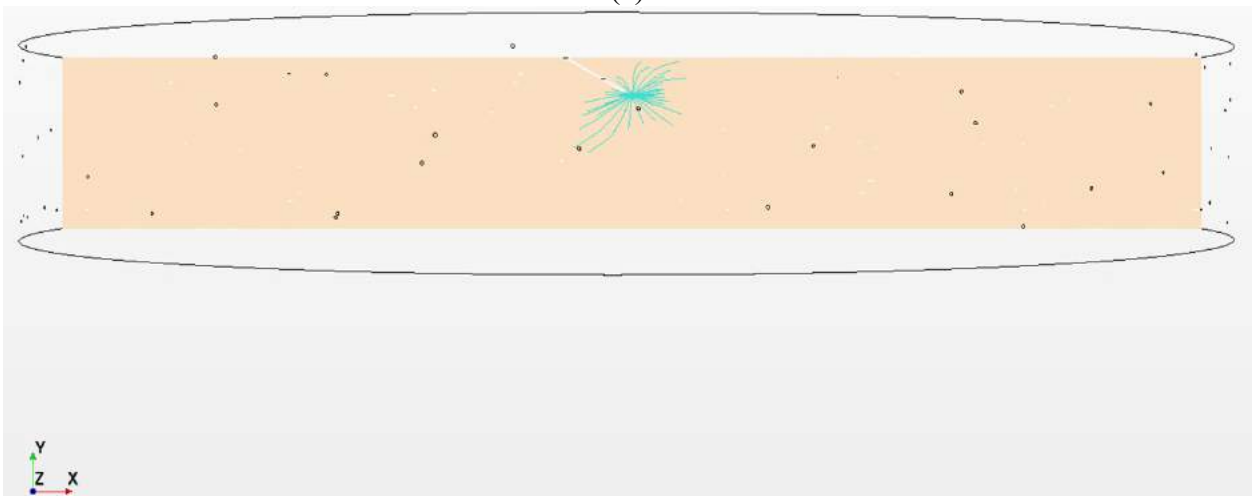

(b)

Figure F-7. Average drug dispersion from cannula for 18 mm tissue and 30° cannula (a) top view (b) side view.

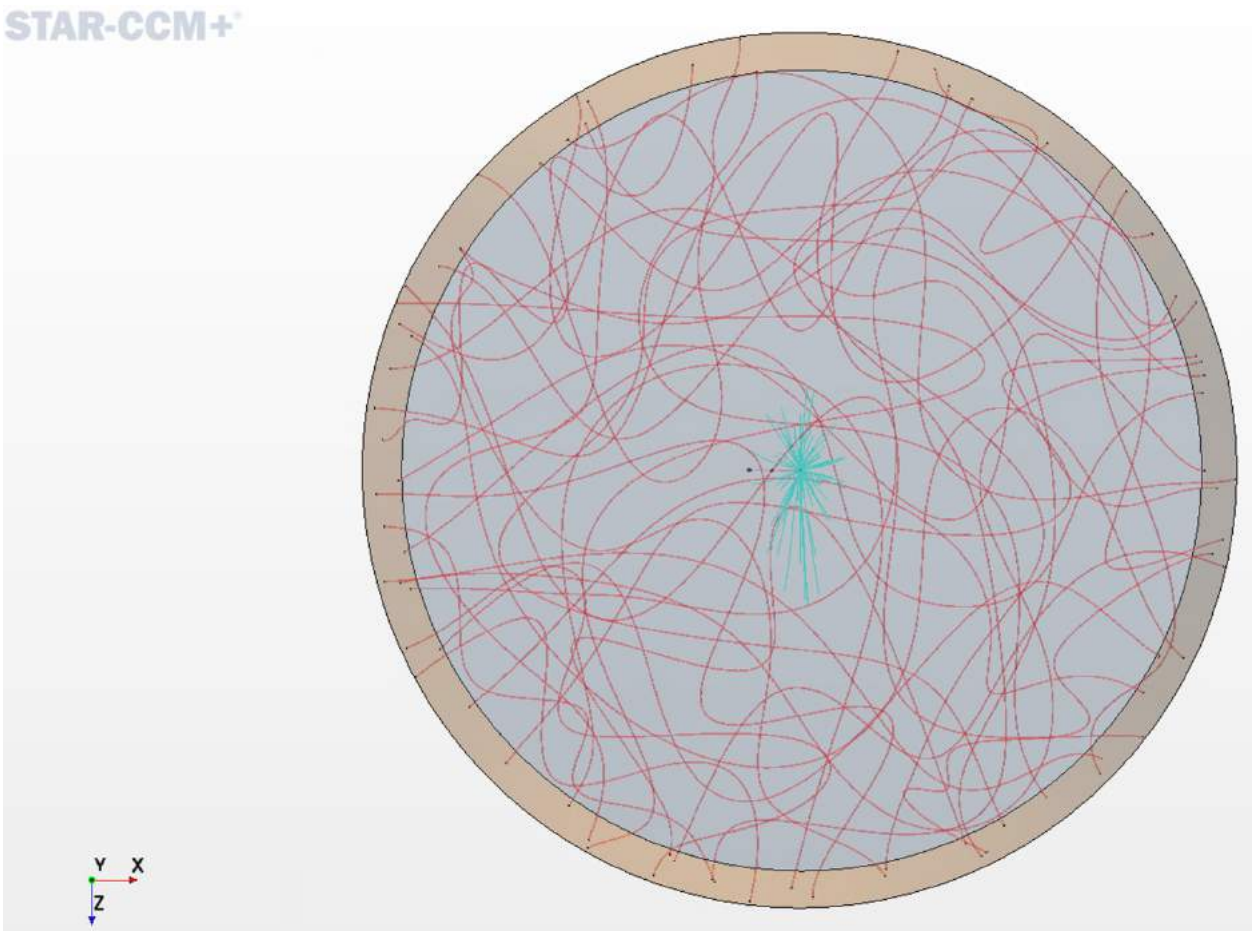

(a)

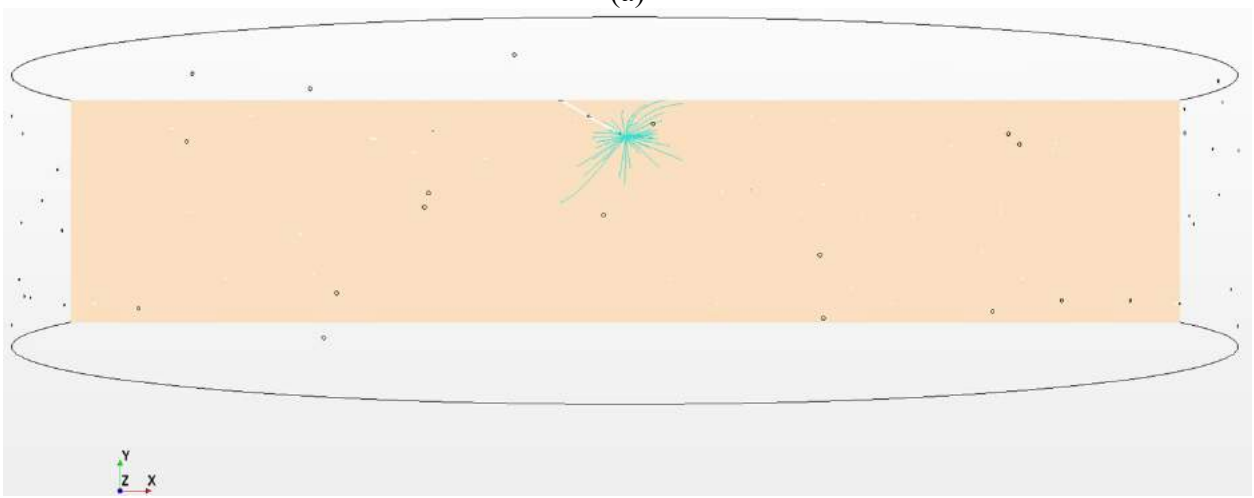

(b)

Figure F-8. Average drug dispersion from cannula for 24 mm tissue and 30° cannula (a) top view (b) side view.

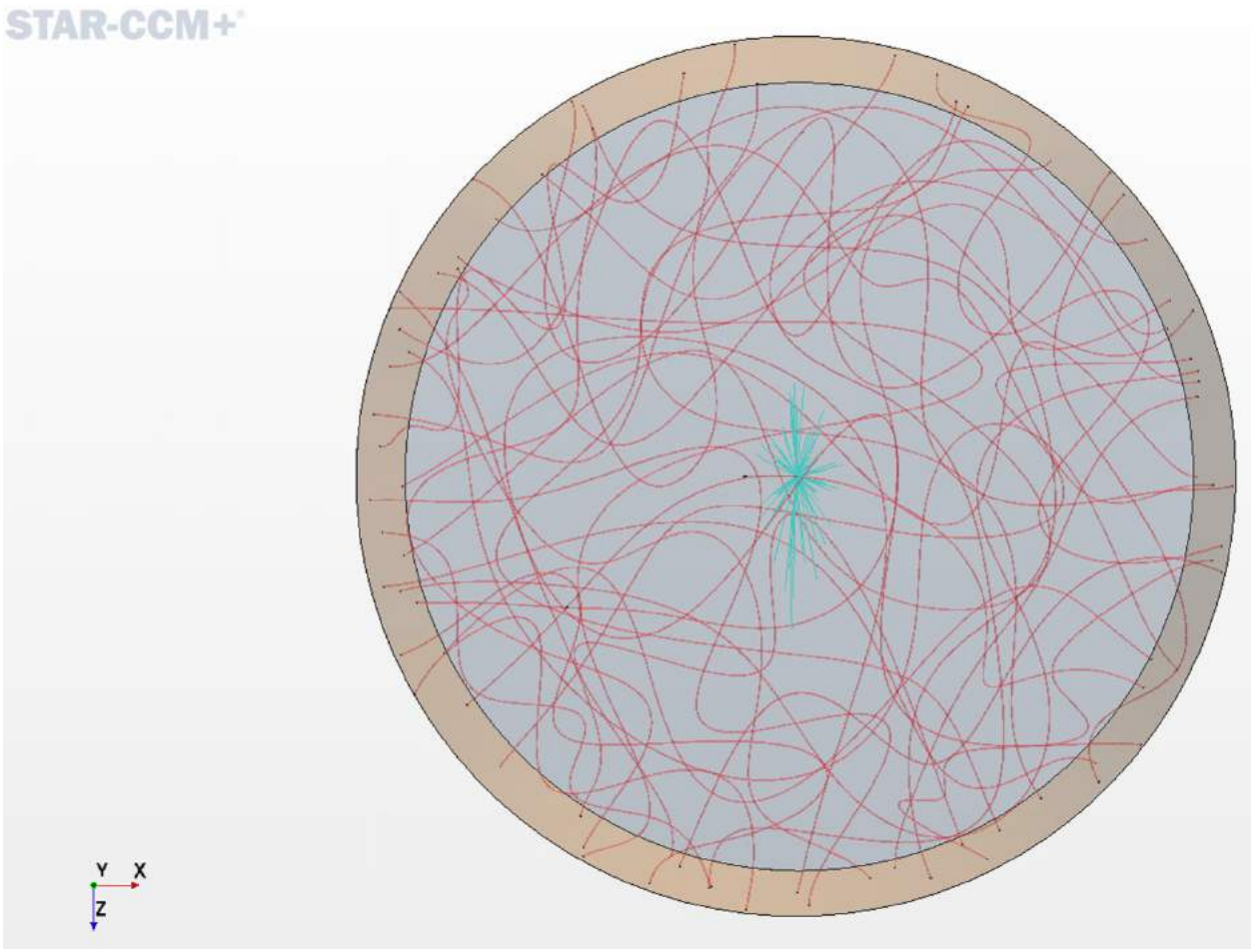

(a)

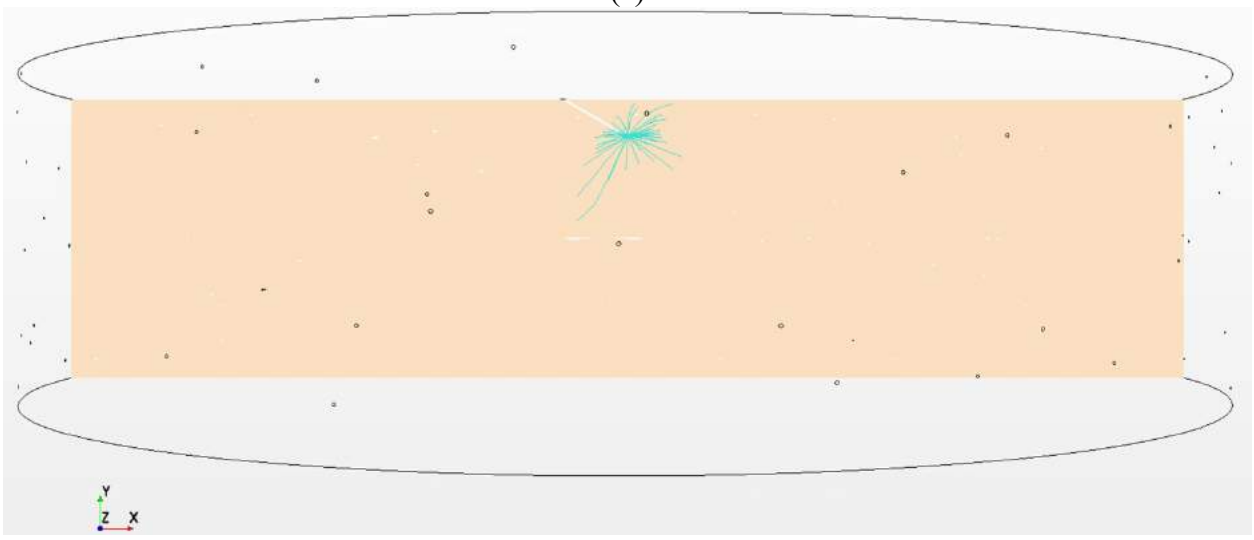

(b)

Figure F-9. Average drug dispersion from cannula for 30 mm tissue and 30° cannula (a) top view (b) side view.

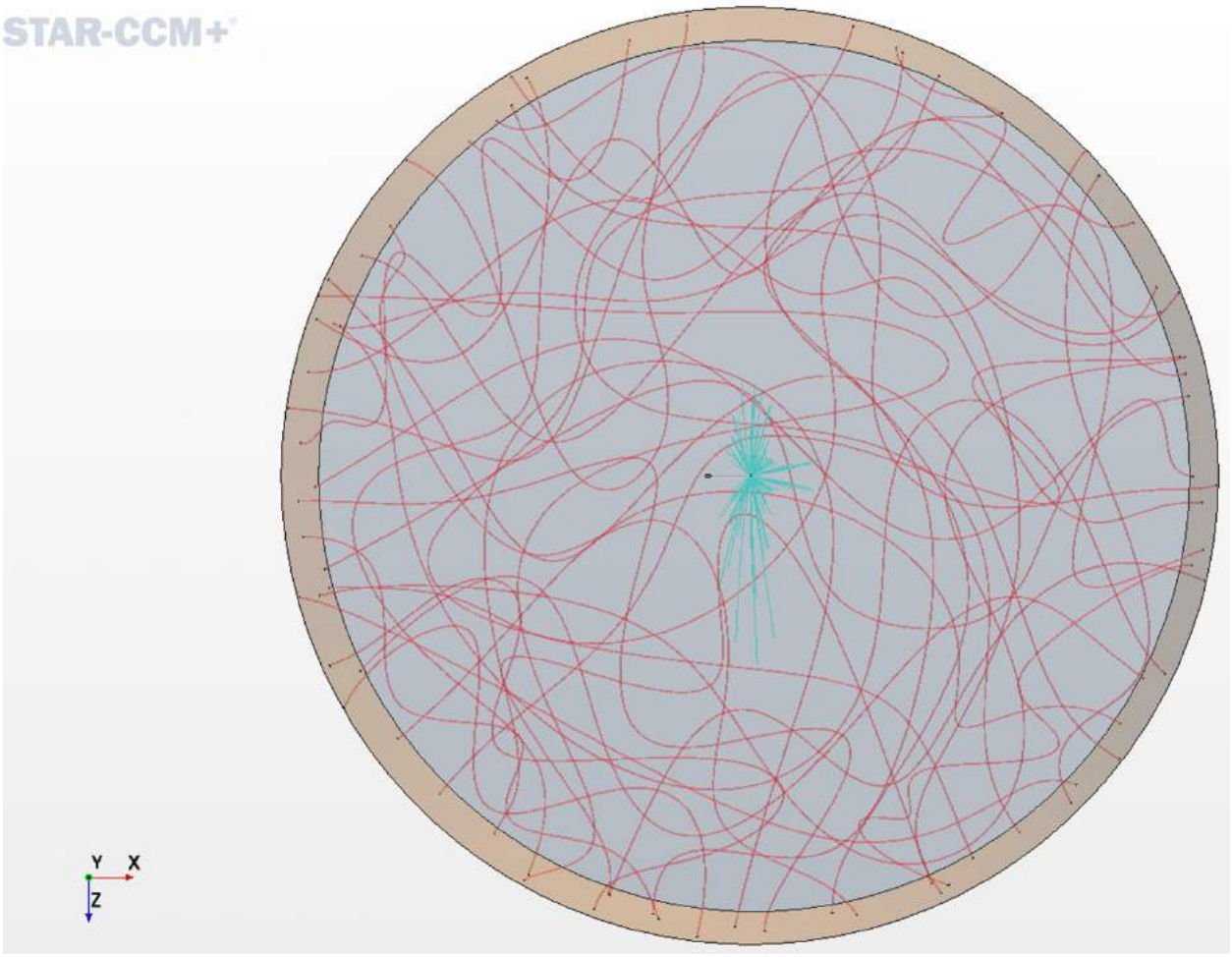

(a)

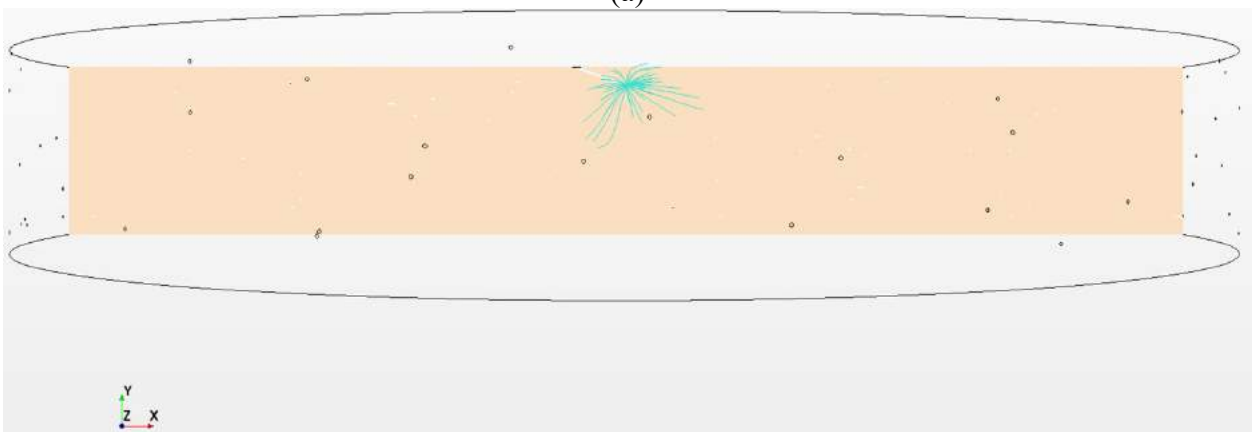

(b)

Figure F-10. Average drug dispersion from cannula for 18 mm tissue and 20° x 13 mm Lg. cannula (a) top view (b) side view.

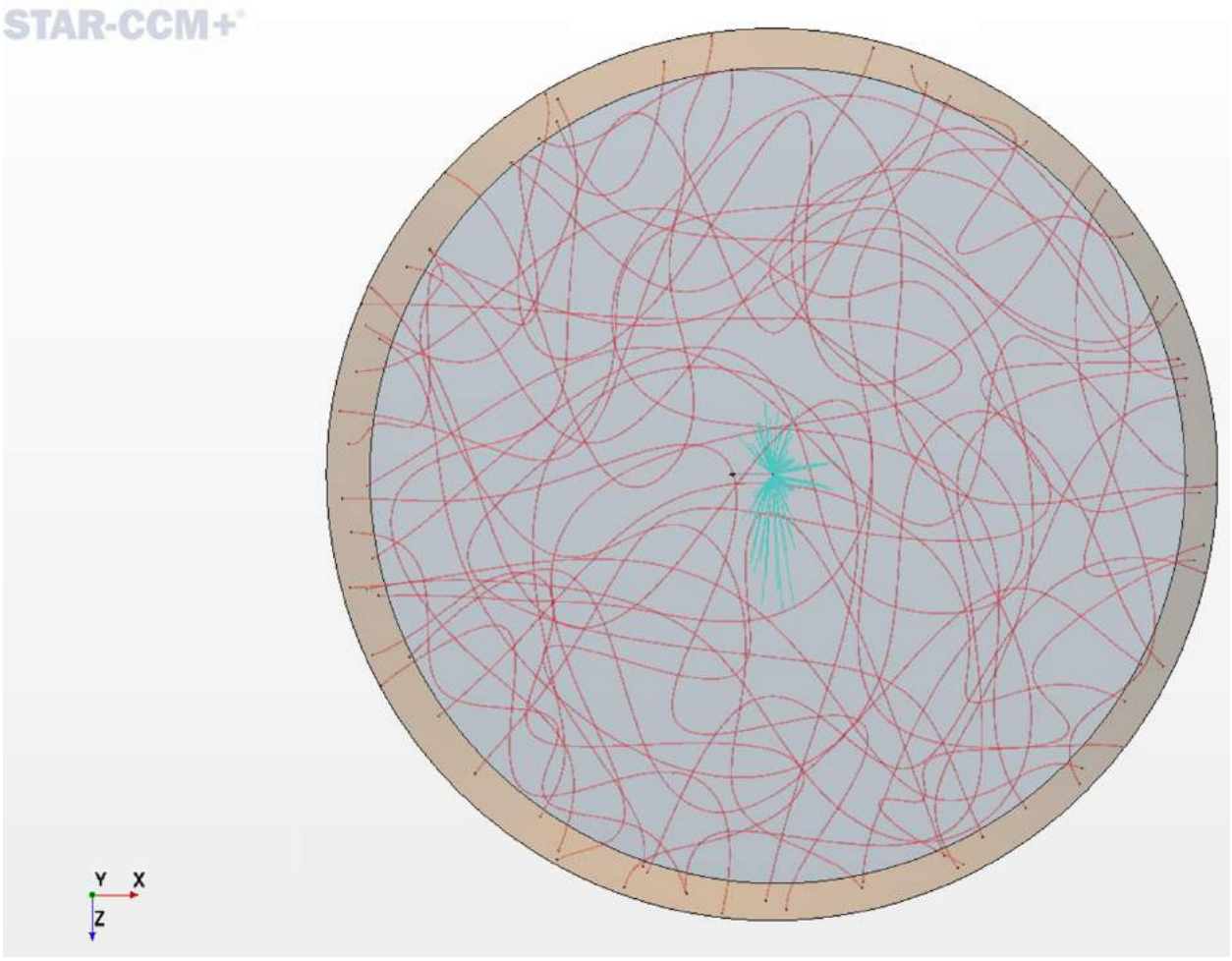

(a)

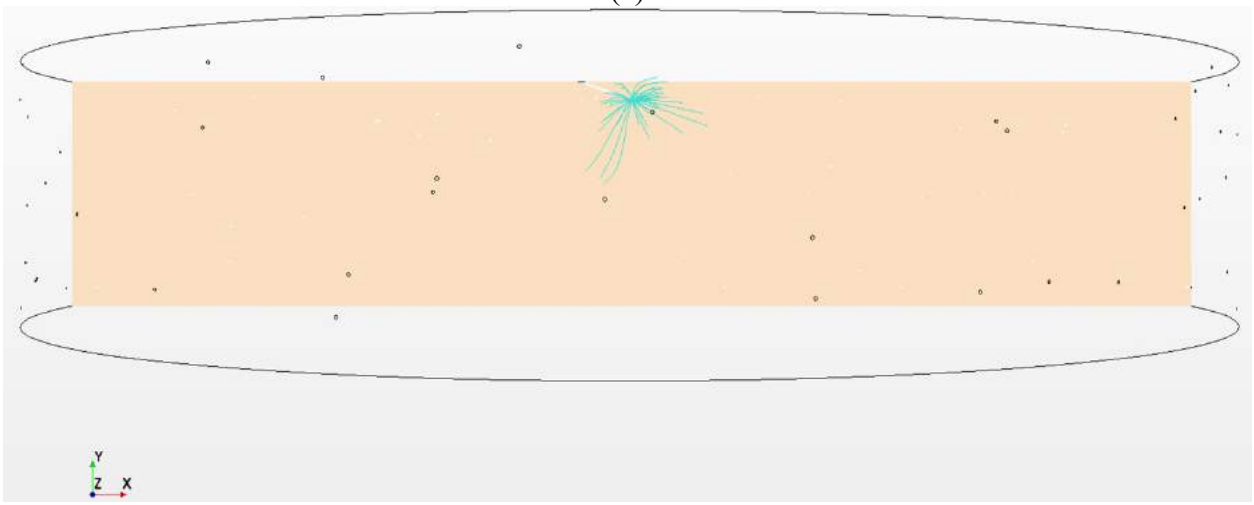

(b)

Figure F-11. Average drug dispersion from cannula for 24 mm tissue and 20° x13 mm Lg. cannula (a) top view (b) side view.

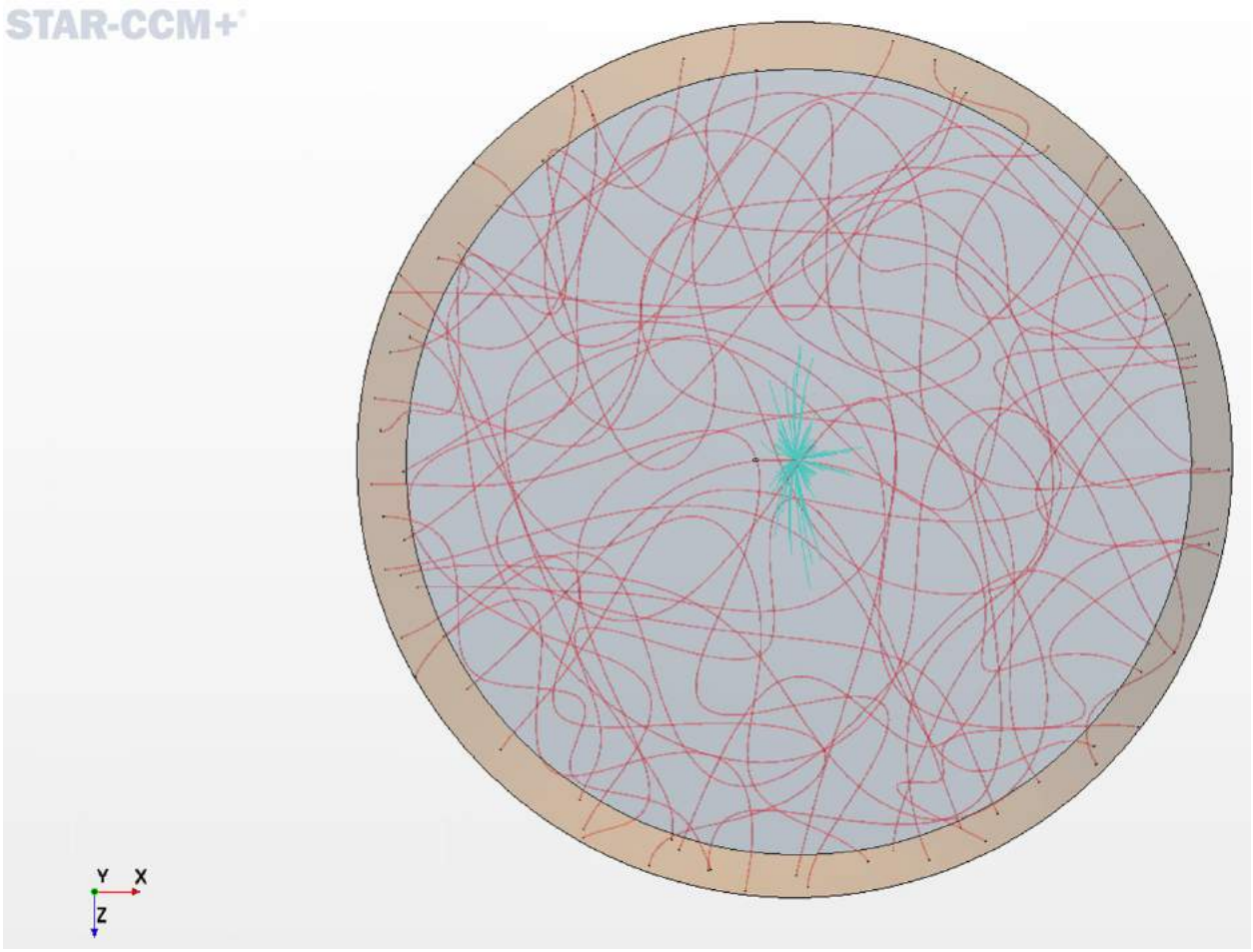

(a)

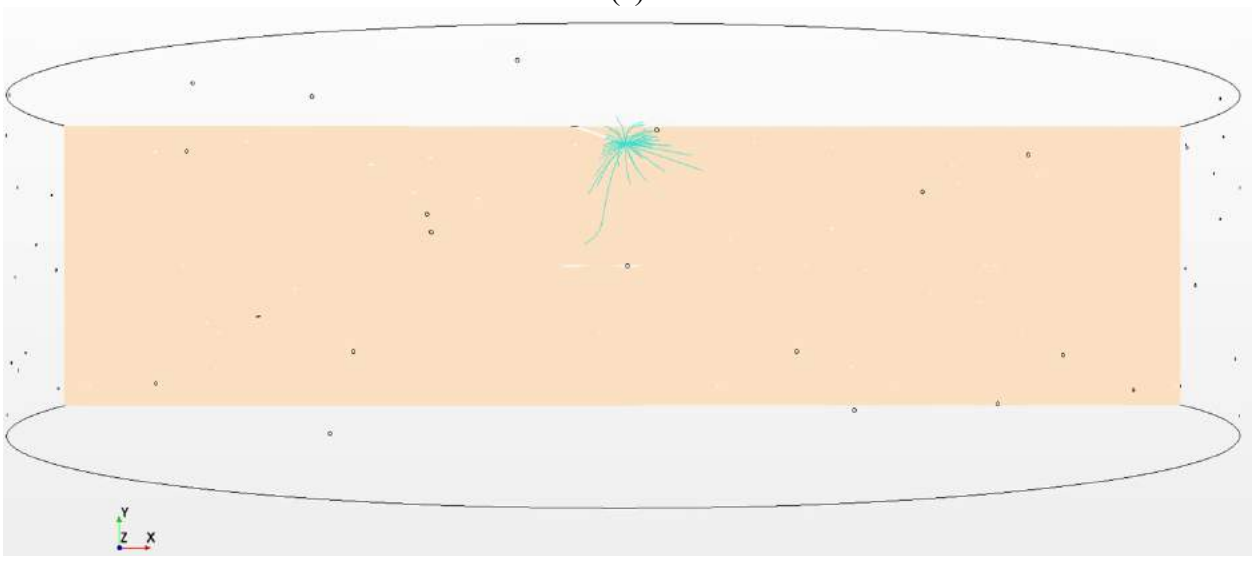

(b)

Figure F-12. Average drug dispersion from cannula for 30 mm tissue and 20° x 13 mm Lg. cannula (a) top view (b) side view.

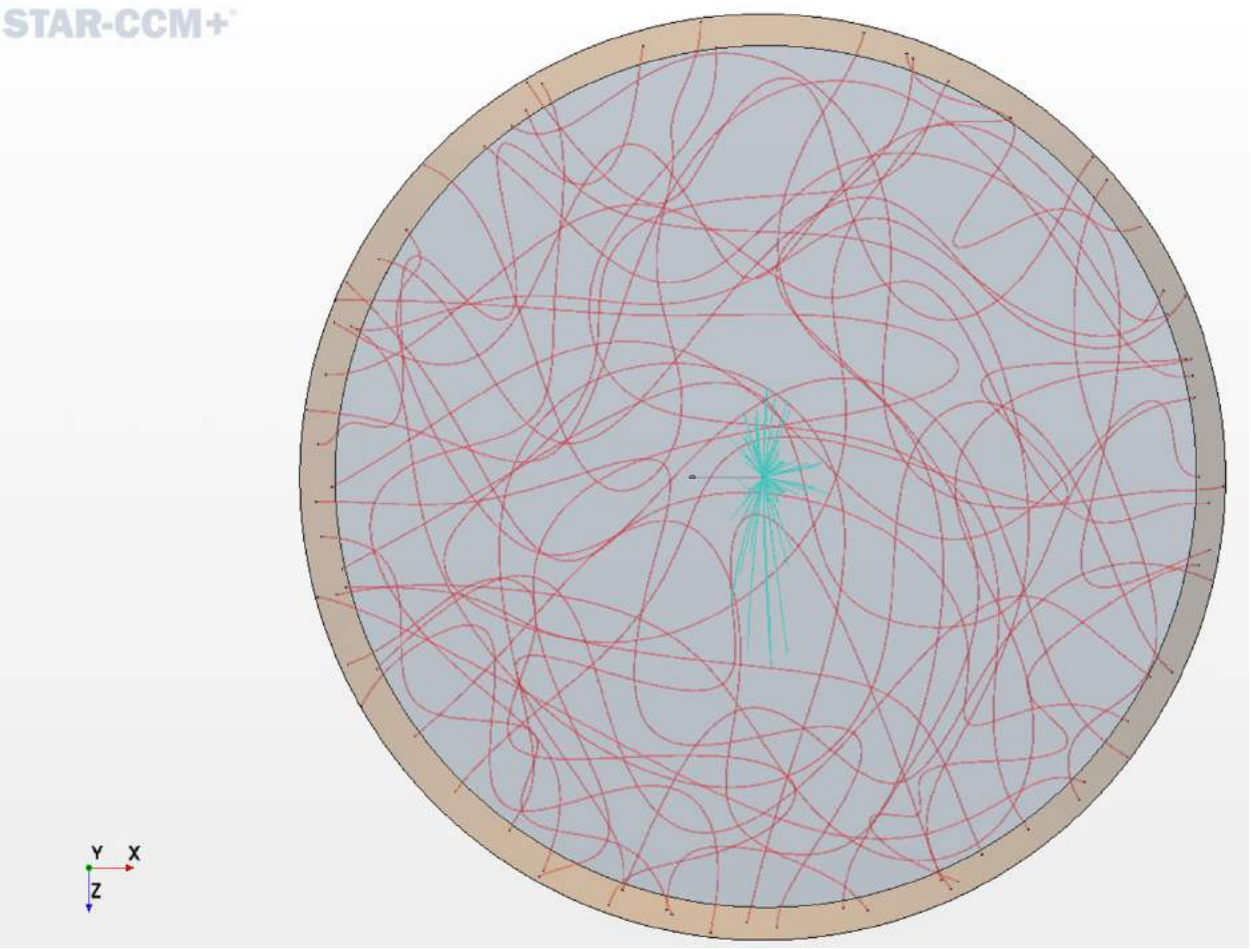

(a)

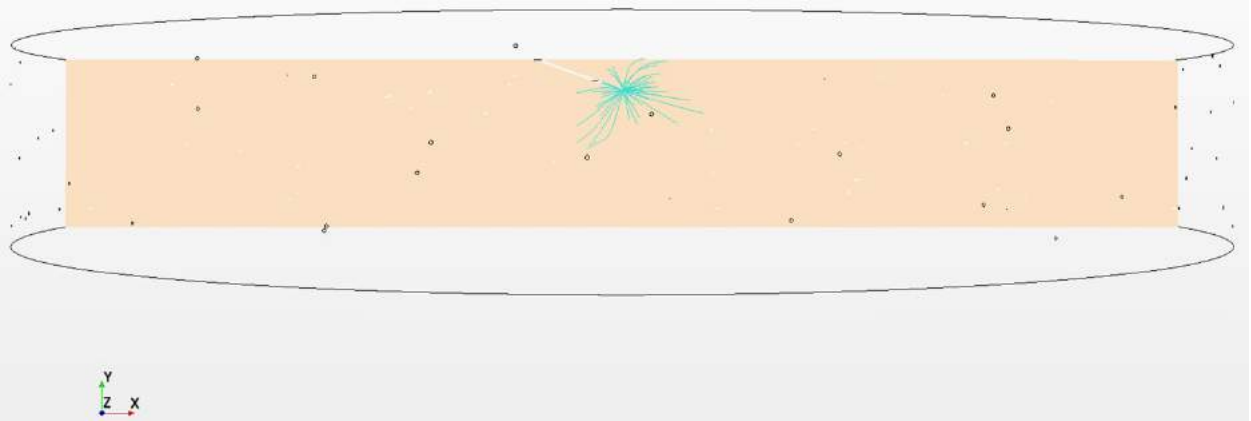

(b)

Figure F-13. Average drug dispersion from cannula for 18 mm tissue and 20° x 17 mm Lg. cannula (a) top view (b) side view.

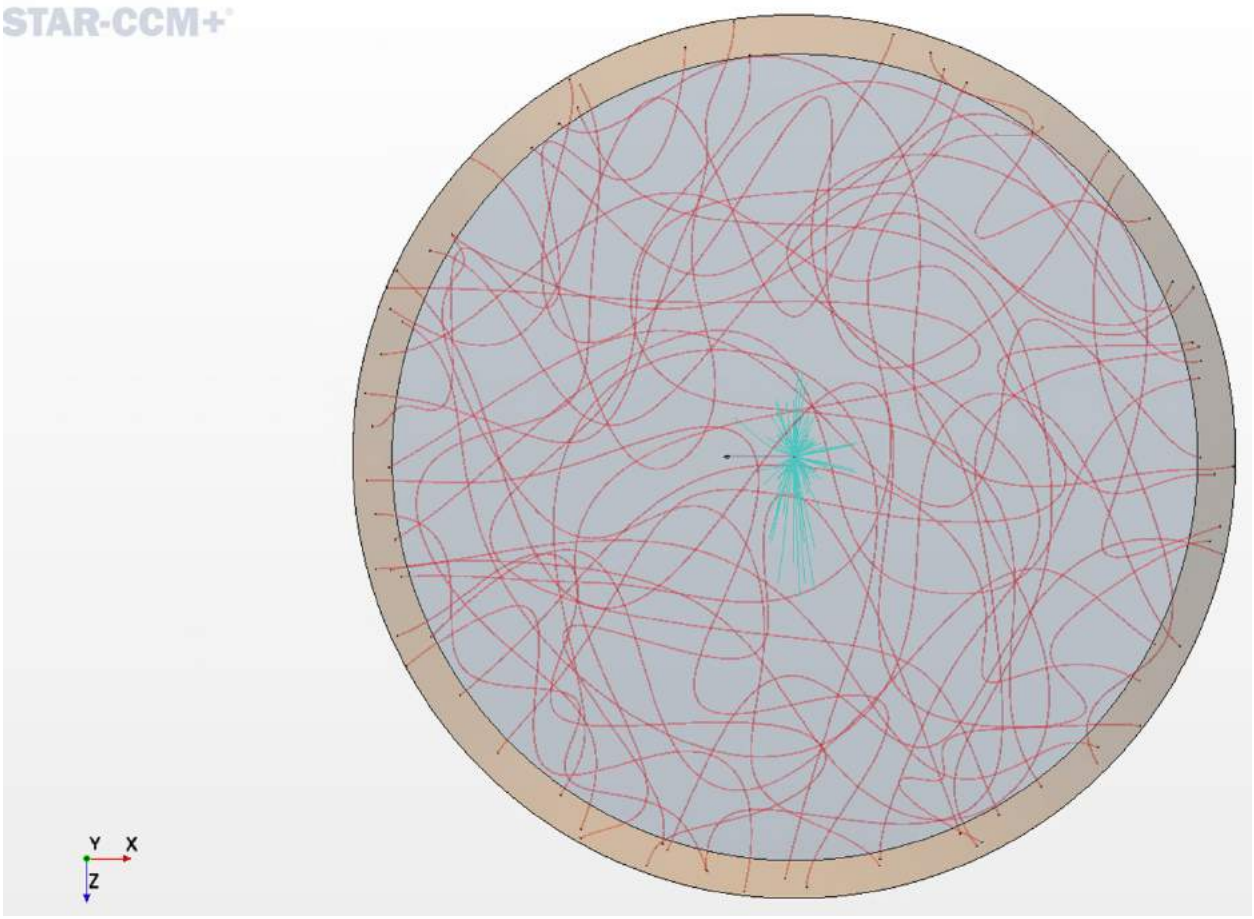

(a)

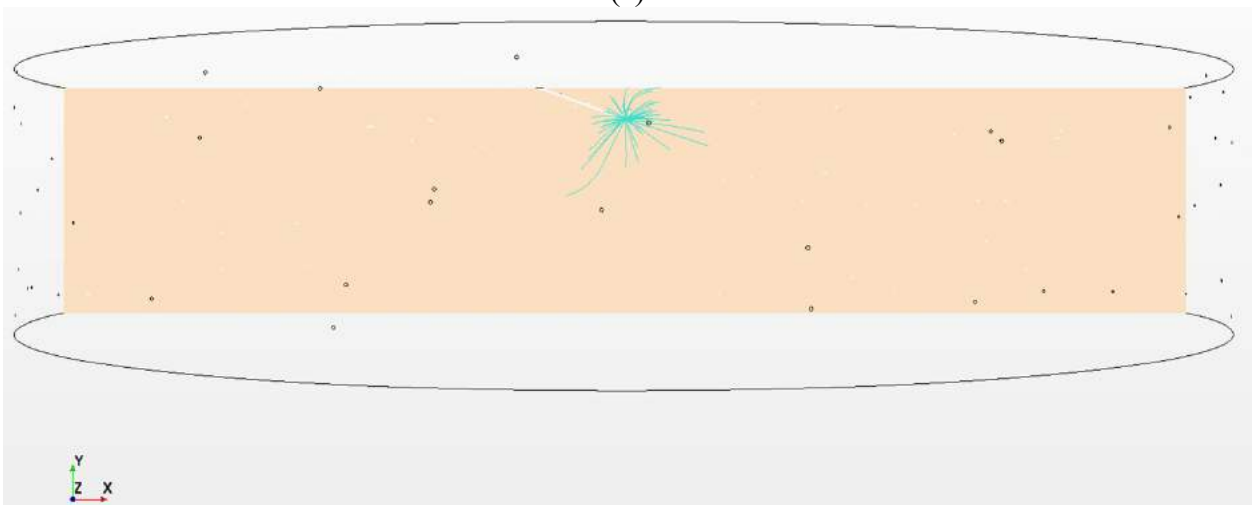

(b)

Figure F-14. Average drug dispersion from cannula for 24 mm tissue and 20° x 17 mm Lg. cannula (a) top view (b) side view.

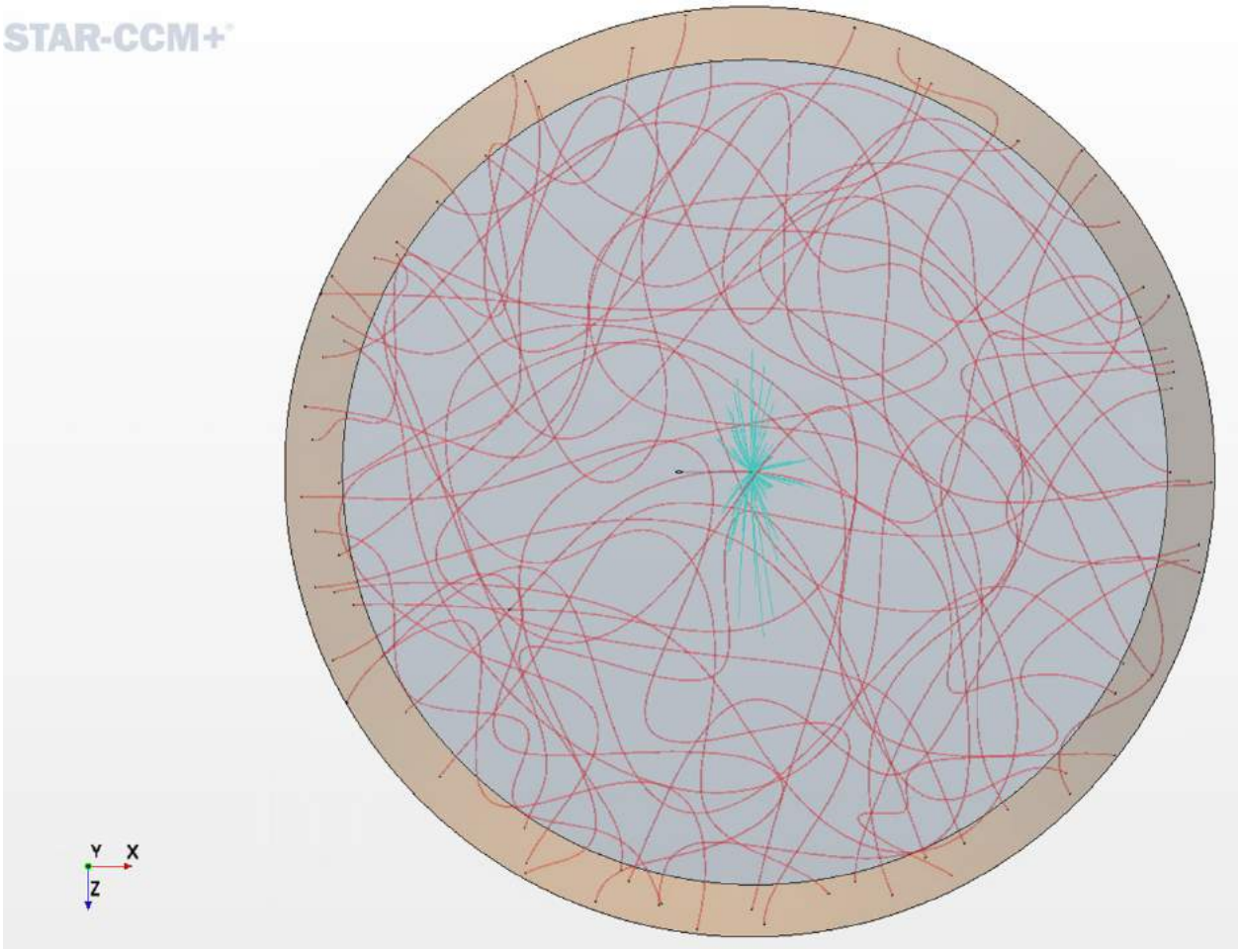

(a)

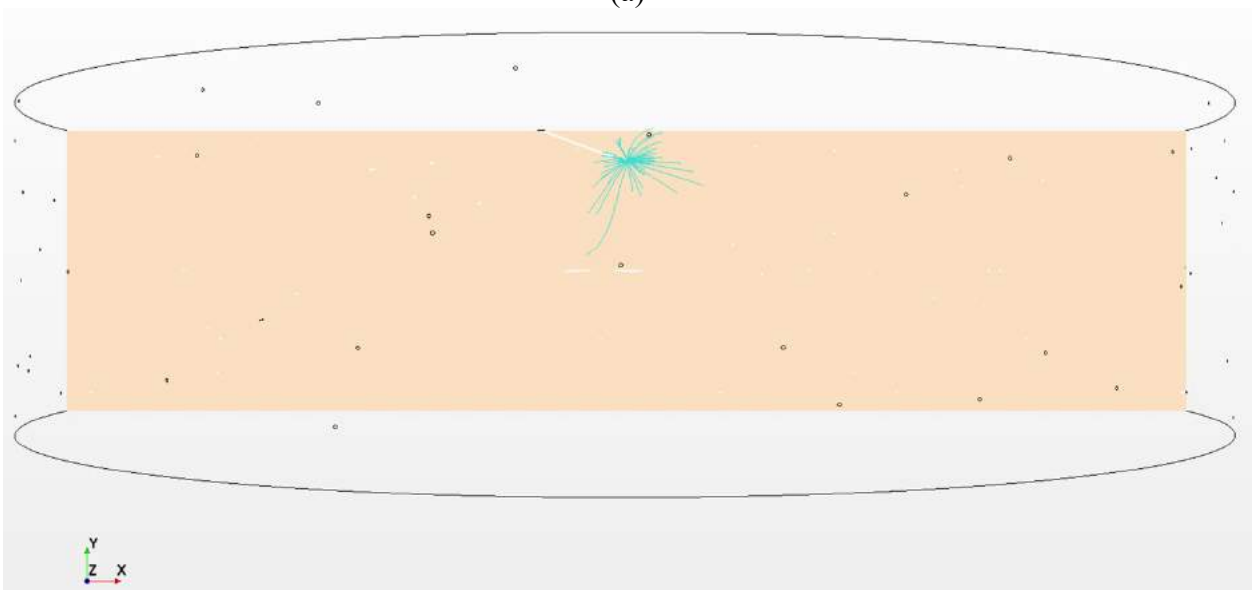

(b)

Figure F-15. Average drug dispersion from cannula for 30 mm tissue and 20° x 17 mm Lg. cannula (a) top view (b) side view.

References

1. Albright, A.L., & Stern, J.N. (1998). Encyclopedia of Sports Medicine and Science. *Adipose Tissue*. Retrieved from http://www.sportsci.org/encyc/adipose/adipose.html
2. McLennan, D.N., Porter, C.J.H., & Charman, S.A. (2005). Subcutaneous drug delivery and the role of lymphatics. *Drug Discovery Today: Technologies, 2(1)*, 89-96.
3. G.I. Frost, G.I. (2007) Recombinant human hyaluronidase (rHuPH20): an enabling platform for subcutaneous drug and fluid administration. *Expert Opinion on Drug Delivery, 4(4),* 427-440.
4. Yilmaz, M., & Hotamisligil, G.S. (2013). Damned If You Do, Damned If You Don't: The Conundrum of Adipose Tissue Vascularization. *Cell Metabolism, 17(1),* 7-9.
5. Peurichard, D., et al. (2017) Simple mechanical cues could explain adipose tissue morphology. *Journal of Theoretical Biology, 429,* 61-81.
6. Rushing, J. (2004). How to administer a subcutaneous injection. *Nursing, 36(6),* 32.
7. Torun, S., & Mutluay, S.D. (2017) Applicability of calf subcutaneous tissue to subcutaneous injection in young adults. *Applied Nursing Research, 34,* 66-69.
8. Heinemann, L., & Krinelke, L. (2012). Insulin Infusion Set: The Achilles Heel of Continuous Subcutaneous Insulin Infusion. *Journal of Diabetes Science and Technology, 6(4),* 954-964.
9. Anselmo, A.C., Gokarn, Y., & Mitragotri, S. (2019) Non-invasive delivery strategies for biologics. *Nature Reviews Drug Discovery, 18,* 19-40.
10. Wasserman, R.L., et al. (2012). Recombinant human hyaluronidase-facilitated subcutaneous infusion of human immunoglobulins for primary immunodeficiency. *Journal of Allergy and Clinical Immunology, 130(4),* 951-957.
11. Kim, H., Park, H., & Lee, S.J. (2017). Effective method for drug injection into subcutaneous tissue. *Scientific Reports, 7(1),* 1-11.
12. Heinemann, L., Weyer, C., Rauhaus, M., Heinrichs, S., & Heise, T. (1998) Variability of the metabolic effect of soluble insulin and the rapid-acting insulin analog insulin aspart. *Diabetes Care, 21(11),* 1910-4.
13. Heinemann, L. (2002) Variability of Insulin Absorption and Insulin Action. *Diabetes Technology & Therapeudics, 4(5),* 673-682.
14. Heinemann, L. (2008) Variability of Insulin Action: Does It Matter? *Insulin, 3(1),* 37-45.

15. Caccialanza, R., Constans, T., Cotogni, P., Zaloga, G.P., & Pontes-Arrunda, A. (2018). Subcutaneous Infusion of Fluids for Hydration or Nutrition: A Review. *Journal of Parenteral and Enteral Nutrition, 42(2),* 296-307.
16. Chen, W., Yung, B.C., Qian, Z., & Chen, X. (2018). Improving long-term subcutaneous drug delivery by regulating material-bioenvironment interaction. *Advanced Drug Delivery Reviews, 127(1),* 20-34.
17. Simonneau, G., et al. (2002). Continuous subcutaneous infusion of reprostinil, a prostacyclin analogue, in patients with pulmonary arterial hypertension. *American Journal of Respiratory and Critical Care Medicine, 165(6),* 800-804.
18. Centers for Disease Control and Prevention. (2017). *National Diabetes Statistics Report*. Atlanta, GA: United States Department of Health and Human Services.
19. van den Boom, L., et al. (2019). Temporal trends and contemporary use of insulin pump therapy and glucose monitoring among children, adolescents, and adults with type 1 diabetes between 1995 and 2017. *Diabetes Care, 42(11),* 2050-2056.
20. Heinemann, L., Walsh, J., & Roberts, R. (2014). We need more research and better designs for insulin infusion sets. *Journal of Diabetes Science and Technology, 8(2),* 199-202.
21. McDonald, T.A., Zepeda, M.L., Tomlinson, M.J., Bee, W.H., & Ivens, I.A. (2010). Subcutaneous administration of biotherapeutics: Current experience in animal models. *Current Opinions in Molecular Therapeutics, 12(4),* 461-470.
22. Collins, D.S., et al. (2017). Optimizing the bioavailability of subcutaneously administered biotherapeutics through mechanochemical drivers. *Pharm. Res., 34(10),* 2000-2011.
23. Ritcher, W.F., & Jacobsen, B. (2014). Subcutaneous Absorption of Biotherapeutics: Knowns and Unknowns. *Drug Metab Dispos, 42(11),* 1881-1889.
24. Rasmussen, C.H., et al. (2014). Insulin aspart pharmacokinetics: an assessment of its variability and under- lying mechanisms. *European Journal of Pharmaceutical Sciences, 62,* 65–75.
25. Thomsen, M., Hernandez-Garcia, A., Mathiesen, J., Poulsen, M., Sorensen, D.N., Tarnow, L., & Fiedenhans'l, R. (2014). Model Study of the Pressure Build-Up during Subcutaneous Injection. *PloS ONE, 9(8),* e104054.
26. Leuenberger Jockel, J.P., Roebrock, P., & Shergold, O.A. (2013). Insulin Depot Formation in Subcutaneous Tissue. *J Diabetes Sci Technol, 7(1),* 227-237.

27. Bhave, G. & Neilson, E.G. (2011). Body Fluid Dynamics: Back to the Future. *J Am Soc Nephrol, 22(12),* 2166-2181.
28. Yao, W., Shen, Z., & Ding, G. (2013). Simulation of Interstitial Fluid Flow in Ligaments: Comparison among Stokes, Brinkman and Darcy Models. *International Journal of Biological Sciences, 9(10),* 1050-1056.
29. Grodzinsky A.J., Levenston M.E., & Jin M., (2000). Cartilage tissue remodeling in response to mechanical forces. *Annu Rev Biomed Eng, 2,* 691-713.
30. Swartz M.A., & Fleury M.E. (2007). Interstitial Flow and Its Effects in Soft Tissues. *Annu Rev Biomed Eng, 9,* 229-256.
31. Tarbell, J.M., Weinbaum, S., & Kamm, R.D. (2005). Cellular fluid mechanics and mechanotransduction. *Annals of Biomed Eng, 33(12),* 1719–1723.
32. Ng, C.P., & Swartz, M.A. (2003). Fibroblast alignment under interstitial fluid flow using a novel 3-D tissue culture model. *American Journal of Physiology, 284(5),* H1771– H1777.
33. Yao, W., Li, Y., & Ding, G. (2012). Interstitial fluid flow: the mechanical environment of cells and foundation of meridians. *Evidence-Based Complementary and Alternative Medicine, 2012,* 1-9.
34. Frayn, K.N., & Karpe, F. (2014). Regulation of human subcutaneous adipose tissue blood flow. *International Journal of Obesity, 38,* 1019-1026.
35. Polacheck, W.J., Charest, J.L. & Kamm, R.D. (2011). Interstitial flow influences direction of tumor cell migration through competing mechanisms. *Proc Natl Acad Sci USA, 108(27),* 11115-11120.
36. Sarntinoranont, M., Chen, X., Zhao, J., & Mareci, T.H. (2006). Computational Model of Interstitial Transport in the Spinal Cord using Diffusion Tensor Imaging. *Annals of Biomed Eng, 34(8),* 1304-1321.
37. Kuttler, A., Dimke, T., Kern, S., Helmlinger, G., Stanski, D., & Finelli, L.A. (2010). Understanding pharmacokinetics using realistic computational models of fluid dynamics: biosimulation of drug distribution within the CSF space for intrathecal drugs. *J Pharmacokinet Pharmacodyn, 37(6),* 629-644.
38. Steuperaert, M., et al. (2019). A 3D CFD model of the interstitial fluid pressure and drug distribution in heterogeneous tumor nodules during intraperitoneal chemotherapy. *Drug Delivery, 26(1),* 404-415.

39. Gao, Y., Shi, Y., Fu, M., Feng, Y., Lin, G., Kong, D., Jiang, B. (2020). Simulation study of the effects of interstitial fluid pressure and blood flow velocity on transvascular transport of nanoparticles in tumor microenvironment. *Computer Methods and Programs in Biomedicine, 193,* 105493.

40. d'Esposito, A., et al. (2018). Computational fluid dynamics with imaging of cleared tissue and of in vivo perfusion predicts drug uptake and treatment responses in tumours. *Nature Biomed Eng, 2(10),* 773-787.

41. Yao, W., & Li, Y. (2013). Analytic solutions of the interstitial fluid flow models. *Journal of Hydrodynamics, 25(3),* 683-694.

42. Yao, W., & Ding, G.H. (2011). Interstitial fluid flow: simulation of mechanical environment of cells in the interosseous membrane. *Acta Mech Sin, 27(4),* 602-610.

43. Lee, J.S., & Fung, Y.C. (1969). Stokes flow around a circular cylindrical post confined between two parallel plates. *J Fluid Mech, 37(4),* 657-670.

44. Pedersen, J.A., Boschetti, F., & Swartz, M.A. (2007). Effects of extracellular fiber architecture on cell membrane shear stress in a 3D fibrous matrix. *J Biomech, 40(7),* 1484-1492.

45. Pedersen, J.A., Lichter, S., & Swartz, M.A. (2010). Cells in 3D matrices under interstitial flow: Effects of extracellular matrix alignment on cell shear stress and drag forces. *J Biomech, 43(5),* 900-905.

46. Zedelmair, M. (2016). *Numerical simulation of insulin depot formation and absorption in subcutaneous tissue modeled as a porous media* [Master's thesis dissertation, California State University, Northridge]. Zedelmair-Michael-thesis-2016.

47. Ludescher, B., Rommel, M., Willmer, T., Fritsche, A., Schick, F., & Machann, J. (2011). Subcutaneous adipose tissue thickness in adults – correlation with BMI and recommendations for pen needle lengths for subcutaneous self-injection. *Clinical Endocrinology, 75(6),* 786-790.

48. Störchile, P., et al. (2017). Standardized ultrasound measurement of subcutaneous fat patterning: high reliability and accuracy in groups ranging from lean to obese. *Ultrasound in Med & Biol, 43(2),* 427-438.

49. Kelso, A., Müller, W. Fürhapter-Rieger, A., Sengeis, M., Ahammer, H., & Steinacker, J.M. (2020). High inter-observer reliability in standardized ultrasound measurements of subcutaneous adipose tissue in children aged three to six years. *BMC Pediatrics, 20,* 145.

50. Chirita-Emandi, A., Dobrescu, A., Papa, M., & Puiu, M. (2015). Reliability of Measuring Subcutaneous Fat Tissue Thickness Using Ultrasound in Non-Athletic Young Adults. *MAEDICA – A Journal of Clinical Medicine, 1093),* 204-209.

51. de Albuquerque Garcia Redondo, P., et al. (2020). Lymphatic vessels in human adipose tissue. *Cell and Tissue Research, 379(8),* 511-520.

52. Brown, N.K., et al. (2014). Perivascular adipose tissue in vascular function and disease. *Arterioscler Throm Vasc Biol, 34(8),* 1621-1630.

53. Spencer, M., et al. (2011). Adipose Tissue Extracellular Matrix and Vascular Abnormalities in Obesity and Insulin Resistance. *J Clin Endocrinol Metab, 96(12),* E1990-E1998.

54. Mihai, L.A., Chin, L. Janmey, P.A., & Goriely, A. (2015). A comparison of hyperelastic constitutive models applicable to brain and fat tissues. *J R Soc Interface, 12,* 20150486.

55. Starly, B., Yildirim, E., & Sue, W. (2007). A tracer metric numerical model for predicting tortuosity factors in three-dimensional porous tissue scaffolds. *Computer Methods and Programs in Biomedicine, 87(1),* 21-27.

56. Bini, F., Pica, A., Marinozzo, A., & Marinozzo, F. (2019). A 3D model of the effect of tortuosity and constrictivity on the diffusion in mineralized collagen fibril. *Scientific Reports, 9(1),* 2658.

57. Ashworth, J.C., Best, S.M., & Cameron, R.E. (2014). Quantitative architectural description of tissue engineering scaffolds. *Material Technology: Advanced Performance Materials, 29(5),* 281-295.

58. Hrabe, J., Hrabetová, S., & Segeth, K. (2004). A model of effective diffusion and tortuosity in the extracellular space of the brain. *Biophysical Journal, 87(3),* 1606-1617.

59. Wei, J.C.J., Edwards, G.A., Martin, D.J., Huang, H., Crichton, M.L., & Kendall, M.A.F. (2017). Allometric scaling of skin thickness, elasticity, viscoelasticity to mass for micro-medical device translation: from mice, rats, rabbits, pigs to humans. *Scientific Reports,7(1),* 15885.

60. Burren, D. Bolus speeds – how fast is your pump? (n.d.) *Bionic Wookie*. Retrieved on July 1, 2020 from https://bionicwookiee.com/2019/07/30/bolus-speeds-how-fast-is-your-pump/

61. Versteeg, H. K., & Malalasekera, W. (2010). *An Introduction to Computational Fluid Dynamics: The Finite Volume Method (2nd ed.).* Harlow, Essex: Pearson/Prentice Hall.
62. Khaled, A.-R.A., & Vafai, K. (2003). The role of porous media in modeling flow and heat transfer in biological tissues. *Inter J of Heat and Mass Transfer, 46(26),* 4989-5003.
63. Sherar, M.D., Gladman, A.S., Davidson, S.R.H., Trachtenberg, J., & Gertner, M.R. (2001). Helical antenna arrays for interstitial microwave thermal therapy for prostate cancer: tissue phantom testing and simulations for treatment. *Phys Med Biol, 46(7),* 1905-1918.
64. Sanyal, D.C., & Maji, N.K. (2001). Thermoregulation through skin under variable atmospheric and physiological conditions. *J Theor Biol, 208(4),* 451-456.
65. Sternberg, R.L., Kalinowski, A.J., & Papadakis, J.S. (1980). Nonlinear partial differential equations in engineering and applied science. *Lecture Notes in Pure and Applied Mathematics, 54,* 429-443.
66. White, F.M. (2003). *Fluid Mechanics, Fifth Edition.* New York, NY: McgrawHill.
67. Compass (2018, November). *Tdyn-CFD+HT – Validation Case 5*. Retrieved on August 30, 2020 from https://www.compassis.com//downloads/Manuals/Validation/Tdyn-ValTest5-Flow_through_porous_media.pdf
68. Wood, B.D., Xiaoliang, H., & Sourabh, V.A. (2020). Modeling turbulent flows in porous media. *Annu Rev Fluid Mech, 52(1),* 171-203.
69. Huang, H. & Ayoub, J.A. (2008). Applicability of the Forchheimer equations for non-Darcy flow in porous media. *SPE Journal, 13(1),* 112-122.
70. Bird, R.B., Stewart, W.E., & Lightfoot, E.N. (2002). *Transport Phenomena, 2nd Edition.* New York, NY: John Wiley & Sons.
71. Hausman G.J., & Richardson, R.L. (1983). Cellular and vascular development in immature rat adipose tissue. *Journal of Lipid Research, 24(5),* 522-532.
72. Robciuc, M.R., et al. (2016). VEGFB/VEGFR1-induced expansion of adipose vasculature counteracts obesity and related metabolic complications. *Cell Metabolism, 23(4),* 712-724.
73. Rutkowski, J.M., & Swartz, M.A. (2007). A driving force for change: interstitial flow as a morphoregulator. *Trends in Cell Biology, 17(1),* 44-50.
74. Scallan, J., Huxley, V.H., & Korthuis, R.J. (2010). *Capillary Fluid Exchange: Regulation, Functions, and Pathology.* San Rafael, CA: Morgan & Claypool Life Science.

75. Hansen, K.C., D'Alessandro, A., Clement, C.C., & Santambrogio, L. (2015). Lymph formation, composition, and circulation: a protein perspective. *International Immunology, 27(5),* 219-227.

76. Fox, S. & Rompolski, K. (2022). *Human Physiology, Sixteenth Edition.* New York, NY: McGraw Hill LLC.

77. Lv, Y., Liu, J., Gao, Y., & Xu, B. (2006) Modeling of transdermal drug delivery with a micro needle array. *Journal of Micromechanics and Microengineering, 16,* 1492-2501.

78. Farvid, M.S., Ng, T.W.K., Chan, D.C. Barrett, P.H.R., & Watts, G.F. (2005). Association of adiponectin and resistin with adipose tissue compartments, insulin resistance and dyslipidaemia. *Diabetes Obes Metab, 7(4),* 406-413.

79. Hasgall, P.A., et al. (2018, May 15). IT'IS Database for thermal and electromagnetic parameters of biological tissues, Version 4.0. DOI: 10.13099/VIP21000-04-0. Retrieved on June 10, 2020 from it is.swiss/database.

80. Tsai, C.K., Wang, T.D., Lin, J.W., Hsu, R.B., Guo, L.Z., Chen, S.T., & Liu, T.M. (2012). Virtual optical biopsy of human adipocytes with third harmonic generation microscopy. *Biomedical Optics Express, 4(1),* 178-186.

81. Zhao, F., et al. (2014). A multiscale computational fluid dynamics approach to simulate the micro-fluidic environment within a tissue engineering scaffold with highly irregular pore geometry. *Biomechanics and Modeling in Mechanobiology, 18(6),* 1965-1977.

82. Tu, J., Yeoh, G.H., & Liu, C. (2018). *Computational Fluid Dynamics (Third Edition).* Cambridge, MA: Butterworth-Heinemann.

83. Ward, L.G., Heckman, M.G., Warren, A.I., & Tran, K. (2013). Dosing accuracy of insulin aspart *FlexPens* after transport through the pneumatic tube system. *Hosp. Pharm., 48(1),* 33-38.